THE STRUCTURE AND FUNCTION OF THE VASOPRESSIN V_{1A} RECEPTOR

RICHARD THOMAS LOGAN

A thesis submitted to the University of Birmingham

for the degree of Doctor of Philosophy

School of Biosciences
College of Life and Environmental Science
University of Birmingham
Birmingham
B15 2TT
September 2012

ABSTRACT

The neurohypophysial hormone [arginine^{8}]vasopressin (AVP) exerts the majority of its physiological roles through the G-protein-coupled receptor, $V_{1a}R$. AVP binding to the $V_{1a}R$ promotes receptor activation and generates signalling though the inositol phosphate pathway.

ICL 2 has been implicated in many aspects of GPCR signalling and crystallographic data highlight the structurally dynamic nature of this region. A complete alanine-scanning study of ICL 2 has not previously been conducted in a GPCR but is presented here in the prototypical peptide-ligand GPCR, $V_{1a}R$. However, a role of Leu$^{3.58}$ in mediating G-protein-dependent signalling was observed in the $V_{1a}R$ – a finding that has previously been reported in other GPCRs.

Upon agonist binding, the structural rearrangements of TM V and TM VI are integral in signal transduction in GPCRs. Two highly conserved residues, Tyr$^{5.58}$ and Ile$^{6.40}$ are key players in the activation process. Given their high conservation, it was presumed that their roles are universal throughout the rhodopsin-like GPCR family. The systematic substitution of these two residues in the $V_{1a}R$ demonstrate the receptor-specific nature of substitutions of Tyr$^{5.58}$ and Ile$^{6.40}$ given that findings in the $V_{1a}R$ are not recapitulated in the generally limited mutagenic studies in other receptors.

I would like to dedicate this thesis to Mum and Dad.

Thank you for the belief you have in me with everything that I do.

ACKNOWLEDGEMENTS

Firstly I would like to thank Professor Mark Wheatley for his supervision and continued support throughout my PhD. My thanks also go to members of the Wheatley lab, past and present (Denise, Michelle, Matt, Rosemary, Mohammed, Jack and particularly Rachel) who have provided invaluable discussion and much enjoyment whilst working alongside them. Also, other members of the 7th floor, Eva, Tim, Umbreen, Martin, Craig, Matt, have made my time at Birmingham University very enjoyable. In particular, Sandeep and Raul, thank you for being the best neighbours in the research office and for being tolerant of my talking to myself. Thank you to the great friends that I have made over the past four years and I know will be life-long friends. Particularly I am thankful for to the support of the people I started and finished this experience with; Emanuela, Jen, Rach, and Sarah. Cheers Jen for all of the cake too.

I would also like to extend my gratitude to my parents and Kirsty for their enthusiasm and support and to Chris for his understanding, particularly whilst writing up.

Finally I would like to thank the BBSRC and Schering-Plough for their financial support.

TABLE OF CONTENTS

ABBREVIATIONS

Throughout this thesis, abbreviations are used as recommended by the Journal of Biological Chemistry. In addition, the following abbreviations have been used:

5-HT	5-hydroxytryptamine
AC	adenylyl cyclase
ACTH	adrenocorticotrophin hormone
ADH	antidiuretic hormone
ATP	adenosine triphosphate
$AT_{1a}R$	angiotensin II type 1a receptor
AVP	[arginine^8]vasopressin
bRho	bovine rhodopsin
BSA	bovine serum albumin
CAM	constitutively active mutant
cAMP	cyclic 3', 5'-adenosine monophosphate
cDNA	complementary DNA
CXCR4	chemokine receptor type 4
D2R	dopamine D2 receptor
D3R	dopamine D3 receptor
DAG	diacylglycerol
DMEM	Dulbecco's modified Eagle's medium
ECL	extracellular loop
ELISA	enzyme-linked immunosorbent assay
ER	endoplasmic reticulum
ERK1/2	extracellular regulated protein kinase 1/2
EtBr	ethidium bromide
FBS	foetal bovine serum
FSHR	follicle-stimulating hormone receptor
G-protein	guanine nucleotide binding protein
GABA	γ-aminobutyric acid
GAP	GTPase activating protein
GDP	guanosine diphosphate
ghrelin-R	ghrelin receptor
GPCR	G-protein-coupled receptor
GRK	G-protein-coupled receptor kinase
Gt-CT	carboxyl terminus of transducin
GTP	guanosine triphosphate
H8	helix 8
HA	haemagglutinin-epitope
ICL	intracellular loop
InsP	inositol phosphate

$InsP_3$	inositol 1,4,5 trisphosphate
LB	lysogeny broth
LHR	lutropin receptor
mAChR	muscarinic acetylcholine receptor
MAPK	mitogen activated protein kinase
MC4R	melanocortin 4 receptor
OPD	*O*-phenlyenediamine dihydrochloride
OR	opioid receptor
OT	oxytocin
OTR	oxytocin receptor
PBS	phosphate-buffered saline
PCR	polymerase chain reaction
PDL	poly-D-lysine
PEI	polyethylenimine
PIP_2	phosphatidylinositol 4,5-bisphosphate
PKA	protein kinase A
PKC	protein kinase C
PLC	phospholipase C
RGS	regulators of G-protein signalling
Rho	rhodopsin
rho	rho small GTPase
SP	substance P
T4L	T4 lysozyme
TBE	tris-borate-EDTA buffer
TM	transmembrane
TSHR	thyroid-stimulating hormone receptor
$V_{1a}R$	vasopressin 1a receptor
$V_{1b}R$	vasopressin 1b receptor
V_2R	vasopressin 2 receptor
Wt	wild-type
$\alpha_{1B}AR$	α_{1B} adrenoceptor
α_2AR	α_2 adrenoceptor
β_1AR	β_1 adrenoceptor
β_2AR	β_2 adrenoceptor

CHAPTER 1: INTRODUCTION

1.1 G-protein-coupled receptors

G-protein-coupled receptors (GPCRs) are the largest family of integral membrane proteins and as such conduct the majority of signal transduction across cell membranes. Approximately 2 % of genes within the human genome encode ~ 800 GPCRs (Millar and Newton, 2010). Being so numerous, GPCRs participate in a vast array of physiological processes and elicit sight, smell and taste perception. Although 30-50 % of clinically approved drugs modulate GPCRs (Hopkins and Groom, 2002; Klabunde and Hessler, 2002), only a subset of this superfamily are currently druggable, making the potential for pharmaceutical development enormous.

GPCR are expressed at the cell surface and transmit the binding of extracellular ligands across the cell membrane, initiating intracellular signalling cascades. The canonical view of signalling by GPCRs is through activating the family of heterotrimeric GTPases, the guanine nucleotide-binding (G-) proteins.

1.2 G-proteins

G-proteins are made up of three subunits, Gα, Gβ and Gγ. 21 Gα subunits, 6 Gβ and 12 Gγ subunits are encoded in the human genome (Downes and Gautam, 1999). Primary sequence similarity subdivides Gα subunits into four distinct classes: $G\alpha_s$ $G\alpha_i$ $G\alpha_q$ and $G\alpha_{12}$ (Simon *et al.*, 1991). Gα subunits are comprised of a GTPase domain and a helical domain. This conserved protein framework has been confirmed by X-ray crystallography which additionally provides insight into structural changes involved in G-protein activation (Sprang, 1997; Oldham and Hamm, 2006; Singh *et al.*, 2012). The GTPase domain within the Gα

subunit is conserved throughout the entire G-protein superfamily. The six, α-helical domain forms a lid over the nucleotide binding pocket and differentiates the Gα proteins from the monomeric, small G-proteins. The Gα subunit is post-translationally acylated at the N-terminus which facilitates plasma membrane localization (Chen and Manning, 2001).

The Gβ subunit possesses a seven-bladed β-propeller structure and the amino-terminus forms a coiled-coiled with the amino-terminus of Gγ. The C-terminus of Gγ also forms contacts with blades five and six of Gβ (Wall *et al.*, 1995; Sondek *et al.*, 1996). Denaturing conditions are required to separate the obligate Gβγ dimer (Schmidt *et al.*, 1992). The action of G-proteins is discussed further in section 1.6.

1.3 Classification of GPCRs

GPCRs are characterised by a conserved 7 transmembrane (TM) α-helical motif with conserved topology (Figure 1.1). With an extracellular amino-terminus and intracellular carboxyl-terminus, transmembrane regions are connected by alternating intracellular loops (ICL I-III) and extracellular loops (ECL I-III). GPCRs are commonly classified into six familes, Families A-F, according to sequence analysis (Attwood and Findlay, 1994; Kolakowski, 1994). This classification incorporates both vertebrate and invertebrate GPCRs. Human GPCRs may be classified into five groups in the GRAFS classification system (Fredriksson *et al.*, 2003); the glutamate, rhodopsin, adhesion, frizzled/taste2 and secretin families.

The glutamate receptor family represents eight metabotropic glutamate receptors (mGluR), the non-ion channel GABA (γ-aminobutyric acid) receptors, the calcium-sensing receptor and a subfamily of proposed taste receptors. These receptors possess extended amino-termini that are responsible for ligand recognition. For example the mGlu receptors possess the

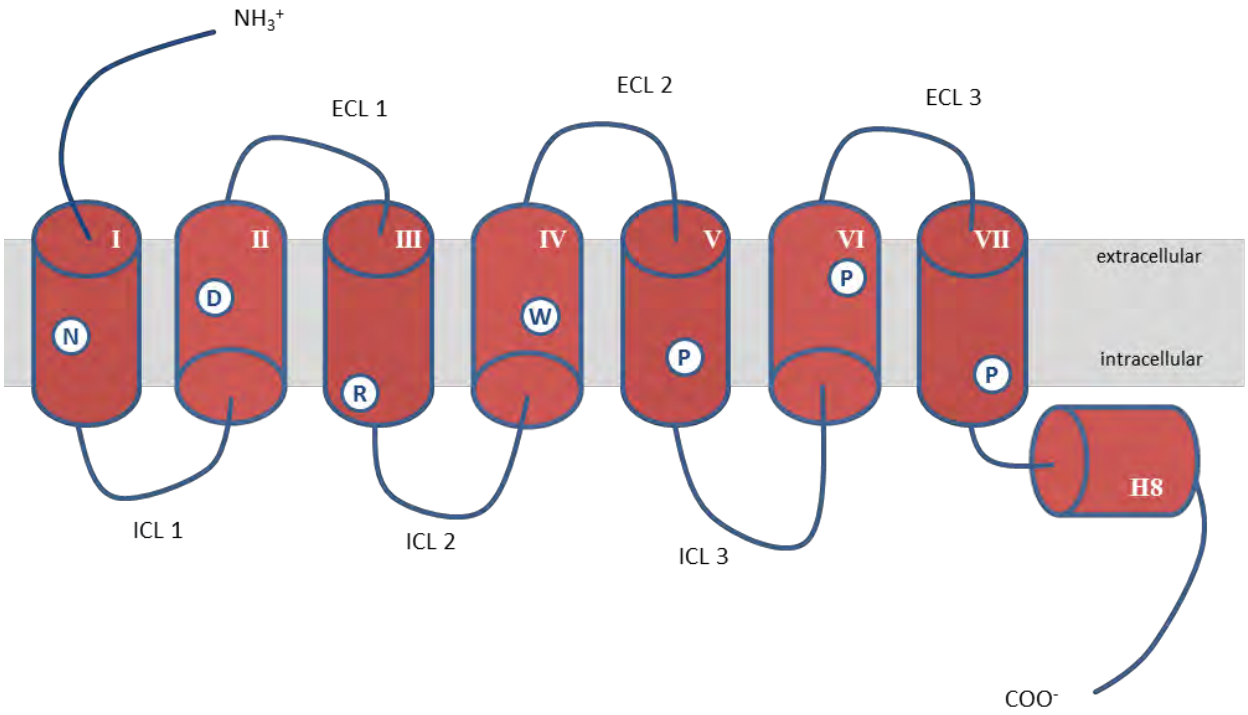

Figure 1.1 A two-dimensional representation of a typical GPCR

The amino terminus is located on the extracellular side and the carboxyl-terminus on the intracellular face. Helices are shown as red cylinders and TM helices are labelled by roman numerals (TM I-VII and H8). Extracellular loops (ECL) and intracellular loops (ICL) are down and labelled. The most conserved residue of each helix is shown in a circle. $Asn^{1.50}$, $Asp^{2.50}$ and $Arg^{3.50}$ are involved in receptor activation and G-protein coupling (discussed further in section 1.5.3). $Trp^{4.50}$, $Pro^{5.50}$, $Pro^{6.50}$ and $Pro^{7.50}$ have more general structural roles dictated by their side chain properties. $Trp^{4.50}$ participates in hydrophobic interactions and the conserved proline residues introduce kinks into the TM regions.

characteristic “Venus flytrap” module that closes around the glutamate ligand upon binding (Pin *et al.*, 2003). The rhodopsin-like family is the largest of all the GPCR families, representing approximately 90% of all vertebrate GPCRs (Fredriksson *et al.*, 2003). This group is identified by characteristic amino acid sequence motifs such as the NPxxY and D/ERY motifs discussed in more detail in section 1.5.3. The rhodopsin GPCR family includes the olfactory receptors. The adhesion receptor family are characterised by motifs in the amino-termini that may participate in cell adhesion (Stacey *et al.*, 2000). Frizzled/taste 2 receptors comprise a fourth group of vertebrate GPCRs. These two receptor subfamilies share consensus sequence motifs that are distinct from the other four families. The taste 2 receptors are distinct from the taste 1 receptors in the glutamate family given that they possess short amino-termini that are unlikely to participate in ligand recognition. The secretin family of GPCRs possess amino-termini ~ 150-180 amino acids in length stabilised by six conserved cysteine residues. The large peptide ligands of the secretin family of GPCRs demonstrate high amino acid sequence identity (Wheatley *et al.*, 2012).

While the ligand-amino-terminal interactions have been elucidated for a number of secretin family GPCRs (Parthier *et al.*, 2009), atomic detail of transmembrane regions is, at present, limited to a subset of rhodopsin family receptors.

1.4 Structure of rhodopsin-like GPCRs

In order to compare the relative position of residues between different rhodopsin-like GPCRs, the Ballesteros-Weinstein numbering system is utilised (Ballesteros and Weinstein, 1995). Each TM helix is referenced regarding helix number, and from sequence alignment, the most conserved residue of each helix is denoted the value 50 (Figure 1.1). The number progressively decreases from 50 for amino acids upstream of the reference residue and

increases towards to carboxyl-terminus. For example, the residue three residues preceding the most conserved residue in TM VI is denoted by the reference 6.47.

1.4.1 Rhodopsin at 2.8 Å

The first crystal structure of a GPCR was that of bovine rhodopsin (bRho) by Palczewski *et al*. in 2000 (Figure 1.2). Rhodopsins are activated by light and produce vision by signalling through the visual G-protein, transducin. Rhodopsin is composed of the protein opsin and a vitamin A derivative – 11-*cis*-retinal – covalently linked through Lys^{296} of opsin. Absorption of a photon of light by 11-*cis*-retinal isomerises the chromophore to all-*trans*-retinal, activating opsin.

From the crystal structure of bRho at 2.8 Å, the precise location of the retinal binding pocket was elucidated. The presence of an eighth cytoplasmic helix (H8) following TM VII and extracellular N-linked glycosylation sites were also identified. The bRho structure has since been refined by obtaining crystals at a higher resolutions (Okada and Palczewski, 2001; Riek *et al.*, 2001; Teller *et al.*, 2001; Krebs *et al.*, 2003; Shimamura *et al.*, 2008).

bRho has an intermediate molecular weight with respect to family A GPCRs and was thought to be representative of the family. However, bRho possesses a covalently bound ligand – an uncommon feature amongst GPCRs. The first crystal structure of a GPCR with a diffusible ligand came in 2007 with the human β_2-adrenoceptor, β_2AR (Rosenbaum *et al.*, 2007).

1.4.2 Crystal structures of diffusible-ligand GPCRs

Increasing amounts of structural data are now available due to various strategies developed to facilitate crystallisation. The major inherent difficulties in obtaining crystals of GPCRs are: i) that as membrane proteins, they must be solubilised by detergent prior to purification and the lateral pressure which maintains their tertiary structure is removed when taken from their

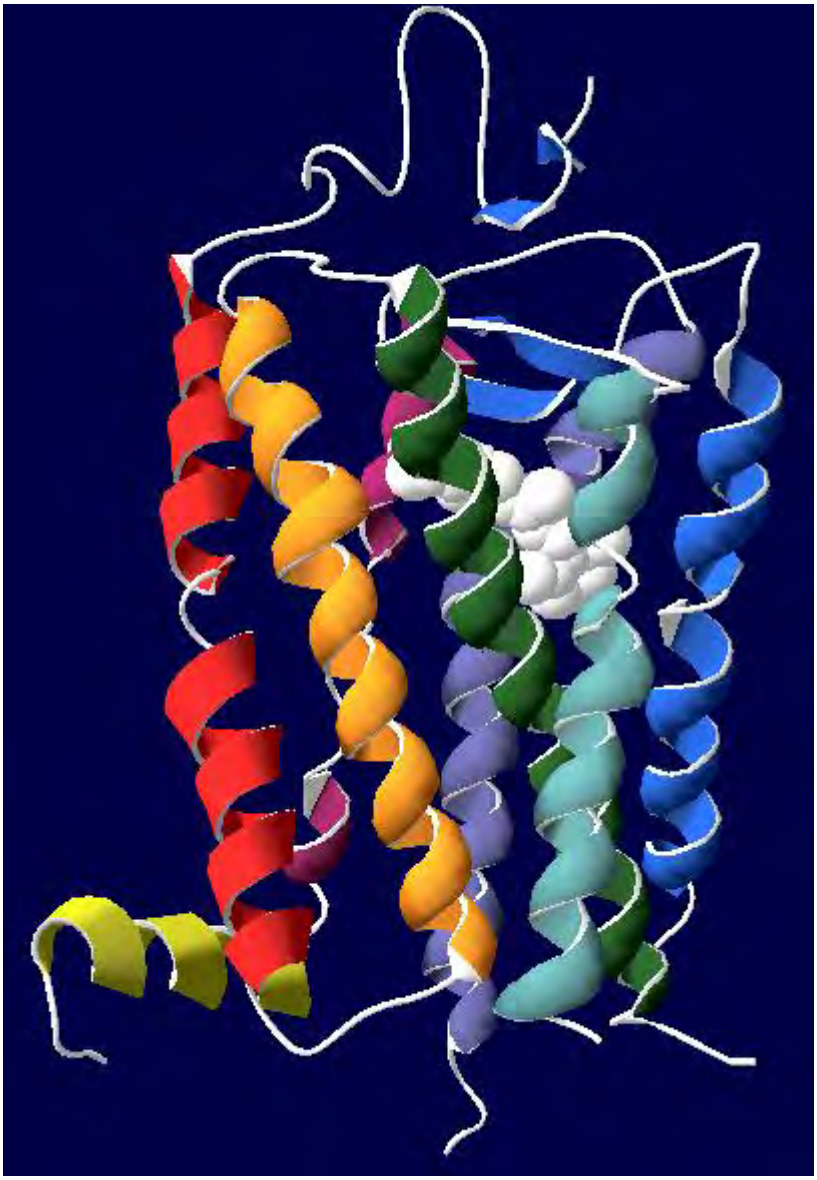

Figure 1.2 Bovine rhodopsin: The first crystal structure of a GPCR

The 11-*cis*-retinal ligand is shown in white space-filled. Helices are coloured according to colour; TM I , red; TM II, orange; TM III green; TM IV, teal; TM V, blue; TM VI, lilac; TM VII, purple and H8, yellow. Glycosylation sites are not shown. pdb: 1F88.

membrane environment, ii) the receptors are unstable in the detergent used in their solubilisation and purification and iii) the conformational dynamism of GPCRs decreases the likelihood that the GPCR will exist as single receptor conformation required for crystallisation. Protein engineering has enhanced success in obtaining crystals suitable to obtain molecular structural detail.

Removal of carbohydrate chains by deglycosylation or mutagenesis of glycosylation sites increases homogeneity of GPCR crystals. The first two β_2AR receptor structures were obtained by crystallisation with inverse agonists, truncating the carboxyl-terminus and stabilising the most flexible of the loop regions, ICL 3. Two methods were used to decrease flexibility of ICL 3; binding an antibody raised against ICL 3 (Rasmussen *et al.*, 2007) or by substituting the ICL 3 region with the relatively inflexible T4-lysozyme, T4L (Cherezov *et al.*, 2007). A completely different strategy was employed for crystallising the avian β_1 adrenoceptor (β_1AR), utilising thermostabilising point mutations to aid in crystallisation (Warne *et al.*, 2008). Ligand-free opsin was crystallised (Park *et al.*, 2008) and showed marked differences to the previously published bRho structure (Palczewski *et al.*, 2000) and gave the first insights into a *pseudoactive* receptor structure. The first G-protein-interacting structure came from crystallising opsin in the presence of the carboxyl terminus of transducin, Gt-CT (Scheerer *et al.*, 2008).

The publication of structures of the human A_{2A} adenosine receptor, A_{2A}R (Jaakola *et al.*, 2008); CXCR4 chemokine receptor (Wu *et al.*, 2010); human dopamine D3 receptor, D3R (Chien *et al.*, 2010) and human histamine H1 receptor, H_1R (Shimamura *et al.*, 2011) have added further structural information to the field. Still these structures provided further insight to the inactive receptor conformation. The structures of agonist-bound receptor conformations have recently become available from the human β_2AR (Rasmussen *et al.*, 2011a; Rasmussen

et al., 2011b; Rosenbaum *et al.*, 2011), avian β_1AR (Warne *et al.*, 2011), metarhodopsin II (Choe *et al.*, 2011) and A_{2A}R (Lebon *et al.*, 2011; Xu *et al.*, 2011). The publication of the first active receptor in a GPCR-G-protein complex (Rasmussen *et al.*, 2011b) represents a milestone structure. Here, T4L is engineered at the amino terminus of the β_2AR and the interface of Gα and Gβγ are stabilised by a camelid nanobody (Figure 1.3).

More recently, the diversity of GPCR structures solved has increased with crystal structures of the human sphingosine 1-phosphate receptor (Hanson *et al.*, 2012); human M2 and rat M3 muscarinic acetylcholine receptors, mAChR (Haga *et al.*, 2012; Kruse *et al.*, 2012). The human κ-opioid receptor, κ-OR (Nagase *et al.*, 2012; Wu *et al.*, 2012); mouse μ-opioid receptor, μ-OR (Manglik *et al.*, 2012), δ-opioid receptor, δ-OR (Granier *et al.*, 2012) and most recently the related nociceptin/orphanin FQ peptide receptor (Thompson *et al.*, 2012) crystal structures have been resolved is inactive conformations.

1.5 Receptor activation

The basis of all GPCR activation models is that the receptor exists in an equilibrium between inactive (R) and active (R*) states (discussed further in 1.7). Agonists have a higher affinity for R* whereby binding stabilises an active state and moves the equilibrium towards R*. The binding event stabilises particular intramolecular rearrangements that initiate intracellular signalling.

Given the important functional roles of particular amino acid motifs conserved in rhodopsin-like GPCRs, it is suggested that mechanisms are shared throughout the family.

Figure 1.3 The crystal structure of the β_2AR-G_s complex

The agonist BI-167107 is shown in space-filled. Helices are coloured according to colour; TM I , red; TM II, orange; TM III green; TM IV, teal; TM V, blue; TM VI, lilac; TM VII, purple and H8, yellow. T4L (brown) is engineered at the amino-terminus of the β_2AR. Heterotrimeric G-protein is shown in white. Nb35 nanobody is shown in pink. pdb: 3SN6

1.5.1 Ligand binding

The binding modes of different families of GPCRs largely correlate to orthosteric (natural) ligand size and architectures of the receptors' amino-termini. As such, the diversity of GPCR ligands of the rhodopsin-like GPCRs requires diverse modes of binding. Orthosteric ligands vary in both chemical composition and size; from small monoamine ligands and nucleotides to peptides, lipids and large glycoproteins. The general location of the orthosteric binding sites of subfamilies of the rhodopsin-like and mGluR-like families of GPCRs are summarised in Figure 1.4. Before the advent of crystallographic GPCR data, site-directed mutagenesis and radioligand binding assays were invaluable in identifying specific residues involved in ligand binding. Key residues may be conserved within families, such as $Asp^{3.32}$ of monoamine ligand receptors, (Gantz *et al.*, 1992; Ho *et al.*, 1992; Mansour *et al.*, 1992; Spalding *et al.*, 1994) which form a counter-ion to the amine group conserved within their cognate ligands. Furthermore, the ligand binding domains of 11-*cis*-retinal and all-*trans*-retinal in opsins occupy a similar position in the GPCR as the monoamine ligands (Palczewski *et al.*, 2000). Nethertheless, crystal structures have revealed that there is a diversity of TM contacts made by ligands which induce common helical rearrangements that confer an active receptor conformation (Unal and Karnik, 2012).

Crystallographic data provides high resolution detail of ligand binding sites that site-directed mutagenesis could previously only infer. An emerging picture is that activation is accompanied by contraction of the ligand binding pocket although how this is achieved seems to vary between receptors. β_1AR crystal structures identified a contraction of the ligand binding pocket of 1 Å of full agonists isoprenaline and carmoterol; and partial agonists dobutamin and salbutamol (Warne *et al.*, 2011). However it was apparent that a specific contact with $Ser^{5.46}$ is required to confer full-agonism. Similarly a contraction by 1.2 Å of the

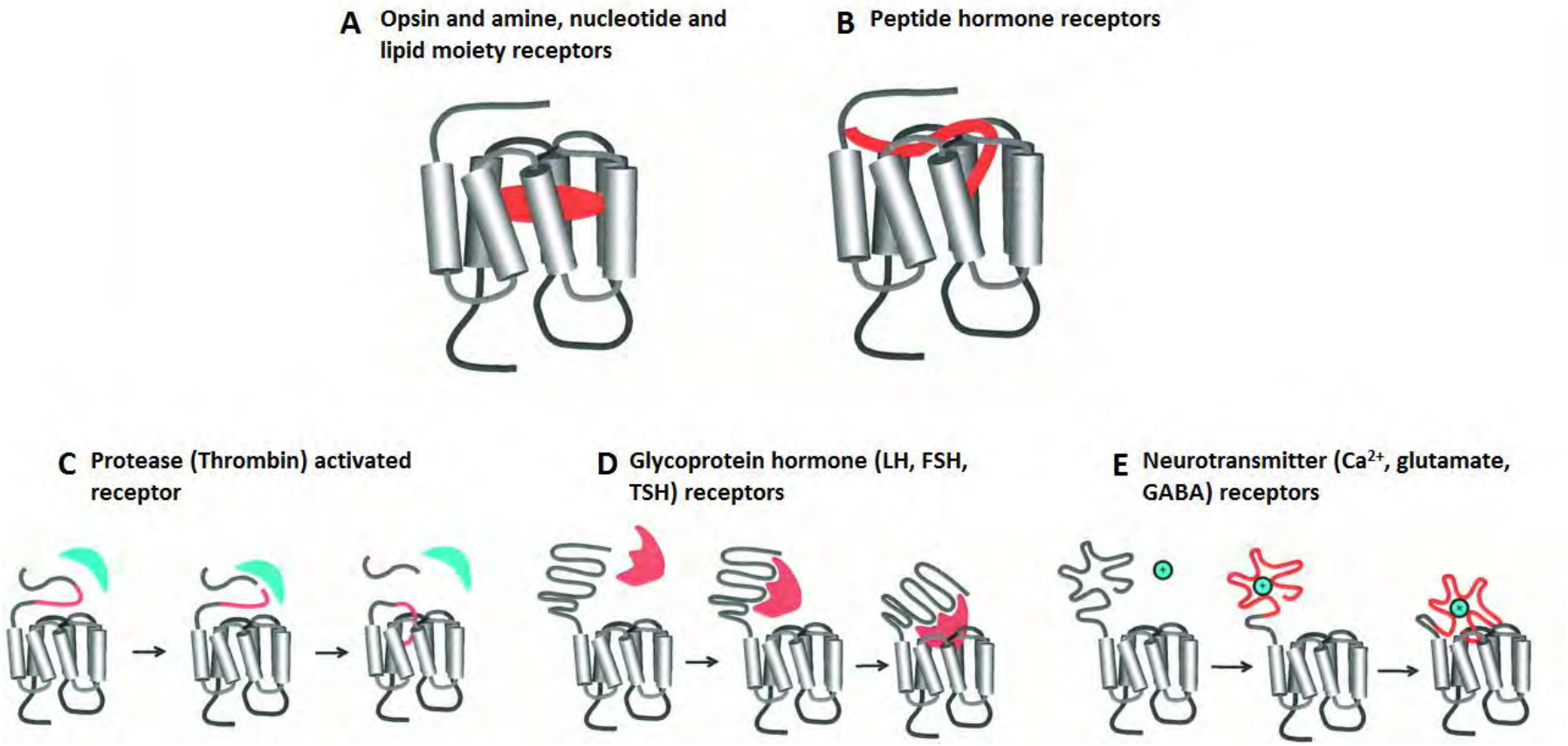

Figure 1.4 Representation of ligand binding domains of GPCRs

A, The opsins and amine, nucleotide and lipid moiety receptors bind orthosteric ligands at TM regions. B, peptide hormone ligands may bind orthosteric ligands at the amino-terminus, ECLs and TM regions. C, proteases cleave the amino-terminus of protease activated receptors which exposes the tethered ligand which subsequently interacts with receptor. D, the large glycoprotein hormones bind and the extended amino-terminus of their respective GPCRs. E, neurotransmitter receptors bind to the large amino-termini of their receptors. Modified from (Ji *et al.*, 1998).

ligand binding site in the β_2AR was observed (Rasmussen *et al.*, 2011a; Rasmussen *et al.*, 2011b; Rosenbaum *et al.*, 2011). The agonist ligands NECA and adenosine at the A_{2A}R likewise induce a 0.7 Å and 0.8 Å contraction of the ligand binding site respectively, but in contrast to β_1AR, key contacts are made with $Ser^{7.42}$ and $His^{7.43}$ rather than TM V (Lebon *et al.*, 2011). Together these data indicate the contraction of the ligand binding site (measured from the Cα of analogous residues 5.42 and 7.39) is induced upon ligand binding, but the precise ligand-receptor contacts are divergent.

1.5.2 Intracellular conformational changes associated with activation

With the advent of GPCR structures stabilised in an active receptor conformation, the direct comparison to inactive structures is now possible. This allows clear observation of structural changes involved in receptor activation which are summarised below. The hallmark structural feature of an activated receptor has been accepted as the outward movement of TM VI relative to TM III to expose the Gα binding site. This has been demonstrated by disulphide cross-linking and site-directed spin labelling experiments in rhodopsin (Farrens *et al.*, 1996) and by fluorescence spectroscopy in the β_2AR (Gether *et al.*, 1997; Yao *et al.*, 2006).

1.5.2.1 Rhodopsin

Crystallographic data of rhodopsin in it ground state demonstrate the close proximity of TM III and TM VI at the intracellular face (Palczewski *et al.*, 2000). Crystallisation of ligand free opsin (Park *et al.*, 2008), opsin with Gt-CT fragment (Scheerer *et al.*, 2008) and most recently crystallographic data of two Meta II conformations (Choe *et al.*, 2011; Deupi *et al.*, 2012) indicate a 6 Å outward movement of TM VI relative to TM III.

1.5.2.2 A_{2A}R

The agonist stabilised A_{2A}R crystal structures represent what are thought to be activation-intermediate structures (Lebon and Tate, 2011; Lebon *et al.*, 2011; Xu *et al.*, 2011) compared

to the ZM241385, inverse agonist-bound structure (Dore *et al.*, 2011). Subtle helical rearrangements included a shift of TM III towards the extracellular surface, 3 Å outward movement of the cytoplasmic portion of TM V and a 40 ° rotation and outward movement of TM VI are similar to those observed in β_2AR structures discussed in section 1.5.2.3. The outward movement of the cytoplasmic portion of TM VI in this structure would not be sufficient to accommodate the C-terminal portion of Gα as observed in opsin and Meta II.

1.5.2.3 β_2AR

Rasmussen *et al*., 2011a crystallised the β_2AR representing the first diffusible-ligand GPCR in an active conformation. A camelid antibody fragment (Nb80) was co-crystallised as a G-protein mimetic in the agonist (BI-167107)-bound β_2AR structure. Nb80 increased the affinity of agonist binding to a similar level as observed in the presence of G-protein. The outward movement of TM VI in the BI-167107-β_2AR-Nb80 complex was 11 Å accompanying a 1.3 Å contraction of the binding pocket.

The BI-167107 agonist and a similar camelid nanobody approach were used in co-crystallising the elusive G-protein-β_2AR complex (Rasmussen *et al.*, 2011b). The Nb35 bound at the interface of Gα and Gβ subunits of the G_s heterotrimer. Although the location of the Gα C-terminus of the intact G-protein is similar to in the opsin crystal structure (Scheerer *et al.*, 2008), the outward movement of TM VI relative to TM III is 14 Å (Figure.1.5). The two active β_2AR structures described here are virtually identical apart from the additional 3 Å movement described in the latter.

It is expected that the outward movement of TM VI relative to TM III allows the binding of G-protein associated with the canonical view of GPCR signalling. What is still not understood is how an active receptor conformation is adopted to elicit G-protein-independent signalling cascades. The publication by (Nakajima and Wess, 2012) concerned designer receptors

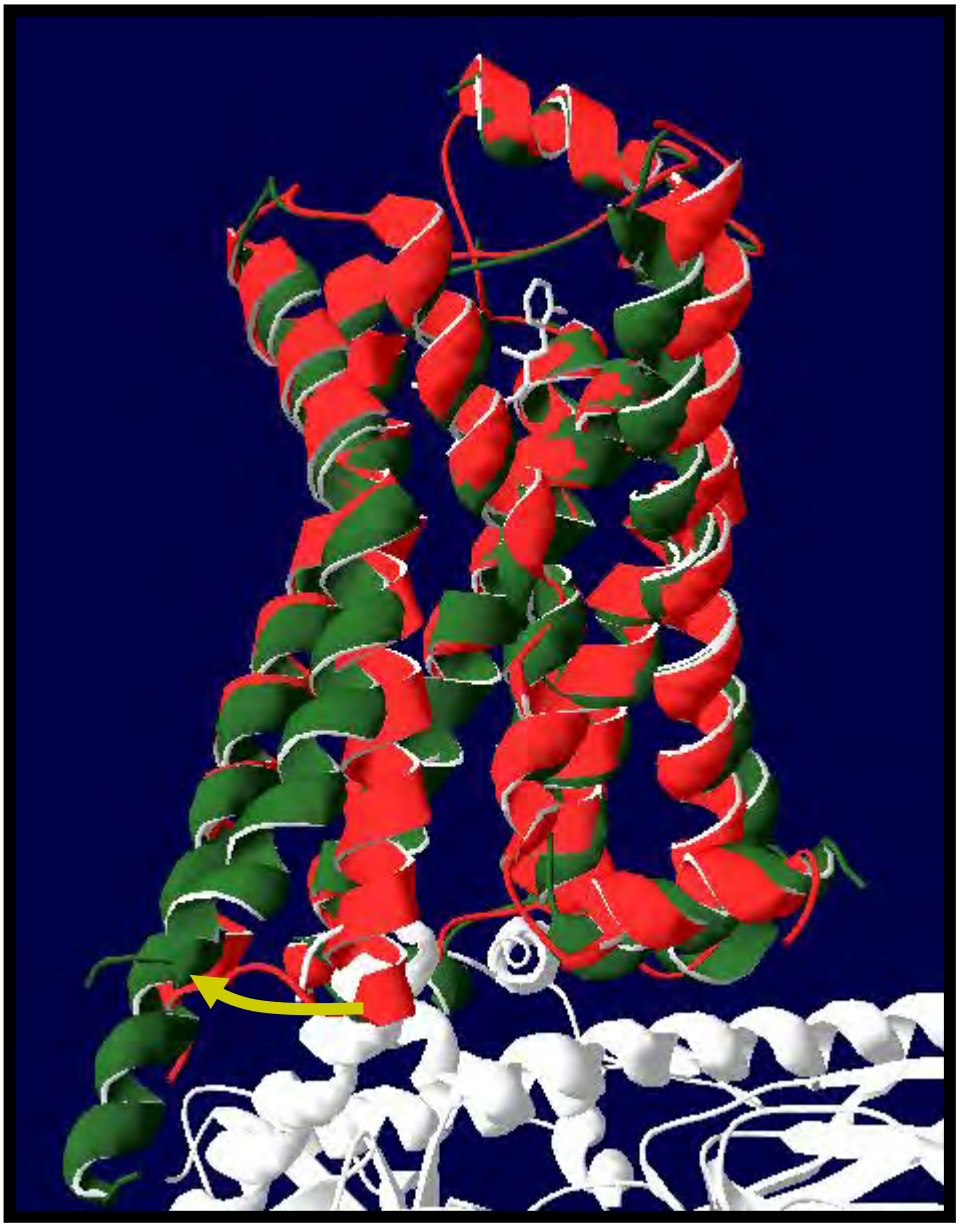

Figure 1.5 An overlay of crystal structures of the β_2AR in an inactive and an active state

The structure of β_2AR in an inactive receptor conformation is shown in red (pdb: 2RH1) and a G-protein interacting conformation is shown in green (pdb: 3SN6). G_s is shown in white (pdb: 3SN6). The outward movement of TM VI away from TM III associated with receptor activation is indicated by the yellow arrow.

exclusively activated by designer drugs (DREADDs). These receptors that selectively signalling through G-protein-independent pathways will perhaps provide inside into the appropriate conformational changes required.

1.5.3 Conserved motifs of rhodopsin-like GPCRs

There are numerous conserved residues that define the rhodopsin-like GPCR family. It is accepted that the conserved motifs possess conserved roles and hence universal modes of activation. Key, conserved amino acids motifs are discussed here with respect to their role in GPCR activation.

1.5.3.1 D/ERY

In the rhodopsin GPCR family, residues Asp/Glu$^{3.49}$-Arg$^{3.50}$-Tyr$^{3.51}$ are located at the membrane boundary of TM III. Arg$^{3.50}$ is the most conserved residue in TM III being present in 96% of rhodopsin-like GPCRs. An acidic residue precedes Arg$^{3.50}$ in 86 % of receptors while Tyr$^{3.51}$ is conserved in 67 % of the family (Mirzadegan *et al.*, 2003). In the bRho crystal structure, Glu$^{3.49}$ side chain forms an ionic interaction with neighbouring Arg$^{3.50}$, maintaining an inactive receptor conformation (Palczewski *et al.*, 2000). Breakage of the interaction by protonation of the acidic side chain (Cohen *et al.*, 1992) or mutagenic charge neutralisation results increased activation in the absence of agonist in the α_{1b}AR and β_2AR (Scheer *et al.*, 1996; Scheer and Cotecchia, 1997; Rasmussen *et al.*, 1999). Additionally, the bRho crystal structure possesses an 'ionic lock' between Glu$^{3.49}$/Arg$^{3.50}$ with Glu$^{6.30}$/Thr$^{6.34}$ at the cytoplasmic face of TM VI (Palczewski *et al.*, 2000) in an inactive conformation. Although Glu$^{3.60}$ is only conserved in the monoamine-ligand GPCRs, the proximity of TM III and TM VI is thought to be important in conferring a G-protein-interacting conformation in general. However, the majority of GPCR crystal structures do not demonstrate an 'ionic lock' with the

exceptions of the D3R (Chien *et al.*, 2010) and one $A_{2A}R$ structure (Dore *et al.*, 2011) although how much this is due to the T4L-fusion replacing ICL 3 is debatable.

1.5.3.2 CWXP

The $Cys^{6.47}$-$Trp^{6.48}$-$Xxx^{6.49}$-$Pro^{6.50}$ motif is located below the ligand-binding domain of rhodopsin-like GPCRs. The 'rotamer toggle switch' involves the side chain indole of $Trp^{6.48}$ switching between two preferred rotamers to modulate the kink in TM VI about $Pro^{6.50}$. The bond angle of the proline kink is decreased when $Trp^{6.48}$ breaks interactions with TM VII normally stablising the R state. A straightening of TM VI and produces a movement of TM VI away from TM III at the cytoplasmic face (Shi *et al.*, 2002; Ruprecht *et al.*, 2004; Schwartz *et al.*, 2006). However, crystallographic data of active receptor conformations thus far does not support this as a mechanism of the conformational changes undergone during GPCR activation.

1.5.3.3 NPXXY

$Asn^{7.49}$, $Pro^{7.50}$ and $Tyr^{7.53}$ comprise the conserved NPxxY motif. $Asn^{7.49}$ is proposed to act as an on/off switch, stabilising an active conformation through a hydrogen bond network with the two most conserved residues in TM I and TM II, $Asn^{1.50}$ and $Asp^{2.50}$ (Govaerts *et al.*, 2001; Urizar *et al.*, 2005). The side chain of $Tyr^{7.53}$ participates in the 'tyrosine toggle switch' with $Tyr^{5.58}$ which translocate into the helical bundle upon activation. This side chain movement extends a hydrogen bond network towards the D/ERY motif and the C-terminus of the G-protein (Standfuss *et al.*, 2011).

1.6 Intracellular signalling

1.6.1 G-protein dependent signalling

GPCRs are named as such by their ability to activate G-proteins and hence initiate intracellular signalling cascades. G-proteins are activated by exchanging a bound GDP (guanosine diphosphate) for GTP (guanosine triphosphate) – a process catalyses by active GPCRs.

1.6.1.1 G-protein activation

The GDP molecule is bound to the Gα GTPase domain which maintains the association of the Gαβγ heterotrimer and hence inactivation of the G-protein (Figure 1.6). An active GPCR promotes the exchange of the GDP molecule for a GTP molecule which causes the heterotrimer to dissociate into Gα-GTP and the functional Gβγ dimer. The two G-protein units activate effector molecules that generate second messengers until such time that the GTPase activity of the α-subunit hydrolyses GTP. Hydrolysis of GTP to GDP results in reassociation of the Gαβγ heterotrimer, inactivating the G-protein and terminating G-protein-dependent signalling.

The β_2AR structure in complex with G_s has now revealed conformational changes that mediated exchange of GDP in the heterotrimer for GTP (Rasmussen *et al.*, 2011b). Hydrogen-deuterium exchange experiments also demonstrate how the active GPCR destabilises the 'P-loop' of G_s that stabilises the GDP molecule, promoting nucleotide exchange (Chung *et al.*, 2011).

1.6.1.2 Activation of adenylyl cyclase

The $G\alpha_s$ and $G\alpha_{i/o}$ subtypes of G-proteins modulate the activity of the intracellular effector adenylyl cyclase, AC (Figure 1.7). AC is a membrane localised enzyme that generates the

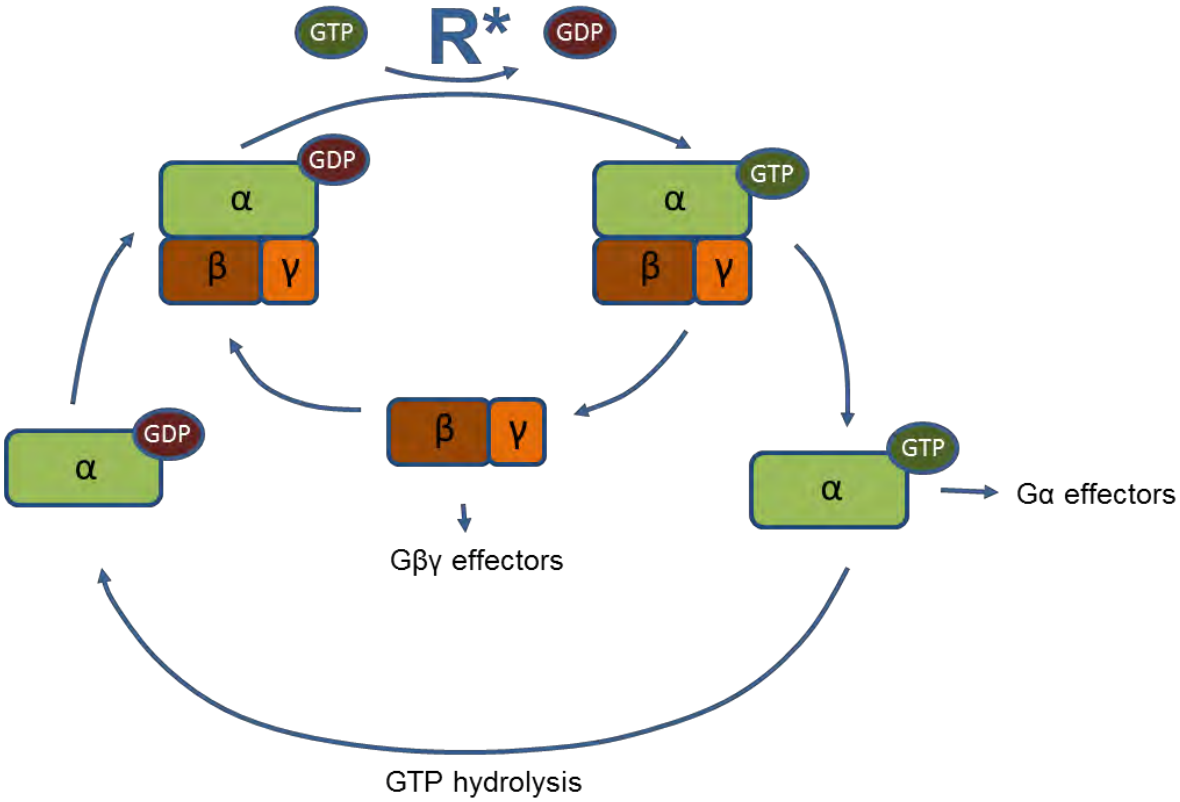

Figure 1.6 G-protein activation by G-protein-coupled receptors

Activated GPCR (R*) catalyses the exchange of GDP for GTP, causing G-protein (Gαβγ) dissociation into Gα-GTP and Gβγ. Both G-protein units may activate downstream effectors until such time that the GTP is hydrolysed. Gα-GDP reassociates with the Gβγ dimer, rendering the heterotrimeric G-protein inactive.

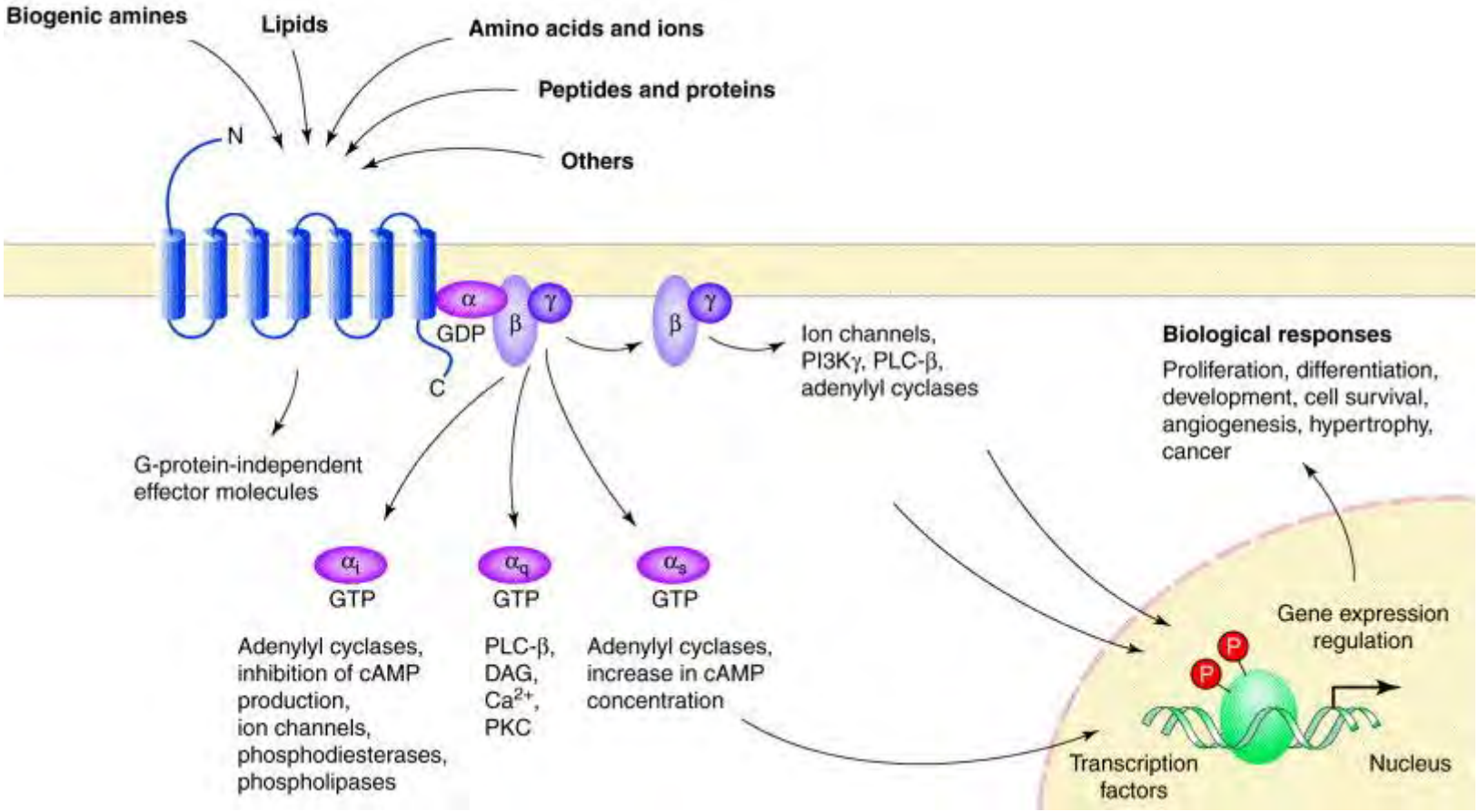

Figure 1.7 Signalling through GPCRs

Binding of diverse extracellular ligands causes the activation of G-proteins at the intracellular face of GPCRs. The subunits of G-protein activate specific effector molecules resulting in activation and inhibition of the production of second messengers (Marinissen and Gutkind, 2001).

second messenger cyclic adenosine 3,5-monophosphate (cAMP) from ATP (adenosine triphosphate). cAMP in turn regulates the activity of protein kinase A (PKA). $G\alpha_s$ increases intracellular levels of cAMP whereas $G\alpha_i$ α-subunits cause inhibition of AC.

1.6.1.3 Activation of phospholipase C-β

Phospholipase C (PLC)-β is activated by the $G\alpha_{q/11}$ subtype of Gα (Figure 1.7). Particular PLC-β isoforms may also be activated by the obligate Gβγ dimer (Morris and Scarlata, 1997). PLC catalyses the hydrolysis of phosphatidylinositol 4,5-bisphosphate (PIP_2), liberating the second messengers inositol 1,4,5-trisphosphate ($InsP_3$) and diacylglycerol (DAG). $InsP_3$ stimulates calcium release from the intracellular stores and DAG activates protein kinase C (PKC).

1.6.2 G-protein-independent signalling

β-arrestins are well documented to be involved in the internalisation of a plethora of membrane proteins. However, β-arrestins also partake in the propagation of intracellular signalling in GPCRs. They were first implicated as mediators of receptor signalling in the β_2AR whereby mitogen-activated protein kinase (MAPK) signalling was inhibited by dominant negative β-arrestin mutants (Daaka *et al.*, 1998; Luttrell *et al.*, 1999). The function of β-arrestin as a scaffold in G-protein-independent signalling has been reported in the angiotensin II receptor type I (AT1R) (Tohgo *et al.*, 2002) and CXCR4 (Sun *et al.*, 2002).

The β_2AR has been shown to activate MAPK through G_s at low agonist concentrations and activate Src at higher concentrations of the same agonist (Sun *et al.*, 2007). Interestingly, this later mechanism is β-arrestin-independent, further highlighting the complexity of GPCR signal transduction.

1.6.3 Constitutive activity

Receptors exist in equilibrium between inactive and active states whereby the binding of an agonist moves the equilibrium towards the active conformation. However, GPCRs may adopt an active receptor conformation in the absence agonist. Constitutively active mutants (CAMs) may be generated by disrupting interactions associated with maintaining an inactive receptor state (Kjelsberg *et al.*, 1992; Robinson *et al.*, 1992; Han *et al.*, 1998). Some such CAMs are associated with pathologies in humans such as retinitis pigmentosa (Stojanovic *et al.*, 2003) and obesity (Proneth *et al.*, 2006). Constitutive activity may be an endogenous feature of a receptor as in the ghrelin receptor (ghrelin-R). In this case, mutations reducing its agonist-independent signalling are associated with pathology (DelParigi *et al.*, 2002; Holst and Schwartz, 2006). The constitutive activity of the ghrelin-R has been shown to be inherent in the receptor itself and not due to interaction with intracellular components (Damian *et al.*, 2012).

1.7 Activation models

Models of activation of GPCRs have developed over the years which accommodate new insights from experimental data.

1.7.1 Ternary complex model

The ternary complex model (TCM) described that a receptor may exist in two affinity forms (De Lean *et al.*, 1980). A cellular component X is required to form a high affinity ternary complex with hormone (H)-bound receptor (HR). The ternary complex HRX is capable of activating effector molecules, connecting the agonist (H) binding event and the initiation of intracellular signalling. Addition of non-hydrolysable guanine nucleotides destabilised the ternary complex, suggesting that component X is an intracellular guanine-nucleotide binding

site or G-protein. The formation of RG accounts for agonist-independent signalling observed experimentally.

1.7.2 Extended ternary complex and cubic ternary complex models

The extended ternary complex elaborates on the TCM to accommodate constitutive activity observed in an engineered β_2AR construct (Samama *et al.*, 1993). Three observations of the mutant β_2AR were made: i) increased agonist-independent signalling, ii) increased agonist affinity and iii) increased intrinsic efficacy of partial agonists. These properties of the mutant β_2AR when compared to Wt can, in part, be accommodated by the increased coupling of receptor to G-protein. However, an increased affinity of agonist for mutant β_2AR was observed even in the absence of G-protein which cannot be accommodated in the TCM. The extended ternary complex model incorporated constant *J* which governs the conversion between two receptor population, R and an active R* (Figure 1.8). Constant β describes the effect of hormone binding on the equilibrium between R and R*. These inclusions accommodate the observations in the constitutively active β_2AR construct such that HR*G is the only ternary complex formed.

The cubic ternary complex elaborates on the extended ternary complex model, permitting distinct receptor conformations binding to a common G-protein (Weiss *et al.*, 1996). To this point, agonist-independent signalling is explained in addition to the action of agonists stabilising an active receptor conformation. Additionally, inverse agonism can be accommodated, whereby an inverse agonist ligand may stabilise an inactive receptor state, decreasing a receptors inherent basal activity. However, only one signalling component, i.e. G-protein, is assumed responsible for all intracellular signalling pathways. A model whereby a receptor can signal through multiple pathways, either through multiple G-proteins and/or

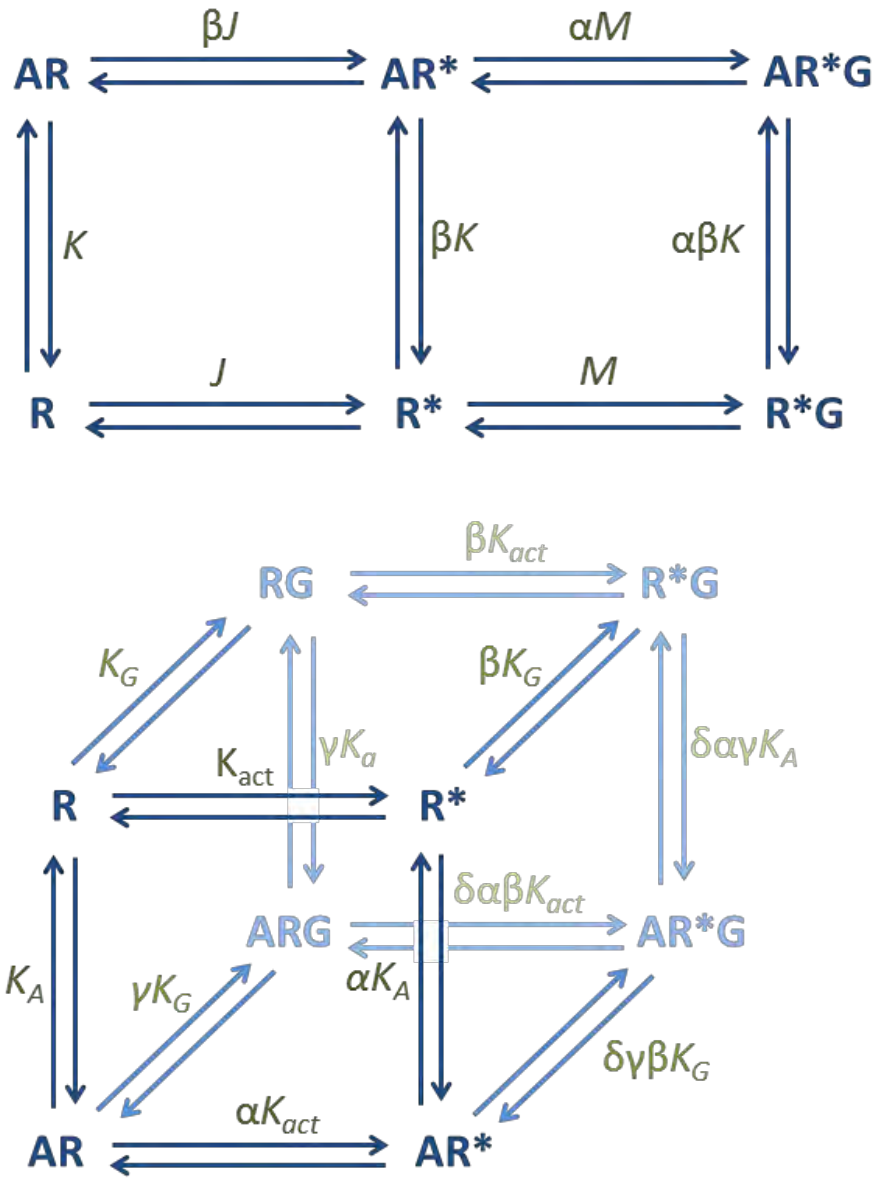

Figure 1.8 The extended ternary complex model and the cubic ternary complex model

Upper panel: The extended ternary complex. Inactive receptor (R) undergos conversion to active receptor (R*) governed by *J*. Agonist (A) interacts with R and R* may interact with A and intracellular G-protein (G). β describes the allosteric effect of A on *J*; *K* describes the affinity of A for R; *M*, the affinity of R* for G. α the ability of A to form the ternary complex AR*G (Samama *et al.*, 1993). Lower panel: The cubic ternary complex model. Both R and R* may interact with G therefore both R*G and AR*G are the active receptor species (Weiss *et al.*, 1996).

other intracellular components such as the β-arrestins must be considered, presumable through multiple active (and inactive) receptor conformations (Gurevich *et al.*, 1997).

1.8 Modulating receptor function

1.8.1 Allostery

Allosteric modulators are ligands that may bind to GPCR regions distinct to the site of orthosteric ligand binding. As such, the binding of an allosteric modulator may modulate the affinity, potency or efficacy of orthosteric ligands for their receptor (Monod *et al.*, 1963; Wess, 2005; Conn *et al.*, 2009).

The monovalent cation, Na^+ is a well-documented allosteric modulator of GPCR function. Na^+ is proposed to neutralise the charged $Asp^{2.50}$, affecting both ligand binding affinity and G-protein activation (Limbird, 1984). The α2 adrenoceptor α_2AR; dopamine D2 receptor. D2R and serotonin receptor, 5-HT_1R (Horstman *et al.*, 1990; Neve *et al.*, 1991; McLoughlin and Strange, 2000) are allosterically modulated by Na^+. An A_{2A}R crystal structure demonstrated how Na^+ ions and structural water molecules contribute to GPCR function (Liu *et al.*, 2012). Additionally this structure shows how cholesterol stabilises the conformation of TM VI.

The ubiquitous steroid-lipid cholesterol has been implicated in the allosteric regulation of a number of GPCRs. Cholesterol shifts the equilibrium to stabilise an inactive receptor conformation in rhodopsin (Straume and Litman, 1988; Mitchell *et al.*, 1990; Bennett and Mitchell, 2008). In contrast cholesterol stabilises an active receptor state in the oxytocin receptor (OTR) (Fahrenholz *et al.*, 1995; Klein *et al.*, 1995).

It is also apparent that GPCRs can be activated via allosteric sites in the absence of agonist in the orthosteric site. So called ago-allosteric modulation was first observed in adenosine A_1 receptor where the allosteric ligand PD81723 activated $G\alpha_{i/o}$ even in the absence of orthosteric ligand (Bruns and Fergus, 1990). This phenomenon has also been described in M_2 mAChR (May *et al.*, 2007) and free fatty acid 2 receptor (Milligan *et al.*, 2009).

1.8.2 Dimerisation

Dimerisation is a well-recognised mechanism by which GPCR signalling may be honed. GPCRs of the rhodopsin family may form dimers through association of transmembrane segments. TM I and TM IV are implicated as interfaces in the formation of homodimers of the α_{1b}AR (Carrillo *et al.*, 2004) and D2R (Guo *et al.*, 2005). Rhodopsin dimers involve TM I and II in native membranes (Liang *et al.*, 2003). The implication of dimer formation is evident in the β_2AR where disruption of dimer formation reduced agonist-induced AC activity (Hebert *et al.*, 1996). Heterodimer formation of somatostatin SST_3:SST_{2A} dimers prevented activation of SST_3 by selective ligand (Pfeiffer *et al.*, 2001). Heterocompexes of the 5-HT_{2A}R and $mGlu_2$R enabled 5-HT_{2A} agonists to induce signalling through $G_{i/o}$ normally associated with $mGlu_2$R signalling (Gonzalez-Maeso *et al.*, 2008). The neurotensin receptor 1 (NTS1) reconstituted in lipid bilayers eliminates the requirement of cellular components to form functional dimers (Harding *et al.*, 2009). Dimerisation is often required for transport to the cell surface but is not a prerequisite for G-protein activation given that β_2AR (Whorton *et al.*, 2007) and rhodopsin (Bayburt *et al.*, 2007) are capable of functioning as monomers.

1.8.3 Post-translational modifications

GPCRs possess post-translational modifications, the resultant effects of which are diverse and largely receptor specific.

1.8.3.1 Glycosylation

Many membrane proteins are modified by the addition of carbohydrate moieties as part of their maturation. N-linked glycosylation of asparagine residues (consensus site Asn-Xxx-Ser/Thr) occurs in the endoplasmic reticulum whereas O-linked glycosylation at serine or threonine residues occurs in the Golgi and cytosol. There is no consensus sequence known for O-linked glycosylation. It has been demonstrated that glycosylation of GPCRs plays multiple roles in their function. N-linked glycosylation occurs in rhodopsin where mutations of the glycosylation consensus sequence cause autosomal retinitis pigmentosa (Murray *et al.*, 2009). The human μ-OR is modified by N-linked glycosylation which is essential in maintaining protein stability (Huang *et al.*, 2012). The vasopressin V2 receptor may be modified by O-linked glycosylation at extracellular serine/threonine residues (Sadeghi and Birnbaumer, 1999).

1.8.3.2 Palmitoylation

The addition of a 16-carbon saturated fatty acid, palmitic acid, often occurs at cysteine residues on the intracellular side of GPCRs near the end of H8. Palmitoylation of two adjacent cysteine resides in the cytoplasmic tail was first demonstrated in bRho (Ovchinnikov Yu *et al.*, 1988). Incorporation of the palmitic acid moieties into the plasma membrane results in the formation of a fourth intracellular loop composed of H8 (Palczewski *et al.*, 2000). The effects of palmitoylation on GPCR function are receptor dependent. The lack of palmitoylation causes in reduced receptor number at the cell surface in the histamine H1 (Fukushima *et al.*, 2001), dopamine D1 (Ng *et al.*, 1994) and TSH (Tanaka *et al.*, 1998) receptors. Signalling efficacy of the β_2AR was greatly reduced in non-palmitoylated receptor constructs (O'Dowd *et al.*, 1989) whereas G_s activation was unaffected in serotonin 4A receptor (Ponimaskin *et al.*, 2002). V_{1a}R is

palmitoylated and agonist-stimulation results in turnover of the palmitate which has structural implications (Hawtin *et al.*, 2001).

The presence of carboxyl-terminal cysteine residues is not indicative of receptor palmitoylation. The cysteine residues in the carboxyl-terminus of the μ-OR are not palmitoylated but a cysteine residue in ICL 2 may be (Chen *et al.*, 1998). Palmitoylation of the ICL 2 cysteine is required for effective intracellular signalling but does not affect ligand binding (Zheng *et al.*, 2012).

1.8.3.3 Ubiquitination

Ubiquitin is a 76 amino acid protein which when covalently linked to intracellular lysine residues, marks proteins for lysosomal degradation (Ciechanover, 2010). This post-translational modification has been characterised in the β_2AR where all intracellular lysine residues were mutated, rendering the receptor incapable of ubiquitination and subsequent degradation upon agonist stimulation (Shenoy *et al.*, 2007). Substitution of lysyl side chains in the CXCR4 (Marchese and Benovic, 2001) and V_2R (Martin *et al.*, 2003) also prevented the lysosomal degradation owing to ubiquitination being prevented.

1.9 Terminating receptor signalling

To effectively regulate receptor signalling, it is essential that receptor activation can be terminated. This may be achieved by a number of mechanisms and utilises a plethora of intracellular proteins (Figure 1.9).

1.9.1 Receptor desensitisation

GPCR-G-protein interactions – and hence intracellular signalling – may be disrupted by a family of GPCR kinases (GRKs). Kinases in this family are comprised of three domains; a regulator of

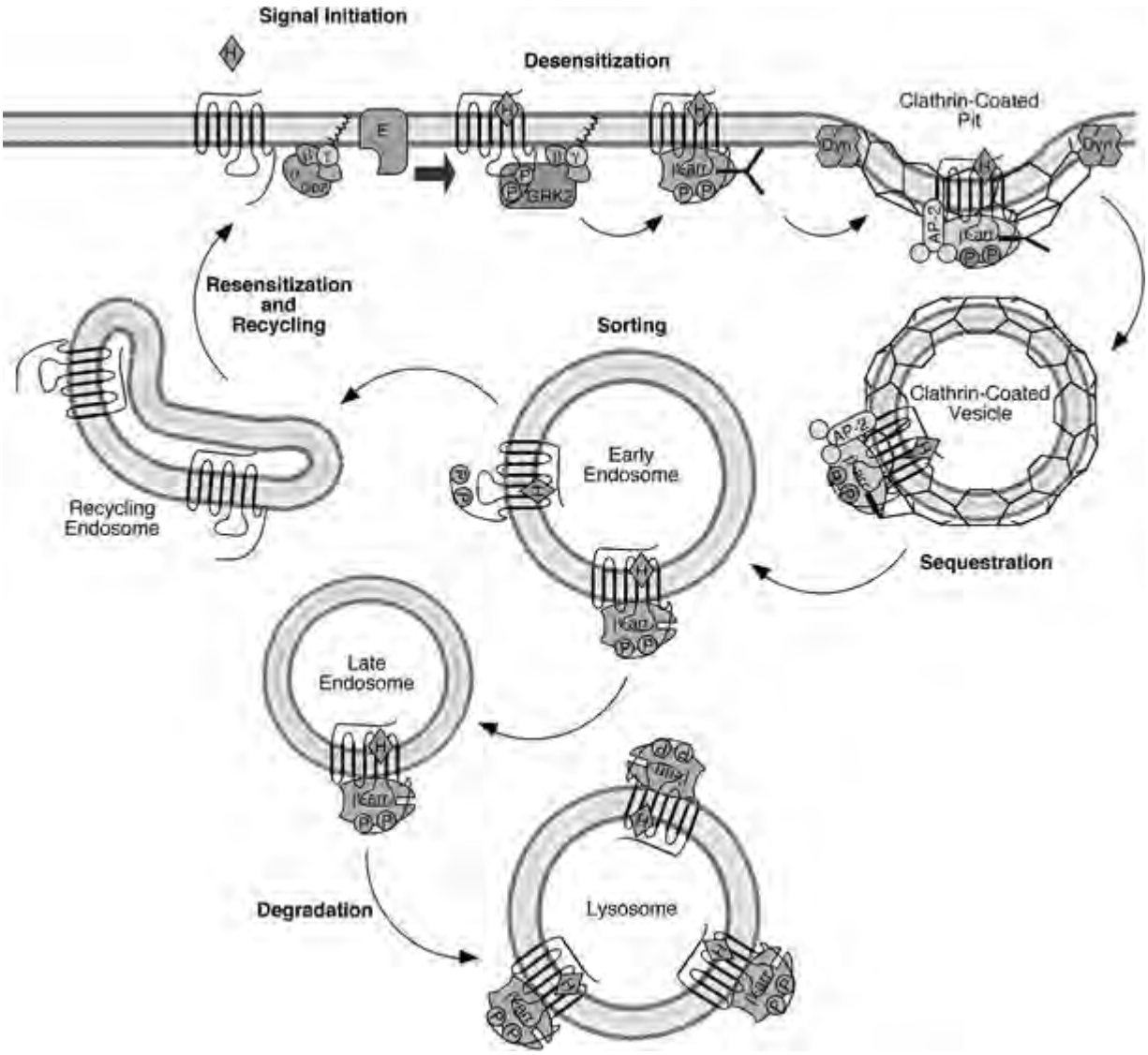

Figure 1.9 Desensitisation, sequestration and receptor fate

Receptors are activated by ligand binding (H), inducing phosphorylation at intracellular portions by GRKs which promotes β-arrestin (β-arr) recruitment. AP-2 (β2-adaptin) associates with receptor-β-arrestin complexes and clathrin, causing formation of clathrin-coated pits. Dynamin (Dyn) causes scission of clathrin-coated vesicle. Receptors are either recycled to the plasma membrane or targetted to late endosomes, resulting in lysosomal degradation. Adapted from Luttrell *et al.*, 2008.

G-protein signalling (RGS) homology domain at the amino-terminus, a catalytic domain and a membrane targeting domain at the carboxyl-terminus (Magalhaes *et al.*, 2012). The GRK family comprises seven members in mammals (GRK 1-7). GRK 1 and GRK 7 are expressed exclusively in the visual system and of the remaining members, all but GRK 4 are expressed ubiquitously (Pitcher *et al.*, 1998; Ferguson, 2001). Association of GRK 2 and GRK 3 with $G\alpha_{q/11}$-coupled GPCRs is in itself enough to uncouple the active receptor from the G-protein in a phosphorylation-independent manner (Ferguson, 2007). Phosphorylation-dependent desensitisation involves phosphorylation of active-receptors by GRKs at serine and threonine residues in the ICL 3 and the carboxy-terminus. Although, this is often not enough to uncouple GPCR and G-protein but does initiate the recruitment of arrestins, of which there are four isoforms in mammals (Ferguson, 2001). Arrestin1 and arrestin4 are expressed in the visual system and the two non-visual arrestins, β-arrestin1 (arrestin2) and β-arrestin2 (arrestin3) are ubiquitously expressed. Association of arrestins to phosphorylated GPCRs uncouples receptor from G-protein, preventing the generation of second messengers.

1.9.2 Sequestration

Further to the desensitisation of active GPCRs, the binding of β-arrestins may initiate the internalisation of receptors from the cell-surface. This reduction of receptor number at the cell-membrane is known as sequestration. Clathrin-mediated endocytosis is induced by β-arrestin1 and β-arrestin2 binding to the clathrin heavy chain of clathrin and β2-adaptin, AP-2 (Ferguson *et al.*, 1996; Goodman *et al.*, 1996). Assembly of the heterotetrameric adaptor complex promotes the invagination of the cell membrane and hence the internalisation of active receptor. Consequently, internalised receptors may undergo two fates; trafficking down the endocytic

pathway if β-arrestins bind with high affinity, or recycling back to the cell membrane if β-arrestin binds with a relatively lower affinity (Oakley *et al.*, 2000).

1.9.3 Regulating G-protein activity

Enhancing the hydrolysis of GTP in the catalytic domain of $G\alpha_q$ and $G\alpha_{i/o}$ proteins is an additional mechanism by which intracellular signalling is halted. Regulators of G-protein signalling (RGS) act as GTPase activating proteins (GAPs), thus promoting the reassociation of the G-protein heterodimer (Nunn *et al.*, 2006). An RGS box of approximately 120 amino acids is conserved among all RGS protein which elicits their GAP activity with flanking regions determining their specificity. Targeting this vast family of GPCR-signalling-regulators is rapidly becoming an area of therapeutic interest (Sjogren and Neubig, 2010).

1.10 Human neurohypophysial hormones

In 1953, the neurophyophysial hormones [arginine^8]vasopressin (AVP) and oxytocin (OT) were the first neuropeptides to be chemically synthesised (Duvigneaud, 1955). AVP and OT are co-translated with specific neurophysin (NP-I for AVP and NP-II for OT) in the supraoptic nuclei (SON) and paraventricular nuclei (PVN) of the hypothalamus. The prohormones are cleaved, in neurosecretory granules and AVP and OT are released into the blood stream with their respective neurophysin as a hormone-binding protein complex (Hadley, 1996)

1.10.1 The structure of AVP and OT

Neurohypophysial hormones are nonapeptide hormones that possess a six amino acid ring structure generated by a characteristic disulphide bond between Cys^1 and Cys^6 (Figure 1.10). The tripeptide carboxyl-terminal tail is amidated (Hadley 1996). A phenylalanine residue is present at

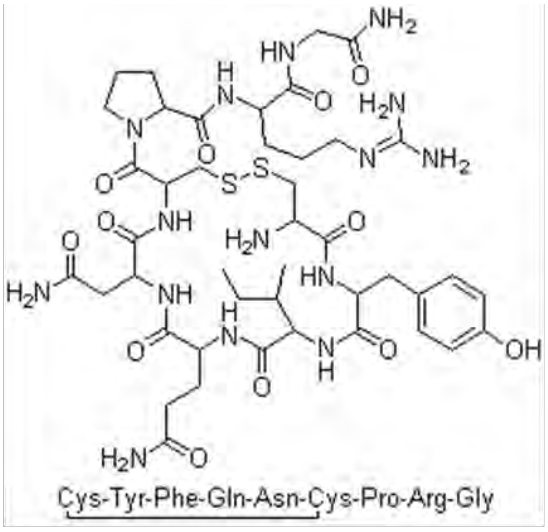

[arginine^{8}]vasopressin

oxytocin

Figure 1.10 Structures of AVP and OT

The molecular structure and amino acid sequences of AVP and OT are shown in the upper and lower panels respectively.

position 3 in AVP compared to an isoleucine residue on OT. Additionally, AVP possesses an arginine residue at position 8 whereas OT has a neutral amino acid, leucine.

1.10.2 AVP and OT receptors

The human neurohypophysial hormone receptors were characterised initially based upon their pharmacology and second messenger generation (Michell *et al.*, 1979). OT binds with high affinity to the oxytocin receptor (OTR) which stimulates PLC-β. AVP also acts at the OTR as a high affinity partial agonist (Wootten *et al.*, 2011), in addition to binding to three distinct vasopressin receptor subtypes; $V_{1a}R$, $V_{1b}R$ and V_2R. The $V_{1a}R$ and $V_{1b}R$ signal through the inositol-phosphate pathway like the OTR whereas the V_2R generates the second messenger cAMP through stimulation of AC (Birnbaumer, 2000). The tissues in which neurohypophysial hormone receptors are expressed dictate the physiological roles of OTR and AVP.

1.10.3 Physiology of neurohypophysial hormones

There are numerous roles for AVP acting through the three primary vasopressin receptors. The $V_{1a}R$ mediates the majority of the physiological roles of AVP including the contraction of vascular smooth muscle (den Ouden and Meinders, 2005) in blood homeostasis, as highlighted by mouse knockout (KO) studies (Oikawa *et al.*, 2010). This study revealed a role of the $V_{1a}R$ in elevation of arterial blood pressure in response to increased plasma salt concentrations. The homeostatic roles of AVP are further highlighted by a study that demonstrated increased locomotion in dehydrated mice, a response that was attenuated in $V_{1a}R$ KO mice (Tsunematsu *et al.*, 2008). Additionally the roles of AVP in platelet aggregation (Filep and Rosenkranz, 1987) and glycogenolysis in the liver and insulin secretion (Howl *et al.*, 1991) are mediated through the

$V_{1a}R$. The intricacy of neurohypophysial hormone physiology is exemplified by the analgesic effects of OT which are not observed in $V_{1a}R$ KO mice (Schorscher-Petcu *et al.*, 2010).

Adrenocorticotropin (ACTH) release from the anterior pituitary is stimulated through the $V_{1b}R$ (Griebel *et al.*, 2003) implicating AVP in stress and anxiety. KO studies identified that ACTH release is mediated by the $V_{1b}R$ under basal and stress conditions (Tanoue *et al.*, 2004).

The V_2R mediates the antidiuretic effects of AVP by two mechanisms (Deen *et al.*, 1995). The V_2R is expressed in the principal cells of the distal nephron in the kidney. V_2R activation promotes the transcription of the water channel aquaporin 2 and stimulates insertion of aquaporin 2 water channels, promoting water reabsorption (Conner *et al.*, 2012). V_2R KO mice exhibited all of the features of X-linked nephrogenic diabetes insipidus (NDI), lacking antidiuretic responses to AVP in addition to polyuria and polydipsia (Li *et al.*, 2009). It is from this antidiuretic effect that AVP is also known as antidiuretic hormone (ADH).

OT plays a duel role in labour. Uterine contraction and prostaglandin $F_{2\alpha}$ release are induced by OT at the OTR in addition to stimulating lactation post-partum (Jenkins and Nussey, 1991). OT was shown to provide antidepressant effects in male mice in an OTR KO study (Matsushita *et al.*, 2010). Both OT and AVP play roles in anxiety, depression and social behaviour including autism (Neumann and Landgraf, 2012), bond formation and maternal care (Bosch and Neumann, 2012).

1.11 Strategy and aims of this study

The aim of this study is to probe regions of the $V_{1a}R$ with regards their contribution to receptor structure and function. Evolution of the GPCR superfamily in general and specifically the $V_{1a}R$ has resulted in amino acids at particular loci, and the side chain properties fulfilling specific roles in receptor structure and function. In substituting specific amino acids to those with different side chain properties, the role of the endogenous residue may be probed. For example, the substitution of any amino acid to alanine affectively removes the side chain as far as the β-carbon. Additionally, the similarities/differences between amino acid side chains may be utilised to assess the role of side chains. For example, in mutating a tyrosine residue to phenylalanine, any perturbation in structure and function, may be attributed to the hydroxyl of the endogenous tyrosine and not the benzene moiety. Together, it is hypothesised that the resultant effects in receptor structure and function observed are due to the differences in the side chains introduced my amino acid substitution. Perturbations in receptor structure and function where assessed following mutagenesis by characterisation of ligand binding, signalling capabilities and cell-surface expression within three regions of the $V_{1a}R$.

Since the publication of crystallographic data, ICL 2 has become an area of increasing interest in the GPCR field owing to its key location within the receptor architecture close to the receptor:G-protein interface. The individual contribution of the amino acids within ICL 2 to the structure and function of the $V_{1a}R$ are focused upon – paying particular attention to areas of conservation within the GPCR superfamily.

The $V_{1a}R$ demonstrates little, if any, detectable constitutive activity through the inositol-phosphate pathway. Constitutively active mutants have previously identified particular residues

within the GPCR superfamily that are integral maintaining an inactive receptor conformation. One such residue is a conserved hydrophobic residue at position 6.40, yet there seems to be no consensus as to the effects of substitutions introduced at this locus. Mutagenesis of the residue $Ile^{6.40}$, and neighbouring residues aim to look at the role of this conserved hydrophobic residue in the $V_{1a}R$.

A conserved tyrosine residue within TM V has been attributed many roles in GPCR function. Here, systematic substitution of $Tyr^{5.58}$ by all other 19 encoded amino acids is utilised to attempt to understand the structural requirements at this locus and how this relates to its functional role.

CHAPTER 2: MATERIALS AND METHODS

2.1 Materials

2.1.1 Antibodies

Monoclonal anti-haemagglutanin (HA) (mouse clone HA-7) primary antibody was purchased from Sigma (Dorset UK). Horse, anti-mouse IgG, horseradish peroxidase (HRP)-conjugated antibody was purchased from New England Biolabs (Hitchin, UK).

2.1.2 Cell tissue culture

Dulbecco's modified Eagle's medium (DMEM) and Dulbecco's phosphate-buffered saline (PBS) were purchased from Lonza (Slough, UK). Inositol-free DMEM was custom made by Life Technologies (Paisley, UK). Foetal bovine serum, (FBS) was purchased from PAA (Yeovil, UK). Poly-D-lysine (PDL) and polyethyleneimine (PEI) transfection reagent were purchased from Sigma (Dorset, UK). Cell-culture plastic ware was purchased from Fisher Scientific (Loughborough, UK) and Triple Red (Long Crendon, UK).

2.1.3 Molecular biology reagents

Deoxyribonucleotide triphosphates (dNTPs) were purchased from Bioline (London, UK). *Pfu* DNA polymerase enzyme was purchased from Promega (Southampton, UK) and *Dpn*I restriction enzyme from New England Biolabs (Hitchin, U.K.). Mammalian expression vector pcDNA3.1(+) (Figure 2.1) was purchased from Invitrogen (Paisley, UK). Promega Wizard® Plus SV Miniprep Kit (Southampton, UK) and High Purity Maxiprep System, Marligen Biosciences (High Wycombe, UK) were used for isolation and purification of plasmid DNA.

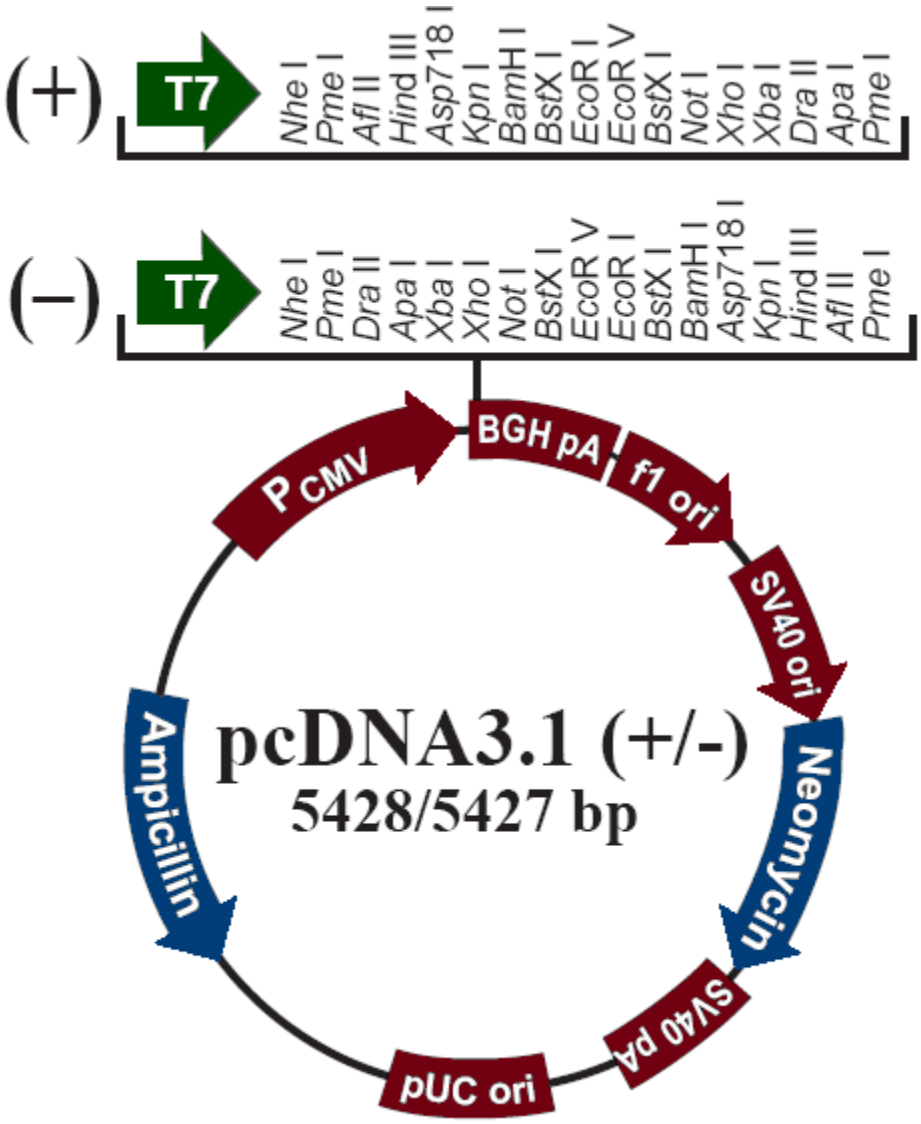

Figure 2.1 Mammalian expression vector pcDNA3.1

T7 promoter (green) and adjacent restriction sites within the multiple cloning sites of pcDNA3.1(+) and pcDNA3.1(-) are shown. SV40 enhancer regions are indicated and region encoding ampicillin resistance utilise for clonal selection is shown (adapted from Invitrogen.com).

2.1.4 Oligonucleotides

Sense and antisense oligonucleotides were designed to incorporate the nucleotide substitutions to create mutant receptor constructs by QuikChange™ (oligonucleotide sequences can be found in the appropriate experimental chapters). Oligonucleotides were synthesized by Invitrogen (Paisley, UK) on a 0.2 μmole scale. Lyophilised oligonucleotides were dissolved in sterile distilled water to 100 pmol/μl and stored at –20 °C. Similarly, oligonucleotides, 5'-TAATACGACTCACTAT-3' and 5'-TAGAAGGCACAGTCGAGGCTG-3', flanking the coding sequences of the $V_{1a}R$ and ghrelin-R were synthesised and used to confirm mutant receptor sequences.

2.1.5 Peptides and hormone analogues

[Arginine^{8}]vasopressin, AVP; cyclic antagonist (CA), [d$(CH_2)_5^{1}$, Tyr(Me)^{2}]AVP; and human ghrelin were purchased from Bachem (Weil am Rhine, Germany).

2.1.6 Radiochemicals

Tritiated AVP, [Phe^{3}-3,4,5-^{3}H]AVP (specific activity: 55.90 – 61.86 Ci/mmol) and myo-[2-^{3}H]inositol (specific activity: 21.70 – 23.75 Ci/mmol) were purchased from Perkin Elmer (Stevenage, UK).

2.1.7 Substrates

Sigma-fast *O*-phenlyenediamine dihydrochloride (OPD) was purchased from Sigma (Dorset, UK).

2.2 Methods

2.2.1 QuikChange™ PCR

Mutagenesis was performed using the coding (cDNA) sequences for $V_{1a}R$ and ghrelin-R in the mammalian expression vector pcDNA3.1(+). Both coding sequences contained a nine amino acid, haemagglutanin (HA)-epitope tag (YPYDVPDYA) engineered after the initiation methionine (Wheatley *et al*., 2007; Kendrick, PhD thesis, University of Birmingham 2010).

The QuikChange™ based mutagenesis method designed by Strategene (Cambridge, UK) was employed to engineer point mutations into the $V_{1a}R$ and ghrelin-R coding sequences. 100 ng of an appropriate template (generally wildtype (Wt)) was used in a final reaction volume of 50 µl. Reaction mixture included sense and antisense oligonucleotide primers at 0.4 pmol/µl; dATP, dCTP, dGTP and dTTP each at 0.2 nmol/µl; *Pfu* DNA polymerase (0.5-2.0 u) in 1x *Pfu* buffer. Using Biometra T3000 Thermocycler, DNA was amplified under conditions: 95 °C for 1 min (preheating); denaturing, 95 °C, 1 min; annealing, 55 °C, 1 min; extension, 68 °C 14 min and repeat from denaturing step for 12 cycles. Methylated template DNA was digested by *Dpn*I at 30 °C for 90 min.

2.2.2 Gel electrophoresis

QuikChange™ reactions were analysed by gel electrophoresis before and after digestion by *Dpn*I to confirm presence of mutant cDNA. Samples were mixed (1:9) with 10 x loading dye buffer (0.25 % (w/v) bromophenol blue, 10 mM Tris, 1mM EDTA and 30 % (v/v) glycerol) and loaded into 1 % (w/v) agarose gels in 1 x TBE buffer (89 mM Tris, 89 mM boric acid, 2 mM EDTA)

containing ethidium bromide (0.5 μg/ml). Horizontal gel electrophoresis was run at approximately 80 mV for 60 min. Gels were visualized using ultraviolet light transilluminator.

2.2.3 Transformation

XL-10 gold ultracompetent cells were made using a standard protocol (Sambrook *et al.*, 1989) and stored at -80 °C. Cells were thawed on ice and 30 μl XL-10 gold cells were incubated with cDNA for 30 min on ice. Cells were heat-shocked at 42 °C for 30 sec and returned to ice for 2 min. 800 μl lysogeny broth (LB)-Lennox (1 % (w/v) peptone, 0.5 % (w/v) yeast extract, 0.5 % (w/v) NaCl) was added and incubated at 37 °C for 1 h. Cells were sedimented by centrifugation at 13,000 rpm for 10 min, resuspended in approximately 30 μl LB and spread on LB agar plates containing 100 μg/ml ampicillin. Plates were incubated for 16 h, 37 °C. Single colonies were selected to inoculate 5-10 mL LB containing 100 μl/ml ampicillin. Cultures were grown for 16 h, 37 °C for cDNA extraction and purification.

2.2.4 Plasmid cDNA extraction and purification

Promega Wizard® Plus SV Miniprep Kit (centrifugation protocol according to manufacturer's instructions) was used to purify culture to yield 1-10 μg cDNA for automated fluorescence DNA sequencing. XL-10 gold ultracompetent cells transformed with cDNA of confirmed sequence were cultured and purified by Marligen High Purity Maxiprep System (column flow-through method according to manufacturer's instructions) to yield 0.5-2.5 mg cDNA. cDNA concentration was determined by absorbance spectroscopy at 260 nm of samples diluted 1:99 in sterile distilled water measured on Bio-Tek Kontron, Unikon 923 spectrometer. Sample purity was determined by measuring the absorbance ratio at 260/280 nm.

2.2.5 Automated fluorescence DNA sequencing

All receptor constructs modified by QuikChange™ were confirmed by automated fluorescence sequencing using primers cited in 2.1.4 (Functional Genomics and Proteomics Laboratories, University of Birmingham, UK).

2.2.6 Cell culture

HEK 293T cells were incubated in humidified 5 % (v/v) CO_2 at a constant temperature of 37 °C. Routine passage in DMEM supplemented with 10 % (v/v) FBS was carried out twice weekly. Cell stocks (low-passage, log phase growth, 1 x 10^6 cells/vial) were stored in liquid nitrogen in freezing medium (90 % (v/v) FBS, 10 % (v/v) DMSO).

For cell membrane preparations for ligand binding assays, cells were seeded at an approximate density of 5 x 10^5 cells/100 mm dish and transfected after 48 h. For measurement of agonist-induced inositol phosphate production PDL-coated, 12-well plates were seeded at a density of 2.5 x 10^5/well and transfected after 24 h. In preparation of enzyme-linked immunosorbent assay (ELISA) protocol, PDL-coated, 24-well plates were seeded at approximate density 1.5x10^5 cells/well and transfected after a further 24 h.

2.2.7 PEI transfection

All transfection solutions of sterile 5 % glucose, sterile 10mM PEI and DNA were incubated without media for 30 min, room temperature prior to being added to dishes/wells. Tranfection solution for radioligand binding cell membrane extracts were composed of 1 ml sterile 5% glucose, 60 µl sterile 10 mM PEI and 5 µg DNA per 100 mm dish. Seeded wells for agonist-induced inositol phosphate production assays were transfected with 60 µl sterile 5% glucose, 8 µl

sterile PEI, 1 µg DNA and 1 ml full media per well, 0 µg DNA for untransfected wells. For ELISA, 30 µl sterile 5% glucose, 4 µl sterile 10 mM PEI, 0.5 µg DNA and 500 µl full media was used per well, 0 µg DNA as blank.

2.2.8 Cell membrane harvesting

Cell membrane extracts were prepared as described previously (Wheatley *et al.*, 2007). Cells were washed twice in ice-cold PBS and scraped in harvest buffer (20 mM HEPES, 1 mM EGTA, 10 mM $Mg(CH_3COO)_2$; pH 7.4) containing 0.1 mg/ml bacitracin and 250 mM sucrose. Cell membranes were sedimented (4000 rpm; 10 min at 4 °C) and resuspended in harvest buffer containing 0.1 mg/ml bacitracin. Membranes were incubated on ice for 20 min and centrifuged as before. Sedimented cell membranes were resuspended in harvest buffer containing 250mM sucrose and stored in 500 µl aliquots at -20 °C.

2.2.9 Protein assay

The Pierce BCA protein assay kit (Northumberland, UK) was used to determine protein concentration of cell membrane extracts. Using a standard BSA standard curve, the approximate total protein concentration of unknown samples was determined.

2.2.10 Radioligand binding assays

Radioligand binding assays were performed on harvested cell membrane preparations using a tritiated natural agonist [Phe^3-3,4,5-^{3}H]AVP as previously described (Wheatley *et al*., 1997). In a final volume of 500 µl, radioligand binding assays contained tritiated radioligand, competing ligand (AVP or CA) at final concentrations 10^{-6} to 10^{-12} M and membranes (50-300 µg protein) diluted in assay buffer (20 mM HEPES, 1 mM EGTA, 10 mM $Mg(CH_3COO)_2$, 1 mg/ml BSA;

pH 7.4). Non-specific binding was defined by a saturating concentration of unlabelled ligand (10 μM). Incubation for 90 min at 30 °C established equilibrium and subsequent centrifugation (13,000 rpm for 10 min) separated bound and free ligand. Membranes pellets were twice washed in water and solubilised with 50 μl Soluene 350 (Packard). 1 ml of HiSafe3 liquid scintillation cocktail (Perkin Elmer) was added to solubilised membranes and dpm calculated using a Packard 1600 TR liquid scintillation analyser counter; 3 min counts.

2.2.10.1 Analysis of radioligand binding data

Experimental data were expressed as a percentage of maximum binding. Replicates of three independent experiments performed in triplicate were analysed by non-linear regression to fit theoretical Langmuir binding isotherms using the GraphPad Prism 4.0 program (San Diego, USA). Individual IC_{50} values for competing ligands were corrected for radioligand occupancy to give individual K_i values using the equations below. K_i values are quoted as the mean of three values ± s.e.m.

$$[^3H]\text{ligand concentration (nM)} = \frac{\text{counts (dpm)}}{\text{specific activity (Ci/mmol)} + \text{sample volume (μl)} \times 2.22}$$

$$K_i \text{ (nM)} = IC_{50} - [\text{free radioligand}] \text{ (nM)}$$

$$K_i \text{ (nM)} = IC_{50} \times \frac{K_d[H^3]\text{ligand}}{K_d[^3H]\text{ligand} \times [\text{free radioligand}]}$$

2.2.11 AVP-induced inositol phosphate production assay

AVP-induced accumulation of inositol phosphates were carried out as previously described (Wheatley *et al*., 1997). 24 h post transfection, media was replaced with inositol-free DMEM

containing 1 μCi/ml myo-[2-^{3}H]inositol. Cells were washed with PBS 24 h after media change and incubated in fresh inositol-free DMEM containing 10 mM LiCl at 37 °C for 30 min. Cells were then incubated at 37 °C for 30 min with varying concentrations of AVP ranging from 10^{-10} – 10^{-6} M. Media was removed by aspiration and the assay was terminated with the addition of 0.5 ml per well of perchloric acid solution (5 % (v/v) $HClO_4$, 1 mM EDTA and 1 mg/ml phytic acid hydrolysate) and incubated at room temperature for 15 min. Samples were neutralised with 1.2 M KOH containing 10 mM EDTA and 50 mM HEPES in 1 ml microcentrifuge tubes and stored overnight at -20 °C. Samples were sedimented at 13,000 rpm for 30 min and supernatent loaded onto Bio-Rad AG1-X8 (formate form) (Hemel Hempstead, UK) filled columns. Following the elution of free inositol and glycerophosphoinositol with 10 ml, 60 mM NH_4COOH containing 0.1 M HCOOH, a mixed fraction of inositol mono-, bis- and trisinositolphosphates was eluted by 10 ml, 850 mM NH_4COOH containing 0.1 M HCOOH. 10 ml UltimaFlo AF scintillation cocktail (Perkin Elmer) was added to the mixed fraction eluent and radioactivity quantified by a Packard 1600 TR liquid scintillation analyser counter; 3 min counts, three times per vial.

2.2.11.1 Analysis of AVP-induced inositol phosphate production

Data were analysed by non-linear regression to generate sigmoidal dose-response curves using GraphPad Prism 4.0 (San Diego, USA). Data were normalised to Wt E_{max} and basal signalling levels. Mean EC_{50} values of three independent experiments performed in triplicate were determined and are stated ± mean 95 % confidence intervals. E_{max} values are stated ± s.e.m.

2.2.12 ELISA to measure cell-surface expression

HEK 293T wells were transfected with receptor constructs as previously described (Wheatley *et al*., 1997). To induce internalisation, $V_{1a}R$ construct were stimulated for 30 min with 10^{-7} M AVP

and incubated in humidified 5% CO_2 at 37 °C. Growth media was removed by aspiration and cells were treated with 3.7 % (v/v) formaldehyde in PBS for 15 min. Cells were washed with PBS three times and blocked with 1% (w/v) BSA in PBS for 45 minutes shaking at room temperature. The cells were incubated with 250 µl mouse, α-HA antibody (diluted 1:2500-3500) in PBS with 1% (w/v) BSA at room temperature, 1 h (shaken). Cells were washed three times with PBS and blocked as before for 15 min. Cells were incubated with 250 µl α-mouse IgG, HRP-linked antibody diluted (diluted 1:2500-3500) for 1 h. The cells were washed a further three times before addition of OPD substrate made up according to manufacturer's instructions. Colour was allowed to develop in the dark and reaction terminated by transferring 100 µl volumes into a 96 well plate containing 100 µl/well of 1 M H_2SO_4. The absorbance at 492 nm was measured.

2.2.12.1Analysis of ELISA

Data were analysed using GraphPad Prism 4.0 program (San Diego, USA). Histograms were constructing of cell-surface expression of three independent experiments performed in triplicate, normalised to total Wt expression and untransfected cells. For $V_{1a}R$ constructs, the presence of receptor at the cell surface after agonist challenge was analysed similarly.

CHAPTER 3: INVESTIGATING INTRACELLULAR LOOP 2 IN $V_{1A}R$

3.1 Introduction

Intracellular loop 2 (ICL 2) connecting transmembrane helices III and IV is the most conserved intracellular loop of the rhodopsin-like family of GPCRs with respect to length (Mirzadegan *et al.*, 2003). This intracellular region has been shown to contain binding determinants for arrestin (Raman *et al.*, 2003; Marion *et al.*, 2006) and GRK 2 (Dhami *et al.*, 2005) in addition to contact points for Gα (Timossi *et al.*, 2002; Havlickova *et al.*, 2003; Rasmussen *et al.*, 2011b). The importance of ICL 2 in GPCR function is further highlighted by human pathologies caused by point mutations within ICL 2 in GPR54 (Wacker *et al.*, 2008), V_2R (Vargas-Poussou *et al.*, 1997) and the melanocortin 1 receptor (Sanchez-Laorden *et al.*, 2009).

Crystallographic data have demonstrated the potential of ICL 2 to adopt multiple conformations. Crystal structures of the β_1AR (Warne *et al.*, 2008) and the $A_{2A}R$ (Jaakola *et al.*, 2008) first demonstrated α-helical portions of ICL 2 whereas the β_2AR adopted an L-shaped conformation (Cherezov *et al.*, 2007). It has been suggested that an α-helix conformation of ICL2 is associated with the ability to bind β-arrestin and that in general, GPCRs are able to adopt both conformations with varied probability (Shan *et al.*, 2010). This dynamic nature is highlighted by the dopamine D3 receptor (Chien *et al.*, 2010), where ICL 2 of one unit of the asymmetric dimer is helical and the other is unresolved indicting structural heterogeneity.

Few mutagenic studies of the entire ICL 2 have been conducted. The most extensive study to date was the cannabinoid CB_1 receptor which signals through G_i and G_s (Chen *et al.*, 2010). Much mutagenesis has been concentrated around the conserved $Pro^{3.57}$ residue and the adjacent residue

which is usually a bulky hydrophobic. $Pro^{3.57}$ is associated with arrestin binding and internalisation (Raman *et al.*, 2003; Marion *et al.*, 2006) whereas the adjacent residue 3.58 is more implicated in the activation of many classes of G-protein (Moro *et al.*, 1993; Sugimoto *et al.*, 2004; Chen *et al.*, 2010).

The aim of this chapter is to assess the contribution of individual amino acids within ICL 2 on the pharmacology, signalling properties and cell-surface expression of the G_q-coupled $V_{1a}R$. The DRY motif of the $V_{1a}R$ has been characterised previously (Hawtin, 2005). The first section of this chapter will encompass the systematic alanine-scanning mutagenesis of the residues proximal to the DRY motif continuing through to the basic cluster at the juxtamembrane segment of TM IV (Figure 3.1). Particular attention will then be paid to the residues $Pro^{3.57}$-$Leu^{3.58}$ and the downstream residues which correspond to the helical region revealed in recent GPCR crystal structures. In addition, some complementary experiments were conducted in ICL 2 of the ghrelin-R to characterise the effects of specific residue substitutions in a $G_{q/11}$-coupled GPCR possessing substantial constitutive activity, signalling through the inositol phosphate pathway like $V_{1a}R$ (Holst *et al.*, 2003).

3.2 Results

All $V_{1a}R$ receptor constructs discussed in this chapter are summarised in Figure 3.1. The oligonucleotides utilised to generate the receptor constructs (as described in section 2.2.1) are summarised in Table 3.1. The $V_{1a}R$ constructs were characterised by radioligand binding assay with respect to their ability to bind the endogenous agonist ligand AVP and synthetic peptide ligand CA. All receptor constructs characterised by radioligand binding expressed at

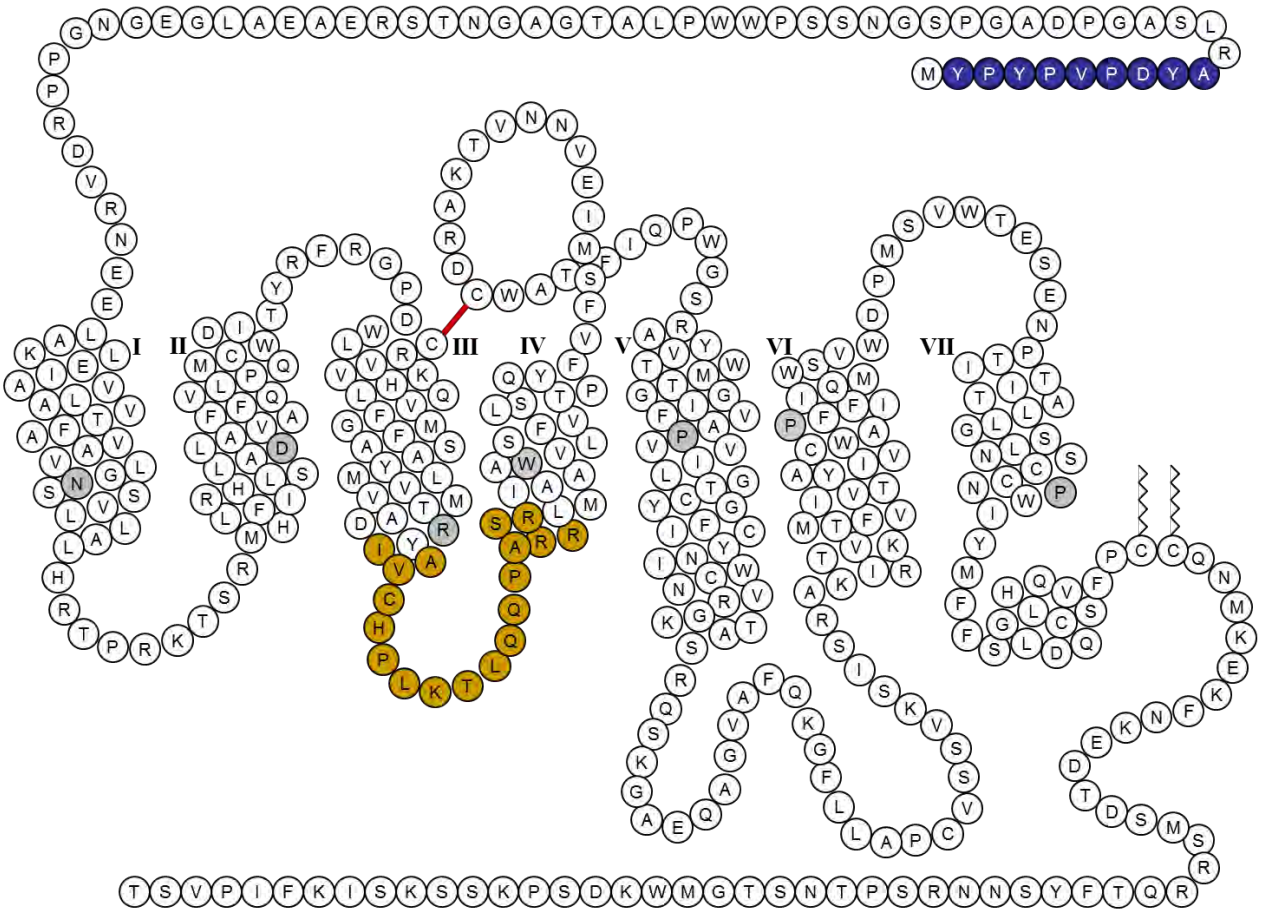

Figure 3.1 Two-dimensional representation of the $V_{1a}R$

The N-terminal, HA-epitope tag (extracellular side) is shown as blue circles. Helices are labelled by roman numerals. The most conserved residue of each helix of rhodopsin-like GPCRs is shown in grey circles and conserved disulphide bridge is shown in red. Palmitoylation sites are shown as zigzags (intracellular side). The residues discussed within this chapter are shown as yellow circles.

Receptor construct	Sense oligonucleotide	Antisense oligonucleotide
[I3.52A]V_{1a}R	5' – GCC–GAC–CGC–TAC–**GCC**-GCG-GTG-TGC-CAC – 3'	5' – GTG-GCA-CAC-CGC-**GGC**-GTA-GCG-GTC-GGC – 3'
[I3.52F]V_{1a}R	5' – GAC-CGC-TAC-**TTC**-GCG-GTG-TG – 3'	5' – CA-CAC-CGC-**GAA**-GTA-GCG-GTC – 3'
[A3.53G]V_{1a}R	5' – AC-CGC-TAC-ATC-**GGG**-GTG-TGC-CAC-CC – 3'	5' – GG-GTG-GCA-CAC-**CCC**-GAT-GTA-GCG-GT – 3'
[V3.54A]V_{1a}R	5' – GC-TAC-ATC-GCG-**GCG**-TGC-CAC-CCG-CT – 3'	5' – AG-CGG-GTG-GCA-**CGC**-CGC-GAT-GTA-GC – 3'
[C3.55A]V_{1a}R	5' – C-TAC-ATC-GCG-GTG-**GCC**-CAC-CCG-CTC-AAG – 3'	5' – CTT-GAG-CGG-GTG-**GGC**-CAC-CGC-GAT-GTA-G – 3'
[H3.56A]V_{1a}R	5' – C-ATC-GCG-GTG-TGC-**GCC**-CCG-CTC-AAG-AC – 3'	5' – GT-CTT-GAG-CGG-**GGC**-GCA-CAC-CGC-GAT-G – 3'
[H3.56F]V_{1a}R	5' – GCG-GTG-TGC-**TTC**-CCG-CTC-AAG – 3'	5' – CTT-GAG-CGG-**GAA**-GCA-CAC-CGC – 3'
[P3.57A]V_{1a}R	5' – GCG-GTG-TGC-CAC-**GCG**-CTC-AAG-ACT-CTG – 3'	5' – CAG-AGT-CTT-GAG-**CGC**-GTG-GCA-CAC-CGC – 3'
[P3.57L]V_{1a}R	5' – GCG-GTG-TGC-CAC-**CTG**-CTC-AAG-ACT-CTG – 3'	5' – CAG-AGT-CTT-GAG-**CAG**-GTG-GCA-CAC-CGC – 3'
[L3.58A]V_{1a}R	5' – GTG-TGC-CAC-CCG-**GCC**-AAG-ACT-CTG-CAA-C– 3'	5' – G-TTG-CAG-AGT-CTT-**GGC**-CGG-GTG-GCA-CAC – 3'
[L3.58M]V_{1a}R	5' – G-TGC-CAC-CCG-**ATG**-AAG-ACT-CTG – 3'	5' – G-TTG-CAG-AGT-CTT-**CAT**-CGG-GTG-GCA-C – 3'
[L3.58S]V_{1a}R	5' – G-TGC-CAC-CCG-**TCC**-AAG-ACT-CTG – 3'	5' – G-TTG-CAG-AGT-CTT-**GGA**-CGG-GTG-GCA-C – 3'
[K3.59A]V_{1a}R	5' – G-TGC-CAC-CCG-CTC-**GCG**-ACT-CTG-CAA-CAG – 3'	5' – CTG-TTG-CAG-AGT-**CGC**-GAG-CGG-GTG-GCA-C – 3'
[K3.59R]V_{1a}R	5' – GC-CAC-CCG-CTC-**AGG**-ACT-CTG-CAA-C – 3'	5' – G-TTG-CAG-AGT-**CCT**-GAG-CGG-GTG – 3'
[T3.60A]V_{1a}R	5' – CAC-CCG-CTC-AAG-**GCT**-CTG-CAA-CAG – 3'	5' – CTG-TTG-CAG-**AGC**-CTT-GAG-CGG-GTG-GC – 3'
[T3.60F]V_{1a}R	5' – CAC-CCG-CTC-AAG-**TTT**-CTG-CAA-CAG-C – 3'	5' – G-CTG-TTG-CAG-**AAA**-CTT-GAG-CGG-GTG – 3'
[T3.60S]V_{1a}R	5' – CAC-CCG-CTC-AAG-**TCT**-CTG-CAA-CAG-C – 3'	5' – G-CTG-TTG-CAG-**AGA**-CTT-GAG-CGG-GTG – 3'
[T3.60Y]V_{1a}R	5' – CAC-CCG-CTC-AAG-**TAT**-CTG-CAA-CAG-C – 3'	5' – G-CTG-TTG-CAG-**ATA**-CTT-GAG-CGG-GTG – 3'
[L3.61A]V_{1a}R	5' – CCG-CTC-AAG-ACT-**GCG**-CAA-CAG-CCC-GCG – 3'	5' – CGC-GGG-CTG-TTG-**CGC**-AGT-CTT-GAG-CGG – 3'
[L3.61K]V_{1a}R	5' – CCG-CTC-AAG-ACT-**AAG**-CAA-CAG-CCC-GCG – 3'	5' – CGC-GGG-CTG-TTG-**CTT**-AGT-CTT-GAG-CGG – 3'
[Q3.62A]V_{1a}R	5' – CTC-AAG-ACT-CTG-**GCA**-CAG-CCC-GCG-CGC – 3'	5' – GCG-CGC-GGG-CTG-T**GC**-CAG-AGT-CTT-GAG – 3'

[Q3.62V]V_{1a}R	5' – CTC-AAG-ACT-CTG-**GTA**-CAG-CCC-GCG-CGC – 3'	5' – GCG-CGC-GGG-CTG-**TAC**-CAG-AGT-CTT-GAG – 3'
[Q3.63A]V_{1a}R	5' – G-CTC-AAG-ACT-CTG-CAA-**GCG**-CCC-GCG-C – 3'	5' – G-CGC-GGG-**CGC**-TTG-CAG-AGT-CTT-GAG-C– 3'
[P3.64A]V_{1a}R	5' – CT-CTG-CAA-CAG-**GCC**-GCG-CGC-CGC-TC – 3'	5' – GA-GCG-GCG-CGC-**GGC**-CTG-TTG-CAG-AG – 3'
[A3.65G]V_{1a}R	5' – G-CAA-CAG-CCC-**GGG**-CGC-CGC-TCG-CGC – 3'	5' – GCG-CGA-GCG-GCG-**CCC**-GGG-CTG-TTG-C – 3'
[R3.66A]V_{1a}R	5' – CAA-CAG-CCC-GCG-**GCC**-CGC-TCG-CGC-CTC – 3'	5' – GAG-GCG-CGA-GCG-**GGC**-CGC-GGG-CTG-TTG – 3'
[R3.67A]V_{1a}R	5' – CAG-CCC-GCG-CGC-**GCC**-TCG-CGC-CTC-ATG – 3'	5' – CAT-GAG-GCG-CGA-**GGC**-GCG-CGC-GGG-CTG – 3'
[S3.68A]V_{1a}R	5'– GCG-CGC-CGC-**GCG**-CGC-CTC-ATG-ATC – 3'	5'– GAT-CAT-GAG-GCG-**CGC**-GCG-GCG-CGC – 3'
[R3.69A]V_{1a}R	5' – GCG-CGC-CGC-TCG-**GCC**-CTC-ATG-ATC-GCG – 3'	5' – CGC-GAT-CAT-GAG-**GGC**-CGA-GCG-GCG-CGC – 3'
[R3.66A/R3.67A]V_{1a}R	5' – CAA-CAG-CCC-GCG-**GCC**-**GCC**-TCG-CGC-CTC-ATG – 3'	5' – CAT-GAG-GCG-CGA-**GGC**-**GGC**-CGC-GGG-CTG-TTG– 3'
[R3.66A/R3.69A]V_{1a}R	5' – CAA-CAG-CCC-GCG-**GCC**-CGC-TCG-**GC**C-CTC – 3'	5' – GAG-G**GC**-CGA-GCG-**GGC**-CGC-GGG-CTG-TTG – 3'
[R3.67A/R3.69A]V_{1a}R	5' – CAG-CCC-GCG-CGC-**GCC**-TCG-**GC**C-CTC-ATG – 3'	5' – CAT-GAG-G**GC**-CGA-**GGC**-GCG-CGC-GGG-CTG – 3'
[R3.66A/R3.67A/ R3.69A]V_{1a}R	5' – GCG-**GC**C-**GC**C-TCG-**GCC**-CTC-ATG-ATC-GCG – 3'	5' – CGC-GAT-CAT-GAG-**GGC**-CGA-G**GC**-G**GC**-CGC– 3'
[β_2AR-ICL2$_H$]V_{1a}R	RXN1: 5' – G-TGC-CAC-CCG-**TTC**-AAG-**TAT**-CTG-CAA-C – 3' RXN2: 5' – CCG-**T**TC-AAG-**TA**T-**CAG**-**TCA**-CAG-CCC-GCG-CGC – 3'	RXN1: 5' – G-TTG-CAG-**ATA**-CTT-**GAA**-CGG-GTG-GCA – 3' RXN2: 5' – GCG-CGC-GGG-CTG-**TGA**-**CTG**-A**TA**-CTT-GA**A**-CGG – 3'
[ghrelinR-ICL2$_H$]V_{1a}R	RXN1: 5' – GC-CAC-CCG-CTC-**AGG**-**GCT**-**AAG**-CAA-CAG – 3' RXN2: 5' – CTC-A**GG**-**G**CT-**AA**G-**GTA**-CAG-CCC-GCG-CGC – 3'	RXN1: 5' – CTG-TTG-**CTT**-**AGC**-**CCT**-GAG-CGG-GTG-GC – 3' RXN2: 5' – GCG-CGC-GGG-CTG-**TAC**-**CTT**-AG**C**-C**C**T-GAG – 3'

Table 3.1 Oligonucleotide sequences utilised to generate receptor constructs

Receptor constructs were generated as previously described in section 2.2.1. The codon encoding the amino acid substituted is highlighted in red and nucleotide substitutions in bold. Non-bold bases show the complementary template sequence.

1-2 pmol/mg protein. In order to determine the effects of point mutations on the receptors' capabilities to activate PLC, receptor constructs were transiently transfected into HEK 293T cells and the accumulation of inositol phosphates, InsP-$InsP_3$ was measured. Cell-surface expression of each receptor construct was also quantified relative to Wt by exploiting the HA epitope–tag in an ELISA.

3.2.1 Alanine-scanning mutagenesis of ICL 2

To investigate the contribution of individual amino acids in ICL 2 to the structure and function of the $V_{1a}R$, each amino acid was individually mutated to alanine. In doing so, the amino acid side chain from the β-carbon is effectively removed. Natural alanine residues were mutated to glycine generating the receptor constructs [I3.52A]$V_{1a}R$, [A3.53G]$V_{1a}R$, [V3.54A]$V_{1a}R$, [C3.55A]$V_{1a}R$, [H3.56A]$V_{1a}R$, [P3.57A]$V_{1a}R$, [L3.58A]$V_{1a}R$, [K3.59A]$V_{1a}R$, [T3.60A]$V_{1a}R$, [L3.61A]$V_{1a}R$, [Q3.62A]$V_{1a}R$, [Q3.63A]$V_{1a}R$, [P3.64A]$V_{1a}R$, [A3.65G]$V_{1a}R$, [R3.66A]$V_{1a}R$, [R3.67A]$V_{1a}R$, [S3.68A]$V_{1a}R$ and [R3.69A]$V_{1a}R$. Radioligand competition binding curves of alanine substitutions of ICL 2 residues are shown in Figures 3.3-3.7. InsP-$InsP_3$ dose-response curves and cell-surface expression levels are represented in Figures 3.8-3.1. All data are summarised in Table 3.2. All figures and tables are presented together in the following pages.

All receptor constructs with the exception of [I3.52A]$V_{1a}R$, [P3.64A]$V_{1a}R$, [R3.66A]$V_{1a}R$, [R3.67A]$V_{1a}R$ and [R3.69A]$V_{1a}R$ bound the agonist ligand AVP and synthetic antagonist CA with Wt-like binding affinity (Figure 3.3-3.7, Table 3.2). [I3.52A]$V_{1a}R$ displayed 4.5-fold and 6-fold increases in affinity for AVP and CA respectively (Figure 3.3). [P3.64A]$V_{1a}R$ did not bind [^{3}H]AVP at experimental concentrations so could not be pharmacologically characterised (Figure 3.6). [R3.66A]$V_{1a}R$, [R3.67A]$V_{1a}R$ and [R3.69A]$V_{1a}R$ bound AVP with increase affinity of 4-,

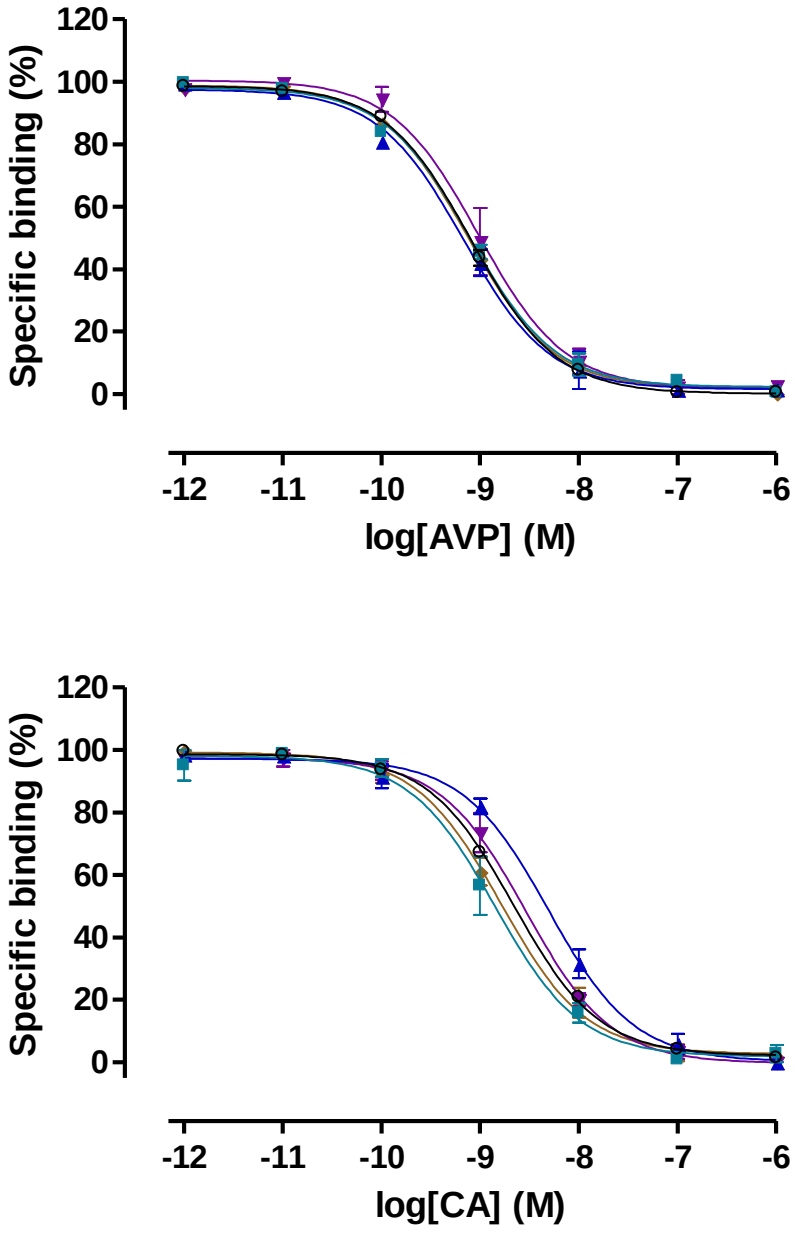

Figure 3.3 Competition radioligand binding curves of alanine substituted ICL 2 residues

Competition radioligand binding assays were performed on HEK 293T cells, transiently transfected with receptor constructs [Wt]$V_{1a}R$, (○); [I3.52A]$V_{1a}R$, (■); [A3.53G]$V_{1a}R$, (▲); [V3.54A]$V_{1a}R$, (▼) and [C3.55A]$V_{1a}R$ (♦). Upper panel: [^{3}H]AVP vs AVP competition; lower panel: [^{3}H]AVP vs CA competition. A theoretical Langmuir binding isotherm was fitted to data expressed as specific binding (%), defining non-specific binding by 1 μM ligand. Data are the mean ± s.e.m. of three experiments performed in triplicate.

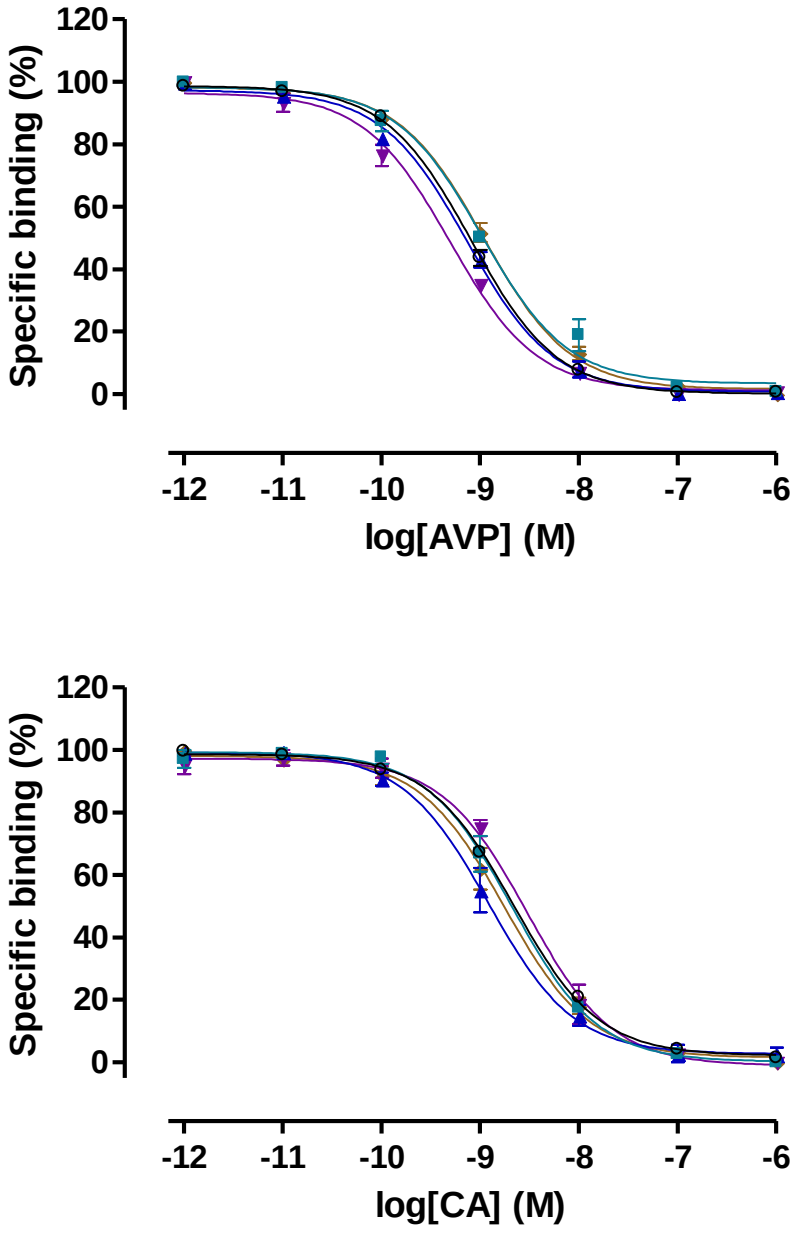

Figure 3.4 Competition radioligand binding curves of alanine substituted ICL 2 residues

Competition radioligand binding assays were performed on HEK 293T cells, transiently transfected with receptor constructs [Wt]$V_{1a}R$, (○); [H3.56A]$V_{1a}R$, (■); [P3.57A]$V_{1a}R$, (▲); [L3.58A]$V_{1a}R$, (▼) and [K3.59A]$V_{1a}R$ (♦). Upper panel: [^{3}H]AVP vs AVP competition; lower panel: [^{3}H]AVP vs CA competition. A theoretical Langmuir binding isotherm was fitted to data expressed as specific binding (%), defining non-specific binding by 1 μM ligand. Data are the mean ± s.e.m. of three experiments performed in triplicate.

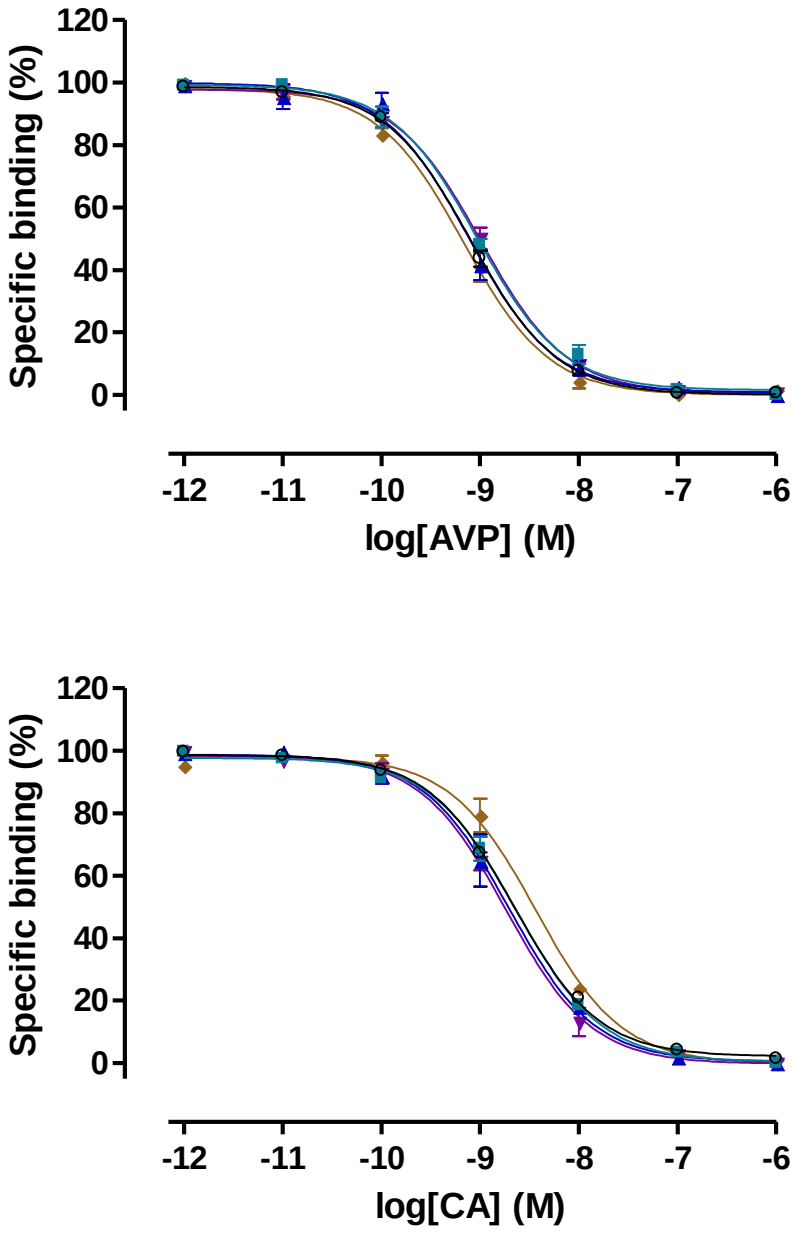

Figure 3.5 Competition radioligand binding curves of alanine substituted ICL 2 residues

Competition radioligand binding assays were performed on HEK 293T cells, transiently transfected with receptor constructs [Wt]$V_{1a}R$, (○); [T3.60A]$V_{1a}R$, (■); [L3.61A]$V_{1a}R$, (▲); [Q3.62A]$V_{1a}R$, (▼) and [Q3.63A]$V_{1a}R$ (♦). Upper panel: [^{3}H]AVP vs AVP competition; lower panel: [^{3}H]AVP vs CA competition. A theoretical Langmuir binding isotherm was fitted to data expressed as specific binding (%), defining non-specific binding by 1 μM ligand. Data are the mean ± s.e.m. of three experiments performed in triplicate.

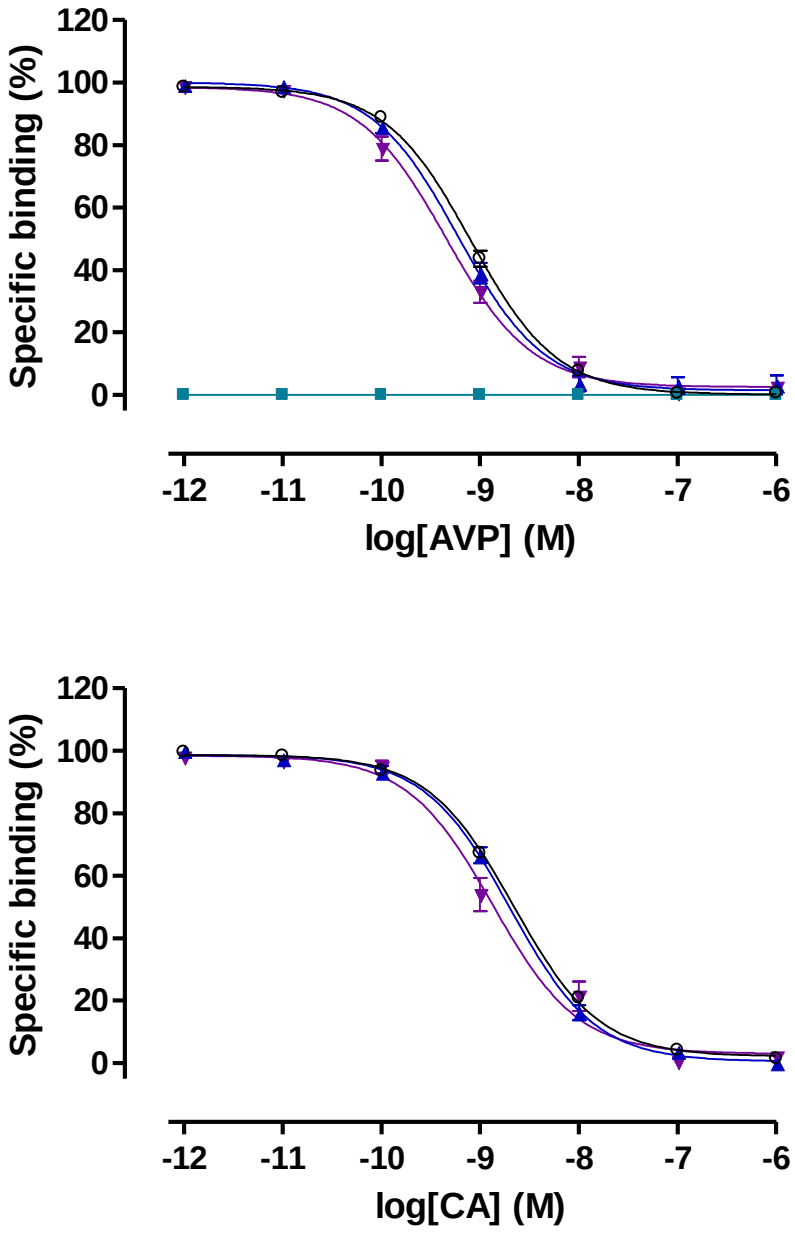

Figure 3.6 Competition radioligand binding curves of alanine substituted ICL 2 residues

Competition radioligand binding assays were performed on HEK 293T cells, transiently transfected with receptor constructs [Wt]V_{1a}R, (○); [P3.64A]V_{1a}R, (■); [A3.65G]V_{1a}R (▲) and [R3.66A]V_{1a}R, (▼). Upper panel: [^{3}H]AVP vs AVP competition; lower panel: [^{3}H]AVP vs CA competition. A theoretical Langmuir binding isotherm was fitted to data expressed as specific binding (%), defining non-specific binding by 1 μM ligand. Data are the mean ± s.e.m. of three experiments performed in triplicate.

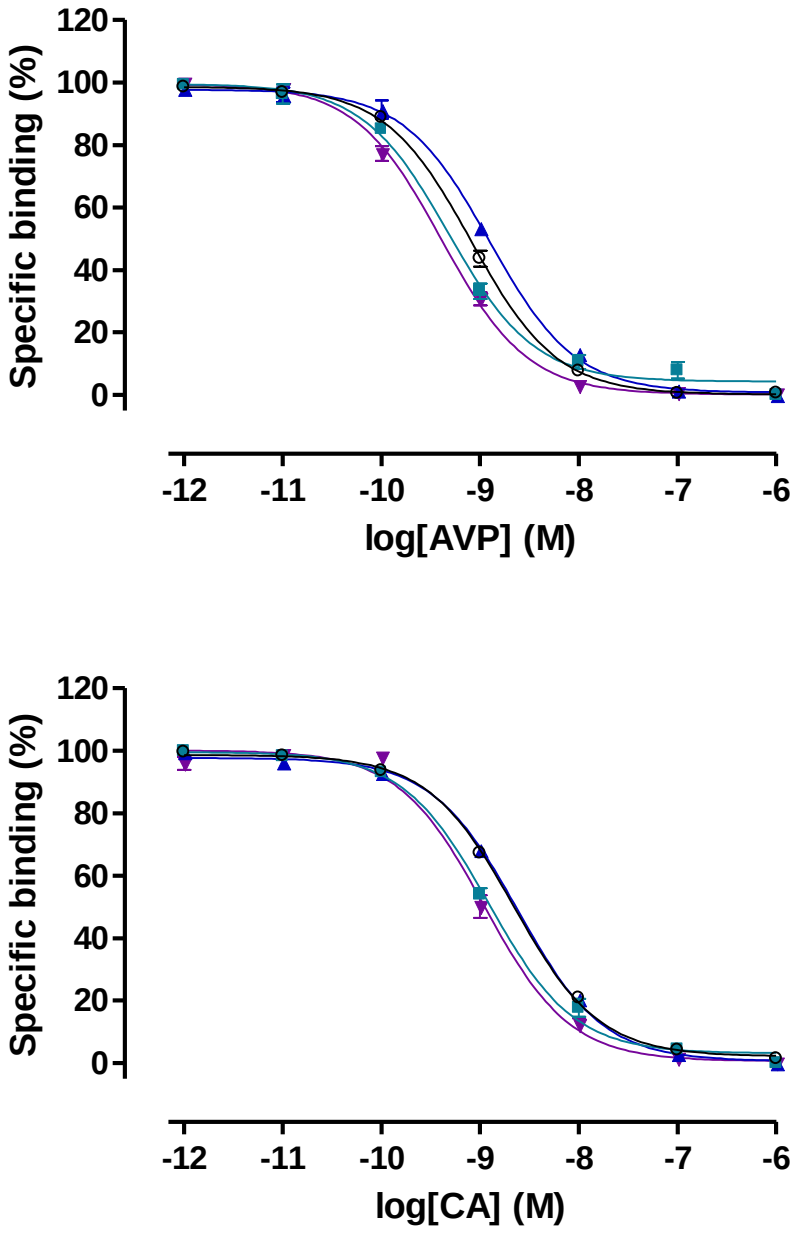

Figure 3.7 Competition radioligand binding curves of alanine substituted ICL 2 residues

Competition radioligand binding assays were performed on HEK 293T cells, transiently transfected with receptor constructs [Wt]$V_{1a}R$, (○); [R3.67A]$V_{1a}R$, (■); [S3.68A]$V_{1a}R$ (▲) and [R3.69A]$V_{1a}R$, (▼). Upper panel: [^{3}H]AVP vs AVP competition; lower panel: [^{3}H]AVP vs CA competition. A theoretical Langmuir binding isotherm was fitted to data expressed as specific binding (%), defining non-specific binding by 1 μM ligand. Data are the mean ± s.e.m. of three experiments performed in triplicate.

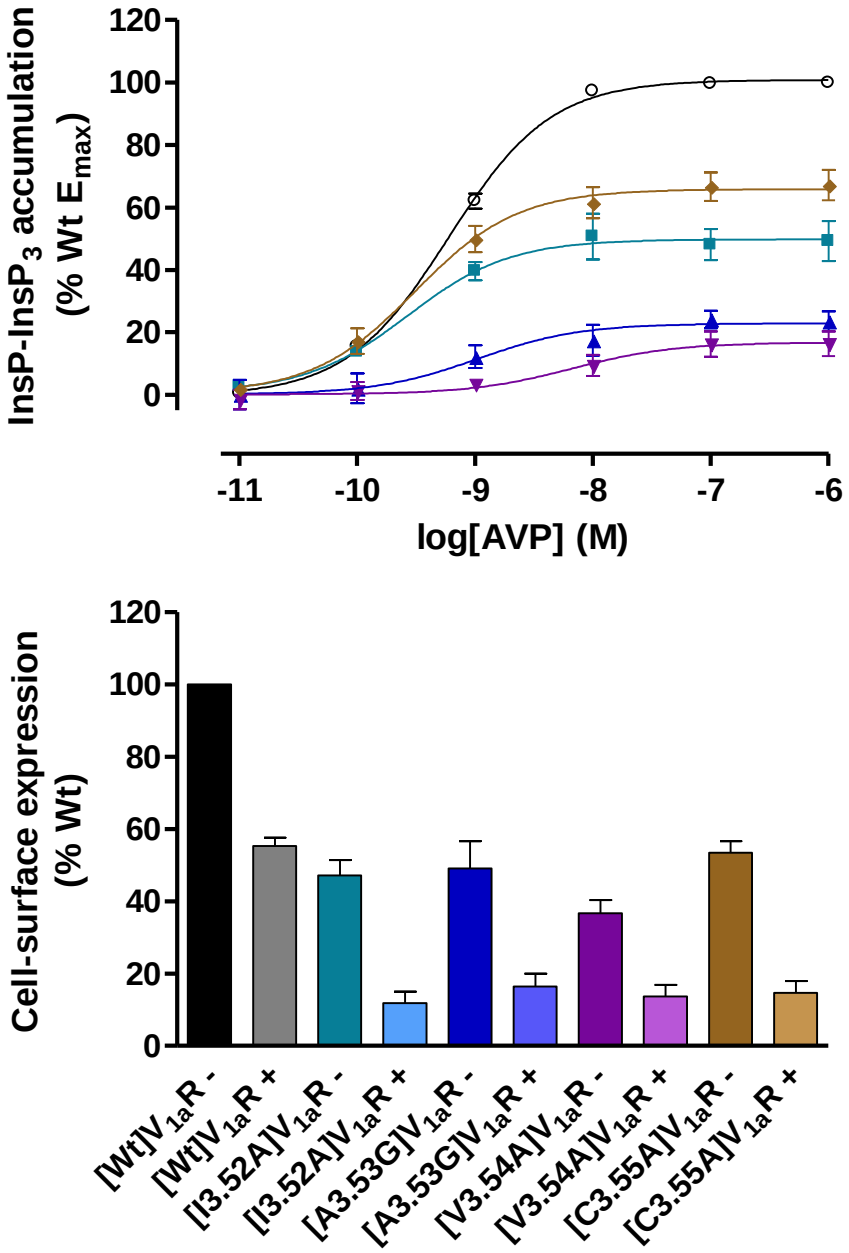

Figure 3.8 InsP-InsP$_3$ dose-response curves and cell-surface expression (+/- agonist challenge) of alanine substitutions of ICL 2 residues

Upper panel: Dose-response curves of inositol phosphates accumulation assays of HEK 293T cells, transiently transfected with receptor constructs [Wt]V_{1a}R, (○); [I3.52A]V_{1a}R, (■); [A3.53G]V_{1a}R, (▲); [V3.54A]V_{1a}R, (▼) and [C3.55A]V_{1a}R (♦). Data are normalised to [Wt]V_{1a}R basal and maximal signalling levels, expressed as the mean ± s.e.m. of three experiments performed in triplicate. Basal signalling is plotted at 10^{-11} M. Lower panel: Cell-surface expression levels of receptor constructs were normalised to untransfected cells and unstimulated (-) [Wt]V_{1a}R expression levels. Data are stated as the mean ± s.e.m. of three experiments performed in triplicate. Stimulated (+) constructs were challenged by 10^{-7}M AVP for 30 min.

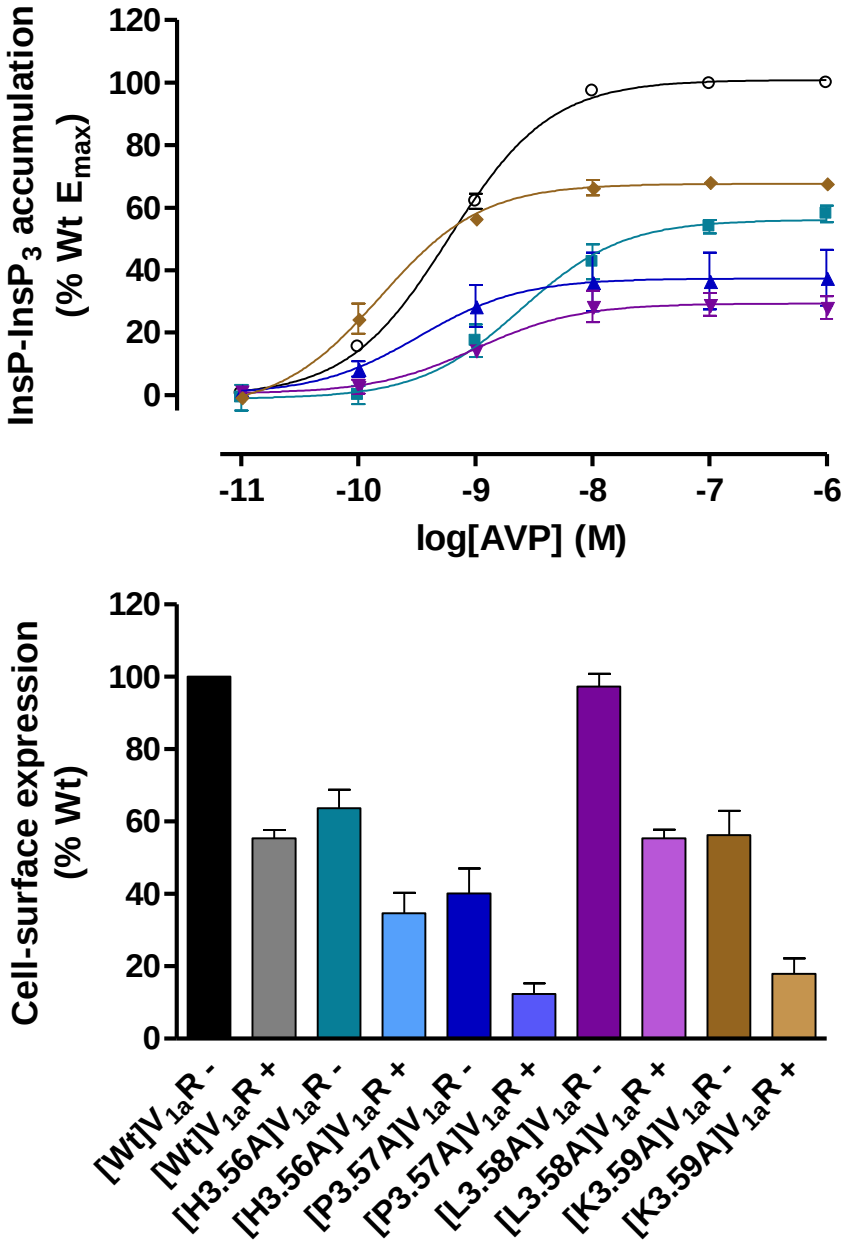

Figure 3.9 InsP-InsP$_3$ dose-response curves and cell-surface expression (+/- agonist challenge) of alanine substitutions of ICL 2 residues

Upper panel: Dose-response curves of inositol phosphates accumulation assays of HEK 293T cells, transiently transfected with receptor constructs [Wt]V_{1a}R, (○); [H3.56A]V_{1a}R, (■); [P3.57A]V_{1a}R, (▲); [L3.58A]V_{1a}R, (▼) and [K3.59A]V_{1a}R (♦). Data are normalised to [Wt]V_{1a}R basal and maximal signalling levels, expressed as the mean ± s.e.m. of three experiments performed in triplicate. Basal signalling is plotted at 10^{-11} M. Lower panel: Cell-surface expression levels of receptor constructs were normalised to untransfected cells and unstimulated (-) [Wt]V_{1a}R expression levels. Data are stated as the mean ± s.e.m. of three experiments performed in triplicate. Stimulated (+) constructs were challenged by 10^{-7}M AVP for 30 min.

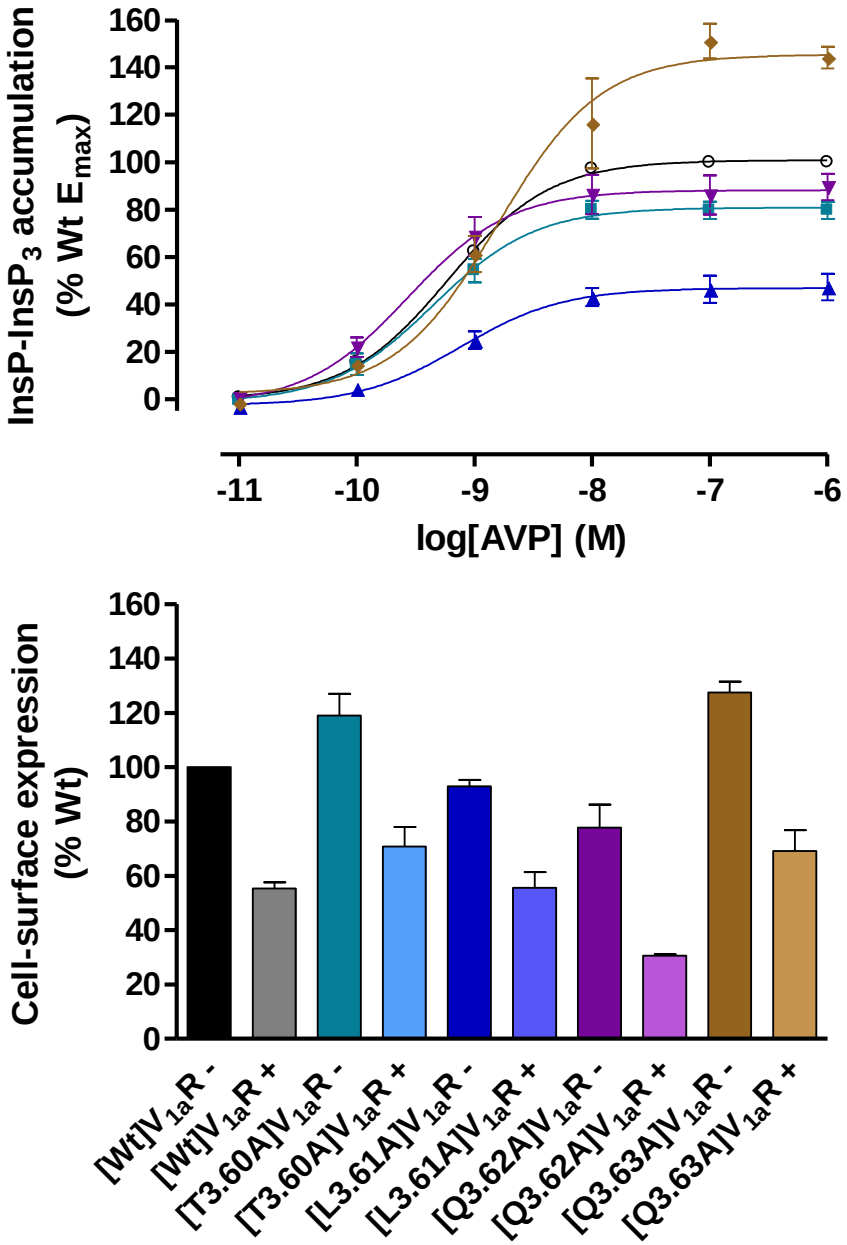

Figure 3.10 InsP-InsP$_3$ dose-response curves and cell-surface expression (+/- agonist challenge) of alanine substitutions of ICL 2 residues

Upper panel: Dose-response curves of inositol phosphates accumulation assays of HEK 293T cells, transiently transfected with receptor constructs [Wt]V_{1a}R, (○); [T3.60A]V_{1a}R, (■); [L3.61A]V_{1a}R, (▲); [Q3.62A]V_{1a}R, (▼) and [Q3.63A]V_{1a}R, (♦). Data are normalised to [Wt]V_{1a}R basal and maximal signalling levels, expressed as the mean ± s.e.m. of three experiments performed in triplicate. Basal signalling is plotted at 10^{-11} M. Lower panel: Cell-surface expression levels of receptor constructs were normalised to untransfected cells and unstimulated (-) [Wt]V_{1a}R expression levels. Data are stated as the mean ± s.e.m. of three experiments performed in triplicate. Stimulated (+) constructs were challenged by 10^{-7}M AVP for 30 min.

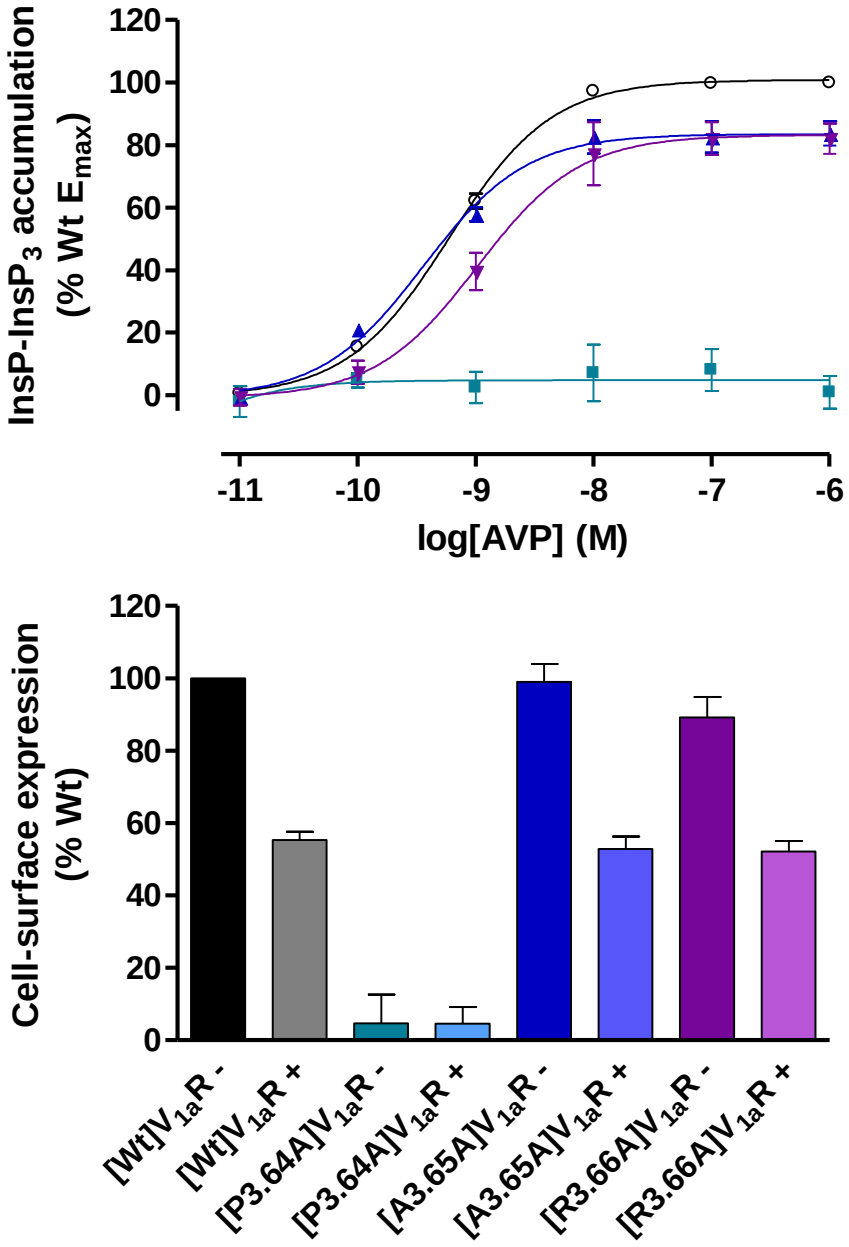

Figure 3.11 InsP-InsP$_3$ dose-response curves and cell-surface expression (+/- agonist challenge) of alanine substitutions of ICL 2 residues

Upper panel: Dose-response curves of inositol phosphates accumulation assays of HEK 293T cells, transiently transfected with receptor constructs [Wt]V_{1a}R, (○); [P3.64A]V_{1a}R, (■); [A3.65G]V_{1a}R, (▲) and [R3.66A]V_{1a}R, (▼). Data are normalised to [Wt]V_{1a}R basal and maximal signalling levels, expressed as the mean ± s.e.m. of three experiments performed in triplicate. Basal signalling is plotted at 10^{-11} M. Lower panel: Cell-surface expression levels of receptor constructs were normalised to untransfected cells and unstimulated (-) [Wt]V_{1a}R expression levels. Data are stated as the mean ± s.e.m. of three experiments performed in triplicate. Stimulated (+) constructs were challenged by 10^{-7}M AVP for 30 min.

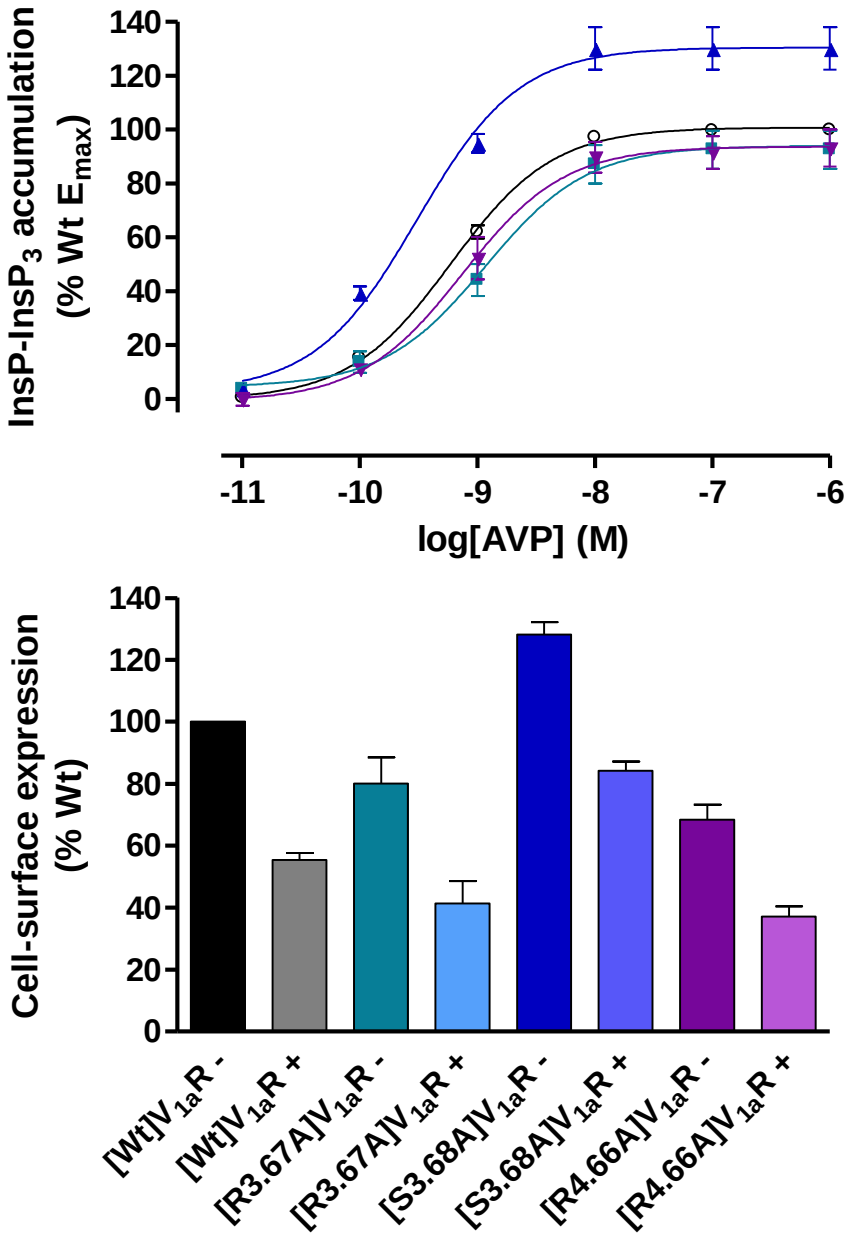

Figure 3.12 InsP-InsP$_3$ dose-response curves and cell-surface expression (+/- agonist challenge) of alanine substitutions of ICL 2 residues

Upper panel: Dose-response curves of inositol phosphates accumulation assays of HEK 293T cells, transiently transfected with receptor constructs [Wt]V_{1a}R, (○); [R3.67A]V_{1a}R, (■); [S3.68A]V_{1a}R, (▲) and [R3.69A]V_{1a}R, (▼). Data are normalised to [Wt]V_{1a}R basal and maximal signalling levels, expressed as the mean ± s.e.m. of three experiments performed in triplicate. Basal signalling is plotted at 10^{-11} M. Lower panel: Cell-surface expression levels of receptor constructs were normalised to untransfected cells and unstimulated (-) [Wt]V_{1a}R expression levels. Data are stated as the mean ± s.e.m. of three experiments performed in triplicate. Stimulated (+) constructs were challenged by 10^{-7}M AVP for 30 min.

Receptor construct	Binding affinity, K_i (nM) ± s.e.m.		InsP-InsP$_3$ accumulation (% Wt E_{max}) ± s.e.m.			Cell-surface expression (% Wt unstimulated) ± s.e.m.	
	AVP	CA	Basal	EC_{50}*	E_{max}	Unstimulated	Stimulated
$V_{1a}R$	**0.45 ± 0.04**	**0.96 ± 0.10**	**0**	**0.60 ± 0.02**	**100**	**100**	**55 ± 2**
[I3.52A]$V_{1a}R$	0.10 ± 0.08	0.15 ± 0.08	3 ± 1	0.28 ± 0.04	51 ± 7	47 ± 4	12 ± 3
[A3.53G]$V_{1a}R$	0.26 ± 0.08	1.06 ± 0.20	0 ± 5	1.05 ± 0.32	24 ± 3	49 ± 7	16 ± 4
[V3.54A]$V_{1a}R$	0.59 ± 0.33	1.45 ± 0.18	-1 ± 3	5.98 ± 2.27	16 ± 4	37 ± 4	14 ± 3
[C3.55A]$V_{1a}R$	0.31 ± 0.11	0.68 ± 0.10	2 ± 2	0.32 ± 0.03	67 ± 5	53 ± 3	15 ± 3
[H3.56A]$V_{1a}R$	0.63 ± 0.11	1.22 ± 0.22	-1 ± 4	2.47 ± 0.40	58 ± 3	64 ± 5	35 ± 6
[P3.57A]$V_{1a}R$	0.73 ± 0.06 #	1.21 ± 0.08#	2 ± 2	0.35 ± 0.03	38 ± 9	40 ± 7	12 ± 3
[L3.58A]$V_{1a}R$	0.33 ± 0.08	1.14 ± 0.43	1 ± 1	1.04 ± 0.19	29 ± 4	97 ± 3	55 ± 2
[K3.59A]$V_{1a}R$	0.43 ± 0.10	0.86 ± 0.25	-1 ± 1	1.70 ± 0.02	68 ± 1	56 ± 7	18 ± 4
[T3.60A]$V_{1a}R$	0.53 ± 0.13	1.39 ± 0.35	0 ± 1	0.46 ± 0.05	80 ± 4	119 ± 8	71 ±7
[L3.61A]$V_{1a}R$	0.38 ± 0.07	0.95 ± 0.15	-3 ± 2	0.78 ± 0.07	47 ± 6	93 ± 2	56 ± 6
[Q3.62A]$V_{1a}R$	0.82 ± 0.22	1.27 ± 0.16	1 ± 0	0.29 ± 0.02	89 ± 6	78 ± 9	31 ± 1
[Q3.63A]$V_{1a}R$	0.50 ± 0.18	2.17 ± 0.63	-2 ± 3	1.51 ± 0.35	151 ± 7	127 ± 4	69 ± 8
[P3.64A]$V_{1a}R$	Did not bind [^{3}H]AVP		-2 ± 5	No detectible signalling		4 ± 8	5 ± 5
[A3.65A]$V_{1a}R$	0.24 ± 0.02	0.74 ± 0.17	-1 ± 1	0.36 ± 0.05	84 ± 4	99 ± 5	53 ± 4
[R3.66A]$V_{1a}R$	0.11 ± 0.04	0.33 ± 0.06	-1 ± 3	1.04 ± 0.06	82 ± 5	89 ± 6	52 ± 3
[R3.67A]$V_{1a}R$	0.14 ± 0.05	0.32 ± 0.03	4 ± 1	1.16 ± 0.10	93 ± 7	80 ± 8	41 ± 7
[S3.68A]$V_{1a}R$	0.93 ± 0.04	1.71 ± 0.16	4 ± 1	0.31 ± 0.05	130 ± 8	128 ± 4	84 ± 3
[R3.69A]$V_{1a}R$	0.16 ± 0.02	0.30 ± 0.05	-1 ± 2	0.75 ± 0.06	93 ± 7	68 ± 5	37 ± 3

Table 3.2 Binding, signalling and cell-surface expression alanine substitutions of ICL 2 residues

All data are shown as the mean ± s.e.m. of three separate experiments performed in triplicate. *EC_{50} is stated as the mean ± mean of 95 % confidence intervals of three separate experiments performed in triplicate. Data in yellow indicate >2.5-fold increase in K_i or EC_{50} or >25 % reduction in E_{max}, cell-surface expression; orange >5-fold increase in K_i or EC_{50} or >50 % reduction in E_{max}, cell-surface expression or internalisation; red >10-fold increase in K_i or EC_{50} or >75 % reduction in E_{max}, cell-surface expression or internalisation. Data in green indicate >2.5-fold increase in K_i or EC_{50} or >25 % increase in E_{max}, cell-surface expression or > 50% increase in internalisation. Data in white are comparable to Wt. # denotes IC_{50} ± mean of 95 % confidence intervals of three separate experiments performed in triplicate.

3- and 2.8-fold respectively and all bound CA with 3-fold increases in affinity (Figures 3.6-3.7, Table 3.2). [P3.57A]V_{1a}R displayed Wt-like IC_{50} values for AVP, 0.73 ± 0.06 nM (Wt 0.80 ± 0.02 nM) and CA, 1.21 ± 0.08 nM (2.17 ± 0.09 nM), Figure 3.4. All receptor constructs displayed Wt-like basal levels of activity so will not be discussed further in this regard (Table 3.2).

Receptor constructs [I3.52A]V_{1a}R, [A3.53G]V_{1a}R, [V3.54A]V_{1a}R, [C3.55A]V_{1a}R exhibited reduced maximal signalling levels and reduced cell-surface expression compared to Wt (Figure 3.8, Table 3.2). The EC_{50} values of [I3.52A]V_{1a}R, [A3.53G]V_{1a}R and [C3.55A]V_{1a}R were comparable to Wt whilst [V3.54A]V_{1a}R increased ~10-fold. In response to agonist, [A3.53G]V_{1a}R, [V3.54A]V_{1a}R internalised at levels of receptor at levels comparable to Wt. [I3.52A]V_{1a}R and [C3.55A]V_{1a}R all displayed an increased tendency to internalise, > 67.5 % of unstimulated expression (Wt, 45 % unstimulated expression).

[P3.57A]V_{1a}R and [L3.58A]V_{1a}R demonstrated Wt-like EC_{50} values while [H3.56A]V_{1a}R and [K3.59A]V_{1a}R achieved small 4.1- and 2.8-fold increases respectively (Figure 3.9, Table 3.2). The maximal signalling levels of [H3.56A]V_{1a}R, [P3.57A]V_{1a}R, [K3.59A]V_{1a}R demonstrated decreased E_{max} values in line with their reduced cell-surface expression. [L3.58A]V_{1a}R expressed at a Wt-like level with a marked reduction in maximal signalling capabilities (29 % of Wt E_{max}). P3.57A and K3.59A internalised a larger proportion of the receptor expressed (70 % and 68 % respectively) compared to Wt (45 % of unstimulated levels).

Receptor constructs [T3.60A]V_{1a}R and [Q3.62A]V_{1a}R signalled like-Wt in all respects (Figure 3.10, Table 3.2). [L3.61A]V_{1a}R and [Q3.63A]V_{1a}R displayed Wt-like EC_{50} values yet maximal InsP-$InsP_3$ generation was 47 % and 151 % of Wt respectively. [Q3.63A]V_{1a}R expressed at the

cell surface at 127 % of Wt levels while the [T3.60A]V_{1a}R, [Q3.62A]V_{1a}R and [L3.61A]V_{1a}R expressed at levels comparable to Wt. All receptor constructs internalised upon agonist challenge.

Figure 3.11 shows that receptor construct [P3.64A]V_{1a}R could not generate second messengers InsP-$InsP_3$ in response to AVP challenge given that is was not expressed at the cell surface as indicated by ELISA (Table 3.2). [A3.65G]V_{1a}R and [R3.66A]V_{1a}R signalled like Wt in all respects, expressed at the cell-surface at levels comparable to Wt and internalised a similar proportion of receptors to Wt (Figure 3.6, Table 3.2).

[R3.67A]V_{1a}R signalled and expressed at the cell surface at levels comparable to Wt (Figure 3.12, Table 3.2). [S3.68A]V_{1a}R generated an EC_{50} comparable to Wt with an E_{max} 130 % of Wt. Cell-surface expression was also increased to 128 % of Wt levels. [R3.69A]V_{1a}R signalled through the inositol phosphate pathway in a manner comparable to Wt although cell-surface expression was slightly reduced. [R3.67A]V_{1a}R, [S3.68A]V_{1a}R and [R3.69A]V_{1a}R all internalised normally in response to AVP challenge.

3.2.2 Extended alanine-scanning of the arginine cluster

A basic residue at the TM IV-cytosolic boundary is thought to contribute to a motif responsible for cholesterol binding (Hanson *et al.*, 2008). As such, double and triple substitutions, [R3.66A/R3.67A]V_{1a}R, [R3.66A/R3.69A]V_{1a}R, [R3.67A/R3.69A]V_{1a}R and [R3.66A/R3.67A/R3.69A]V_{1a}R of the arginine cluster in V_{1a}R were generated to investigate their role in receptor function.

All receptor constructs bound [^{3}H]AVP and generated competition binding curves for the ligands AVP and CA (Figure 3.13). IC_{50} values for constructs [R3.66A/R3.67A]V_{1a}R (AVP, 0.59 ± 0.04 nM; CA, 1.81 ± 0.28 nM) and [R3.66A/R3.69A]V_{1a}R (AVP, 0.40 ± 0.03 nM;

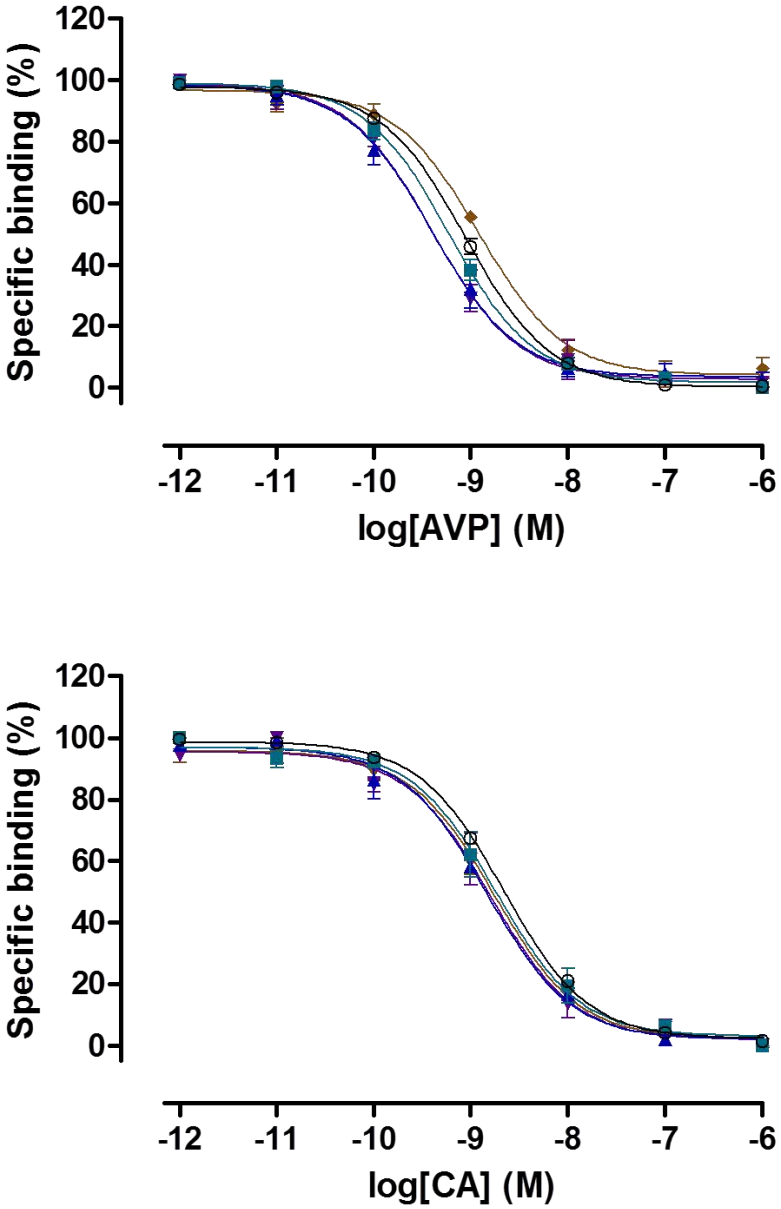

Figure 3.13 Competition radioligand binding curves of multiple arginine substitutions at the cytoplasmic interface of TM IV

Competition radioligand binding assays were performed on HEK 293T cells, transiently transfected with receptor constructs [Wt]V_{1a}R, (○); [R3.66A/R3.67A]V_{1a}R, (■); [R3.66A/R3.67A]V_{1a}R, (▲); [R3.67A/R3.69A]V_{1a}R, (▼) and [R3.66A/R3.67A/R3.69A]V_{1a}R (♦). Upper panel: [^{3}H]AVP vs AVP competition; lower panel: [^{3}H]AVP vs CA competition. A theoretical Langmuir binding isotherm was fitted to data expressed as specific binding (%), defining non-specific binding by 1 μM ligand. Data are the mean ± s.e.m. of three experiments performed in triplicate.

CA 1.45 ± 0.22 nM) were comparable to Wt (AVP, 0.80 ± 0.02 nM; CA, 2.17 ± 0.09 nM). The double substitution receptor construct [R3.67A/R3.69]V_{1a}R increased the binding affinity of AVP 4.1-fold while maintaining Wt-like CA binding (Figure 3.13, Table 3.3). The triple substitution [R3.66A/R3.67A/R3.69A]V_{1a}R maintained a Wt-like pharmacological profile. All multiple-substituted receptor constructs maintained Wt-like basal signalling levels but exhibited decreases in maximal InsP-$InsP_3$ generation and also decreased expression at the cell surface was evident. EC_{50} values of [R3.66A/R3.67A]V_{1a}R and [R3.66A/R3.69A]V_{1a}R were Wt-like while [R3.67A/R3.69A]V_{1a}R decreased 2.6-fold. EC_{50} for the triple substitution decreased 5.4-fold. Double receptor constructs and the triple substitution internalised levels of receptor comparable to Wt upon agonist challenge.

3.2.3 Substitution of conserved residues $Pro^{3.57}$, $Leu^{3.58}$ and $Lys/Arg^{3.59}$

A proline residue is present at locus 3.57 in 64 % of rhodopsin-like GPCRs (Marion *et al.*, 2006). An alanine residue is also common at this position (26 %), therefore the P3.57L mutant construct was generated to elucidate whether proline and alanine contribute similarly at this position with respect to V_{1a}R and ghrelin-R structure and function. An isoleucine, leucine, valine or phenylalanine at position 3.58 is observed in 75 % of rhodopsin-like GPCRs. A basic residue is present at position 3.59 in both V_{1a}R and ghrelin-R, therefore $Lys^{3.59}$ was substituted to alanine in the ghrelin-R to assess the contribution of a basic side chain at this locus in receptor structure and function.

3.2.3.1 Substitution of $Pro^{3.57}$ and $Leu^{3.58}$ in the V_{1a}R

The substitution [L3.58S]V_{1a}R recapitulates a polymorphism in the V_{1a}R documented in GPR54 (Wacker *et al.*, 2008) and [L3.58M]V_{1a}R introduces the methionine residue present in the V_2R

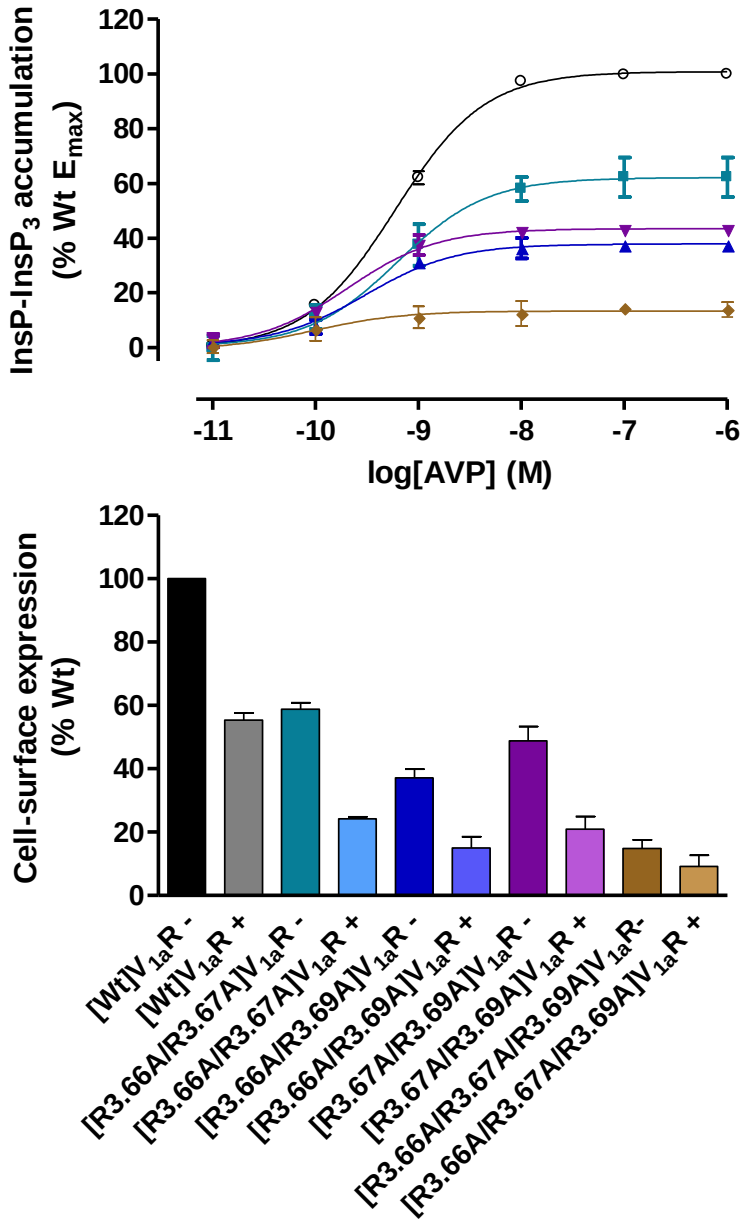

Figure 3.14 InsP-InsP$_3$ dose-response curves and cell-surface expression (+/- agonist challenge) of multiple arginine substitutions at the cytoplasmic interface of TM IV

Upper panel: Dose-response curves of inositol phosphates accumulation assays of HEK 293T cells, transiently transfected with receptor constructs [Wt]V_{1a}R, (○); [R3.66A/R3.67A]V_{1a}R, (■); [R3.66A/R3.69]V_{1a}R, (▲),[R3.67A/R3.69A]V_{1a}R, (▼) and [R3.66A/R3.67A/R3.69A]V_{1a}R, (♦). Data are normalised to [Wt]V_{1a}R basal and maximal signalling levels, expressed as the mean ± s.e.m. of three experiments performed in triplicate. Basal signalling is plotted at 10^{-11} M. Lower panel: Cell-surface expression levels of receptor constructs were normalised to untransfected cells and unstimulated (-) [Wt]V_{1a}R expression levels. Data are stated as the mean ± s.e.m. of three experiments performed in triplicate. Stimulated (+) constructs were challenged by 10^{-7}M AVP for 30 min.

Receptor construct	Binding affinity, K_i (nM) ± s.e.m.		InsP-InsP$_3$ accumulation (% Wt E_{max}) ± s.e.m.			Cell-surface expression (%Wt unstimulated) ± s.e.m.	
	AVP	CA	Basal	EC_{50} *	E_{max}	Unstimulated	Stimulated
$V_{1a}R$	**0.45 ± 0.04**	**0.96 ± 0.10**	**0**	**0.60 ± 0.02**	**100**	**100**	**55 ± 2**
[R3.66A/R3.67]$V_{1a}R$	0.59 ± 0.04#	1.81 ± 0.28#	0 ± 5	0.61 ± 0.06	62 ± 7	59 ± 2	24 ± 1
[R3.66A/R3.69]$V_{1a}R$	0.40 ± 0.03#	1.45 ± 0.22#	3 ± 0	0.33 ± 0.09	37 ± 1	37 ± 3	15 ± 3
[R3.67A/R3.69]$V_{1a}R$	0.11 ± 0.02	0.39 ± 0.09	3 ± 2	0.23 ± 0.03	43 ± 1	49 ± 4	21 ± 4
[R3.66A/R3.67/ R3.69]$V_{1a}R$	0.34 ± 0.08	0.84 ± 0.17	0 ± 2	0.11 ± 0.04	14 ± 2	15 ± 3	9 ± 4

Table 3.3 Binding, signalling and cell-surface expression of multiple arginine substitutions at the cytoplasmic interface of TM IV

All data are shown as the mean ± s.e.m. of three separate experiments performed in triplicate. *EC_{50} is stated as the mean ± mean of 95 % confidence intervals of three separate experiments performed in triplicate. Data in yellow indicate >2.5-fold increase in K_i or EC_{50} or >25 % reduction in E_{max}, cell-surface expression; orange >5-fold increase in K_i or EC_{50} or >50 % reduction in E_{max}, cell-surface expression or internalisation; red >10-fold increase in K_i or EC_{50} or >75 % reduction in E_{max}, cell-surface expression or internalisation. Data in green indicate >2.5-fold increase in K_i or EC_{50} or >25 % increase in E_{max}, cell-surface expression or > 50% increase in internalisation. Data in white are comparable to Wt. # denotes IC_{50} ± mean of 95 % confidence intervals of three separate experiments performed in triplicate.

which couples to G_s. [P3.57L]V_{1a}R bound AVP and CA with Wt-like binding affinities. The substitution of $Leu^{3.58}$ for either serine or methionine produced a receptor construct that bound AVP and CA like Wt (Figure 3.15, Table 3.4).

The receptor construct [P3.57L]V_{1a}R displayed reduction in maximal InsP-$InsP_3$ generation (47 % of Wt) with Wt-like basal and EC_{50} values (Figure 3.16, Table 3.4). A proportional decrease in cell-surface expression was also evident but the construct internalised a Wt-like proportion of receptor upon agonist stimulation (Figure 3.16, Table 3.4). At the locus 3.58, the serine substitution severely reduced maximal signalling capabilities with an E_{max} of just 15 % of Wt but did not affect basal signalling levels or EC_{50}. [L3.58S]V_{1a}R receptor construct displayed a slightly increased presence at the cell surface at 126 % of Wt levels. The conservative [L3.58M]V_{1a}R substitution behaved like Wt with respect to signalling through the inositol phosphate pathway and cell-surface expression. Both [L3.58S]V_{1a}R and [L3.58M]V_{1a}R underwent internalisation upon AVP challenge.

3.2.3.2 Substitution of $Pro^{3.57}$, $Leu^{3.58}$ and $Lys^{3.59}$ in the ghrelin-R

The receptor constructs [P3.57A]ghrelin-R, [P3.57L]ghrelin-R, [L3.58A]ghrelin-R, [R3.59A]ghrelin-R were generated to assess the contribution of these residues on the inositol phosphates generation and cell-surface expression in the ghrelin-R. Naturally, the ghrelin-R possesses a basal activity of 50-60 % of E_{max} signals through with inositol phosphate pathway (Holst *et al.*, 2003).

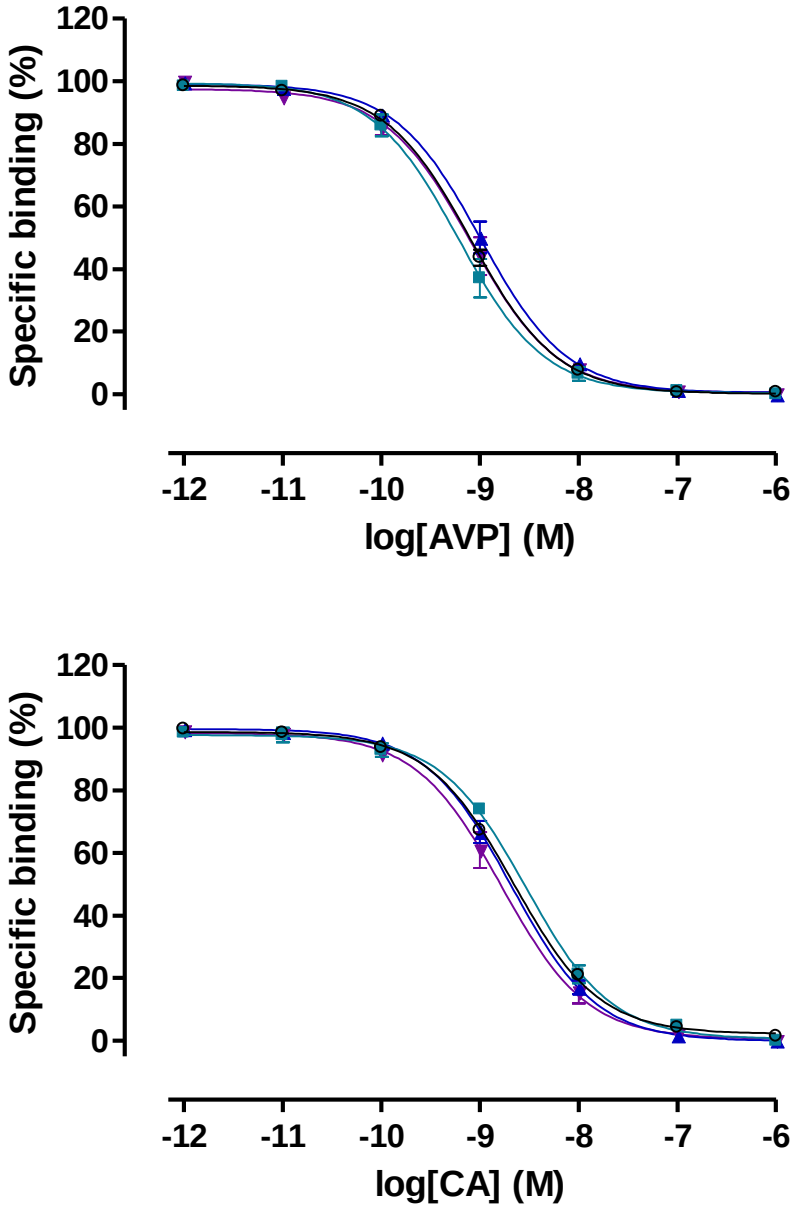

Figure 3.15 Competition radioligand binding curves of Pro$^{3.57}$ and Leu$^{3.58}$ constructs in $V_{1a}R$

Competition radioligand binding assays were performed on HEK 293T cells, transiently transfected with receptor constructs [Wt]$V_{1a}R$, (○); [P3.57L]$V_{1a}R$, (■); [L3.58S]$V_{1a}R$ (▲) and [L3.58M]$V_{1a}R$, (▼). Upper panel: [^{3}H]AVP vs AVP competition; lower panel: [^{3}H]AVP vs CA competition. A theoretical Langmuir binding isotherm was fitted to data expressed as specific binding (%), defining non-specific binding by 1 μM ligand. Data are the mean ± s.e.m. of three experiments performed in triplicate.

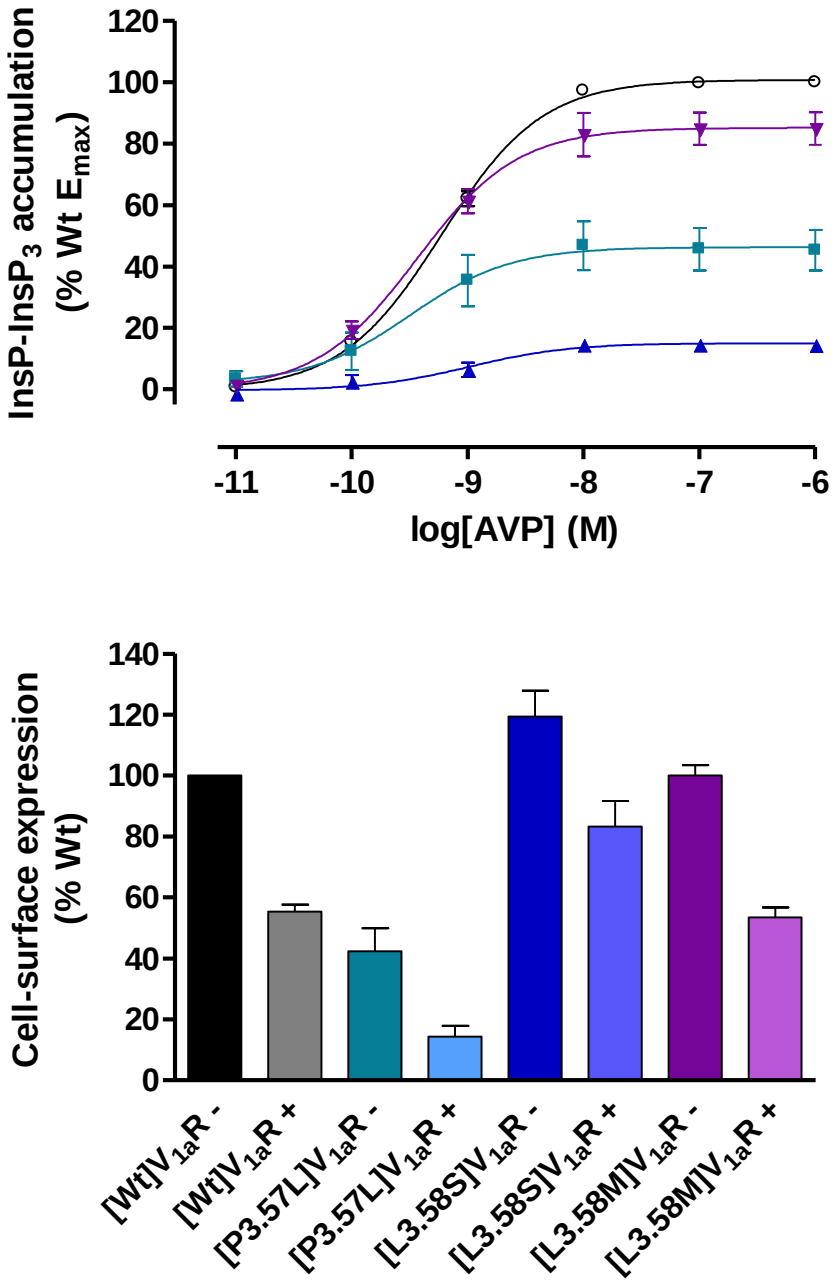

Figure 3.16 InsP-InsP$_3$ dose-response curves and cell-surface expression (+/- agonist challenge) of Pro$^{3.57}$ and Leu$^{3.58}$ constructs in V$_{1a}$R

Upper panel: Dose-response curves of inositol phosphates accumulation assays of HEK 293T cells, transiently transfected with receptor constructs [Wt]V$_{1a}$R, (○); [P3.57L]V$_{1a}$R, (■); [L3.58S]V$_{1a}$R, (▲) and [L3.58M]V$_{1a}$R, (▼). Data are normalised to [Wt]V$_{1a}$R basal and maximal signalling levels, expressed as the mean ± s.e.m. of three experiments performed in triplicate. Basal signalling is plotted at 10^{-11} M. Lower panel: Cell-surface expression levels of receptor constructs were normalised to untransfected cells and unstimulated (-) [Wt]V$_{1a}$R expression levels. Data are stated as the mean ± s.e.m. of three experiments performed in triplicate. Stimulated (+) constructs were challenged by 10^{-7}M AVP for 30 min.

Receptor construct	Binding affinity, K_i (nM) ± s.e.m.		InsP-$InsP_3$ accumulation (% Wt E_{max}) ± s.e.m.			Cell-surface expression (% Wt ustimulated) ± s.e.m.	
	AVP	CA	Basal	EC_{50}*	E_{max}	Unstimulated	Stimulated
$V_{1a}R$	**0.45 ± 0.04**	**0.96 ± 0.10**	**0**	**0.60 ± 0.02**	**100**	**100**	**55 ± 2**
[P3.57L]$V_{1a}R$	0.23 ± 0.10	0.64 ± 0.22	3 ± 3	0.33 ± 0.04	47 ± 8	42 ± 7	14 ± 4
[L3.58S]$V_{1a}R$	0.65 ± 0.20	1.18 ±0.22	-1 ± 2	0.95 ± 0.36	15 ± 2	119 ± 9	83 ± 8
[L3.58M]$V_{1a}R$	0.55 ± 0.20	0.87 ± 0.15	1 ± 2	0.37 ± 0.02	85 ± 4	100 ± 3	53 ± 3

Table 3.4 Binding, signalling and cell-surface expression of $Pro^{3.57}$ and $Leu^{3.58}$ constructs in $V_{1a}R$

All data are shown as the mean ± s.e.m. of three separate experiments performed in triplicate. *EC_{50} is stated as the mean ± mean of 95 % confidence intervals of. Data in yellow indicate >2.5-fold increase in K_i or EC_{50} or >25 % reduction in E_{max}, cell-surface expression; orange >5-fold increase in K_i or EC_{50} or >50 % reduction in E_{max}, cell-surface expression or internalisation; red >10-fold increase in K_i or EC_{50} or >75 % reduction in E_{max}, cell-surface expression or internalisation. Data in green indicate >2.5-fold increase in K_i or EC_{50} or >25 % increase in E_{max}, cell-surface expression or > 50% increase in internalisation. Data in white are comparable to Wt. # denotes IC_{50} ± mean of 95 % confidence intervals three separate experiments performed in triplicate.

While [P3.57A]ghrelin-R and [P3.57L]ghrelin-R were expressed at the same level albeit ~50 % of Wt. However, the P3.57A substitution maintained agonist responsiveness in generating InsP-$InsP_3$ (Figure 3.17, Table 3.5), [P3.57A]ghrelin-R generated a Wt-like EC_{50} with only slight reduction in basal signalling level. In contrast, P3.57L ablated both the basal activity and ghrelin-induced signalling of the ghrelin-R. The [L3.58A]ghrelin-R construct demonstrated a marked inhibition in basal signalling. There was also some decrease in agonist potency (4.2-fold) and E_{max} in response to ghrelin stimulation. Expression was markedly elevated at 148 % of Wt levels. [R3.59A]ghrelin-R maintained Wt-like signalling capabilities and cell-surface expression.

3.2.4 Probing the role of residue 3.60

In peptide ligand-GPCRs, residue 3.60 is generally an amino acid with a small side chain (Figure 3.18). In contrast, the amine-ligand GPCRs generally possess a tyrosine residue. Multiple receptor substitutions were generated in the $V_{1a}R$ and ghrelin-R to assess the roles of their respective naturally occurring amino acids, and the effects of introducing the tyrosine residue conserved among amine-ligand GPCRs. A phenylalanine residue was also substituted into both receptors given its side chain similarity to tyrosine.

3.2.4.1 Probing the role of residue 3.60 in $V_{1a}R$

Naturally, the $V_{1a}R$ has a threonine at this locus, therefore the conservative substitution [T3.60S]$V_{1a}R$ was generated in addition to receptor constructs [T3.60F]$V_{1a}R$ and [T3.60Y]$V_{1a}R$. [T3.60S]$V_{1a}R$ and [T3.60F]$V_{1a}R$ were well tolerated, maintaining Wt-like pharmacology (Figure 3.19, Table 3.6), signalling capabilities, expression and internalisation (Figure 3.20). However the [T3.60Y]$V_{1a}R$ construct bound AVP with 3-fold decrease in affinity but maintained Wt-like CA binding affinity. Basal signalling through the inositol phosphate pathway was unaffected, as

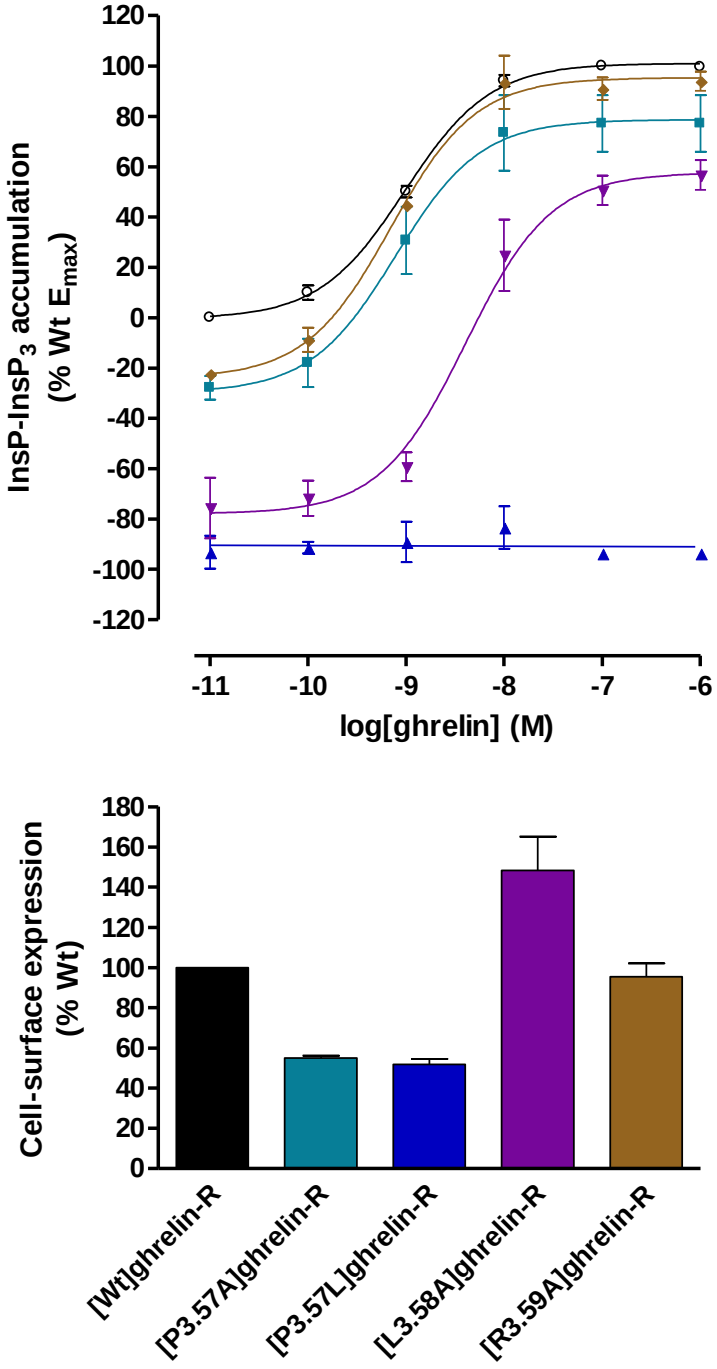

Figure 3.17 InsP-InsP$_3$ dose-response curves and cell-surface expression of Pro$^{3.57}$, Leu$^{3.58}$ and Arg$^{3.59}$ constructs in ghrelin-R

Upper panel: Dose-response curves of inositol phosphates accumulation assays of HEK 293T cells, transiently transfected with receptor constructs [Wt]ghrelin-R, (○); [P3.57A]ghrelin-R, (■); [P3.57L]ghrelin-R, (▲), [L3.58A]ghrelin-R, (▼) and [R3.59A]ghrelin-R, (♦). Data are normalised to basal and maximal signalling levels, expressed as the mean ± s.e.m. of three experiments performed in triplicate. Basal signalling is plotted at 10^{-11} M. Lower panel: Cell-surface expression levels of receptor constructs normalised to untranfected cells and [Wt]ghrelin-R expression levels expressed as the mean ± s.e.m. of three experiments performed in triplicate.

Receptor construct	InsP-InsP$_3$ accumulation (% Wt E_{max}) ± s.e.m.			Cell-surface expression (% Wt unstimulated) ± s.e.m.
	Basal	EC_{50}*	E_{max}	
ghrelin-R	**0**	**0.97 ± 0.03**	**100**	**100**
[P3.57A]ghrelin-R	-28 ± 5	0.80 ± 0.06	77 ± 11	55 ± 1
[P3.57L]ghrelin-R	-93 ± 7	No detectible signalling		52 ± 3
[L3.58A]ghrelin-R	-76 ± 12	4.12 ± 0.61	57 ± 6	148 ± 17
[R3.59A]ghrelin-R	-22 ± 2	0.71 ± 0.10	93 ± 4	96 ± 6

Table 3.5 Binding, signalling and cell-surface expression of Pro$^{3.57}$, Leu$^{3.58}$ and Arg$^{3.59}$ constructs in ghrelin-R

All data are shown as the mean ± s.e.m. of three separate experiments performed in triplicate. *EC_{50} is stated as the mean ± mean of 95 % confidence intervals of three separate experiments performed in triplicate. Data in yellow indicate >2.5-fold increase in EC_{50} or >25 % reduction in basal signalling, E_{max}, cell-surface expression; orange >5-fold increase in EC_{50} or >50 % reduction in basal signalling, E_{max} or cell-surface expression; red >10-fold increase in EC_{50} or >75 % reduction in basal signalling, E_{max} or cell-surface expression. Data in green indicate >2.5-fold increase in EC_{50} or >25 % increase in basal signalling, E_{max} or cell-surface expression. Data in white are comparable to Wt.

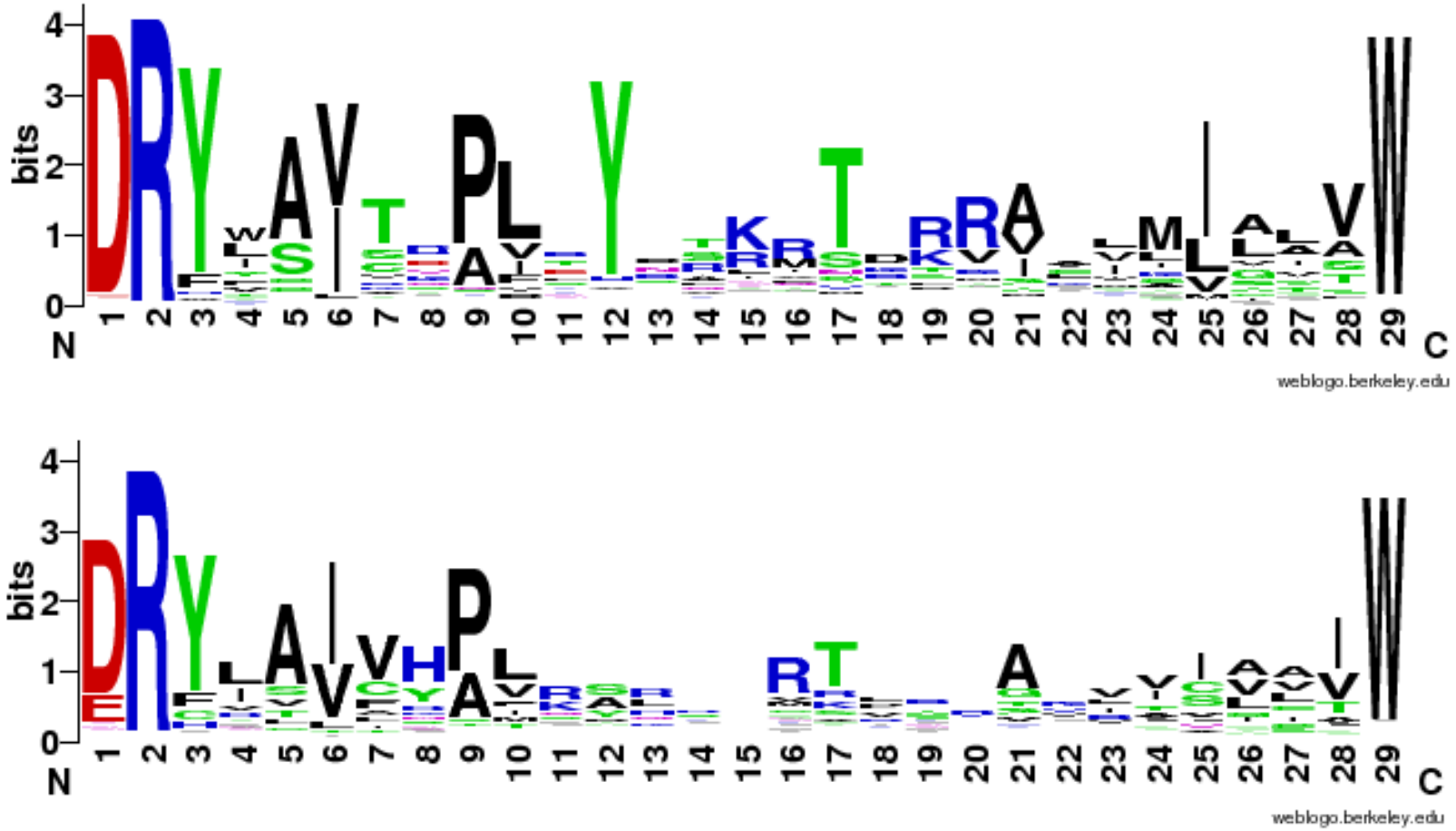

Figure 2.18 Weblogos of sequences of ICL 2 regions in amine-ligand and peptide-ligand GPCRs

Weblogos of amine ligand-GPCRs (upper panel) and peptide ligand-GPCRs (lower panel) from multiple sequence alignments from the GPCR database *http://www.gpcr.org/7tm/*. The logos represent the sequences between $Arg^{3.50}$ and $Trp^{4.50}$. Residue 3.60 is at position 12.

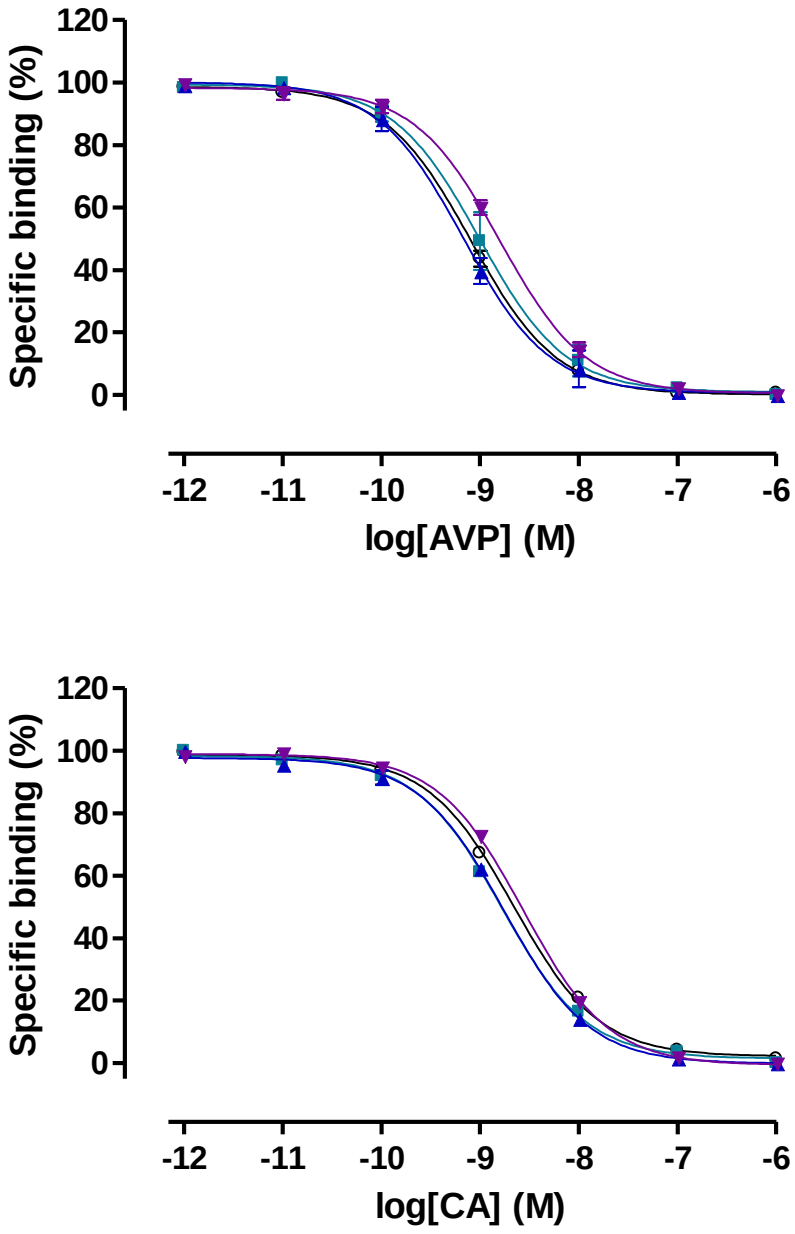

Figure 3.19 Competition radioligand binding curves of Thr$^{3.60}$ substitutions in $V_{1a}R$

Competition radioligand binding assays were performed on HEK 293T cells, transiently transfected with receptor constructs [Wt]$V_{1a}R$, (○); [T3.60S]$V_{1a}R$, (■); [T3.60F]$V_{1a}R$, (▲) and [T3.60Y]$V_{1a}R$, (▼). Upper panel: [^{3}H]AVP vs AVP competition; lower panel: [^{3}H]AVP vs CA competition. A theoretical Langmuir binding isotherm was fitted to data expressed as specific binding (%), defining non-specific binding by 1 μM ligand. Data are the mean ± s.e.m. of three experiments performed in triplicate.

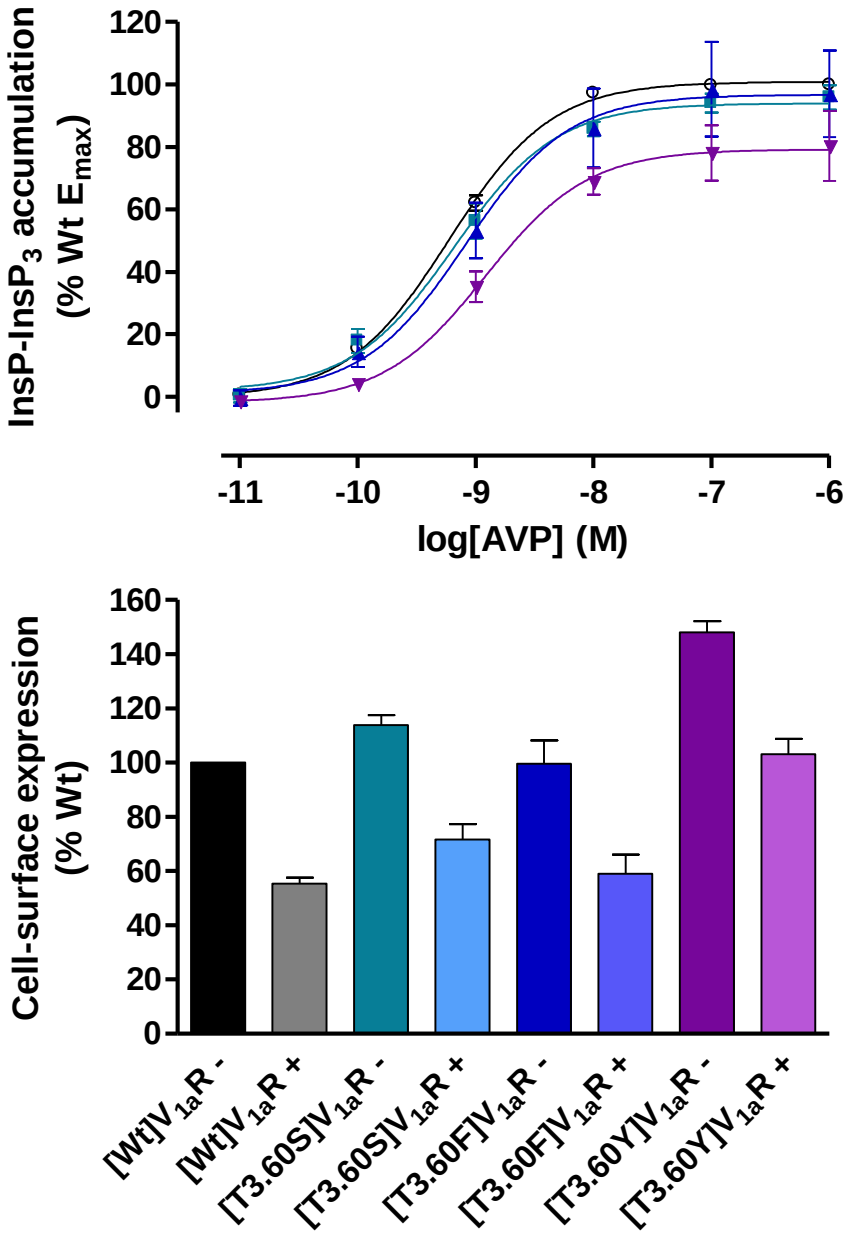

Figure 3.20 InsP-InsP$_3$ dose-response curves and cell-surface expression (+/- agonist challenge) of Thr$^{3.60}$ substitutions in V$_{1a}$R

Upper panel: Dose-response curves of inositol phosphates accumulation assays of HEK 293T cells, transiently transfected with receptor constructs [Wt]V$_{1a}$R, (○); [T3.60S]V$_{1a}$R, (■); [T3.60F]V$_{1a}$R, (▲) and [T3.60Y]V$_{1a}$R, (▼). Data are normalised to [Wt]V$_{1a}$R basal and maximal signalling levels, expressed as the mean ± s.e.m. of three experiments performed in triplicate. Basal signalling is plotted at 10^{-11} M. Lower panel: Cell-surface expression levels of receptor constructs were normalised to untransfected cells and unstimulated (-) [Wt]V$_{1a}$R expression levels. Data are stated as the mean ± s.e.m. of three experiments performed in triplicate. Stimulated (+) constructs were challenged by 10^{-7}M AVP for 30 min.

Receptor construct	Binding affinity, K_i (nM) ± s.e.m.		InsP-$InsP_3$ accumulation (% Wt E_{max}) ± s.e.m.			Cell-surface expression (% Wt unstimulated) ± s.e.m.	
	AVP	CA	Basal	EC_{50}*	E_{max}	Unstimulated	Stimulated
$V_{1a}R$	**0.45 ± 0.04**	**0.96 ± 0.10**	**0**	**0.60 ± 0.02**	**100**	**100**	**55 ± 2**
[T3.60S]$V_{1a}R$	0.85 ± 0.42	1.21 ± 0.09	0 ± 2	0.64 ± 0.10	96 ± 4	114 ± 4	72 ± 6
[T3.60F]$V_{1a}R$	0.44 ± 0.10	0.86 ± 0.11	0 ± 3	0.81 ± 0.09	99 ± 15	100 ± 9	59 ± 7
[T3.60Y]$V_{1a}R$	1.35 ± 0.25	2.18 ± 0.25	-1 ± 1	1.22 ± 0.07	80 ± 11	148 ± 4	103 ± 6

Table 3.6 Binding, signalling and cell-surface expression of $Thr^{3.60}$ substitutions in $V_{1a}R$

All data are shown as the mean ± s.e.m. of three separate experiments performed in triplicate. *EC_{50} is stated as the mean ± mean of 95 % confidence intervals of three separate experiments performed in triplicate. Data in yellow indicate >2.5-fold increase in K_i or EC_{50} or >25 % reduction in E_{max}, cell-surface expression; orange >5-fold increase in K_i or EC_{50} or >50 % reduction in E_{max}, cell-surface expression or internalisation; red >10-fold increase in K_i or EC_{50} or >75 % reduction in E_{max}, cell-surface expression or internalisation. Data in green indicate >2.5-fold increase in K_i or EC_{50} or >25 % increase in E_{max}, cell-surface expression or > 50% increase in internalisation. Data in white are comparable to Wt. # denotes IC_{50} ± mean of 95 % confidence intervals of constructs that bound ligand but K_i could not be calculated.

was agonist potency (Figure 3.20, Table 3.6). The construct was expressed at the cell surface at 148 % of Wt levels but generated a maximal signalling response of 80 % of Wt levels. All $Thr^{3.60}$ substitutions internalised a Wt-like proportion of receptor upon agonist stimulation.

3.2.4.2 Probing the role of residue 3.60 in ghrelin-R

The alanine residue of the ghrelin-R was mutated to the threonine residue present in the $V_{1a}R$ in addition to substitution by phenylalanine and tyrosine. [A3.60T]ghrelin-R, [A3.60F]ghrelin-R and [A3.60Y]ghrelin-R were all expressed at the cell surface at levels comparable to Wt (Figure 3.21, Table 3.7). All substitutions severely reduced the basal signalling capabilities of receptors to generate InsP-$InsP_3$. With only small aberrations in EC_{50} (< 3-fold increases) only the [A3.60Y]ghrelin-R displayed a marked decrease in maximal signalling levels, whereas [A3.60T]ghrelin-R and [A3.60F]ghrelin-R were essentially Wt.

3.2.5 Probing sequences associated with ICL 2 helical elements

Inspection of GPCR crystal structures reveals in general, it is the five residues downstream of $Pro^{3.57}$ that can adopt an α-helical conformation, $ICL2_H$ (Warne *et al.*, 2008; Chien *et al.*, 2010; Haga *et al.*, 2012; Manglik *et al.*, 2012; Wu *et al.*, 2012). Consequently, these residues in the $V_{1a}R$ were mutated to the corresponding residues of the β_2AR which has been shown to adopt a helical conformation (Rasmussen *et al.*, 2011a; Rasmussen *et al.*, 2011b) and the constitutively active ghrelin-R generating chimeric constructs [β_2AR-$ICL2_H$]$V_{1a}R$ and [ghrelin-R-$ICL2_H$]$V_{1a}R$ respectively (Figure 3.22). Each amino acid of the proposed helical region taken from ghrelin-R was also substituted individually into the $V_{1a}R$.

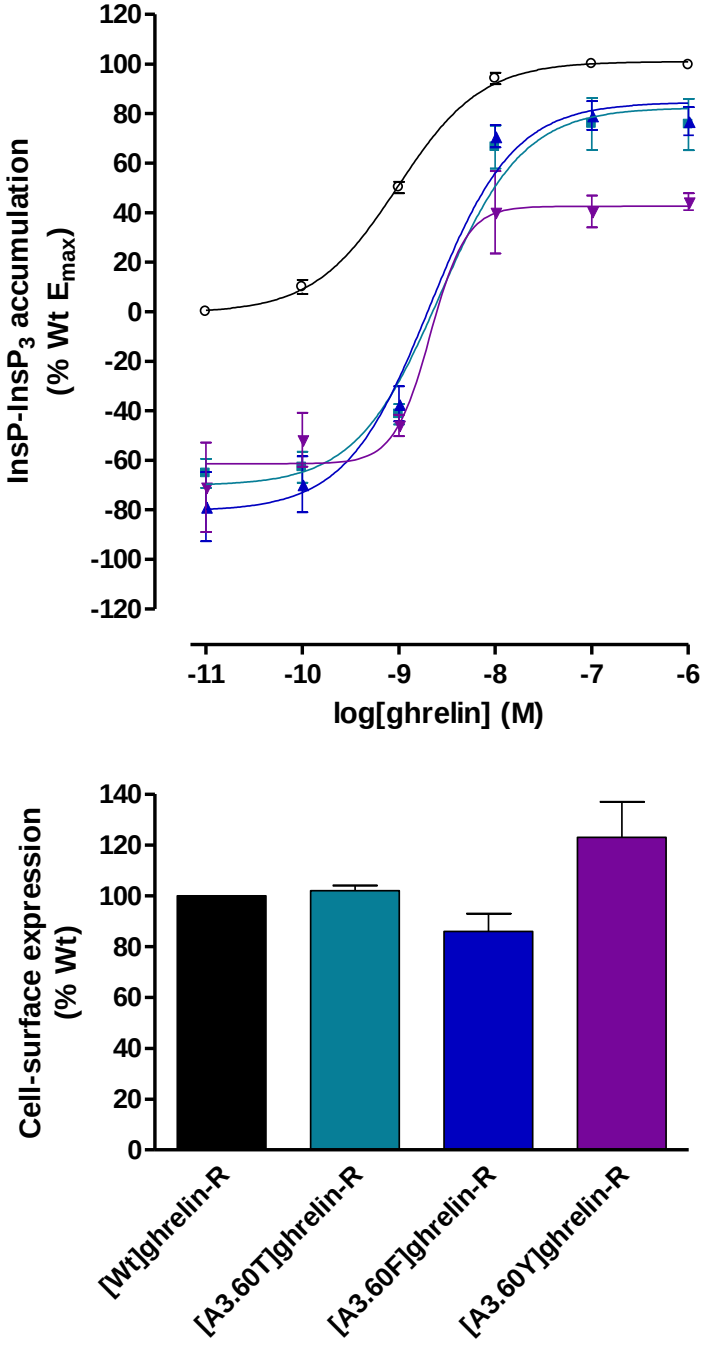

Figure 3.21 InsP-InsP$_3$ dose-response curves and cell-surface expression of Ala$^{3.60}$ substitutions in ghrelin-R

Upper panel: Dose-response curves of inositol phosphates accumulation assays of HEK 293T cells, transiently transfected with receptor constructs [Wt]ghrelin-R, (○); [A3.60T]ghrelin-R, (■); [A3.60F]ghrelin-R, (▲) and [A3.60Y]ghrelin-R, (▼). Data are normalised to basal and maximal signalling levels, expressed as the mean ± s.e.m. of three experiments performed in triplicate. Basal signalling is plotted at 10^{-11} M. Lower panel: Cell-surface expression levels of receptor constructs were normalised to untransfected cells and [Wt]ghrelin expression levels. Data are stated as the mean ± s.e.m. of three experiments performed in triplicate.

Receptor construct	InsP-InsP$_3$ accumulation (% Wt E_{max}) ± s.e.m.			Cell-surface expression (% Wt unstimulated) ± s.e.m.
	Basal	EC_{50}*	E_{max}	
ghrelin-R	**0**	**0.97 ± 0.03**	**100**	**100**
[A3.60T]ghrelin-R	-69 ± 3	2.71 ± 0.01	83 ± 4	102 ± 2
[A3.60F]ghrelin-R	-80 ± 3	2.11 ± 0.61	85 ± 3	86 ±7
[A3.60Y]ghrelin-R	-71 ± 18	2.03 ± 0.25	44 ± 3	123 ± 14

Table 3.7 Binding, signalling and cell-surface expression of Ala$^{3.60}$ substitutions in ghrelin-R

All data are shown as the mean ± s.e.m. of three separate experiments performed in triplicate. *EC_{50} is stated as the mean ± mean of 95 % confidence intervals of three separate experiments performed in triplicate. Data in yellow indicate >2.5-fold increase in EC_{50} or >25 % reduction in basal signalling, E_{max} or cell-surface expression; orange >5-fold increase in EC_{50} or >50 % reduction in basal signalling, E_{max} or cell-surface expression; red >10-fold increase in EC_{50} or >75 % reduction in basal signalling, E_{max} or cell-surface expression. Data in green indicate >2.5-fold increase in EC_{50} or >25 % increase in basal signalling, E_{max} or cell-surface expression. Data in white are comparable to Wt.

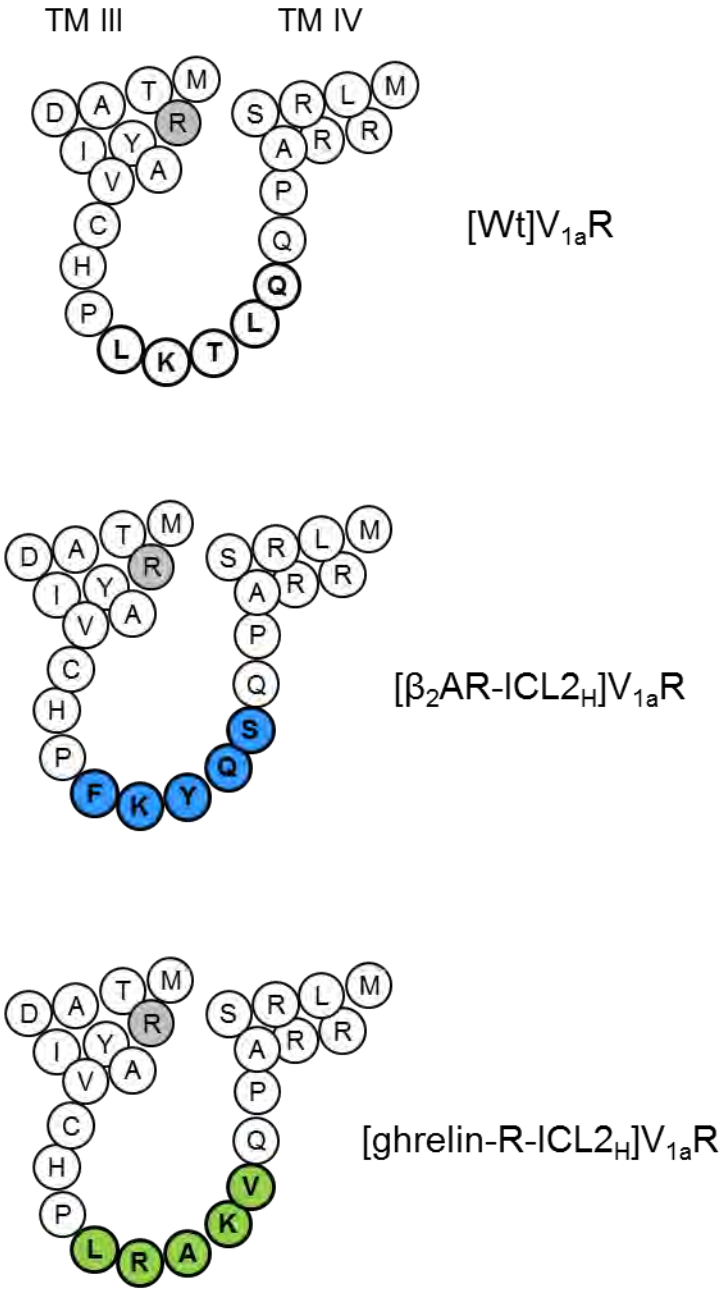

Figure 3.22 Sequences of chimeric receptor constructs

(Top-bottom) ICL 2 sequences of [Wt]V_{1a}R, [β_2AR-ICL2$_H$]V_{1a}R and [ghrelin-R-ICL2$_H$]V_{1a}R constructs. Residues corresponding to α-helical portions of ICL 2 are shown in bold. B2AR and ghrelin-R sequences corresponding to ICL2$_H$ portions are shown in blue and green respectively.

3.2.5.1 Chimeric substitutions of $V_{1a}R$ $ICL2_H$

[β_2AR-$ICL2_H$]$V_{1a}R$ and [ghrelin-R-$ICL2_H$]$V_{1a}R$ bound both AVP and CA with Wt-like binding affinities (Figure 3.23, Table 3.8). [β_2AR-$ICL2_H$]$V_{1a}R$ displayed a Wt-like signalling properties through the inositol phosphate pathway while [ghrelin-R-$ICL2_H$]$V_{1a}R$ exhibited an increased maximal signalling response, 158 % of Wt (Figure 3.24, Table 3.8). Both receptor constructs displayed reduced ability to internalise upon agonist challenge ([β_2AR-$ICL2_H$]$V_{1a}R$, 19 %; [ghrelin-R-$ICL2_H$]$V_{1a}R$, 17 %; Wt, 45 % of unstimulated expression).

3.2.5.2 Individual amino acid substitutions of the ghrelin-R $ICL2_H$ sequence into $V_{1a}R$

$Leu^{3.58}$ is present in both receptors and the T3.60A substitution has been discussed previously. The constructs [K3.59R]$V_{1a}R$, [L3.61K]$V_{1a}R$ and [Q3.62V]$V_{1a}R$ recapitulate amino acids of the ghrelin-R into the $V_{1a}R$.

[K3.59R]$V_{1a}R$ and [Q3.62V]$V_{1a}R$ maintained Wt-like binding affinities for AVP and CA while [L3.61K]$V_{1a}R$ displayed 3-fold decreased affinities for both ligands (Figure 3.25, Table 3.9). The signalling capabilities of all constructs were Wt-like as were the level of cell-surface expression (Figure 3.26, Table 3.9). [K3.59R]$V_{1a}R$, [L3.61K]$V_{1a}R$ and [Q3.62V]$V_{1a}R$ internalised at Wt-like levels upon agonist challenge.

3.2.6 Further substitution of amino acids of ghrelin-R into the $V_{1a}R$

The region preceeding the proposed helical portion of ICL 2 is reasonably similar between the ghrelin-R and $V_{1a}R$ with the exception of postions 3.52 and 3.56. Therefore, the constructs [I3.52F]$V_{1a}R$ and [H3.56F]$V_{1a}R$ were generated. These substitutions yielded constructs that displayed Wt-like pharmacological and signalling properties (Figure 3.27-3.28, Table 3.10).

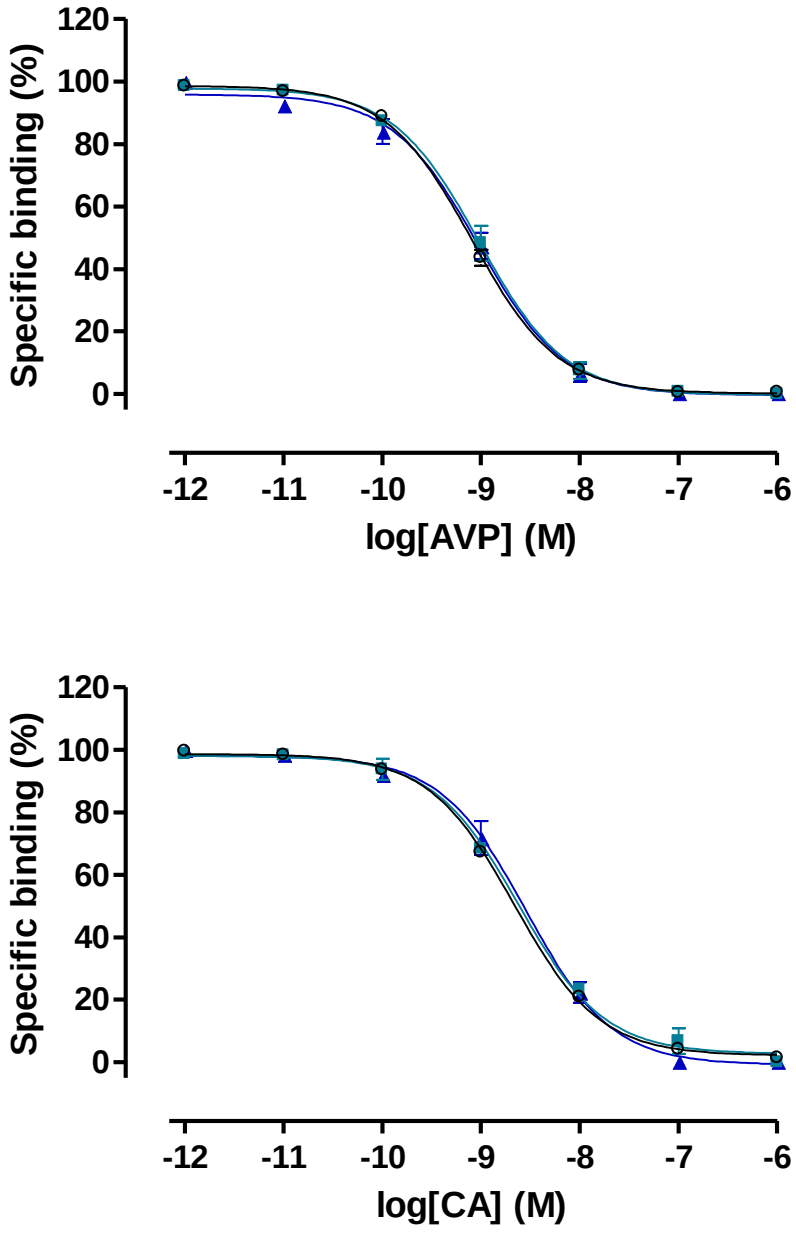

Figure 3.23 Competition radioligand binding curves of chimeric $ICL2_H$ $V_{1a}R$ constructs

Competition radioligand binding assays were performed on HEK 293T cells, transiently transfected with receptor constructs [Wt]$V_{1a}R$, (○); [β_2AR-$ICL2_H$]$V_{1a}R$, (■) and [ghrelin-R-$ICL2_H$]$V_{1a}R$, (▲). Upper panel: [^{3}H]AVP vs AVP competition; lower panel: [^{3}H]AVP vs CA competition. A theoretical Langmuir binding isotherm was fitted to data expressed as specific binding (%), defining non-specific binding by 1 μM ligand. Data are the mean ± s.e.m. of three experiments performed in triplicate.

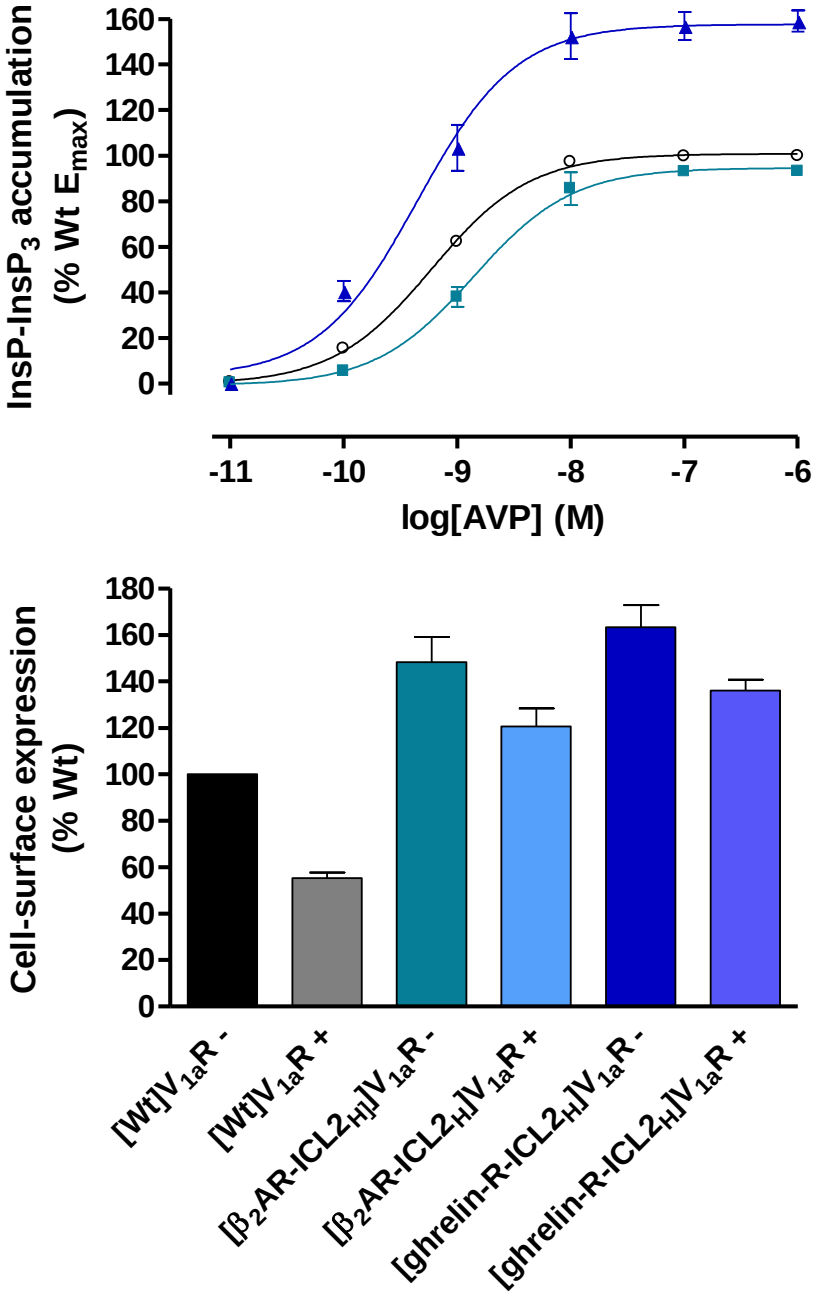

Figure 3.24 InsP-InsP$_3$ dose-response curves and cell-surface expression (+/- agonist challenge) of chimeric ICL2$_H$ V$_{1a}$R constructs

Upper panel: Dose-response curves of inositol phosphates accumulation assays of HEK 293T cells, transiently transfected with receptor constructs [Wt]$V_{1a}R$, (○); [β_2AR-ICL2$_H$]$V_{1a}R$, (■); and [ghrelin-R-ICL2$_H$]$V_{1a}R$, (▲). Data are normalised to [Wt]$V_{1a}R$ basal and maximal signalling levels, expressed as the mean ± s.e.m. of three experiments performed in triplicate. Basal signalling is plotted at 10^{-11} M. Lower panel: Cell-surface expression levels of receptor constructs were normalised to untransfected cells and unstimulated (-) [Wt]$V_{1a}R$ expression levels. Data are stated as the mean ± s.e.m. of three experiments performed in triplicate. Stimulated (+) constructs were challenged by 10^{-7}M AVP for 30 min.

Receptor construct	Binding affinity, K_i (nM) ± s.e.m.		InsP-$InsP_3$ accumulation (% Wt E_{max}) ± s.e.m.			Cell-surface expression (% Wt unstimulated) ± s.e.m.	
	AVP	CA	Basal	EC_{50}*	E_{max}	Unstimulated	Stimulated
$V_{1a}R$	**0.45 ± 0.04**	**0.96 ± 0.10**	**0**	**0.60 ± 0.02**	**100**	**100**	**55 ± 2**
[β_2AR-$ICL2_H$]$V_{1a}R$	0.78 ± 0.19	1.35 ± 0.17	0 ± 2	1.41 ± 0.11	93 ± 2	148 ± 11	120 ± 8
[ghrelin-R-$ICL2_H$]$V_{1a}R$	0.74 ± 0.14	1.96 ± 0.84	0 ± 0	0.43 ± 0.09	159 ± 5	163 ± 10	136 ± 5

Table 3.8 Binding, signalling and cell-surface expression of chimeric $ICL2_H$ $V_{1a}R$ constructs

All data are shown as the mean ± s.e.m. of three separate experiments performed in triplicate. *EC_{50} is stated as the mean ± mean of 95 % confidence intervals of three separate experiments performed in triplicate. Data in yellow indicate >2.5-fold increase in K_i or EC_{50} or >25 % reduction in E_{max}, cell-surface expression; orange >5-fold increase in K_i or EC_{50} or >50 % reduction in E_{max}, cell-surface expression or internalisation; red >10-fold increase in K_i or EC_{50} or >75 % reduction in E_{max}, cell-surface expression or internalisation. Data in green indicate >2.5-fold increase in K_i or EC_{50} or >25 % increase in E_{max}, cell-surface expression or > 50% increase in internalisation. Data in white are comparable to Wt. # denotes IC_{50} ± mean of 95 % confidence intervals of three separate experiments performed in triplicate.

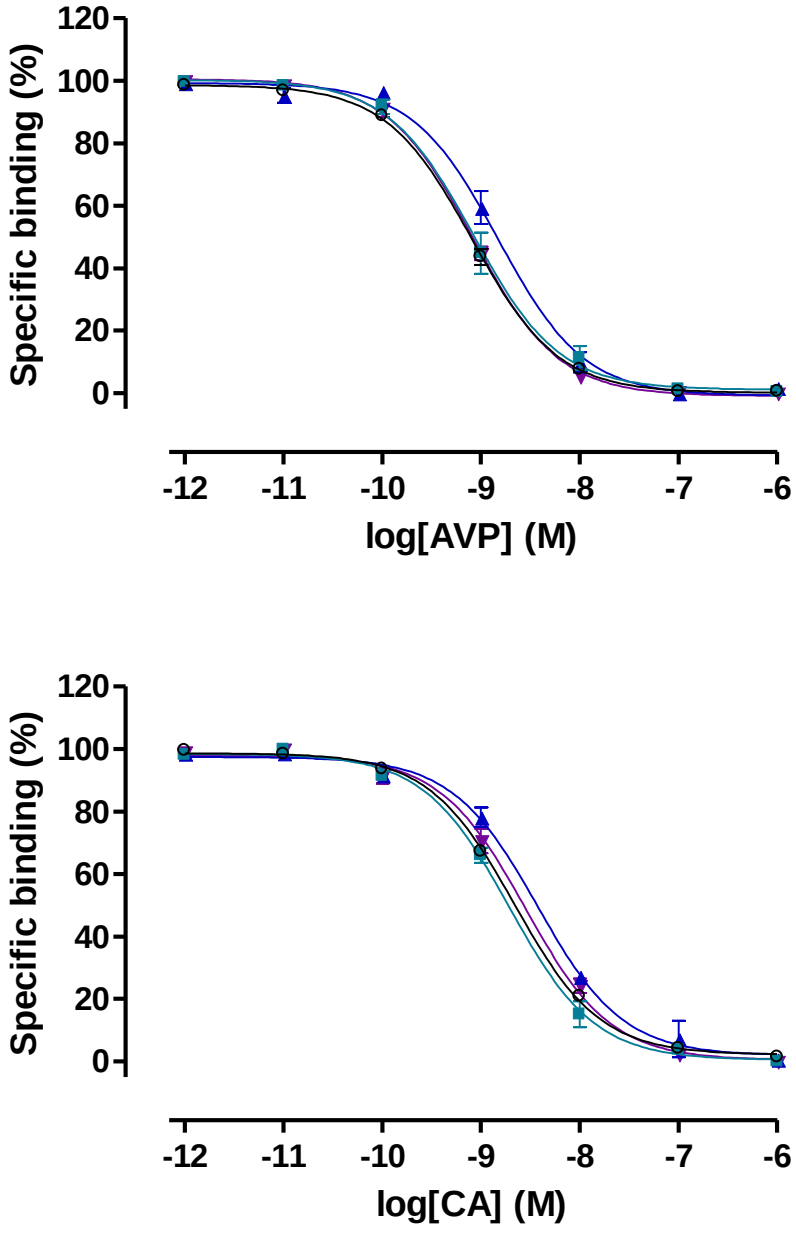

Figure 3.25 Competition radioligand binding curves of ghrelin $ICL2_H$ residues in the $V_{1a}R$

Competition radioligand binding assays were performed on HEK 293T cells, transiently transfected with receptor constructs [Wt]$V_{1a}R$, (○); [K3.59R]$V_{1a}R$, (■); [L3.61K]$V_{1a}R$, (▲) and [Q3.62V]$V_{1a}R$, (▼). Upper panel: [^{3}H]AVP vs AVP competition; lower panel: [^{3}H]AVP vs CA competition. A theoretical Langmuir binding isotherm was fitted to data expressed as specific binding (%), defining non-specific binding by 1 μM ligand. Data are the mean ± s.e.m. of three experiments performed in triplicate.

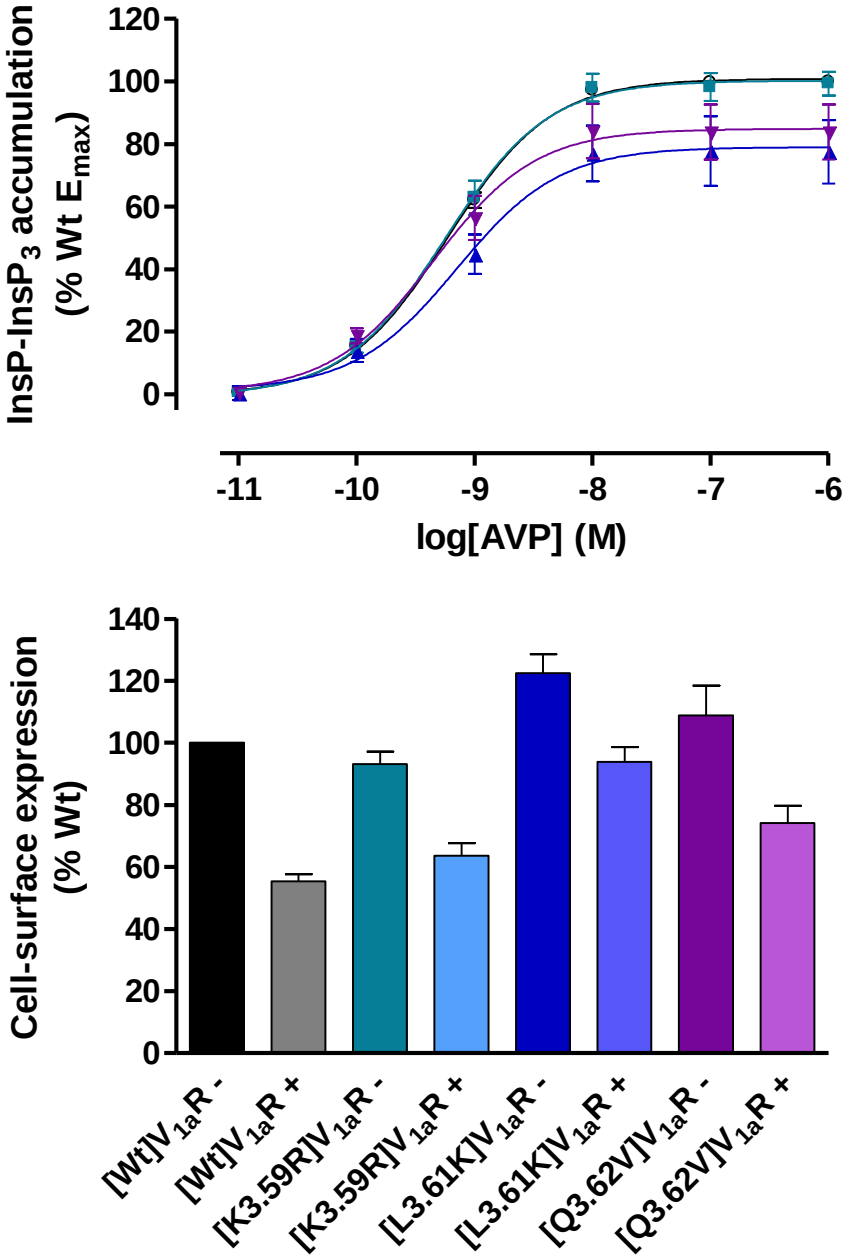

Figure 3.26 InsP-InsP$_3$ dose-response curves and cell-surface expression (+/- agonist challenge) of ghrelin ICL2$_H$ residues in the V$_{1a}$R

Upper panel: Dose-response curves of inositol phosphates accumulation assays of HEK 293T cells, transiently transfected with receptor constructs [Wt]V$_{1a}$R, (○); [K3.59R]V$_{1a}$R, (■); [L3.61K]V$_{1a}$R, (▲) and [Q3.62V]V$_{1a}$R, (▼). Data are normalised to [Wt]V$_{1a}$R basal and maximal signalling levels, expressed as the mean ± s.e.m. of three experiments performed in triplicate. Basal signalling is plotted at 10^{-11} M. Lower panel: Cell-surface expression levels of receptor constructs were normalised to untransfected cells and unstimulated (-) [Wt]V$_{1a}$R expression levels. Data are stated as the mean ± s.e.m. of three experiments performed in triplicate. Stimulated (+) constructs were challenged by 10^{-7}M AVP for 30 min.

Receptor construct	Binding K_i (nM) ± s.e.m.		InsP-$InsP_3$ accumulation (% Wt E_{max}) ± s.e.m.			Cell-surface expression (% $_I$Wt unstimulated) ± s.e.m.	
	AVP	CA	Basal	EC_{50}*	E_{max}	Unstimulated	Stimulated
[Wt]V_{1a}R	**0.45 ± 0.04**	**0.96 ± 0.10**	**0**	**0.60 ± 0.02**	**100**	**100**	**55 ± 2**
[K3.59R]V_{1a}R	0.77 ± 0.24	1.46 ± 0.26	1 ± 1	0.57 ± 0.05	99 ± 4	93 ± 4	64 ± 4
[L3.61K]V_{1a}R	1.45 ± 0.32	3.47 ± 0.37	0 ± 2	0.69 ± 0.11	78 ± 11	122 ± 6	94 ± 5
[Q3.62V]V_{1a}R	0.68 ± 0.06	2.26 ± 0.49	1 ± 1	0.45 ± 0.07	84 ± 9	109 ± 10	74 ± 6

Table 3.9 Binding, signalling and cell-surface expression of ghrelin $ICL2_H$ residues in the V_{1a}R

All data are shown as the mean ± s.e.m. of three separate experiments performed in triplicate. *EC_{50} is stated as the mean ± mean of 95 % confidence intervals of three separate experiments performed in triplicate. Data in yellow indicate >2.5-fold increase in K_i or EC_{50} or >25 % reduction in E_{max}, cell-surface expression; orange >5-fold increase in K_i or EC_{50} or >50 % reduction in E_{max}, cell-surface expression or internalisation; red >10-fold increase in K_i or EC_{50} or >75 % reduction in E_{max}, cell-surface expression or internalisation. Data in green indicate >2.5-fold increase in K_i or EC_{50} or >25 % increase in E_{max}, cell-surface expression or > 50% increase in internalisation. Data in white are comparable to Wt. # denotes IC_{50} ± mean of 95 % confidence intervals of constructs that bound ligand but K_i could not be calculated.

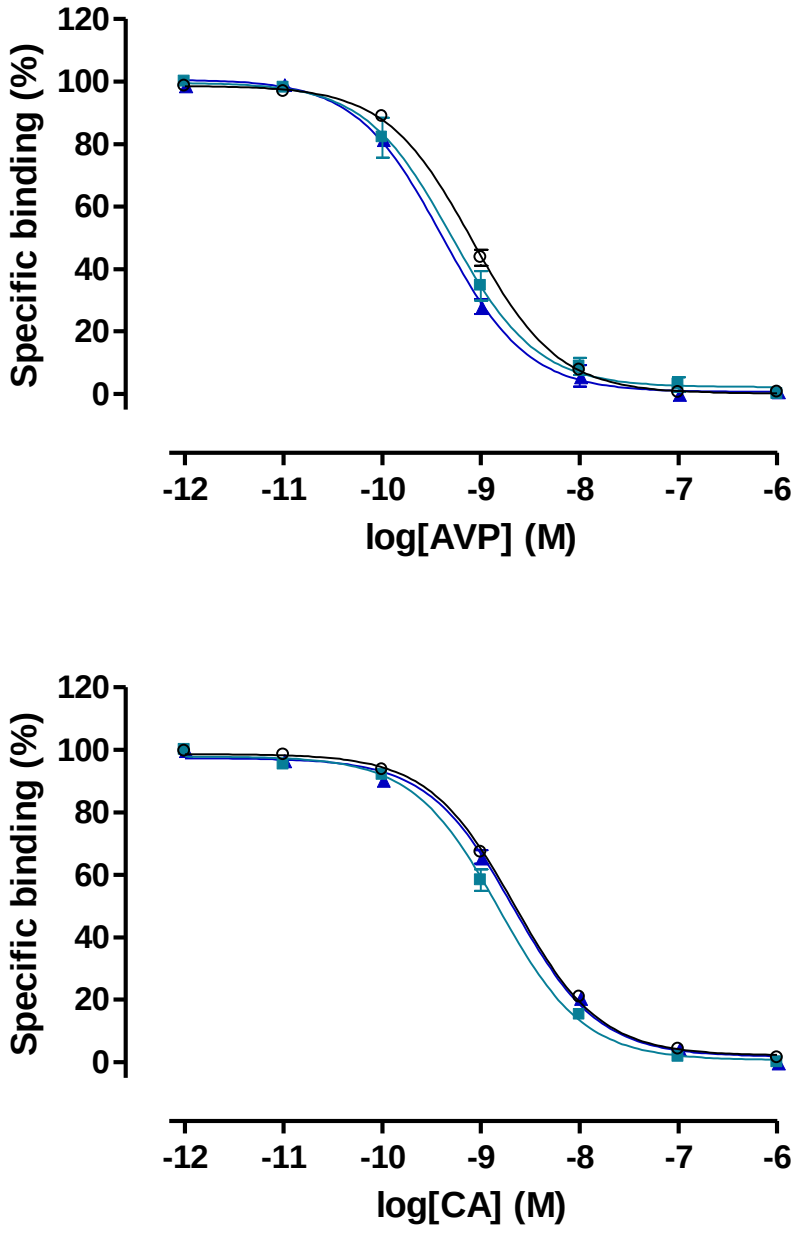

Figure 3.27 Competition radioligand binding curves of ghrelin-R-like amino acid substitutions in $V_{1a}R$

Competition radioligand binding assays were performed on HEK 293T cells, transiently transfected with receptor constructs [Wt]$V_{1a}R$, (○); [I3.52F]$V_{1a}R$, (■) and [H3.56F]$V_{1a}R$. Upper panel: [^{3}H]AVP vs AVP competition; lower panel: [^{3}H]AVP vs CA competition. A theoretical Langmuir binding isotherm was fitted to data expressed as specific binding (%), defining non-specific binding by 1 μM ligand. Data are the mean ± s.e.m. of three experiments performed in triplicate.

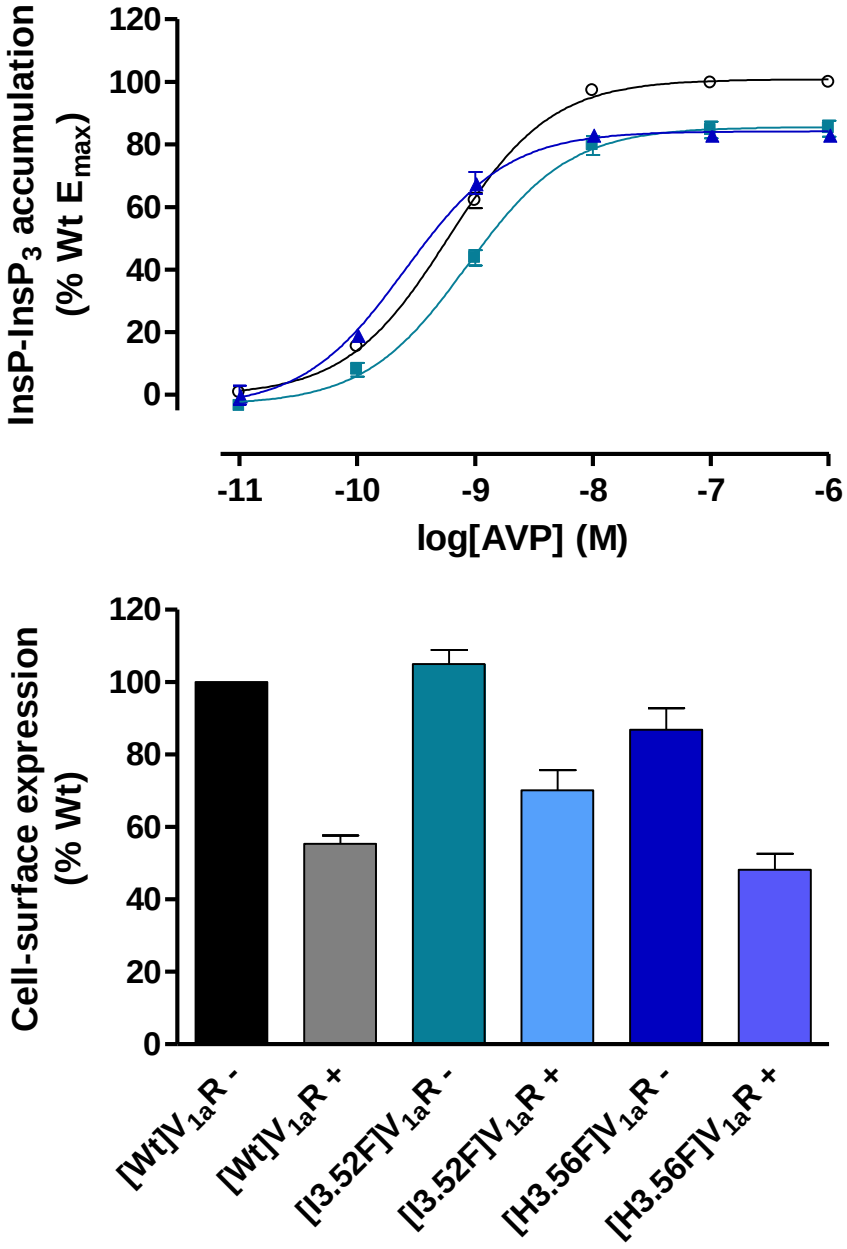

Figure 3.28 InsP-InsP$_3$ dose-response curves and cell-surface expression (+/- agonist challenge) of ghrelin-R-like amino acid substitutions in $V_{1a}R$

Upper panel: Dose-response curves of inositol phosphates accumulation assays of HEK 293T cells, transiently transfected with receptor constructs [Wt]$V_{1a}R$, (○); [I3.52F]$V_{1a}R$, (■) and [H3.56F]$V_{1a}R$, (▲). Data are normalised to [Wt]$V_{1a}R$ basal and maximal signalling levels, expressed as the mean ± s.e.m. of three experiments performed in triplicate. Basal signalling is plotted at 10^{-11} M. Lower panel: Cell-surface expression levels of receptor constructs were normalised to untransfected cells and unstimulated (-) [Wt]$V_{1a}R$ expression levels. Data are stated as the mean ± s.e.m. of three experiments performed in triplicate. Stimulated (+) constructs were challenged by 10^{-7}M AVP for 30 min.

Receptor construct	Binding affinity, K_i (nM) ± s.e.m.		InsP-$InsP_3$ accumulation (% Wt E_{max}) ± s.e.m.			Cell-surface expression (% Wt unstimulated) ± s.e.m.	
	AVP	CA	Basal	EC_{50}*	E_{max}	Unstimulated	Stimulated
[Wt]V_{1a}R	**0.45 ± 0.04**	**0.96 ± 0.10**	**0**	**0.60 ± 0.02**	**100**	**100**	**55 ± 2**
[I3.52F]V_{1a}R	0.36 ± 0.06	0.71 ± 0.20	-4 ± 1	0.86 ± 0.06	85 ± 3	105 ± 4	70 ± 6
[H3.56F]V_{1a}R	0.24 ± 0.09	0.63 ± 0.14	0 ± 3	0.27 ± 0.03	83 ± 2	87 ± 6	48 ± 4

Table 3.10 Binding, signalling and cell-surface expression of ghrelin-R-like amino acid substitutions in V_{1a}R

All data are shown as the mean ± s.e.m. of three separate experiments performed in triplicate. *EC_{50} is stated as the mean ± mean of 95 % confidence intervals of three separate experiments performed in triplicate. Data in yellow indicate >2.5-fold increase in K_i or EC_{50} or >25 % reduction in E_{max}, cell-surface expression; orange >5-fold increase in K_i or EC_{50} or >50 % reduction in E_{max}, cell-surface expression or internalisation; red >10-fold increase in K_i or EC_{50} or >75 % reduction in E_{max}, cell-surface expression or internalisation. Data in green indicate >2.5-fold increase in K_i or EC_{50} or >25 % increase in E_{max}, cell-surface expression or > 50% increase in internalisation. Data in white are comparable to Wt. # denotes IC_{50} ± mean of 95 % confidence intervals of constructs that bound ligand but K_i could not be calculated.

Cell-surface expression levels were comparable to [Wt]V_{1a}R and the proportion of receptors internalised upon agonist challenge Wt-like for both receptor constructs.

3.3 Discussion

3.3.1 The role of amino acids in the amino portion of ICL 2 in the V_{1a}R

Overall, these data provide much insight into the role of ICL 2 in the structure and function of the V_{1a}R. Substitution of residues to alanine in the amino-portion of ICL 2 was the most sensitive to reducing expression at the cell surface. This suggests that $Ile^{3.52}$, $Ala^{3.53}$, $Val^{3.54}$, $Cys^{3.55}$, $His^{3.56}$, $Pro^{3.57}$ and $Lys^{3.59}$ all contribute to the expression level of the V_{1a}R, presumably though contributing stability through their side chains that cannot be provided by the methyl group of alanine. This region in the CB_1R has previously been scanned by alanine mutagenesis but with less disruption to cell surface expression (Chen *et al.*, 2010). Additionally, I3.52A, C3.55A, P3.57A and K3.59A substitutions generated a receptor constructs that display an increased tendency to internalise upon agonist stimulation. The [I3.52A]V_{1a}R construct displayed a 4-fold increase in AVP affinity which is probably the cause of the 2-fold increase in agonist potency in generating InsP-$InsP_3$. Cell-surface expression levels were 'rescued' by the substitution of the corresponding residue observed in the ghrelin-R in the constructs [I3.52F]V_{1a}R and [H3.56F]V_{1a}R. These substitutions also recovered the signalling characteristics of the V_{1a}R, restoring the increased potency of [I3.52F]V_{1a}R and decreased potency of [H3.56F]V_{1a}R to Wt-like levels. It is noteworthy that no increase in basal activity was observed in the V_{1a}R when corresponding ghrelin-R residues were introduced, indicating that these residues alone are not sufficient to confer constitutive activity. Together these data indicate the importance of side chain volume – greater than that of alanine – at positions 3.52 and 3.56 in maintaining cell-surface expression. However, in the prokineticin-2 (PKR2) receptor, co-immunoprecipitation experiments indicated that $His^{3.56}$ is

not necessary for interaction with G-protein (Peng *et al.*, 2011), as supported by these data given that [H3.56A]$V_{1a}R$ could still signal though the inositol-phosphate pathway.

[A3.53G]$V_{1a}R$ was expressed less than Wt at the cell surface but the decrease in E_{max} was greater than the decrease in expression. This apparent decrease in efficacy may be due to the added flex introduced into the peptide backbone conferred by the glycine substitution. An isoleucine, leucine, valine or phenylalanine residue occurs at position 3.54 in 98 % of rhodopsin-like GPCRs (Marion *et al.*, 2006), highlighting the importance of the $Val^{3.54}$ in the $V_{1a}R$. Substitution to alanine in the [V3.54A]$V_{1a}R$ construct resulted in a ~10-fold decrease in AVP potency and decreased efficacy in generating InsP-$InsP_3$ establishing that alanine cannot substitute for this group conservation. Alanine-substitution of neighbouring resides $Ile^{3.52}$ and $Cys^{3.55}$ reduced cell-surface expression to ~50 % of Wt but displayed 50 % and 67 % of Wt E_{max} respectively. Given that [A3.53G]$V_{1a}R$ and [V3.54A]$V_{1a}R$ expressed at 49 % and 37 % of Wt but signalled at 24 % and 17 % of Wt E_{max} respectively, their reduced efficacy in generating InsP-$InsP_3$ is clearly not due to simply a reduction in cell-surface expression. The crystal structure of β_2AR in complex with G_s (Rasmussen *et al.*, 2011b) indicates that residues $Ala^{3.53}$ and $Val^{3.54}$ do not form direct contacts with the G-protein so their substitution may affect the ability of the receptor to adopt an active conformation. This region has been previously implicated in contributing to the ability of the receptor to adopt an active state together with other ICL 2 residues. In the follicle-stimulating hormone receptor (FSHR), agonist-induced cAMP accumulation was abolished despite proper expression upon the introduction of an alanine residue in place of the native $Thr^{3.53}$ (Nakamura *et al.*, 1998; Timossi *et al.*, 2002).

3.3.2 The role of $Pro^{3.57}$-$Leu^{3.58}$ in the $V_{1a}R$

Alanine and leucine substitution of $Pro^{3.57}$ are able to maintain Wt-like pharmacology and signalling capabilities through the inositol phosphate pathway. However, either substitution leads to a reduction in expression of $V_{1a}R$ at the cell-surface. In contrast the P3.57A substitution in the $AT_{1a}R$ maintained agonist binding, E_{max} was reduced to ~60 % of Wt while cell-surface expression was Wt-like (Gaborik *et al.*, 2003). As in the $V_{1a}R$, the [P3.57A]ghrelin-R maintained near-Wt signalling capabilities with a only slight reduction in agonist-independent signalling. In contrast, substitution to leucine generated a ghrelin-R that completely ablated both basal and agonist-induced InsP-$InsP_3$ accumulation. This is not due to reduced cell-surface expression given that the [P3.57L]ghrelin-R and [P3.57A]ghrelin-R constructs expressed at similar levels. Therefore in the $V_{1a}R$ which possesses little constitutive activity, an alanine or leucine residue can maintain the role of the native $Pro^{3.57}$ albeit with a reduced maximal signalling capability as a result of reduced cell-surface expression. However, although the P3.57A substitution in the ghrelin-R is well tolerated, the leucine substitution (uncommon at position 3.57 in rhodopsin-like GPCRs) completely prevented both basal and agonist-induced inositol phosphates accumulation. $Pro^{3.57}$ has been implicated in G_q coupling in the $5HT_{2c}R$ whereby under basal conditions, a 4-fold decrease in co-immunoprecipitation of receptor and G-protein was observed when a P3.57A substitution was introduced compared to Wt (Marion *et al.*, 2006)

The reduced efficacy of non-conservative substitutions of $Leu^{3.58}$ is has been reported for other GPCRs (Moro *et al.*, 1993; Gaborik *et al.*, 2003; Ulloa-Aguirre *et al.*, 2007; Wacker *et al.*, 2008; Chen *et al.*, 2010) whilst maintaining cell-surface expression. The hydrophobic residue at position 3.58 promotes GDP-GTP exchange (Wacker *et al.*, 2008) and is supported by the structure of β_2AR in its G-protein-interacting conformation where it interacts with the

P-loop of the G-protein (Rasmussen *et al.*, 2011b). This may be supported by findings in the $V_{1a}R$ given that substitution to both alanine and serine severely reduced AVP efficacy through the inositol phosphate pathway. Agonist-induced internalisation was prevented by L3.58A in the M_1R (Lechleiter *et al.*, 1990) but this was not observed in the $V_{1a}R$ for alanine substitution, at least after 30 minutes of AVP stimulation. [L3.58A]ghrelin-R construct replicates these signalling impairments, displaying a reduction in both basal and maximal signalling levels. Additionally, the increase in cell-surface expression is consistent with a loss in the ability to internalise given that the ghrelin-R undergoes constitutive internalisation (Kendrick, PhD thesis, University of Birmingham 2010). The L3.58M substitution in the $V_{1a}R$ retained Wt functionality in all respects, further highlighting the absolute requirement of a bulky, hydrophobic residue at the locus 3.58.

3.3.3 The role of putative $ICL2_H$ residues in the $V_{1a}R$

The ICL 2 amino acid sequences of the chimeric receptor constructs [β_2AR-$ICL2_H$]$V_{1a}R$ and [ghrelin-R-$ICL2_H$]$V_{1a}R$ are shown in Figure 3.22. Substitution of ICL2 by corresponding residues of β_2AR or ghrelin-R increased $V_{1a}R$ expression by a similar amount. Interestingly, the $ICL2_H$ region of the G_s-coupled GPCR, β_2AR demonstrated no detrimental effect on InsP-$InsP_3$ signalling but the substitution of ghrelin-R $ICL2_H$ residues increased E_{max}. This being said, the increase in the [ghrelin-R-$ICL2_H$]$V_{1a}R$ construct may be due to increased efficacy of AVP. Both receptor constructs drastically reduced the proportion of receptor internalised upon agonist challenge indicating that the ICL 2 sequence $Leu^{3.58}Lys^{3.59}Thr^{3.60}Leu^{3.61}Gln^{3.62}$ together is important in modulating internalisation in the $V_{1a}R$. Although it cannot be suggested that these residues are, or are not, adopting an α-helical conformation, it has previously been suggested that the ability to adopt an α-helix is associated with an ability to interact with β-arrestins (Shan *et al.*, 2010).

Comparison of known crystal structures indicates that, $Leu^{3.58}$ in the $V_{1a}R$ is the first residue proposed to be capable of adopting an α-helical conformation. Alanine substitutions of $Thr^{3.60}$ and $Gln^{3.62}$ indicated that neither residue is specifically involved in the intracellular signal generation or cell-surface expression of the $V_{1a}R$. Introducing the ghrelin-like valine at position 3.62 maintained Wt-like receptor function. $Lys^{3.59}$ plays a minor role in receptor stability, trafficking or folding given that the alanine substitution was expressed at a lesser extent at the cell surface. The reduced E_{max} can be accounted for by this reduced expression, although the decreased AVP potency in InsP-$InsP_3$ generation was also observed. Wt inositol phosphate accumulation and cell-surface expression was recovered by the ghrelin-like substitution K3.59R. Together these data indicate the importance of a basic residue at this locus for cell-surface expression and InsP-$InsP_3$ accumulation in the $V_{1a}R$. However, this may not be true of GPCRs in general as the loss of the basic character at position 3.59 conferred by the [R3.59A]ghrelin-R construct yielded a Wt-like signalling and cell-surface expression indicating that the ghrelin-R is not sensitive to amino acid changes at 3.59. Substitution of $Thr^{3.60}$ to alanine, serine or phenylalanine maintained Wt-like functionality of the $V_{1a}R$ in all respects. However substitution to the amine-like $Tyr^{3.60}$ increased cell-surface expression and decreased the affinity of AVP agonist 3-folds. Given that a large proportion of $V_{1a}R$ adopt an inactive state without agonist stimulation and the decrease in agonist affinity, it is likely the T3.60Y substitution is stabilising an inactive conformation. A small residue that is incapable of forming hydrogen bonds is required at position 3.60 to maintain constitutive activity in the ghrelin-R. When substituted for serine (may hydrogen bond), phenylalanine (bulky) or tyrosine (bulky and may hydrogen bond) a decreased basal activity was observed. However hydrogen bond or bulk alone is not enough to reduce the E_{max} of ghrelin-R but contribution of both in [A3.60Y]ghrelin-R decreased ghrelin-induced signalling markedly although the

construct was well expressed. Together, substitution of 3.60 to amine ligand-GPCR tyrosine residue in the peptide-ligand GPCRs provides inactivating effects.

3.3.4 The role ICL 2 residues downstream of putative $ICL2_H$ in the $V_{1a}R$

Q3.63A demonstrates a slight decreased efficacy of AVP in generating InsP-$InsP_3$ although the maximum signalling capabilities are increased compared to Wt implicating the glutamine side chain in signal transduction. The P3.64A substitution would relieve the constrained orientation of the peptide backbone provided by Pro3.64 in the $V_{1a}R$. The loss of receptor expression indicates that the restricted torsion angle of the N-Cα bond of proline is absolutely required to maintain the integrity of the $V_{1a}R$. This particular conformation may be essential in maintaining the relative orientation of ICL 2 with respect to TM IV. $Ser^{3.68}$ contributes to the level of expression of the $V_{1a}R$ at the cell surface as substitution to alanine substantially increased expression. Given that this residue is potentially positioned in TM IV the replacement of serine for alanine is more preferable in an α-helical conformation as substitution removes the serine hydroxyl group which may disrupt the stability of the helix.

Removal of arginine residues at the ICL 2-TM IV interface by alanine substitution decreases the basic character in this area. Fewer arginine residues at position results in decreased cell-surface expression and consequently maximal signalling capabilities. This loss in cell-surface expression may be due to the reduction of interaction of the arginine residues with membrane lipids such as cholesterol as suggested previously (Hanson *et al.*, 2008). Interestingly, double and single alanine substitutions produced apparent increased affinities for AVP and CA while the triple mutant construct, substituting all arginine residues maintained Wt-like pharmacology. However, in general, it is clear that basic character at the ICL2-TM IV interface is essential to maintain the cell-surface expression and integrity of $V_{1a}R$.

CHAPTER 4: INTERACTIONS OF HYDROPHOBIC BARRIER RESIDUES IN THE $V_{1A}R$

4.1 Introduction

Upon agonist binding to a GPCR, receptor activation is transmitted to the intracellular face to initiate the appropriate signalling cascades. This activation is conferred by the rearrangement of intramolecular interactions stabilising an inactive state. One such rearrangement is the 'global toggle switch' whereby the kink of TMVI is modulated by $Trp^{6.48}$. The decreased bend-angle of the proline-induced kink straightens TMVI, moving it away from TMIII (Shi *et al.*, 2002; Ruprecht *et al.*, 2004; Schwartz *et al.*, 2006) accompanied by a rotation of TM VI. However GPCR crystal structures suggest that a less drastic rearrangement of $Trp^{6.48}$ accompanies the rotation and outward movement of TM VI relative to TM III to expose a G-protein binding site. In a subset of rhodopsin-like GPCRs, exposure of G-protein binding epitopes requires the breakage of the ionic interactions between $Asp/Glu^{3.49}$-$Arg^{3.50}$ and consequently an interhelical ionic bond between $Arg^{3.50}$ and $Glu^{6.30}$. Preventing the $Arg^{3.50}$-$Glu^{6.30}$ interaction by mutagenesis of the β_2AR resulted in CAMs, implicating the interactions in maintaining an inactive state (Ballesteros *et al.*, 2001). Although not all GPCRs possess the appropriate residues to maintain an 'ionic lock' interaction, the outward movement of TM VI relative to TM III is generally accepted as a requirement to allow G-protein interaction.

Positioned near the membrane-cytosolic boundary are residues that are implicated in stabilising an inactive receptor conformation. In opsin and H_1R, mutation of the residue at position $^{6.40}$ has been show to modulate constitutive activity of the receptors depending on the substitution introduced (Han *et al.*, 1998; Bakker *et al.*, 2008). A L6.40Q polymorphism in the melanocortin-4 receptor (Proneth *et al.*, 2006) was identified in an obesity patient, a

pathology caused by agonist-independent signalling. To date, the effects of the specific mutations seem to be receptor specific. Rhodopsin, which possesses no basal activity due to a bound inverse agonist, showed a remarkable ability to generate constitutively active receptor constructs upon mutation at this locus.

Residue 6.40 is either a valine, isoleucine or leucine in 84 % of rhodopsin-like GPCRs (Mirzadegan *et al.*, 2003). The methionine of rhodopsin in relatively atypical, conserved in 5 % of rhodopsin-like GPCRs. It is one of a number of conserved hydrophobic residues that form a hydrophobic barrier separating an interhelical hydrogen bond network near the ligand binding region from the DRY motif at the intracellular face (Trzaskowski *et al.*, 2012). The hydrophobic barrier comprises residues 2.43, 2.46, 3.43, 3.46, 6.36 and 6.40, and is disrupted upon agonist binding, resulting in the hydrogen bond network extending from the ligand binding pocket through to the G-protein binding domain. These rearrangements are supported by structures of active GPCRs (Lebon *et al.*, 2011; Rasmussen *et al.*, 2011b; Standfuss *et al.*, 2011).

This study aims to utilise a systematic mutagenic approach to probe the role of $Ile^{6.40}$ in the structure and function of the $V_{1a}R$. Initially $Ile^{6.40}$ was substituted to every encoded amino acid and pharmacologically and functionally characterised. Double mutations were generated to attempt to identify interaction partners of $Ile^{6.40}$ and additionally $Leu^{3.43}$ which also participates in the hydrophobic barrier maintaining an inactive receptor conformation.

4.2 Results

The residues discussed within this chapter are represented in Figure 4.1. The oligonucleotides utilised to generate the receptor constructs (as described in section 2.2.1) are summarised in Table 4.1. Receptor constructs were characterised by radioligand binding assay with respect

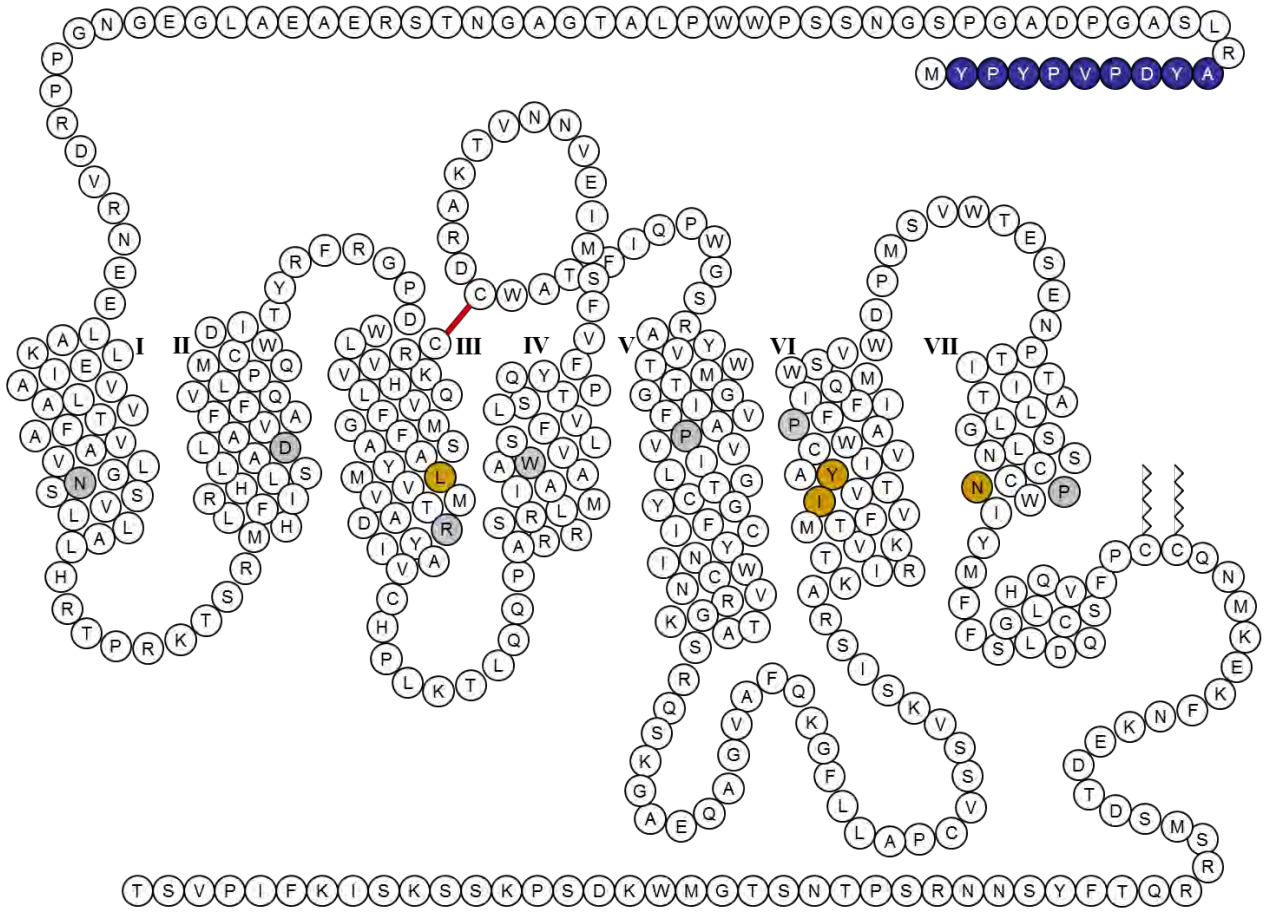

Figure 4.1 Two-dimensional representation of the $V_{1a}R$

The N-terminal, HA-epitope tag (extracellular side) is shown as blue circles. Helices are labelled by roman numerals. The most conserved residue of each helix of rhodopsin-like GPCRs is shown in grey circles and conserved disulphide bridge is shown in red. Palmitoylation sites are shown as zigzags (intracellular side). The residues discussed within this chapter are shown as yellow circles.

Receptor Construct	Sense Oligonucleotide	Antisense Oligonucleotide
[L3.43D]V_{1a}R	5' – CG-GCC-TAC-ATG-**GAC**-GTA-GTC-ATG-AC – 3'	5' – GT-CAT-GAC-TAC-**GTC**-CAT-GTA-GGC-CG – 3'
[L3.43K]V_{1a}R	5' – CG-GCC-TAC-ATG-**AAG**-GTA-GTC-ATG-AC – 3'	5' – GT-CAT-GAC-TAC-**CTT**-CAT-GTA-GGC-CG – 3'
[I6.40C]V_{1a}R	5' – G-ATG-ACT-TTT-GTG-**TGC**-GTG-ACG-GCT-TAC – 3'	5' – GTA-AGC-CGT-CAC-**GCA**-CAC-AAA-AGT-CAT-C– 3'
[I6.40D]V_{1a}R	5' – G-ATG-ACT-TTT-GTG-**GAC**-GTG-ACG-GCT-TAC – 3'	5' – GTA-AGC-CGT-CAC-**GTC**-CAC-AAA-AGT-CAT-C– 3'
[I6.40E]V_{1a}R	5' – G-ATG-ACT-TTT-GTG-**GAA**-GTG-ACG-GCT-TAC – 3'	5' – GTA-AGC-CGT-CAC-**TTC**-CAC-AAA-AGT-CAT-C– 3'
[I6.40F]V_{1a}R	5' – G-ATG-ACT-TTT-GTG-**TTC**-GTG-ACG-GCT-TAC – 3'	5' – GTA-AGC-CGT-CAC-**GAA**-CAC-AAA-AGT-CAT-C– 3'
[I6.40G]V_{1a}R	5' – G-ATG-ACT-TTT-GTG-**GGC**-GTG-ACG-GCT-TAC – 3'	5' – GTA-AGC-CGT-CAC-**GCC**-CAC-AAA-AGT-CAT-C– 3'
[I6.40H]V_{1a}R	5' – G-ATG-ACT-TTT-GTG-**CAC**-GTG-ACG-GCT-TAC – 3'	5' – GTA-AGC-CGT-CAC-**GTG**-CAC-AAA-AGT-CAT-C– 3'
[I6.40K]V_{1a}R	5' – G-ATG-ACT-TTT-GTG-**AAA**-GTG-ACG-GCT-TAC – 3'	5' – GTA-AGC-CGT-CAC-**TTT**-CAC-AAA-AGT-CAT-C– 3'
[I6.40P]V_{1a}R	5' – G-ATG-ACT-TTT-GTG-**CCC**-GTG-ACG-GCT-TAC – 3'	5' – GTA-AGC-CGT-CAC-**GGG**-CAC-AAA-AGT-CAT-C– 3'
[I6.40Q]V_{1a}R	5' – G-ATG-ACT-TTT-GTG-**CAA**-GTG-ACG-GCT-TAC – 3'	5' – GTA-AGC-CGT-CAC-**TTG**-CAC-AAA-AGT-CAT-C– 3'
[I6.40R]V_{1a}R	5' – G-ATG-ACT-TTT-GTG-**CGC**-GTG-ACG-GCT-TAC – 3'	5' – GTA-AGC-CGT-CAC-**GCG**-CAC-AAA-AGT-CAT-C– 3'
[I6.40T]V_{1a}R	5' – G-ATG-ACT-TTT-GTG-**ACC**-GTG-ACG-GCT-TAC – 3'	5' – GTA-AGC-CGT-CAC-**GGT**-CAC-AAA-AGT-CAT-C– 3'
[I6.40V]V_{1a}R	5' – G-ATG-ACT-TTT-GTG-**GTC**-GTG-ACG-GCT-TAC – 3'	5' – GTA-AGC-CGT-CAC-**GAC**-CAC-AAA-AGT-CAT-C– 3'
[I6.40W]V_{1a}R	5' – G-ATG-ACT-TTT-GTG-**TGG**-GTG-ACG-GCT-TAC – 3'	5' – GTA-AGC-CGT-CAC-**CCA**-CAC-AAA-AGT-CAT-C– 3'
[Y6.44D]V_{1a}R	5' – G-ATC-GTG-ACG-GCT-**GAC**-ATC-GTC-TGC-TG – 3'	5' – CA-GCA-GAC-GAT-**GTC**-AGC-CGT-CAC-GAT-C – 3'
[N7.49D]V_{1a}R	5' – G-AAT-AGC-TGC-TGT-**GAT**-CCC-TGG-ATA-TAC – 3'	5' – GTC-TAT-CCA-GGG-**ATC**-ACA-GCA-GCT-ATT-C – 3'
[N7.49K]V_{1a}R	5' – G-AAT-AGC-TGC-TGT-**AAA**-CCC-TGG-ATA-TAC – 3'	5' – GTC-TAT-CCA-GGG-**TTT**-ACA-GCA-GCT-ATT-C – 3'
[N7.49R]V_{1a}R	5' – G-AAT-AGC-TGC-TGT-**CGT**-CCC-TGG-ATA-TAC – 3'	5' – GTC-TAT-CCA-GGG-**ACG**-ACA-GCA-GCT-ATT-C – 3'

Table 4.1 Oligonucleotide sequences utilised to generate receptor constructs

Receptor constructs were generated as described in section 2.2.1. The codon encoding the amino acid substituted is highlighted in red and nucleotide substitutions in bold. Non-bold bases show the complementary template sequence.

to their ability to bind the endogenous agonist AVP and synthetic peptide antagonist CA. All $V_{1a}R$ constructs characterised by competition radioligand binding assay were expressed at 1-2pmol/mg protein. In order to determine the effects of amino acid substitution on the receptors' signalling capabilities, receptor constructs were transiently transfected into HEK 293T cells and the dose-response accumulation of inositol phosphates, InsP-$InsP_3$ measured. The effects on EC_{50}, basal and maximal signalling (E_{max}) were determined. The signalling responses of receptor constructs may be perturbed by amino acid substitutions affecting functional expression at the cell surface. Whole cell ELISA utilised the HA-tag engineered at the amino terminus of all $V_{1a}R$ constructs to detect the presence of receptor constructs at the cell surface.

4.2.1 Systematic substitution of $Ile^{6.40}$

The substitution of $Ile^{6.40}$ in the $V_{1a}R$ to all other encoded amino acids was utilised to assess the contribution of the isoleucine side chain in receptor structure and function. The radioligand competition binding curves of the receptor constructs [I6.40C]$V_{1a}R$, [I6.40D]$V_{1a}R$, [I6.40E]$V_{1a}R$, [I6.40F]$V_{1a}R$, [I6.40G]$V_{1a}R$, [I6.40H]$V_{1a}R$, [I6.40K]$V_{1a}R$, [I6.40P]$V_{1a}R$, [I6.40Q]$V_{1a}R$, [I6.40R]$V_{1a}R$, [I6.40T]$V_{1a}R$, [I6.40V]$V_{1a}R$ and [I6.40W]$V_{1a}R$ are presented in Figures 4.2-4.7. Inositol phosphates dose-response curves and levels of cell-surface expression (+/- agonist challenge) are represented in Figures 4.8-4.13. Six of the 19 substitutions of $Ile^{6.40}$ (alanine, serine, asparagine, leucine, methionine and tyrosine) were engineered and partially characterised with respect to radioligand binding and inositol phosphate accumulation by Wootten (PhD thesis, University of Birmingham, 2007). These data are italicised in Table 4.2 and discussed as an ensemble with the new data presented here. Levels of basal signalling and internalisation were Wt-like unless stated in the text. All graphs and summary data tables are presented together in the following pages.

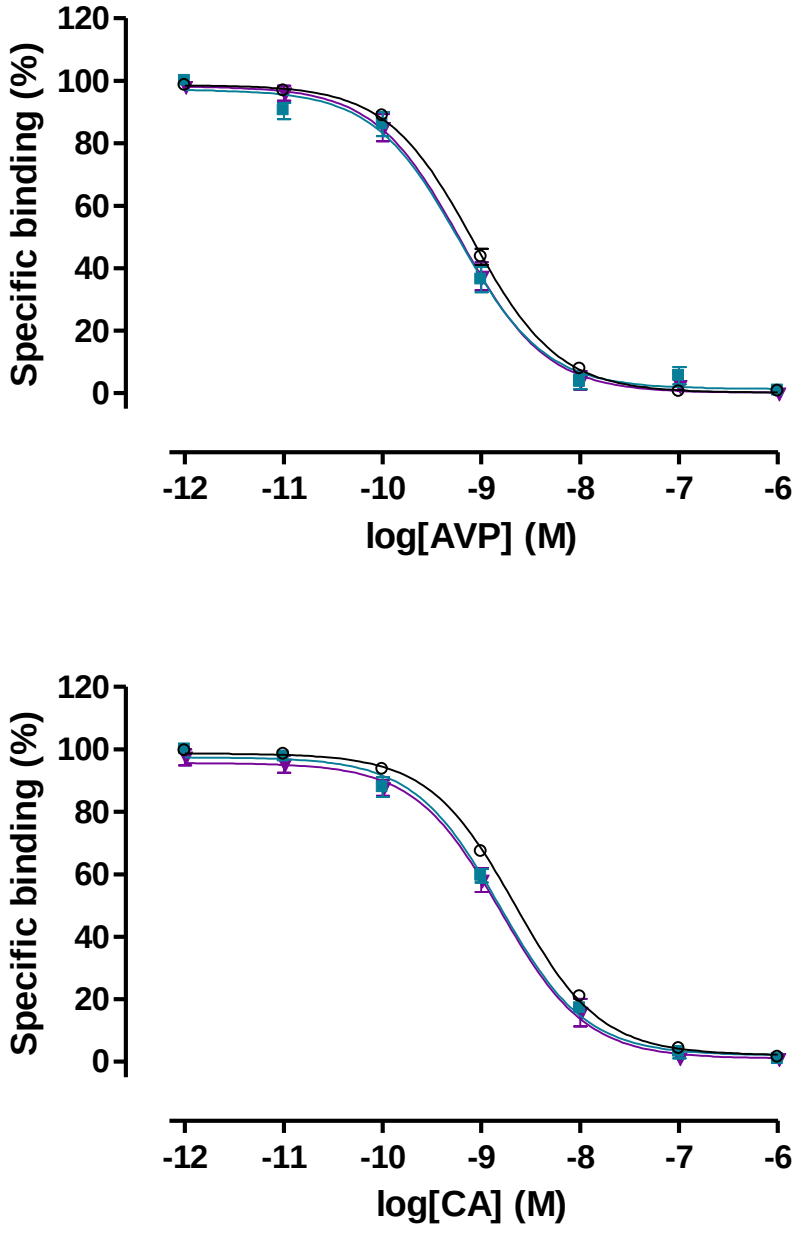

Figure 4.2 Competition radioligand binding curves of substitutions of Ile$^{6.40}$ to small amino acids

Competition radioligand binding assays were performed on HEK 293T cells, transiently transfected with receptor constructs [Wt]V_{1a}R, (○); [I6.40G]V_{1a}R, (■) and [I6.40P]V_{1a}R, (▼). Upper panel: [^{3}H]AVP vs AVP competition; lower panel: [^{3}H]AVP vs CA competition. A theoretical Langmuir binding isotherm was fitted to data expressed as specific binding (%), defining non-specific binding by 1 μM ligand. Data are the mean ± s.e.m. of three experiments performed in triplicate.

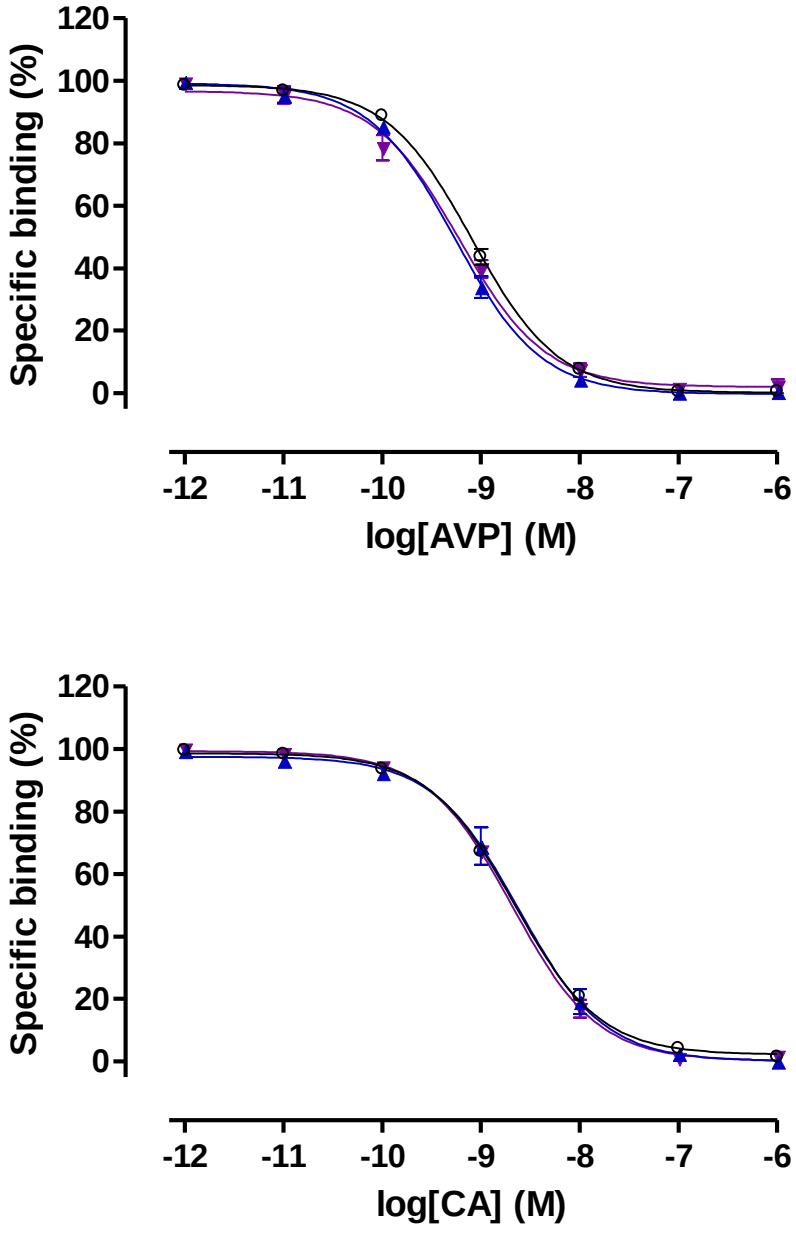

Figure 4.3 Competition radioligand binding curves of substitutions of Ile$^{6.40}$ to small polar amino acids

Competition radioligand binding assays were performed on HEK 293T cells, transiently transfected with receptor constructs [Wt]V_{1a}R, (○); [I6.40T]V_{1a}R, (▲); and [I6.40C]V_{1a}R, (▼). Upper panel: [^{3}H]AVP vs AVP competition; lower panel: [^{3}H]AVP vs CA competition. A theoretical Langmuir binding isotherm was fitted to data expressed as specific binding (%), defining non-specific binding by 1 μM ligand. Data are the mean ± s.e.m. of three experiments performed in triplicate.

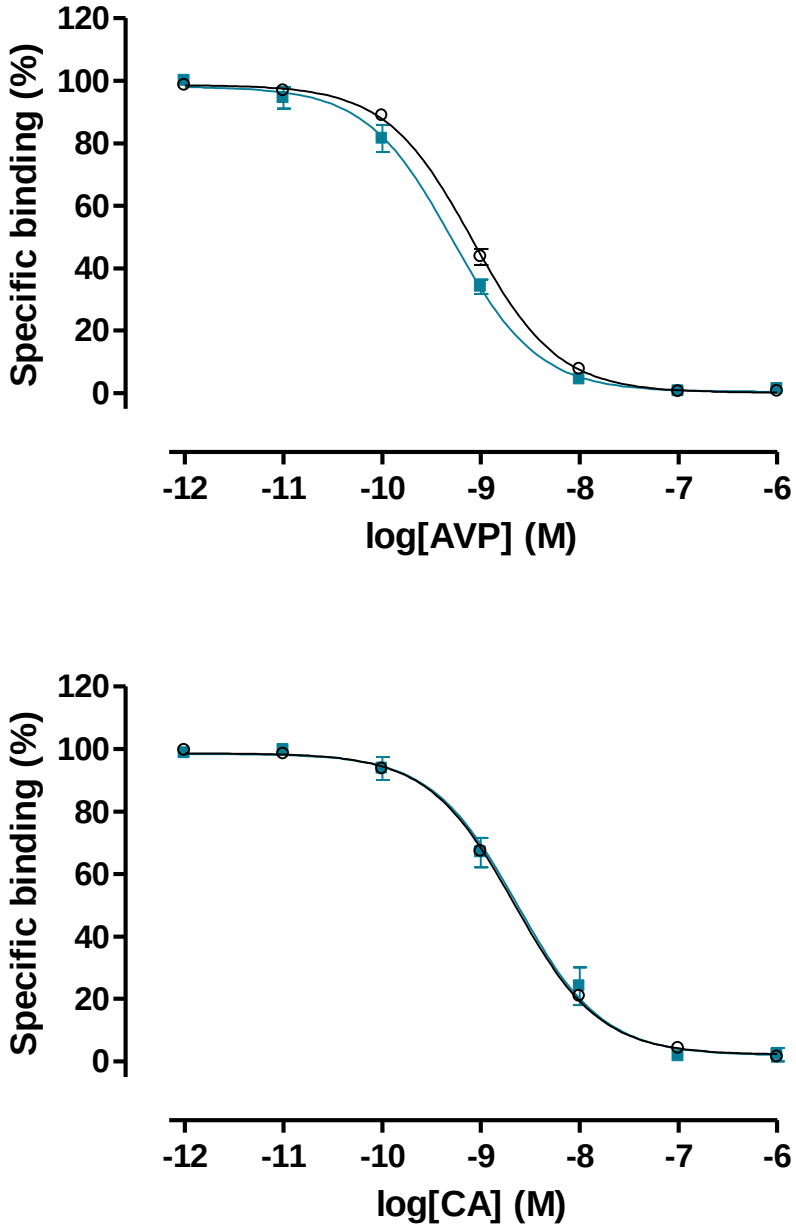

Figure 4.4 Competition radioligand binding curves of substitutions of Ile$^{6.40}$ to valine

Competition radioligand binding assays were performed on HEK 293T cells, transiently transfected with receptor constructs [Wt]$V_{1a}R$, (○) and [I6.40V]$V_{1a}R$ (■). Upper panel: [^{3}H]AVP vs AVP competition; lower panel: [^{3}H]AVP vs CA competition. A theoretical Langmuir binding isotherm was fitted to data expressed as specific binding (%), defining non-specific binding by 1 μM ligand. Data are the mean ± s.e.m. of three experiments performed in triplicate.

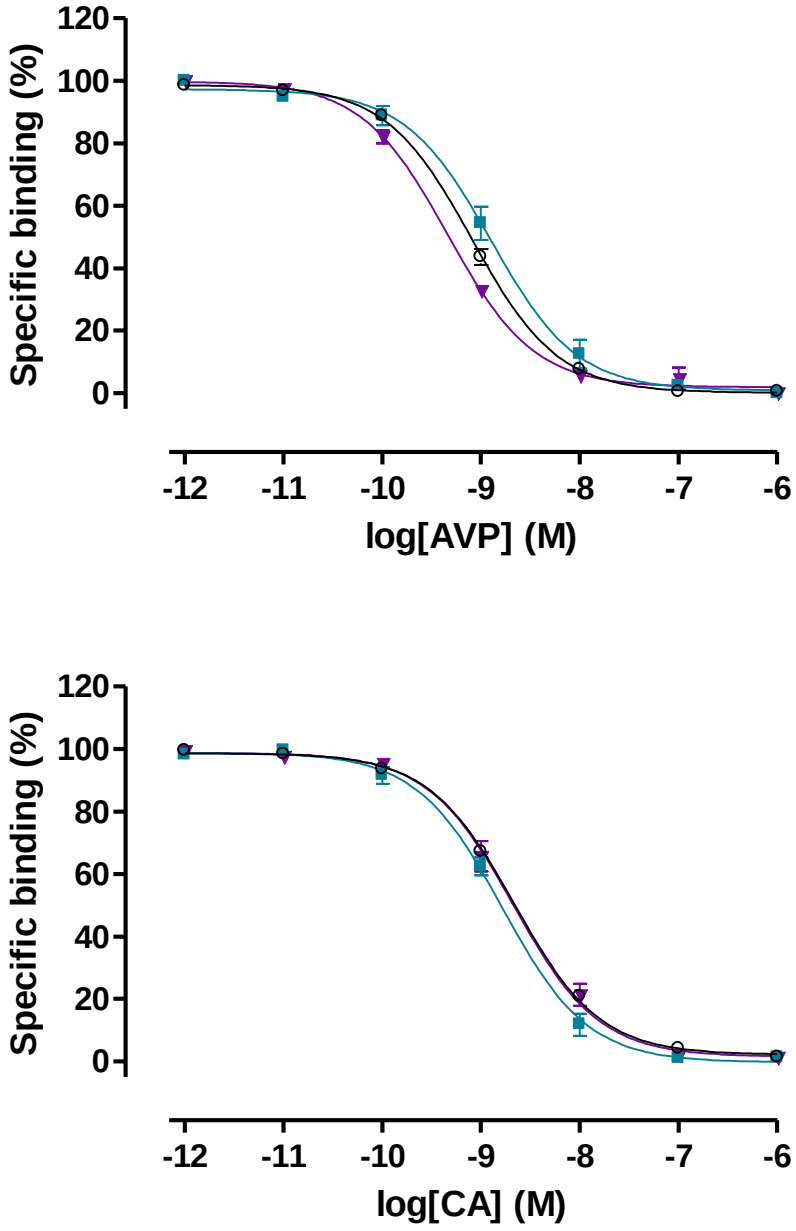

Figure 4.5 Competition radioligand binding curves of substitutions of Ile$^{6.40}$ to aromatic amino acids

Competition radioligand binding assays were performed on HEK 293T cells, transiently transfected with receptor constructs [Wt]V_{1a}R, (○); [I6.40F]V_{1a}R, (■) and [I6.40W]V_{1a}R, (▼). Upper panel: [^{3}H]AVP vs AVP competition; lower panel: [^{3}H]AVP vs CA competition. A theoretical Langmuir binding isotherm was fitted to data expressed as specific binding (%), defining non-specific binding by 1 μM ligand. Data are the mean ± s.e.m. of three experiments performed in triplicate.

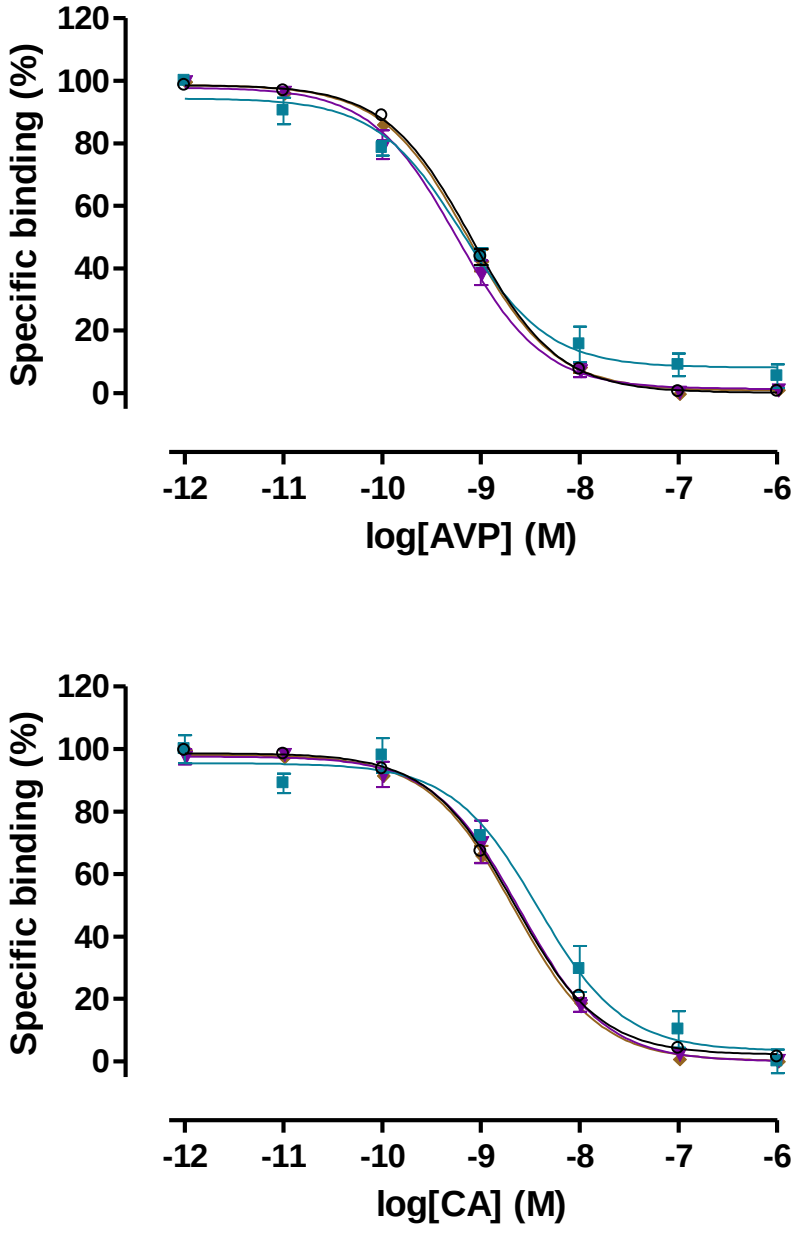

Figure 4.6 Competition radioligand binding curves of substitutions of Ile$^{6.40}$ to acidic and amine amino acids

Competition radioligand binding assays were performed on HEK 293T cells, transiently transfected with receptor constructs [Wt]V_{1a}R, (○); [I6.40D]V_{1a}R, (■); [I6.40E]V_{1a}R, (▼); and [I6.40Q]V_{1a}R (♦). Upper panel: [^{3}H]AVP vs AVP competition; lower panel: [^{3}H]AVP vs CA competition. A theoretical Langmuir binding isotherm was fitted to data expressed as specific binding (%), defining non-specific binding by 1 μM ligand. Data are the mean ± s.e.m. of three experiments performed in triplicate.

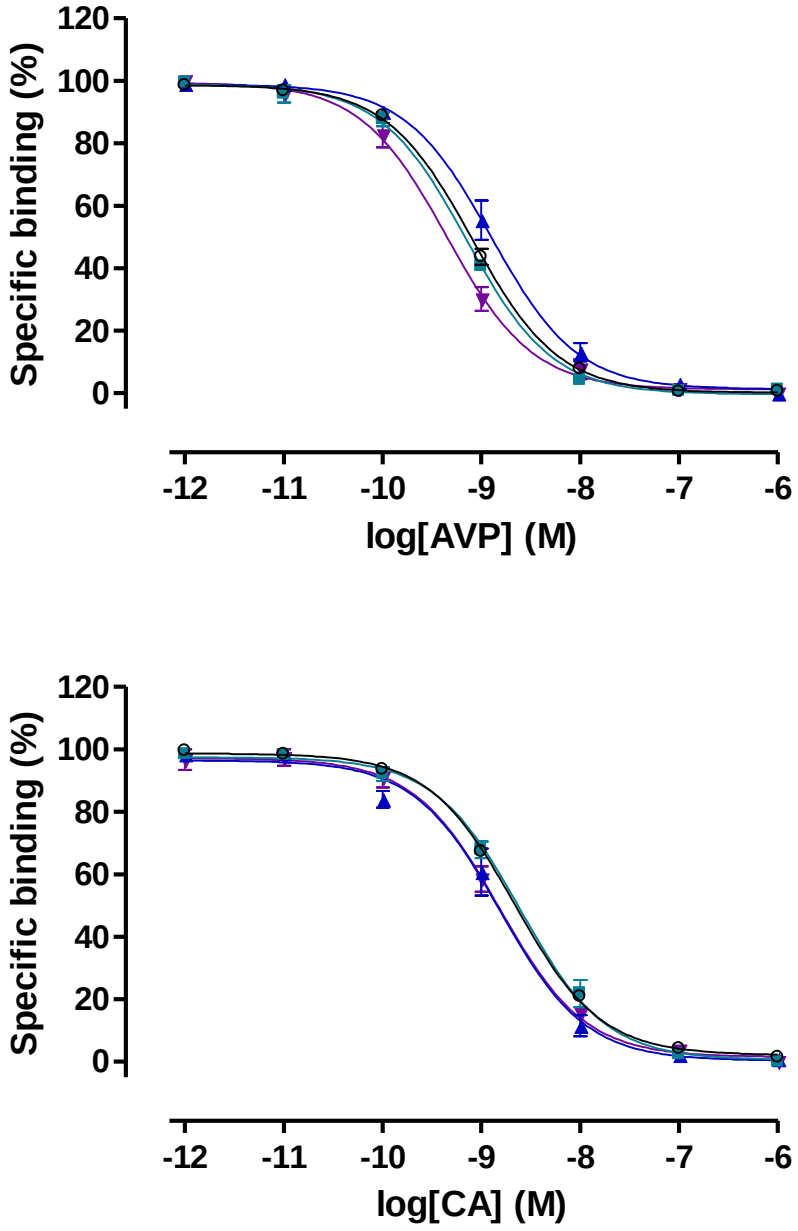

Figure 4.7 Competition radioligand binding curves of substitutions of Ile$^{6.40}$ to basic amino acids

Competition radioligand binding assays were performed on HEK 293T cells, transiently transfected with receptor constructs [Wt]V_{1a}R, (○); [I6.40H]V_{1a}R, (■); [I6.40K]V_{1a}R, (▲); and [I6.40R]V_{1a}R (▼). Upper panel: [^{3}H]AVP vs AVP competition; lower panel: [^{3}H]AVP vs CA competition. A theoretical Langmuir binding isotherm was fitted to data expressed as specific binding (%), defining non-specific binding by 1 μM ligand. Data are the mean ± s.e.m. of three experiments performed in triplicate.

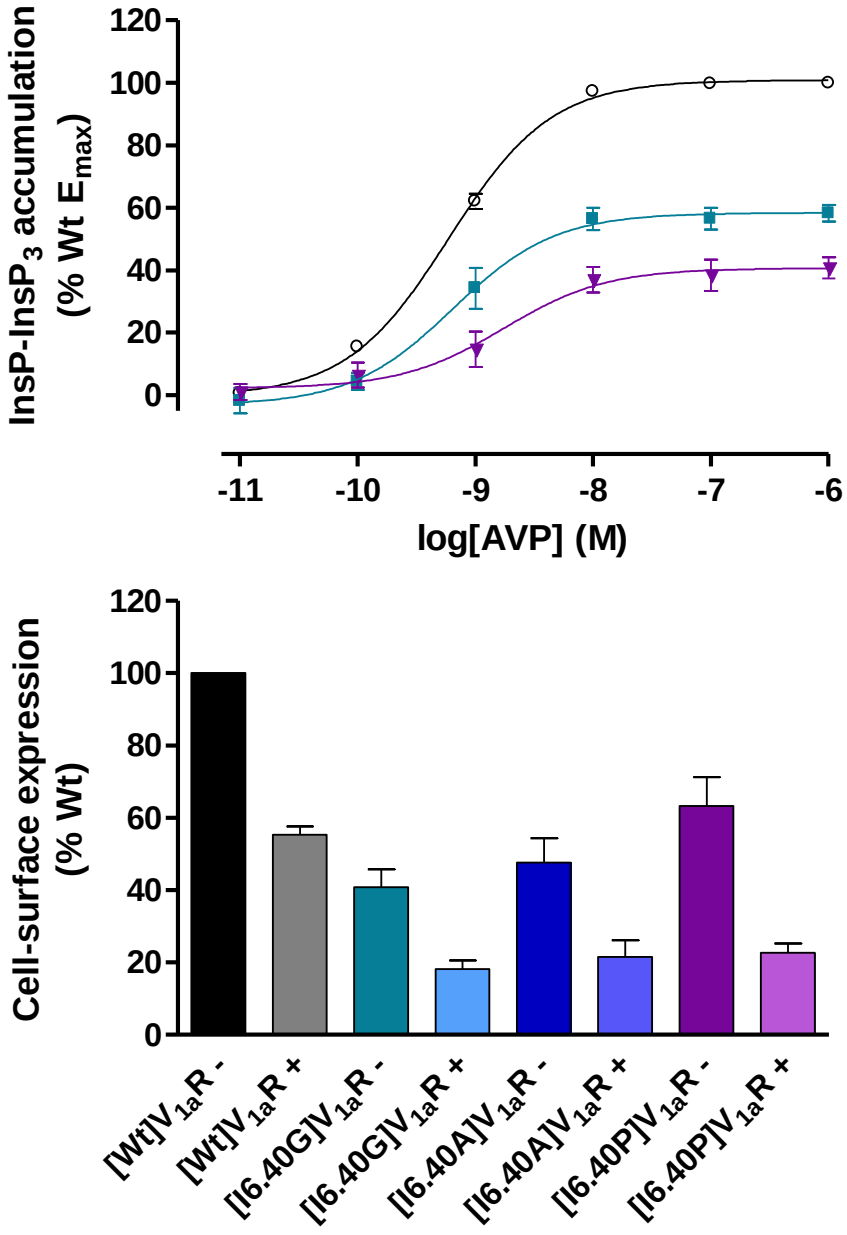

Figure 4.8 InsP-InsP$_3$ dose-response curves and cell-surface expression (+/- agonist challenge) of substitutions of Ile$^{6.40}$ to small amino acids

Upper panel: Dose-response curves of inositol phosphates accumulation assays of HEK 293T cells, transiently transfected with receptor constructs [Wt]V_{1a}R, (○); [I6.40G]V_{1a}R, (■) and [I6.40P]V_{1a}R, (▼). Data are normalised to [Wt]V_{1a}R basal and maximal signalling levels, expressed as the mean ± s.e.m. of three experiments performed in triplicate. Basal signalling is plotted at 10^{-11} M. Lower panel: Cell-surface expression levels of receptor constructs were normalised to untransfected cells and unstimulated (-) [Wt]V_{1a}R expression levels. Data are stated as the mean ± s.e.m. of three experiments performed in triplicate. Stimulated (+) constructs were challenged by 10^{-7}M AVP for 30 min.

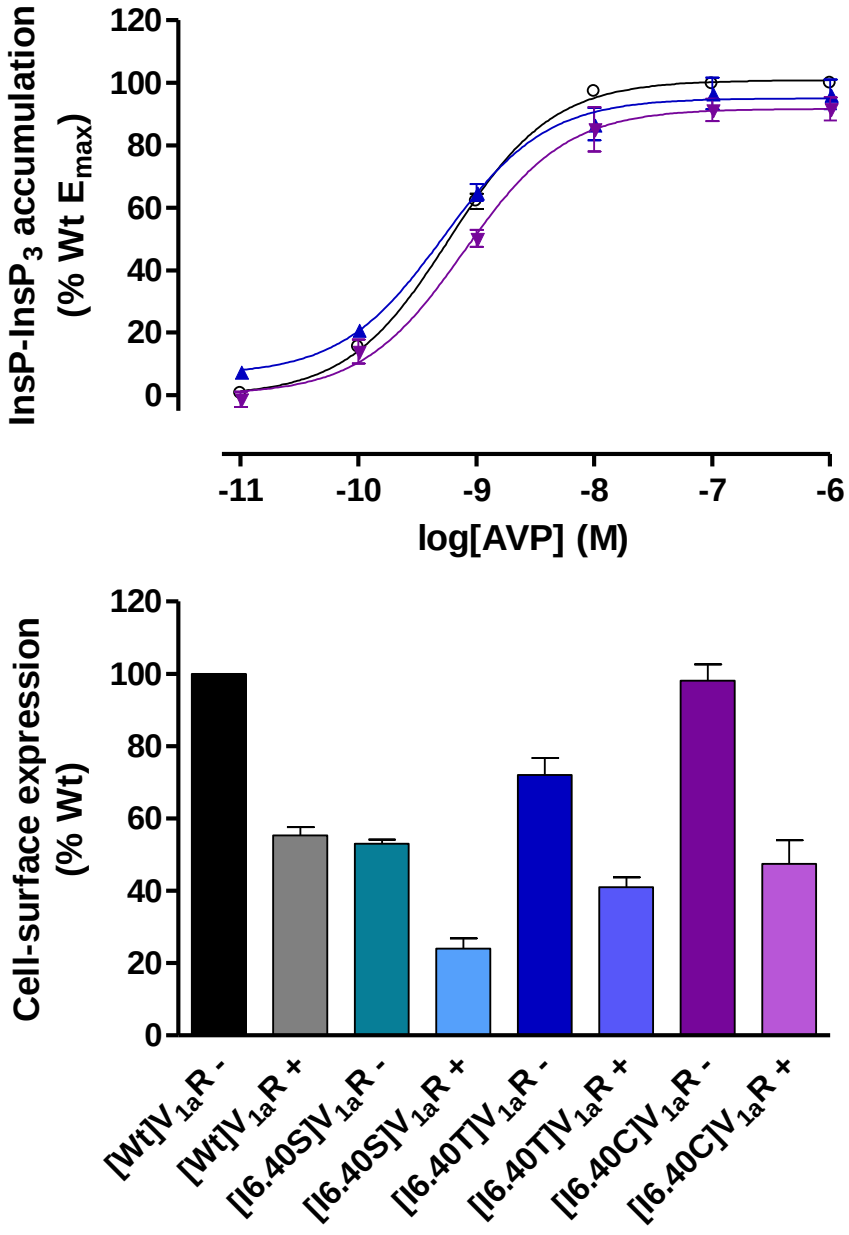

Figure 4.9 InsP-InsP$_3$ dose-response curves and cell-surface expression (+/- agonist challenge) of substitutions of Ile$^{6.40}$ to small, polar amino acids

Upper panel: Dose-response curves of inositol phosphates accumulation assays of HEK 293T cells, transiently transfected with receptor constructs [Wt]V_{1a}R, (○); [I6.40T]V_{1a}R, (▲) and [I6.40C]V_{1a}R, (▼). Data are normalised to [Wt]V_{1a}R basal and maximal signalling levels, expressed as the mean ± s.e.m. of three experiments performed in triplicate. Basal signalling is plotted at 10^{-11} M. Lower panel: Cell-surface expression levels of receptor constructs were normalised to untransfected cells and unstimulated (-) [Wt]V_{1a}R expression levels. Data are stated as the mean ± s.e.m. of three experiments performed in triplicate. Stimulated (+) constructs were challenged by 10^{-7}M AVP for 30 min.

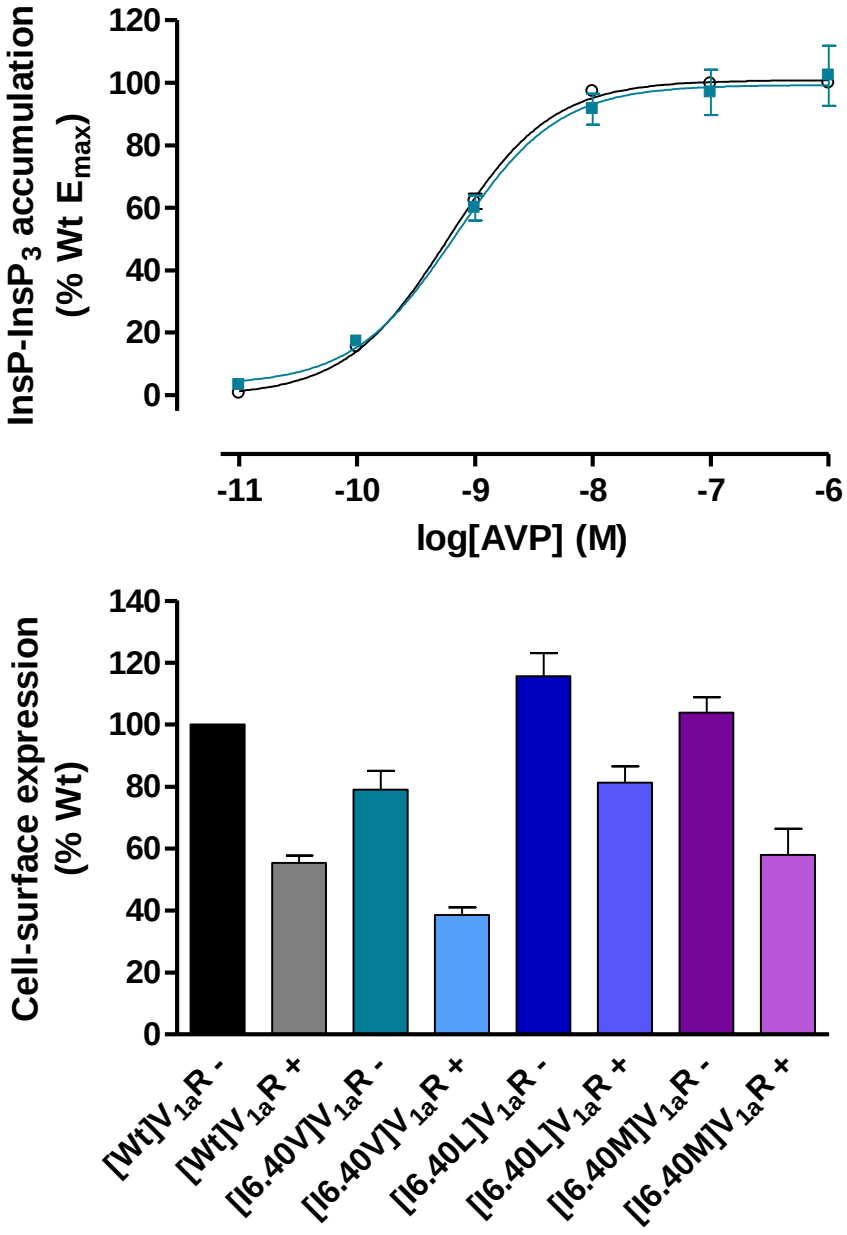

Figure 4.10 InsP-InsP$_3$ dose-response curves and cell-surface expression (+/- agonist challenge) of substitutions of Ile$^{6.40}$ to hydrophobic amino acids

Upper panel: Dose-response curves of inositol phosphates accumulation assays of HEK 293T cells, transiently transfected with receptor constructs [Wt]V_{1a}R, (○) and [I6.40V]V_{1a}R (■). Data are normalised to [Wt]V_{1a}R basal and maximal signalling levels, expressed as the mean ± s.e.m. of three experiments performed in triplicate. Basal signalling is plotted at 10^{-11} M. Lower panel: Cell-surface expression levels of receptor constructs were normalised to untransfected cells and unstimulated (-) [Wt]V_{1a}R expression levels. Data are stated as the mean ± s.e.m. of three experiments performed in triplicate. Stimulated (+) constructs were challenged by 10^{-7}M AVP for 30 min.

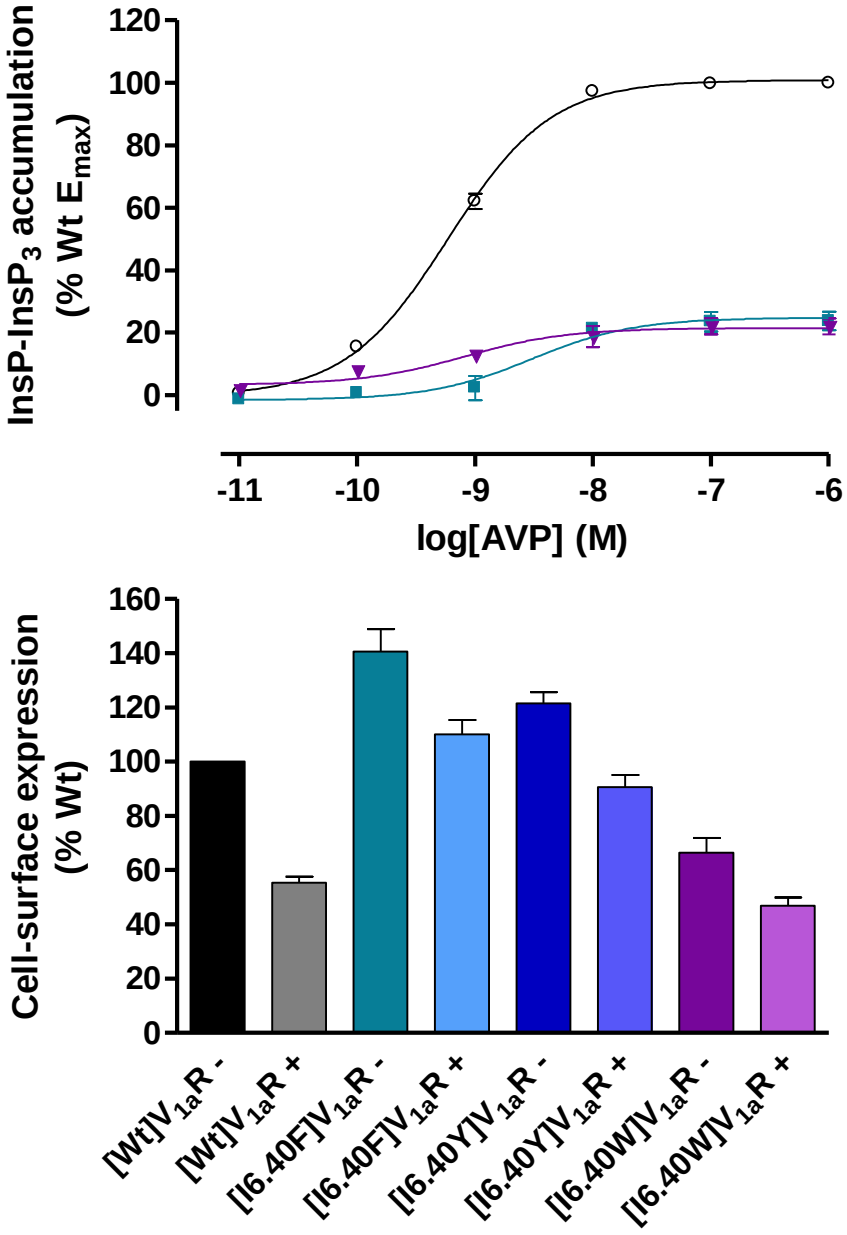

Figure 4.11 InsP-InsP$_3$ dose-response curves and cell-surface expression (+/- agonist challenge) of substitutions of Ile$^{6.40}$ to aromatic amino acids

Upper panel: Dose-response curves of inositol phosphates accumulation assays of HEK 293T cells, transiently transfected with receptor constructs [Wt]V_{1a}R, (○); [I6.40F]V_{1a}R, (■) and [I6.40W]V_{1a}R, (▼). Data are normalised to [Wt]V_{1a}R basal and maximal signalling levels, expressed as the mean ± s.e.m. of three experiments performed in triplicate. Basal signalling is plotted at 10^{-11} M. Lower panel: Cell-surface expression levels of receptor constructs were normalised to untransfected cells and unstimulated (-) [Wt]V_{1a}R expression levels. Data are stated as the mean ± s.e.m. of three experiments performed in triplicate. Stimulated (+) constructs were challenged by 10^{-7}M AVP for 30 min.

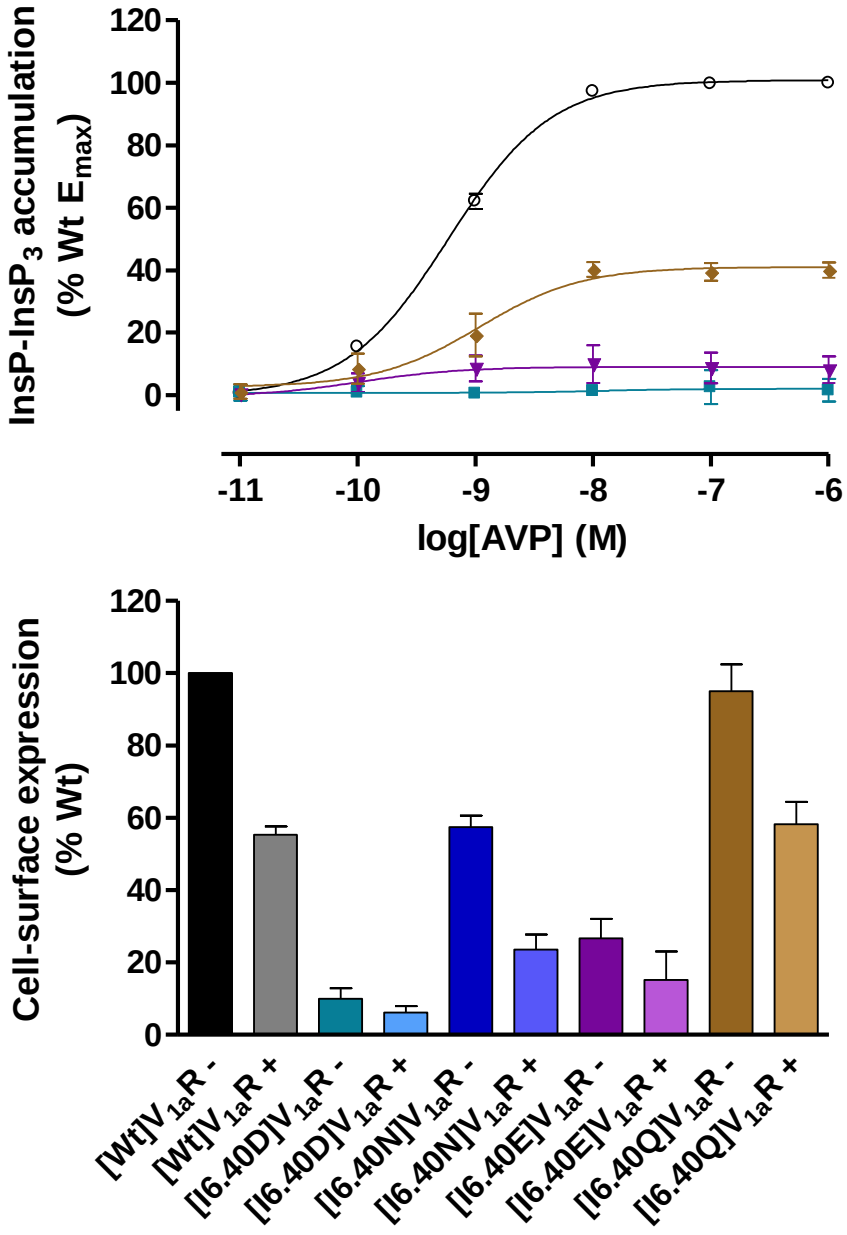

Figure 4.12 InsP-InsP$_3$ dose-response curves and cell-surface expression (+/- agonist challenge) of substitutions of Ile$^{6.40}$ to acid and amine amino acids

Upper panel: Dose-response curves of inositol phosphates accumulation assays of HEK 293T cells, transiently transfected with receptor constructs [Wt]V_{1a}R, (○); [I6.40D]V_{1a}R, (■); [I6.40E]V_{1a}R, (▼); and [I6.40Q]V_{1a}R (♦). Data are normalised to [Wt]V_{1a}R basal and maximal signalling levels, expressed as the mean ± s.e.m. of three experiments performed in triplicate. Basal signalling is plotted at 10^{-11} M. Lower panel: Cell-surface expression levels of receptor constructs were normalised to untransfected cells and unstimulated (-) [Wt]V_{1a}R expression levels. Data are stated as the mean ± s.e.m. of three experiments performed in triplicate. Stimulated (+) constructs were challenged by 10^{-7}M AVP for 30 min.

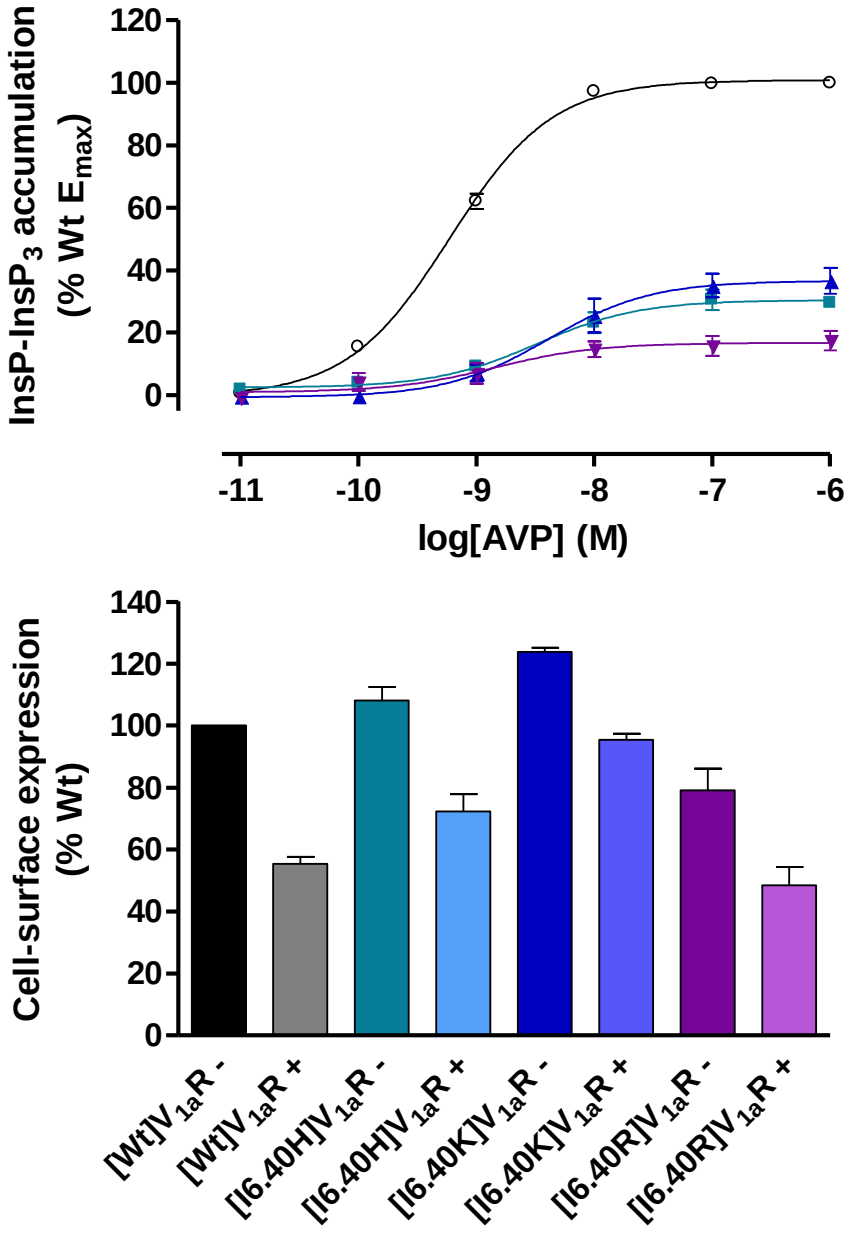

Figure 4.13 InsP-InsP$_3$ dose-response curves and cell-surface expression (+/- agonist challenge) of substitutions of Ile$^{6.40}$ to basic amino acids

Upper panel: Dose-response curves of inositol phosphates accumulation assays of HEK 293T cells, transiently transfected with receptor constructs [Wt]V_{1a}R, (○); [I6.40H]V_{1a}R, (■); [I6.40K]V_{1a}R, (▲) and [I6.40R]V_{1a}R (▼). Data are normalised to [Wt]V_{1a}R basal and maximal signalling levels, expressed as the mean ± s.e.m. of three experiments performed in triplicate. Basal signalling is plotted at 10^{-11} M. Lower panel: Cell-surface expression levels of receptor constructs were normalised to untransfected cells and unstimulated (-) [Wt]V_{1a}R expression levels. Data are stated as the mean ± s.e.m. of three experiments performed in triplicate. Stimulated (+) constructs were challenged by 10^{-7}M AVP for 30 min.

Receptor construct	Binding affinity, K_i (nM) ± s.e.m.		InsP-$InsP_3$ accumulation (% Wt E_{max}) ± s.e.m.			Cell-surface expression (% Wt unstimulated) ± s.e.m.	
	AVP	CA	Basal	EC_{50}*	E_{max}	Unstimulated	Simulated
$V_{1a}R$	**0.45 ± 0.04**	**0.96 ± 0.10**	**0**	**0.60 ± 0.02**	**100**	**100**	**55 ± 2**
[I6.40A]$V_{1a}R$	*0.19 ± 0.07*	*0.86 ± 0.11*	*17 ± 2*	*0.31 ± 0.03*	*104 ± 9*	48 ± 7	22 ± 5
[I6.40C]$V_{1a}R$	0.45 ± 0.11	1.12 ± 0.13	-1 ± 3	0.76 ± 0.09	92 ± 4	98 ± 5	47 ± 7
[I6.40D]$V_{1a}R$	0.64 ± 0.12#	3.74 ± 1.23#	1 ± 3	No detectible signalling		10 ± 3	6 ± 2
[I6.40E]$V_{1a}R$	0.54 ± 0.07#	2.43 ± 0.16#	0 ± 2	0.12 ± 0.05	10 ± 6	27 ± 5	15 ± 8
[I6.40F]$V_{1a}R$	0.59 ± 0.10	0.92 ± 0.15	-1 ± 0	3.06 ± 1.22	24 ± 3	141 ± 8	110 ± 5
[I6.40G]$V_{1a}R$	0.21 ± 0.07	0.60 ± 0.22	-2 ± 4	0.66 ± 0.06	58 ± 3	41 ± 5	18 ± 2
[I6.40H]$V_{1a}R$	0.36 ± 0.12	1.46 ±0.35	2 ± 1	3.18 ± 0.45	31 ± 3	108 ± 4	72 ± 6
[I6.40K]$V_{1a}R$	0.90 ± 0.38	1.19 ± 0.43	0 ± 1	4.14 ± 0.20	37 ± 4	124 ± 1	95 ± 2
[I6.40L]$V_{1a}R$	*1.20 ± 0.25*	*0.72 ± 0.06*	*-9 ± 2*	*42.9 ± 5*	*96 ± 6*	116 ± 7	81 ± 5
[I6.40M]$V_{1a}R$	*0.26 ± 0.09*	*1.16 ± 0.12*	*18 ± 4*	*0.57 ± 0.04*	*146 ± 25*	104 ± 5	58 ± 8
[I6.40N]$V_{1a}R$	*0.89 ± 0.34*	*0.99 ± 0.06*	*5 ± 5*	*0.54 ± 0.10*	*103 ± 8*	57 ± 3	24 ± 4
[I6.40P]$V_{1a}R$	0.40 ± 0.02	0.79 ± 0.10	1 ± 3	1.68 ± 0.40	41 ± 3	63 ± 8	23 ± 3
[I6.40Q]$V_{1a}R$	0.33 ± 0.03	0.84 ± 0.05	1 ± 2	1.04 ± 0.25	41 ± 1	95 ± 7	58 ± 6
[I6.40R]$V_{1a}R$	0.15 ± 0.08	0.56 ± 0.13	-1 ± 2	1.23 ± 0.59	18 ± 3	79 ± 7	48 ± 6
[I6.40S]$V_{1a}R$	*0.36 ± 0.04*	*0.97 ± 0.12*	*12 ± 5*	*0.81 ± 0.06*	*106 ± 8*	53 ± 1	24 ± 3
[I6.40T]$V_{1a}R$	0.23 ± 0.07	0.79 ± 0.05	7 ± 1	0.54 ± 0.06	96 ± 5	72 ± 5	41 ± 3
[I6.40V]$V_{1a}R$	0.28 ± 0.08	1.11 ± 0.33	3 ± 1	0.68 ± 0.07	102 ± 10	79 ± 6	39 ± 3
[I6.40W]$V_{1a}R$	0.12 ± 0.04	0.50 ± 0.06	2 ± 1	0.69 ± 0.32	22 ± 3	67 ± 5	47 ± 3
[I6.40Y]$V_{1a}R$	*1.72 ± 0.76*	*1.94 ±0.04*	*-11 ± 3*	*2.52 ± 0.07*	*31 ± 6*	122 ± 4	91 ± 5

Table 4.2 Binding, signalling and cell-surface expression of $Ile^{6.40}$ substitutions

All data are shown as the mean ± s.e.m. of three separate experiments performed in triplicate. *EC_{50} is stated as the mean ± mean of 95 % confidence intervals of three separate experiments performed in triplicate. Data in yellow indicate >2.5-fold increase in K_i or EC_{50} or >25 % reduction in E_{max}, cell-surface expression; orange >5-fold increase in K_i or EC_{50} or >50 % reduction in E_{max}, cell-surface expression or internalisation; red >10-fold increase in K_i or EC_{50} or >75 % reduction in E_{max}, cell-surface expression or internalisation. Data in green indicate >2.5-fold increase in K_i or EC_{50} or >25 % increase in E_{max}, cell-surface expression or > 50% increase in internalisation. Data in white are comparable to Wt. # denotes IC_{50} ± mean of 95 % confidence intervals of three separate experiments performed in triplicate. Data taken from the thesis of Wootten, University of Birmingham, 2007 are shown in italics.

4.2.1.1 Substitution of Ile$^{6.40}$ for small side chain amino acids

The receptor constructs [I6.40G]V_{1a}R, [I6.40A]V_{1a}R and [I6.40P]V_{1a}R represent the substitution of isoleucine for amino acids with small side chains. The binding characteristics of the receptor constructs were Wt-like with respect to binding both AVP agonist and CA antagonist (Figure 4.2, Table 4.2). A slight increase (2.3-fold) increase in AVP binding affinity to the [I6.40A]V_{1a}R was noted.

[I6.40G]V_{1a}R generated a Wt-like EC_{50} with a decrease in maximal signalling, 58 % of Wt E_{max} (Figure 4.8, Table 4.2). The construct was expressed at the cell-surface at 41 % of Wt levels. Although an EC_{50} and maximal signalling levels comparable to Wt were observed for the [I6.40A]V_{1a}R construct, a substantial increase in basal activity of 17 % was displayed [I6.40A]V_{1a}R expressed at the cell surface at 48 % of Wt levels. [I6.40P]V_{1a}R displayed a 2.8-fold increase in EC_{50} and a reduction in E_{max} (41 % of Wt E_{max}). The receptor construct was expressed at the cell surface at 63 % of Wt levels.

4.2.1.2 Substitution of Ile$^{6.40}$ for small polar amino acids

The receptor constructs [I6.40S]V_{1a}R, [I6.40T]V_{1a}R, [I6.40C]V_{1a}R substituting Ile$^{6.40}$ to amino acids with small polar side chains maintained Wt-like pharmacology (Figure 4.3, Table 4.2). The basal signalling level of [I6.40S]V_{1a}R was considerably increased to 12% of Wt maximal signalling levels although Wt-like EC_{50} and E_{max} values were observed (Figure 4.9, Table 4.2). The receptor construct [I6.40S]V_{1a}R expressed at a reduced 53 % of Wt levels. Wt-like EC_{50} and maximal signalling levels were achieved by the [I6.40T]V_{1a}R receptor construct, but an increase in basal signalling accompanied these findings (7 % of Wt E_{max}). [I6.40T]V_{1a}R displayed slightly reduced cell-surface expression at 72 % of Wt levels. [I6.40C]V_{1a}R was Wt-like with respect to all parameters of InsP-$InsP_3$ signalling and cell-surface expression.

4.2.1.3 Substitution of Ile$^{6.40}$ for hydrophobic amino acids

The receptor constructs [I6.40V]V_{1a}R, [I6.40L]V_{1a}R and [I6.40M]V_{1a}R represent conservative substitutions of Ile$^{6.40}$ and the most commonly residues observed at this locus in rhodopsin-like GPCRs. The pharmacology of [I6.40V]V_{1a}R and [I6.40M]V_{1a}R were comparable to Wt (Figure 4.4, Table 4.2). [I6.40L]V_{1a}R demonstrated a 2.6-fold decrease in agonist binding while maintaining Wt-like antagonist binding.

The signalling capabilities of the receptor construct were essentially Wt in all respects with the introduction of the I6.40V substitution (Figure. 4.10, Table 4.2). Although the receptor construct [I6.40L]V_{1a}R achieved maximal signalling comparable to Wt, a substantial decrease in basal signalling (-9 % of Wt E_{max}) and a 72-fold increase in EC_{50} were observed. [I6.40M]V_{1a}R displayed a considerable increase in basal activity of 18 % of Wt E_{max} with a Wt-like EC_{50}. The maximal signalling capabilities of the [I6.40M]V_{1a}R construct were increased to 146 % compared to Wt E_{max}. Conservative substitutions of Ile$^{6.40}$ to valine, leucine and methionine all expressed at the cell surface at levels comparable to Wt.

4.2.1.4 Substitution of Ile$^{6.40}$ for aromatic amino acids

In substituting Ile$^{6.40}$ to amino acids with aromatic side chains, the receptor constructs [I6.40F]V_{1a}R, [I6.40Y]V_{1a}R and [I6.40W]V_{1a}R were generated. [I6.40F]V_{1a}R maintained Wt-like binding affinities for both AVP and CA (Figure 4.5, Table 4.2). [I6.40Y]V_{1a}R displayed a 3.8-fold decrease in AVP binding and maintained Wt-like CA binding affinity. The receptor construct [I6.40W]V_{1a}R increased the binding affinity of AVP 3.7-fold but maintained a CA binding affinity comparable to Wt.

Inositol phosphates dose-response curve of [I6.40F]V_{1a}R displayed a 5.1-fold increase in EC_{50} and severely reduced maximal signalling capabilities, 24 % of Wt E_{max} (Figure 4.11, Table

4.2). [I6.40Y]V_{1a}R displayed basal signalling of -11 % of Wt E_{max}, 4.2-fold increase in EC_{50} and a reduction in E_{max} to 31 % of Wt levels. The receptor construct [I6.40W]V_{1a}R generated a Wt-like EC_{50} value with respect to InsP-$InsP_3$ accumulation but reached maximal signalling levels only 22 % of Wt. [I6.40F]V_{1a}R, [I6.40Y]V_{1a}R and [I6.40W]V_{1a}R expressed at the cell surface at 141 %, 122 % and 67 % respectively. Although all internalised on AVP challenge, [I6.40F]V_{1a}R showed a greatly reduced tendency to internalise (22 % of total expression; Wt, 45 % of total expression).

4.2.1.5 Substitution of $Ile^{6.40}$ for acidic and amine amino acids

The substitution of $Ile^{6.40}$ to acidic amino acids generated the receptor constructs [I6.40D]V_{1a}R and [I6.40E]V_{1a}R. These constructs bound both AVP and CA, generating competition binding curves (Figure 4.6). IC_{50} values were comparable to Wt (AVP: [I6.40D]V_{1a}R, 0.64 ± 0.12 nM; [I6.40E]V_{1a}R, 0.54 ± 0.07 nM; Wt, 0.85 ± 0.02 nM. CA: [I6.40D]V_{1a}R, 3.74 ± 1.23 nM; [I6.40E]V_{1a}R, 2.43 ± 0.16 nM; Wt, 2.17 ± 0.09 nM). Receptor constructs [I6.40N]V_{1a}R and [I6.40Q]V_{1a}R maintained Wt-like pharmacology (Figure 4.6, Table 4.2).

The receptor construct [I6.40D]V_{1a}R could not generate an inositol-phosphate response and was detectible at the cell surface at only 10 % of Wt levels (Figure 4.12, Table 4.2). [I6.40E]V_{1a}R generated a maximal InsP-$InsP_3$ signal at only 10 % of Wt and 5-fold decrease in EC_{50}. [I6.40E]V_{1a}R displayed a reduction in cell-surface expression (27 % of Wt expression). [I6.40N]V_{1a}R generated InsP-$InsP_3$ in a manner comparable to Wt, with a potential increase in basal activity of 5 % of Wt E_{max}, although cell-surface expression was reduced (57 % of Wt). The receptor construct [I6.40Q]V_{1a}R displayed Wt-like EC_{50} but could only signal to 41 % of Wt E_{max}. Cell-surface expression of [I6.40Q]V_{1a}R was comparable to Wt.

4.2.1.6 Substitution of $Ile^{6.40}$ for basic amino acids

Receptor constructs [I6.40H]$V_{1a}R$, [I6.40K]$V_{1a}R$ and [I6.40R]$V_{1a}R$ generated receptor constructs substituting the leucine reside at position 6.40 for amino acids with basic side chains. [I6.40H]$V_{1a}R$ and [I6.40K]$V_{1a}R$ maintained Wt-like binding affinities for AVP and CA (Figure 4.7, Table 4.2). [I6.40R]$V_{1a}R$ demonstrated a 3-fold increase in AVP binding whilst maintaining CA binding affinity.

Substitution of $Ile^{6.40}$ to basic amino acids severely disrupted the ability to generate InsP-$InsP_3$ (Figure 4.13, Table 4.2). [I6.40H]$V_{1a}R$, [I6.40K]$V_{1a}R$ and [I6.40R]$V_{1a}R$ reached maximal signalling levels of only 31 %, 37 % and 18 % of Wt E_{max} respectively. Only [I6.40R]$V_{1a}R$ maintained Wt-like EC_{50} whilst [I6.40H]$V_{1a}R$ and [I6.40K]$V_{1a}R$ displayed 5.3-fold and 6.9-fold increased EC_{50} respectively. All substitutions of $Ile^{6.40}$ to residues with basic side chains expressed at the cell surface at levels comparable to Wt.

4.2.2 Probing interactions of $Ile^{6.40}$ with the receptor construct [I6.40D]$V_{1a}R$

Given that the most detrimental substitution of $Ile^{6.40}$ was to aspartate, double receptor constructs were generated to attempt to restore expression and functionality. The receptor construct [L3.43K/I6.40D]$V_{1a}R$ was generated to attempt to recapitulate the interaction of $Ile^{6.40}$ with another hydrophobic barrier residue – $Leu^{3.43}$ – with a charge-charge interaction. Additionally an interaction with $Asn^{7.49}$ of the NPXXY was introduced to attempt to recover functionally in the same manner with the receptor construct [I6.40D/N7.49K]$V_{1a}R$. In the carazolol bound structure of the β_2AR, both $Ile^{6.40}$ and $Asn^{7.49}$ point into the helical bundle (Cherezov *et al.*, 2007). Additionally, modelling of a number of CAMs generated by substitution of 6.40 in the H_1R suggested interaction with $Asn^{7.49}$ (Bakker *et al.*, 2008). The single mutations [L3.43K]$V_{1a}R$ and [N7.49K]$V_{1a}R$ were generated to assess the contribution of the individual substitutions on receptor structure and function.

The receptor constructs [L3.43K/I6.40D]$V_{1a}R$ and [I6.40D/N7.49K]$V_{1a}R$ bound both AVP and CA, generating competition radioligand binding curves (Figure 4.14). [L3.43K/I6.40D]$V_{1a}R$ displayed a 2.6-fold decrease in IC_{50} (0.32 ± 0.02 nM; Wt, 0.85 ± 0.02 nM) for AVP binding whilst [I6.40D/N7.49K]$V_{1a}R$ maintaining Wt-like IC_{50} (0.66 ± 0.23 nM; Wt 0.85 ± 0.02 nM). Both [L3.43K/I6.40D]$V_{1a}R$ and [I6.40D/N7.49K]$V_{1a}R$ maintained Wt-like IC_{50} values, 2.23 ± 0.05 nM and 2.96 ± 0.27 nM respectively, for CA (Wt, 2.17 ± 0.09 nM). In contrast, the single substitutions [L3.43K]$V_{1a}R$ and [N7.49K]$V_{1a}R$ displayed 7.8-fold and 20.8-fold decreases in AVP binding affinity whilst CA affinity was comparable to Wt (Figure 4.14, Table 4.3).

The double receptor construct [L3.43K/I6.40D]$V_{1a}R$ displayed basal signalling levels of 10 % of Wt E_{max}, a Wt-like EC_{50} and E_{max} of 35 % of Wt (Figure 4.15, Table 4.3). Expression at the cell surface was 11 % of Wt levels and a decrease in the amount of receptor present after AVP stimulation was observed. The receptor construct [I6.40D/N7.49K]$V_{1a}R$ could not generate detectible InsP-$InsP_3$ when challenged with AVP and was not expressed at the cell surface. The single mutant [L3.43K]$V_{1a}R$ signalled though the inositol phosphate pathway like Wt in all respects. The cell-surface expression observed was increased to 161 % of Wt and underwent internalisation upon agonist challenge. No detectible InsP-$InsP_3$ was observed for the receptor construct [N7.49K]$V_{1a}R$ although it was well expressed at the cell surface (126 % of Wt levels). The substitution of $Asn^{7.49}$ to lysine however, made the receptor construct incapable of internalisation upon agonist stimulation.

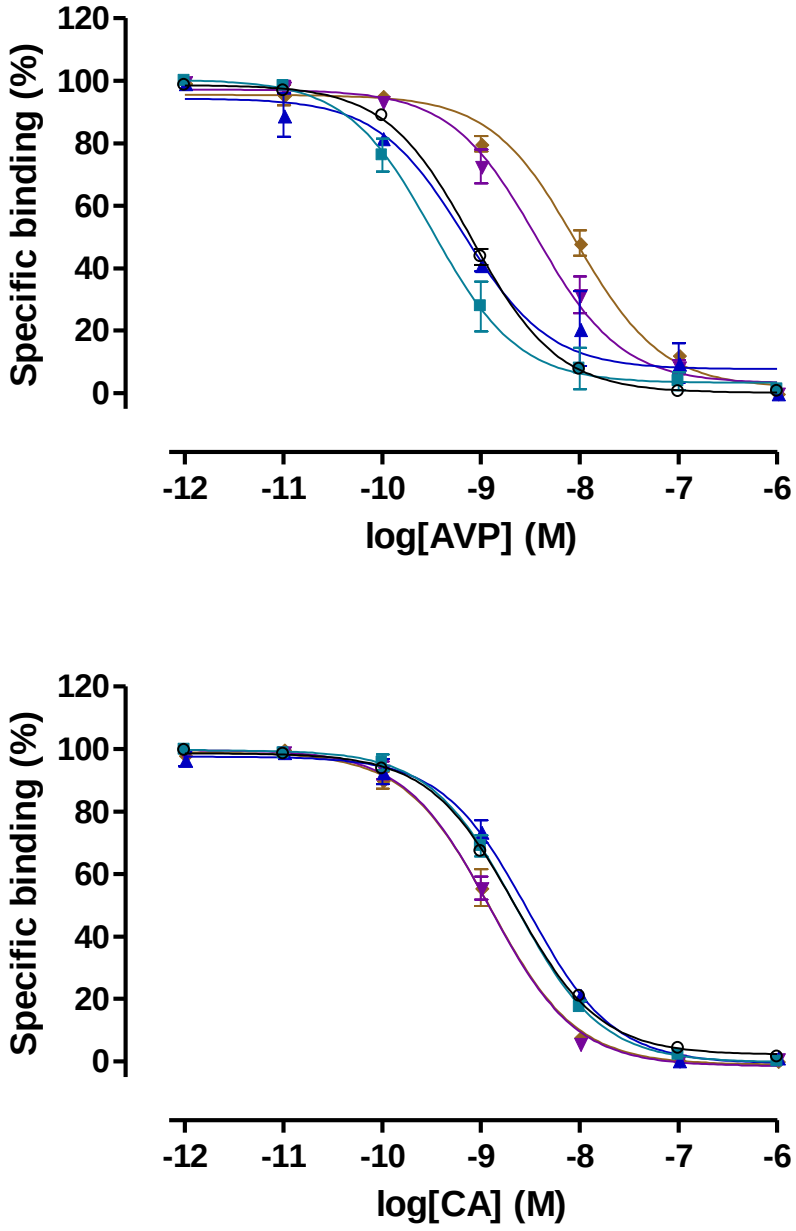

Figure 4.14 Competition radioligand binding curves of constructs probing interactions with Ile$^{6.40}$

Competition radioligand binding assays were performed on HEK 293T cells, transiently transfected with receptor constructs [Wt]$V_{1a}R$, (○); [L3.43K/I6.40D]$V_{1a}R$, (■); [I6.40D/N7.49K]$V_{1a}R$, (▲); [L3.43K]$V_{1a}R$, (▼) and [N7.49K]$V_{1a}R$ (♦). Upper panel: [^{3}H]AVP vs. AVP competition; lower panel: [^{3}H]AVP vs. CA competition. A theoretical Langmuir binding isotherm was fitted to data expressed as specific binding (%), defining non-specific binding by 1 μM ligand. Data are the mean ± s.e.m. of three experiments performed in triplicate.

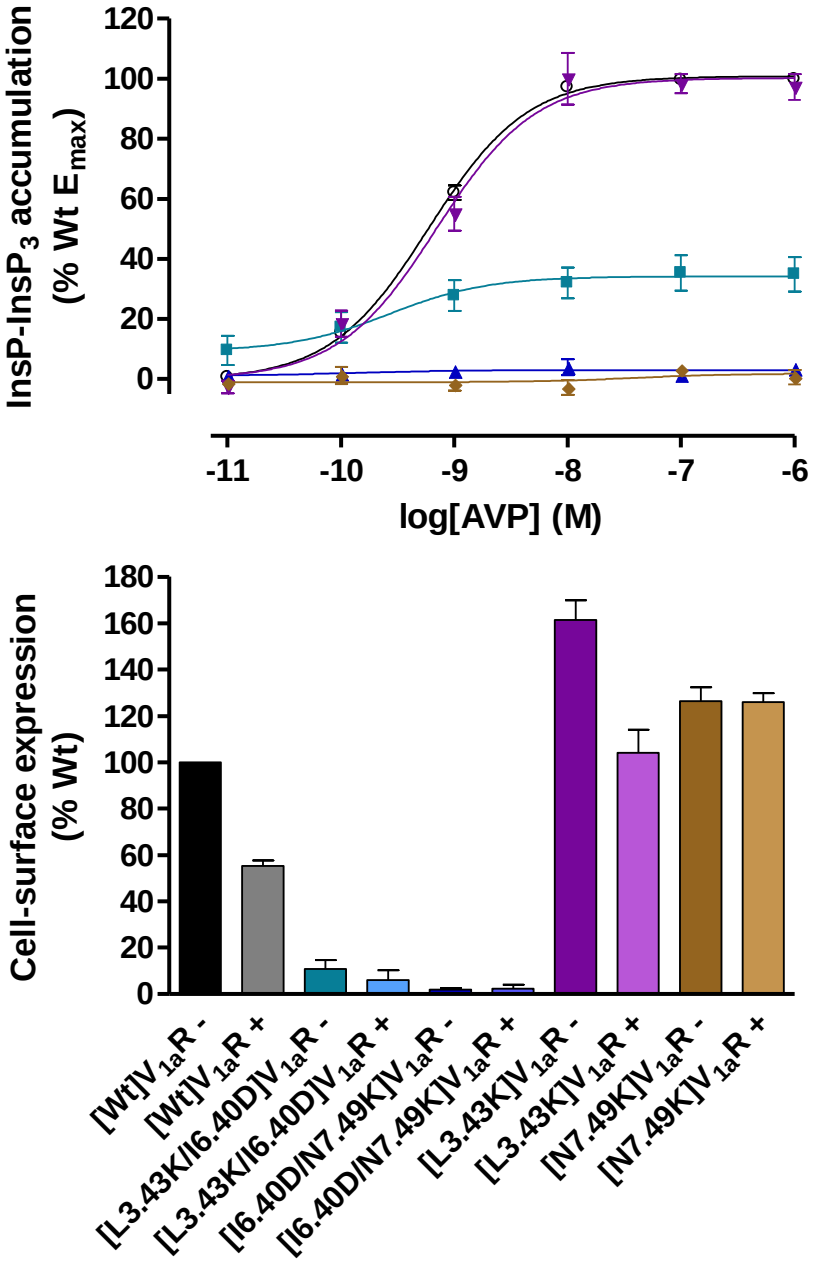

Figure 4.15 InsP-InsP$_3$ dose-response curves and cell-surface expression (+/- agonist challenge) of constructs probing interactions with Ile$^{6.40}$

Upper panel: Dose-response curves of inositol phosphates accumulation assays of HEK 293T cells, transiently transfected with receptor constructs [Wt]V_{1a}R, (○); [L3.43K/I6.40D]V_{1a}R, (■); [I6.40D/N7.49K]V_{1a}R, (▲);[L3.43K]V_{1a}R (▼) and [N7.49K]V_{1a}R (♦). Data are normalised to [Wt]V_{1a}R basal and maximal signalling levels, expressed as the mean ± s.e.m. of three experiments performed in triplicate. Basal signalling is plotted at 10^{-11} M. Lower panel: Cell-surface expression levels of receptor constructs were normalised to untransfected cells and unstimulated (-) [Wt]V_{1a}R expression levels. Data are stated as the mean ± s.e.m. of three experiments performed in triplicate. Stimulated (+) constructs were challenged by 10^{-7}M AVP for 30 min.

Receptor construct	Binding K_i (nM) ± s.e.m.		InsP-$InsP_3$ accumulation (% Wt E_{max}) ± s.e.m.			Cell-surface expression (% Wt unstimulated) ± s.e.m.	
	AVP	CA	Basal	EC_{50}*	E_{max}	Unstimulated	Simulated
$V_{1a}R$	**0.45 ± 0.04**	**0.96 ± 0.10**	**0**	**0.60 ± 0.02**	**100**	**100**	**55 ± 2**
[L3.43K/I6.40D]$V_{1a}R$	0.32 ± 0.02#	2.23 ± 0.05#	10 ± 5	0.27 ± 0.07	35 ± 6	11 ± 4	6 ± 5
[I6.40D/N7.49K]$V_{1a}R$	0.66 ± 0.23#	2.96 ± 0.27#	1 ± 1	No detectible signalling		2 ± 1	2 ± 2
[L3.43K]$V_{1a}R$	3.52 ± 1.27	1.08 ± 0.14	-3 ± 2	0.67 ± 0.14	100 ± 9	161 ± 9	104 ± 10
[N7.49K]$V_{1a}R$	9.36 ± 1.62	1.23 ± 0.27	-1 ± 1	No detectible signalling		126 ± 6	126 ± 4

Table 4.3 Binding, signalling and cell-surface expression of receptor constructs probing interactions with Ile$^{6.40}$

All data are shown as the mean ± s.e.m. of three separate experiments performed in triplicate. *EC_{50} is stated as the mean ± mean of 95 % confidence intervals of three separate experiments performed in triplicate. Data in yellow indicate >2.5-fold increase in K_i or EC_{50} or >25 % reduction in E_{max}, cell-surface expression; orange >5-fold increase in K_i or EC_{50} or >50 % reduction in E_{max}, cell-surface expression or internalisation; red >10-fold increase in K_i or EC_{50} or >75 % reduction in E_{max}, cell-surface expression or internalisation. Data in green indicate >2.5-fold increase in K_i or EC_{50} or >25 % increase in E_{max}, cell-surface expression or > 50% increase in internalisation. Data in white are comparable to Wt. # denotes IC_{50} ± mean of 95 % confidence intervals of three separate experiments performed in triplicate.

4.2.3 The effects of the N7.49R substitution on the$V_{1a}R$

In that the [N7.49K]$V_{1a}R$ receptor construct displayed significant perturbation in function, the [N7.49R]$V_{1a}R$ construct was generated to assess whether the effects observed were as a result of the lysine present at position 7.49 or a basic side chain in general. The pharmacology of the [N7.49R]$V_{1a}R$ receptor construct was Wt-like with respect to both agonist and antagonist binding (Figure 4.16, Table 4.4).

[N7.49R]$V_{1a}R$ was unable to generate detectible InsP-$InsP_3$ signal although it was expressed at the cell surface at levels comparable to Wt (Figure 4.17, Table 4.4). The construct was incapable if internalisation upon agonist challenge.

4.2.4 Probing the interaction of $Leu^{3.43}$ and $Asn^{7.49}$

In order to probe potential interaction of $Leu^{3.43}$ and $Asn^{7.49}$ as both residues are oriented towards each other in the helical bundle of the inactive, carazolol-bound β_2AR (Cherezov *et al.*, 2007), the receptor constructs [L3.43D/N7.49K]$V_{1a}R$ and [L3.43K/N7.49D]$V_{1a}R$ were generated. Additionally the single substitutions [L3.43D]$V_{1a}R$ and [N7.49D]$V_{1a}R$ were generated to assess the effects of single substitutions participating in potential charge-charge interaction.

[L3.43D/N7.49K]$V_{1a}R$ generated radioligand competition curves and IC_{50} values for both AVP, 0.72 ± 0.11 nM and CA, 1.73 ± 0.09 nM that were comparable to Wt (AVP, 0.85 ± 0.02 nM; CA, 2.17 ± 0.09 nM) (Figure 4.18). [L3.43K/N7.49D]$V_{1a}R$ displayed Wt-like binding affinities for both AVP and CA (Figure 4.18, Table 4.5). [L3.43D]$V_{1a}R$ did not binding [^{3}H]AVP at experimental concentrations and [N7.49D]$V_{1a}R$ maintained Wt-like pharmacology.

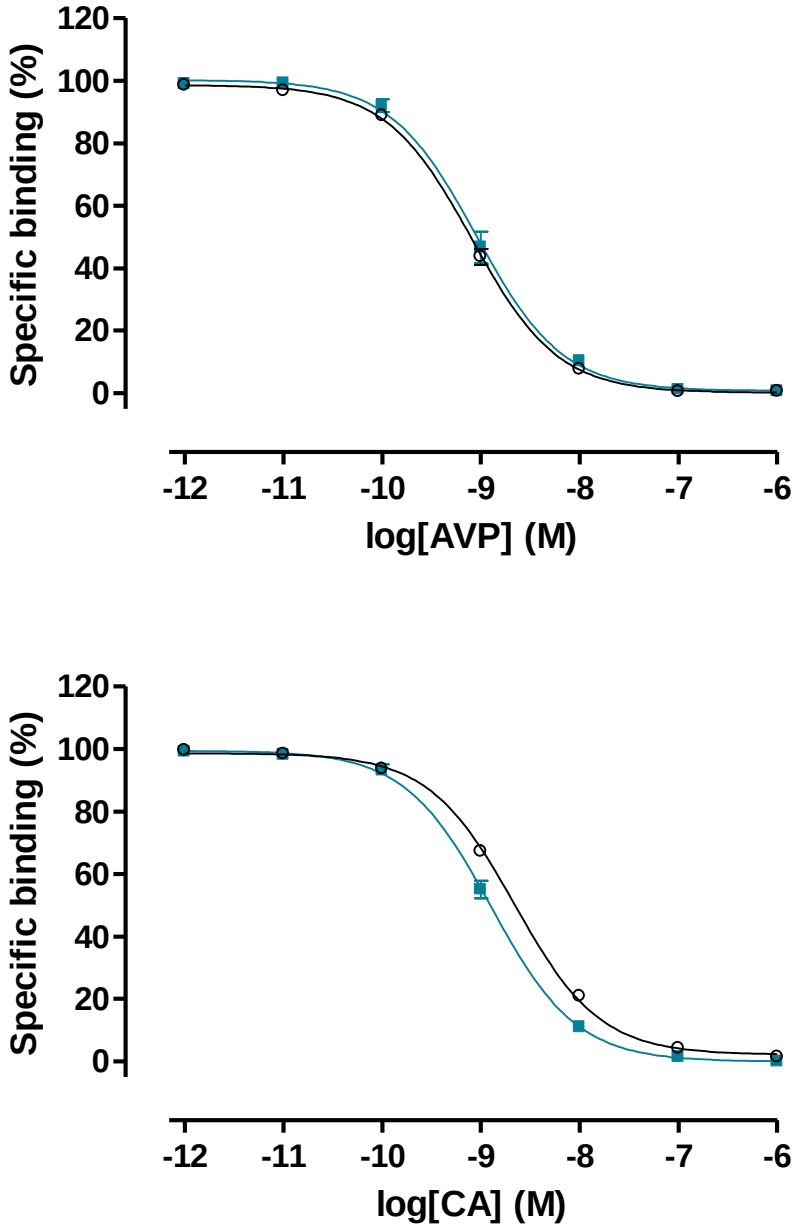

Figure 4.16 Competition radioligand binding profiles of [N7.49R]$V_{1a}R$

Competition radioligand binding assays were performed on HEK 293T cells, transiently transfected with receptor constructs [Wt]$V_{1a}R$, (○) and [N7.49R]$V_{1a}R$, (■). Upper panel: [^{3}H]AVP vs. AVP competition; lower panel: [^{3}H]AVP vs. CA competition. A theoretical Langmuir binding isotherm was fitted to data expressed as specific binding (%), defining non-specific binding by 1 μM ligand. Data are the mean ± s.e.m. of three experiments performed in triplicate.

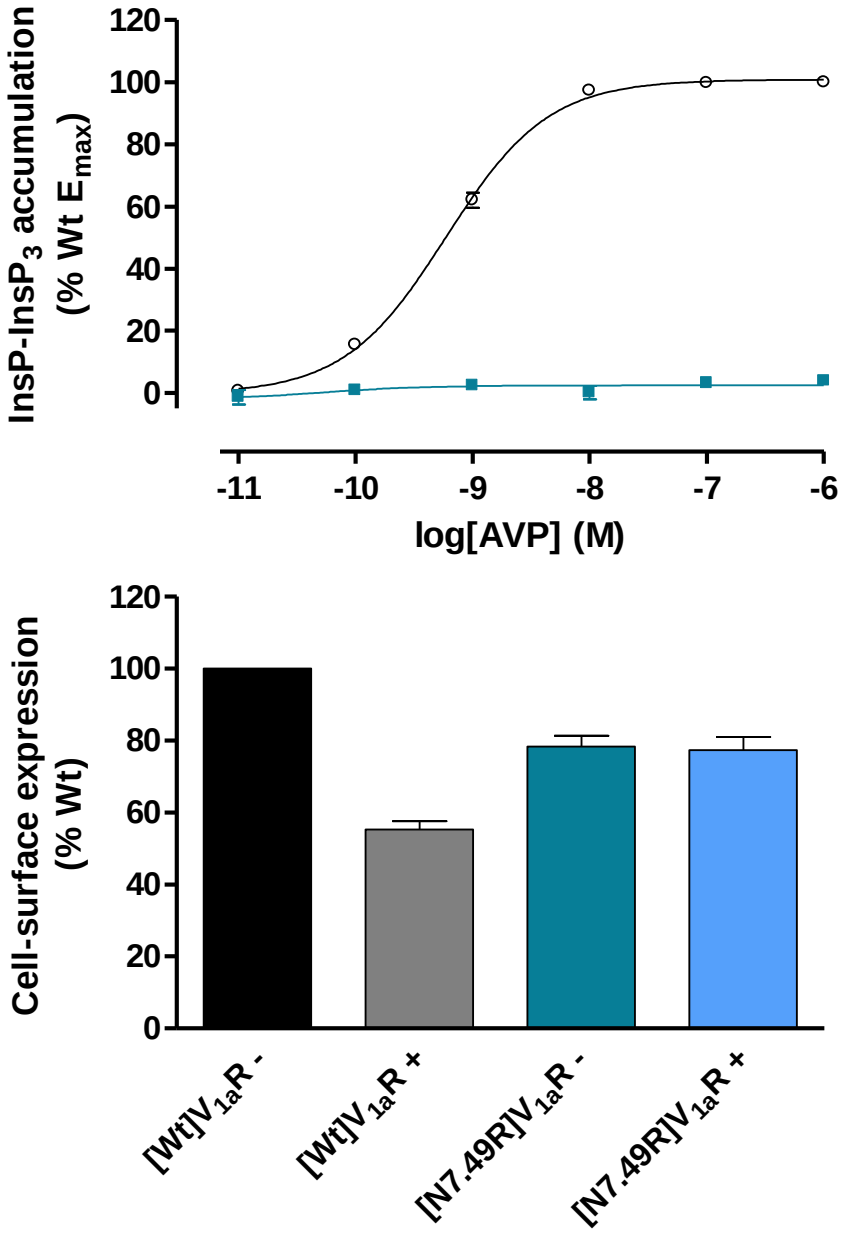

Figure 4.17 InsP-InsP$_3$ dose-response curves and cell-surface (+/- agonist challenge) expression of [N7.49R]V$_{1a}$R

Upper panel: Dose-response curves of inositol phosphates accumulation assays of HEK 293T cells, transiently transfected with receptor constructs [Wt]V$_{1a}$R, (○) and [N7.49R]V$_{1a}$R, (■). Data are normalised to [Wt]V$_{1a}$R basal and maximal signalling levels, expressed as the mean ± s.e.m. of three experiments performed in triplicate. Basal signalling is plotted at 10^{-11} M. Lower panel: Cell-surface expression levels of receptor constructs were normalised to untransfected cells and unstimulated (-) [Wt]V$_{1a}$R expression levels. Data are stated as the mean ± s.e.m. of three experiments performed in triplicate. Stimulated (+) constructs were challenged by 10^{-7}M AVP for 30 min.

Receptor construct	Binding K_i (nM) ± s.e.m.		InsP-$InsP_3$ accumulation (% Wt E_{max}) ± s.e.m.			Cell-surface expression (% Wt unstimulated) ± s.e.m.	
	AVP	CA	Basal	EC_{50}*	E_{max}	Unstimulated	Simulated
$V_{1a}R$	**0.45 ± 0.04**	**0.96 ± 0.10**	**0**	**0.60 ± 0.02**	**100**	**100**	**55 ± 2**
[N7.49R]$V_{1a}R$	0.74 ± 0.16	0.72 ± 0.20	-2 ± 1	No detectible signalling		78 ± 3	77 ± 4

Table 4.4 Binding, signalling and cell-surface expression of [N7.49R]$V_{1a}R$

All data are shown as the mean ± s.e.m. of three separate experiments performed in triplicate. *EC_{50} is stated as the mean ± mean of 95 % confidence intervals of three separate experiments performed in triplicate. Data in yellow indicate >2.5-fold increase in K_i or EC_{50} or >25 % reduction in E_{max}, cell-surface expression; orange >5-fold increase in K_i or EC_{50} or >50 % reduction in E_{max}, cell-surface expression or internalisation; red >10-fold increase in K_i or EC_{50} or >75 % reduction in E_{max}, cell-surface expression or internalisation. Data in green indicate >2.5-fold increase in K_i or EC_{50} or >25 % increase in E_{max}, cell-surface expression or > 50% increase in internalisation. Data in white are comparable to Wt. # denotes IC_{50} ± mean of 95 % confidence intervals of constructs that bound ligand.

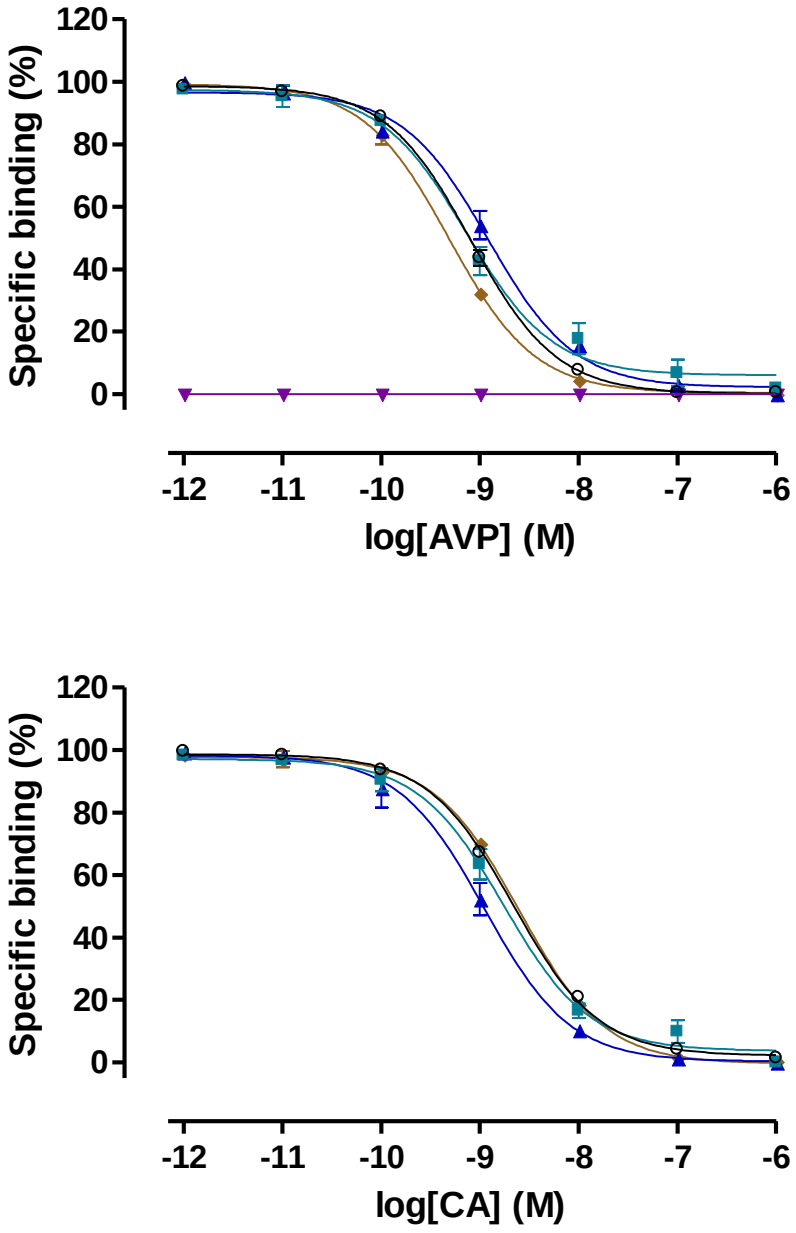

Figure 4.18 Competition radioligand binding profiles of constructs probing the interaction of Leu$^{3.43}$ and Asn$^{7.49}$

Competition radioligand binding assays were performed on HEK 293T cells, transiently transfected with receptor constructs [Wt]$V_{1a}R$, (○); [L3.43D/N7.49K]$V_{1a}R$, (■); [L3.43K/N7.49D]$V_{1a}R$, (▲); [L3.43D]$V_{1a}R$ (▼); and [N7.49D]$V_{1a}R$ (♦). Upper panel: [^{3}H]AVP vs. AVP competition; lower panel: [^{3}H]AVP vs. CA competition. A theoretical Langmuir binding isotherm was fitted to data expressed as specific binding (%), defining non-specific binding by 1 μM ligand. Data are the mean ± s.e.m. of three experiments performed in triplicate.

[L3.43D/N7.49K]V_{1a}R and [L3.43D]V_{1a}R did not generate InsP-$InsP_3$ at levels that could be detected and were expressed at the cell surface at only ~10 % of Wt levels (Figure 4.19, Table 4.5). [L3.43K/N7.49D]V_{1a}R and [N7.49D]V_{1a}R signalled through the inositol phosphate pathway like Wt with only small reductions in maximal signalling levels, 70 % and 74 % of Wt E_{max} respectively. [L3.43K/N7.49D]V_{1a}R expressed at the cell surface at increased density compared to Wt (138 % of Wt levels) and internalised only 20 % of receptors when stimulated by AVP (Wt 45 % internalisation). [N7.49D]V_{1a}R expressed at a reduced level at the cell surface (56 % of Wt) but internalised like Wt upon agonist challenge.

4.2.5 Probing the interaction of Leu$^{3.43}$ and Tyr$^{6.44}$

In the lutropin receptor (LHR), the mutation L3.43R was identified as the cause of gonadotropin-independent precocious puberty in a Brazilian boy (Latronico *et al.*, 1998). This mutation caused salt-bridge formation with Asp$^{6.44}$, resulting in constitutive activity and a lack of hormone responsiveness. This interaction was attempted to be recapitulated in the V_{1a}R by the generation of the receptor construct [L3.43K/Y6.44D]V_{1a}R. The single substitution [Y6.44D]V_{1a}R was also generated.

[L3.43K/Y6.44D]V_{1a}R and [Y6.44D]V_{1a}R displayed 3.7-fold and 5.6-fold increases in affinity to AVP agonist respectively (Figure 4.20, Table 4.6). The receptor construct [L3.43K/Y6.44D]V_{1a}R possessed a 4.8-fold increase in CA affinity whilst [Y6.44D]V_{1a}R displayed a Wt-like affinity to the antagonist.

The double substitution [L3.43K/Y6.44D]V_{1a}R demonstrated a reduced maximal InsP-$InsP_3$ accumulation of 55 % of Wt E_{max} whilst maintaining Wt-like EC_{50} (Figure 4.21, Table 4.6). Cell-surface expression was reduced to 46 % of Wt levels and internalised in response to AVP challenge. [Y6.44D]V_{1a}R achieved maximal signalling levels only 11 % of Wt E_{max} with

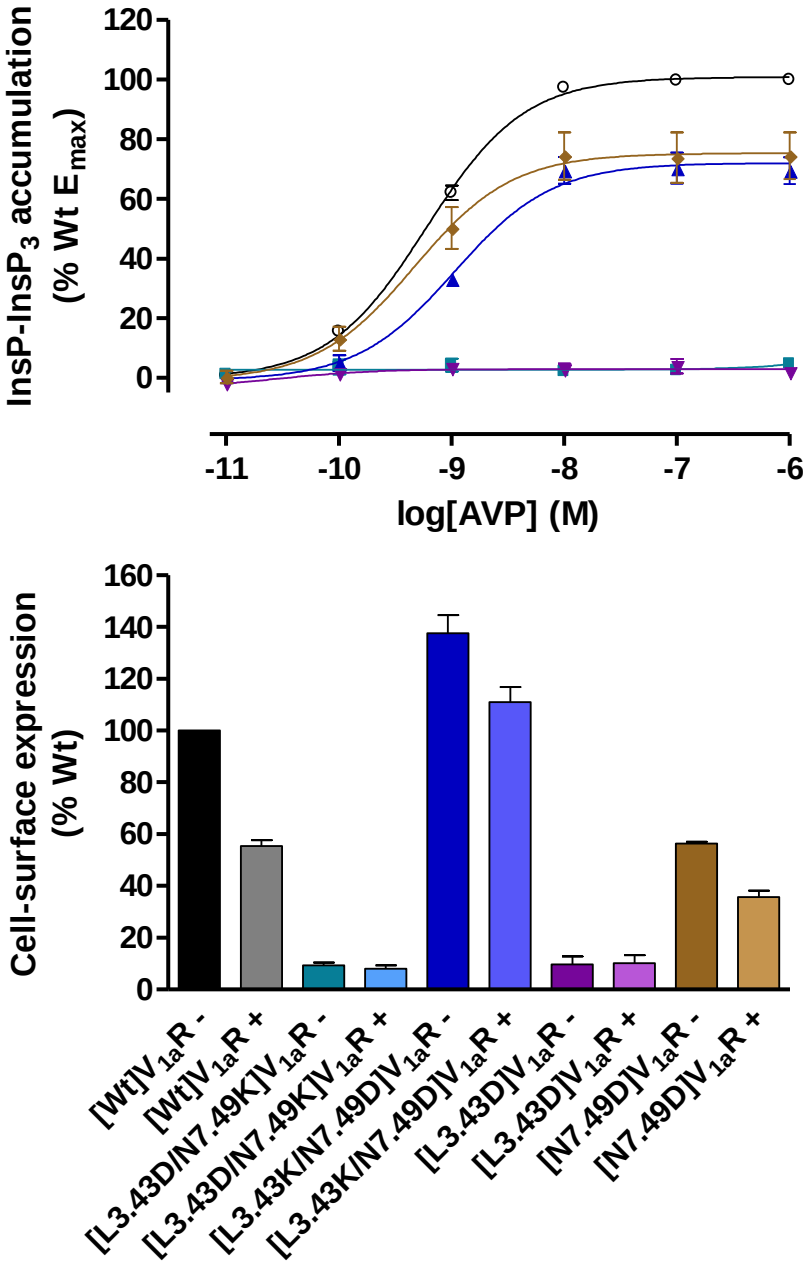

Figure 4.19 InsP-InsP$_3$ dose-response curves and cell-surface expression (+/- agonist challenge) of constructs probing the interaction of Leu$^{3.43}$ and Asn$^{7.49}$

Upper panel: Dose-response curves of inositol phosphates accumulation assays of HEK 293T cells, transiently transfected with receptor constructs [Wt]V_{1a}R, (○); [L3.43D/N7.49K]V_{1a}R, (■); [L3.43K/N7.49D]V_{1a}R, (▲); [L3.43D]V_{1a}R (▼) and [N7.49D]V_{1a}R (♦). Data are normalised to [Wt]V_{1a}R basal and maximal signalling levels, expressed as the mean ± s.e.m. of three experiments performed in triplicate. Basal signalling is plotted at 10^{-11} M. Lower panel: Cell-surface expression levels of receptor constructs were normalised to untransfected cells and unstimulated (-) [Wt]V_{1a}R expression levels. Data are stated as the mean ± s.e.m. of three experiments performed in triplicate. Stimulated (+) constructs were challenged by 10^{-7}M AVP for 30 min.

Receptor construct	Binding affinity, K_i (nM) ± s.e.m.		InsP-$InsP_3$ accumulation (% Wt E_{max}) ± s.e.m.			Cell-surface expression (% Wt unstimulated) ± s.e.m.	
	AVP	CA	Basal	EC_{50}*	E_{max}	Unstimulated	Simulated
[Wt]V_{1a}R	**0.45 ± 0.04**	**0.96 ± 0.10**	**0**	**0.60 ± 0.02**	**100**	**100**	**55 ± 2**
[L3.43D/N7.49K]V_{1a}R	0.72 ± 0.11#	1.73 ± 0.09#	1 ± 1	No detectible signalling		9 ± 1	8 ± 1
[L3.43K/N7.49D]V_{1a}R	1.09 ± 0.31	0.83 ± 0.21	1 ± 2	1.08 ± 0.12	70 ± 5	138 ± 7	111 ± 6
[L3.43D]V_{1a}R	Did not bind [^{3}H]AVP		-2 ± 1	No detectible signalling		10 ± 3	10 ± 3
[N7.49D]V_{1a}R	0.26 ± 0.04	1.09 ± 0.17	0 ± 2	0.48 ± 0.05	74 ± 8	56 ± 1	36 ± 3

Table 4.5 Binding, signalling and cell-surface expression of constructs probing the interaction of Leu$^{3.43}$ and Asn$^{7.49}$

All data are shown as the mean ± s.e.m. of three separate experiments performed in triplicate. *EC_{50} is stated as the mean ± mean of 95 % confidence intervals of three separate experiments performed in triplicate. Data in yellow indicate >2.5-fold increase in K_i or EC_{50} or >25 % reduction in E_{max}, cell-surface expression; orange >5-fold increase in K_i or EC_{50} or >50 % reduction in E_{max}, cell-surface expression or internalisation; red >10-fold increase in K_i or EC_{50} or >75 % reduction in E_{max}, cell-surface expression or internalisation. Data in green indicate >2.5-fold increase in K_i or EC_{50} or >25 % increase in E_{max}, cell-surface expression or > 50% increase in internalisation. Data in white are comparable to Wt. # denotes IC_{50} ± mean of 95 % confidence intervals of three experiments performed in triplicate.

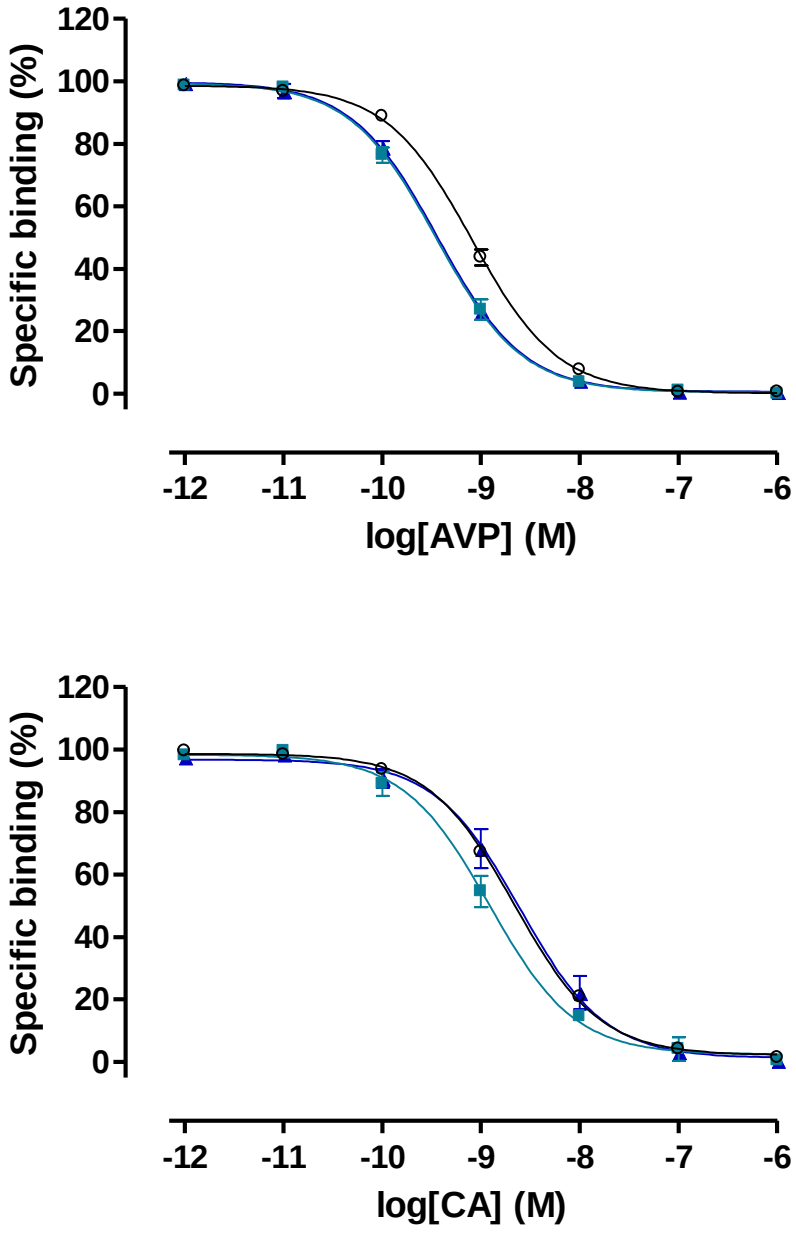

Figure 4.20 Competition radioligand binding profiles of constructs probing the interaction of Leu$^{3.43}$ and Tyr$^{6.44}$

Competition radioligand binding assays were performed on HEK 293T cells, transiently transfected with receptor constructs [Wt]V_{1a}R, (○); [L3.43K/Y6.44D]V_{1a}R, (■) and [Y6.44D]V_{1a}R, (▲). Upper panel: [^{3}H]AVP vs. AVP competition; lower panel: [^{3}H]AVP vs. CA. A theoretical Langmuir binding isotherm was fitted to data expressed as specific binding (%), defining non-specific binding by 1 μM ligand. Data are the mean ± s.e.m. of three experiments performed in triplicate.

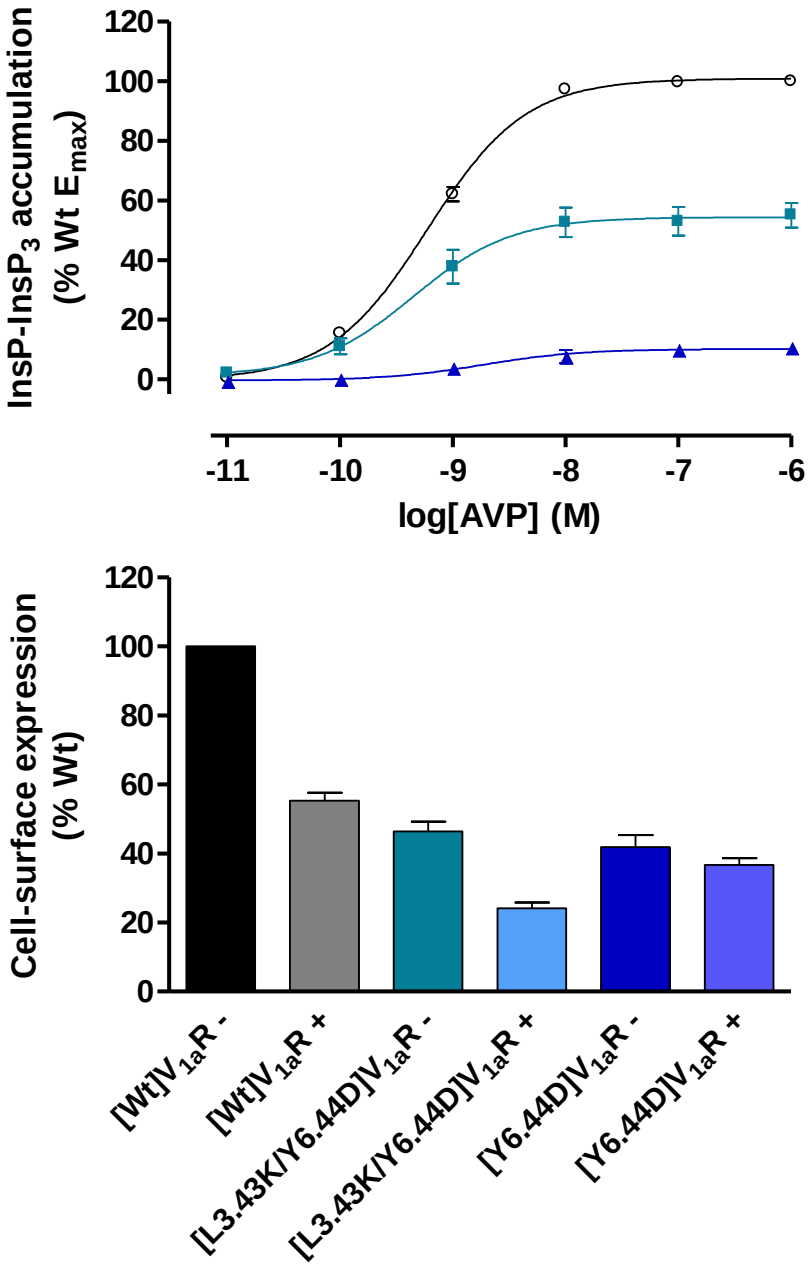

Figure 4.21 InsP-InsP$_3$ dose-response curves and cell-surface expression of constructs probing the interaction of Leu$^{3.43}$ and Tyr$^{6.44}$

Upper panel: Sigmoidal dose-response curves of inositol phosphates accumulation assays of HEK 293T cells, transiently transfected with receptor constructs [Wt]V_{1a}R, (○); [L3.43K/Y6.44D]V_{1a}R, (■) and [Y6.44D]V_{1a}R, (▲). Data are normalised to [Wt]V_{1a}R basal and maximal signalling levels, expressed as the mean ± s.e.m. of three experiments performed in triplicate. Basal signalling is plotted at 10^{-11} M. Lower panel: Cell-surface expression levels of receptor constructs were normalised to untransfected cells and unstimulated (-) [Wt]V_{1a}R expression levels. Data are stated as the mean ± s.e.m. of three experiments performed in triplicate. Stimulated (+) constructs were challenged by 10^{-7}M AVP for 30 min.

Receptor construct	Binding affinity, K_i (nM) ± s.e.m.		InsP-$InsP_3$ accumulation (% Wt E_{max}) ± s.e.m.			Cell-surface expression (% Wt unstimulated) ± s.e.m.	
	AVP	CA	Basal	EC_{50}*	E_{max}	Unstimulated	Simulated
$V_{1a}R$	**0.45 ± 0.04**	**0.96 ± 0.10**	**0**	**0.60 ± 0.02**	**100**	**100**	**55 ± 2**
[L3.43K/Y6.44D]$V_{1a}R$	0.12 ± 0.03	0.20 ± 0.02	2 ± 1	0.46 ± 0.03	55 ± 4	46 ± 3	24 ± 2
[Y6.44D]$V_{1a}R$	0.08 ± 0.03	0.47 ± 0.09	-1 ± 0	1.81 ± 0.50	10 ± 1	42 ± 4	37 ± 2

Table 4.6 Binding, signalling and cell-surface expression of constructs probing the interaction of $Leu^{3.43}$ and $Tyr^{6.44}$

All data are shown as the mean ± s.e.m. of three separate experiments performed in triplicate. *EC_{50} is stated as the mean ± mean of 95 % confidence intervals of three separate experiments performed in triplicate. Data in yellow indicate >2.5-fold increase in K_i or EC_{50} or >25 % reduction in E_{max}, cell-surface expression; orange >5-fold increase in K_i or EC_{50} or >50 % reduction in E_{max}, cell-surface expression or internalisation; red >10-fold increase in K_i or EC_{50} or >75 % reduction in E_{max}, cell-surface expression or internalisation. Data in green indicate >2.5-fold increase in K_i or EC_{50} or >25 % increase in E_{max}, cell-surface expression or > 50% increase in internalisation. Data in white are comparable to Wt. # denotes IC_{50} ± mean of 95 % confidence intervals of three separate experiments performed in triplicate.

a 3-fold increase in EC_{50}. The cell-surface expression was reduced to 42 % of Wt and only 12 % of receptor at the cell surface were internalised upon agonist challenge (Wt, 45 % of unstimulated expression).

4.3 Discussion

4.3.1 The role of $Ile^{6.40}$ in the structure and function of the $V_{1a}R$

The conserved hydrophobic residue at position 6.40 is implicated in forming a hydrophobic barrier, separating the ligand binding site from the intracellular G-protein docking domain (Trzaskowski *et al.*, 2012). The residues partaking in this interaction are shown in Figure 4.22. Mutation of residue 6.40 has resulted in generating constitutively active mutants in opsin, MC4R and H_1R (Han *et al.*, 1998; Proneth *et al.*, 2006; Bakker *et al.*, 2008) by destabilisation of an inactive receptor conformation.

The [I6.40A]$V_{1a}R$ construct effectively removes the isoleucine side chain as far as the β-carbon of the side chain and in doing so, a classical CAM was generated. Constitutively active mutants possess an increased affinity for agonists and a small 2.3-fold increase was observed in the [I6.40A]$V_{1a}R$ construct. The basal signalling level of the [I6.40A]$V_{1a}R$ was increased to 17 % of Wt E_{max} levels and a Wt-like E_{max} although the cell-surface expression was decreased to half of Wt levels. These data clearly implicate the isoleucine side chain at position 6.40 in the $V_{1a}R$ as participating in interactions stabilising the inactive receptor state. Substantial constitutive activity were also generation by substitution of 6.40 to alanine in opsin, 10.9% of light stimulated signalling (Han *et al.*, 1998) and H_1R, ~65 % of E_{max} (Bakker *et al.*, 2008). In contract, the corresponding substitution in the MC4R did not generate a CAM (Proneth *et al.*, 2006). Substituting 6.40 for alanine in MC4R and H_1R reduced expression to about 25 % of Wt levels while [I6.40A]$V_{1a}R$ expressed like Wt. The substitution of the

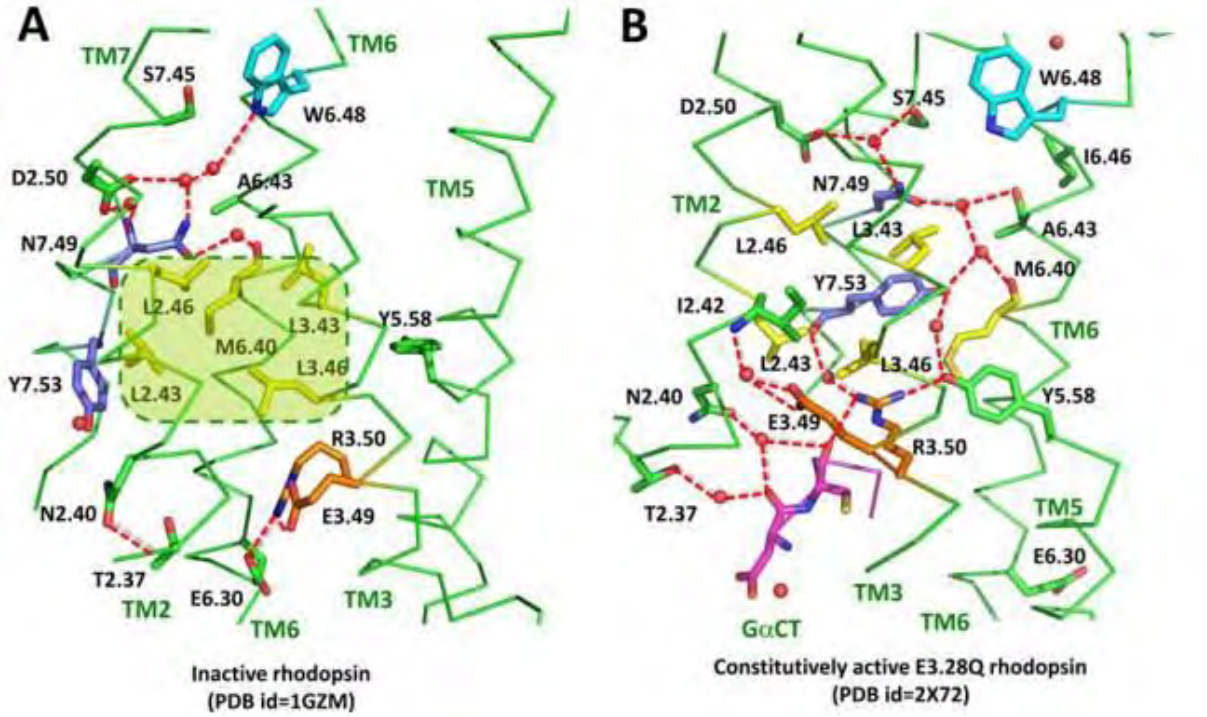

Figure 4.22 Hydrophobic barrier residues in inactive rhodopsin and their rearrangements upon activation

A) The crystal structure of inactive rhodopsin (pdb: 1GZM) highlighting residues of TM II, III and VI comprising the hydrophobic barrier, separating the ligand binding site from the cytoplasmic G-protein binding domain. B) The opening of the hydrophobic barrier, as in the active rhodopsin structure (pdb: 2X72) and formation of a water, channel connecting the ligand binding domain with the ERY motif and G-protein docking domain. (Trzaskowski *et al.*, 2012).

isoleucine side chain for only a hydrogen atom as in the [I6.40G]V_{1a}R receptor construct also increased AVP affinity (2.1-fold) although no increase in the basal signalling level was detected. However, similarly to the alanine substitution, [I6.40G]V_{1a}R displayed E_{max} of 58 % of Wt with a more detrimental effect on cell-surface expression (41 % of Wt). A similar reduction in expression was observed in the H_1R but this construct displayed substantial increase in agonist-independent signalling (Bakker *et al.*, 2008). Increased flexibility introduced into TM VI by the glycine residue may reduce the stability of the receptor, reducing cell-surface expression. Substitution to serine or threonine generated receptors that possessed substantial increases in basal activity at 12 % and 7 % of Wt E_{max} respectively whilst maintaining Wt pharmacology. [I6.40S]V_{1a}R and [I6.40T]V_{1a}R constructs still achieved Wt-like levels of maximal signalling although their expression was reduced to 53 % and 72 % respectively. Particularly for the [I6.40S]V_{1a}R receptor construct, it appears that there in an increased ability for AVP to signal through the inositol phosphate pathway. The serine substitution generated the third highest levels of constitutive activity in opsin at ~16 % of maximum light activated levels and 8.5 % for the threonine substitution (Han *et al.*, 1998). Molecular modelling suggested that serine interacts with $Arg^{3.50}$ through a hydrogen bond network in opsin, stabilising an active conformation and permitting interaction with G-protein (Deupi *et al.*, 2012). The serine substitution in H_1R fully activated the receptor as it was unresponsive to further activation by histamine (Bakker *et al.*, 2008) although the construct could still bind agonist. The [I6.40C]V_{1a}R construct essentially substitutes the hydroxyl of serine for the thiol of cysteine. This substitution generated a receptor construct that was Wt with respects to pharmacology, signalling and cell-surface expression supporting that the hydroxyl moiety in eliciting the basal activity observed in the [I6.40S]V_{1a}R construct. Cysteine substitution in opsin produced one of the lowest basal activities, 3.9 % of light

induced maximum (Han *et al.*, 1998). The [I6.40V]V_{1a}R receptor construct is the approximate side chain volume of [I6.40T]V_{1a}R but is hydrophobic as it does not possess the hydrophilic hydroxyl of threonine. This receptor construct was Wt-like with respect to pharmacology, signalling capabilities, cell-surface expression and internalisation. This further highlights the participation of polar moieties conferring basal activity in the V_{1a}R. This being said, an increase of ~ 9 % in basal activity was observed in opsin when valine was substituted at position 6.40 (Han *et al.*, 1998).

[I6.40M]V_{1a}R displayed basal InsP-$InsP_3$ to 18 % of Wt E_{max}. Wt-like pharmacology was maintained in this receptor construct. E_{max} of 146 % of Wt was displayed while expressing at the cell-surface at a Wt-like density. Together, these data suggest that in the context of the V_{1a}R, the methionine which is capable of maintaining the very low levels of basal activity in rhodopsin cannot fulfil the same role. Only one other V_{1a}R construct demonstrated increased basal activity, [I6.40N]V_{1a}R although the level was not as robust as other receptor constructs. This receptor construct maintained Wt-like pharmacology, EC_{50} and maximal signalling levels even with expression of 57 % of Wt levels. The asparagine substitution of the MC4R generated the greatest increase in constitutive activity of the seven substitutions characterised (Proneth *et al.*, 2006). Similarly, substantial constitutive activity (22.9 % of light-activated maximum) was observed in opsin by asparagine substitution (Han *et al.*, 1998) by interaction with $Arg^{3.50}$ through a hydrogen bond network (Deupi *et al.*, 2012). The naturally occurring polymorphism L6.40Q in MC4R displayed similar levels of constitutive activity to the asparagine substitution and molecular modelling suggests that the glutamine side chain stabilises the orientation of $Tyr^{5.58}$ and $Tyr^{7.53}$ into the helical bundle characteristic of the active state (Proneth *et al.*, 2006). However, the basal activity of the glutamine substitution of 6.40 in opsin did not generate such a large increase in constitutive activity (2.6 % of

signalling in light). [I6.40Q]V_{1a}R displayed decreased AVP efficacy (41 % Wt E_{max} whilst expressing like Wt) indicating that the longer side chain of glutamine compared to asparagine is, at least in part, responsible for the reduced InsP-$InsP_3$ response to AVP.

Introduction of the helix-breaking proline residue in [I6.40P]V_{1a}R was slightly detrimental to the integrity and stability of the construct as suggested from the reduced cell-surface expression. This being said, pharmacology and signalling properties of the construct were well maintained. In opsin, the proline substitution of 6.40 resulted in a slight increase in constitutive activity of only 5.8 % of light activated maximum but the greatest reduction in maximum signalling levels (Han *et al.*, 1998).

The integrity of the V_{1a}R was severely reduced when $Ile^{6.40}$ was substituted for either aspartate or glutamate as indicated by cell-surface expression levels of [I6.40D]V_{1a}R, 10 % of Wt and [I6.40E]V_{1a}R, 27 % of Wt. Substitution of $Ile^{6.40}$ to glutamate in the H_1R also severely decreased receptor expression (~ 10 % of Wt) but was able to be characterised with regards to signalling and the construct was almost full activated (Bakker *et al.*, 2008). The same substitution in the MC4R receptor also increased constitutive activity but expressed at 66 % of Wt levels (Proneth *et al.*, 2006). Basal signalling in opsin of 6.40 substitutions to aspartate and glutamate were 9.7 and 6.4 % of maximum respectively (Han *et al.*, 1998). Given the levels of constitutive activity of receptors possessing an acidic residue at position 6.40, it may be possible that a similar substitution in the V_{1a}R is in fact constitutively active, but the instability introduced by the destabilisation of the inactive receptor state is such that is cannot be expressed at sufficient levels to be functionally characterised. Unlike the substitutions of $Ile^{6.40}$ to acidic residues in the V_{1a}R, the integrity of the receptor constructs substituted by basic amino acids was not affected as constructs were expressed at levels comparable to Wt. Arginine and lysine substitutions in the MC4R generated constructs that expressed at reduced

levels compared to Wt, ~ 54 % of Wt (Proneth *et al.*, 2006). Similarly, in the H_1R, lysine and arginine substitutions at 6.40 were detrimental to cell-surface expression, < 50 % of Wt levels (Bakker *et al.*, 2008). Arginine at 6.40 in opsin resulted in a receptor construct that could not be expressed to levels that could be functionally characterised while histidine and lysine substitutions demonstrated detectible increased in basal activity (~ 6 % maximum activation) and were activated to Wt-like levels in light. However, [I6.40H]$V_{1a}R$, [I6.40K]$V_{1a}R$ and [I6.40R]$V_{1a}R$ displayed decreased efficacy, generating E_{max} (% Wt) of 31 %, 37 % and 18 % respectively although they were expressed at Wt-like levels. Although [I6.40H]$V_{1a}R$ and [I6.40K]$V_{1a}R$ maintained Wt-like pharmacology, the agonist potency to generate InsP-$InsP_3$ were reduced as indicated by the respective 5.3- and 6.9-fold increases in EC_{50}. In MC4R arginine substitution at 6.40 was clearly constitutively active whilst lysine demonstrated only moderate agonist-independent signalling (Proneth *et al.*, 2006). Conversely, although both substitutions to basic amino acids were constitutively active in H_1R, lysine substitution demonstrated full activation of the H_1R (Bakker *et al.*, 2008). Computational modelling (Figure 4.23) suggested the mechanism of constitutive activity by these basic residues in the H_1R is by inducing the conformational reorientation of $Asn^{7.49}$ towards $Asp^{2.50}$ as in the active state (Jongejan *et al.*, 2005; Urizar *et al.*, 2005).

The bulky side chain of phenylalanine in the [I6.40F]$V_{1a}R$ construct maintained receptor pharmacology and conferred increased stability of the $V_{1a}R$ manifesting in an increased cell-surface expression. However, a lesser proportion of the construct internalised when challenged by AVP compared to Wt. This may in part be due to the decreased potency of AVP to activate the receptor construct and hence generate InsP-$InsP_3$. No difference was observed in the basal signalling level of the [I6.40F]$V_{1a}R$ construct, as was the case in MC4R (Proneth *et al.*, 2006) and H_1R (Bakker *et al.*, 2008). The larger tryptophan residue of the

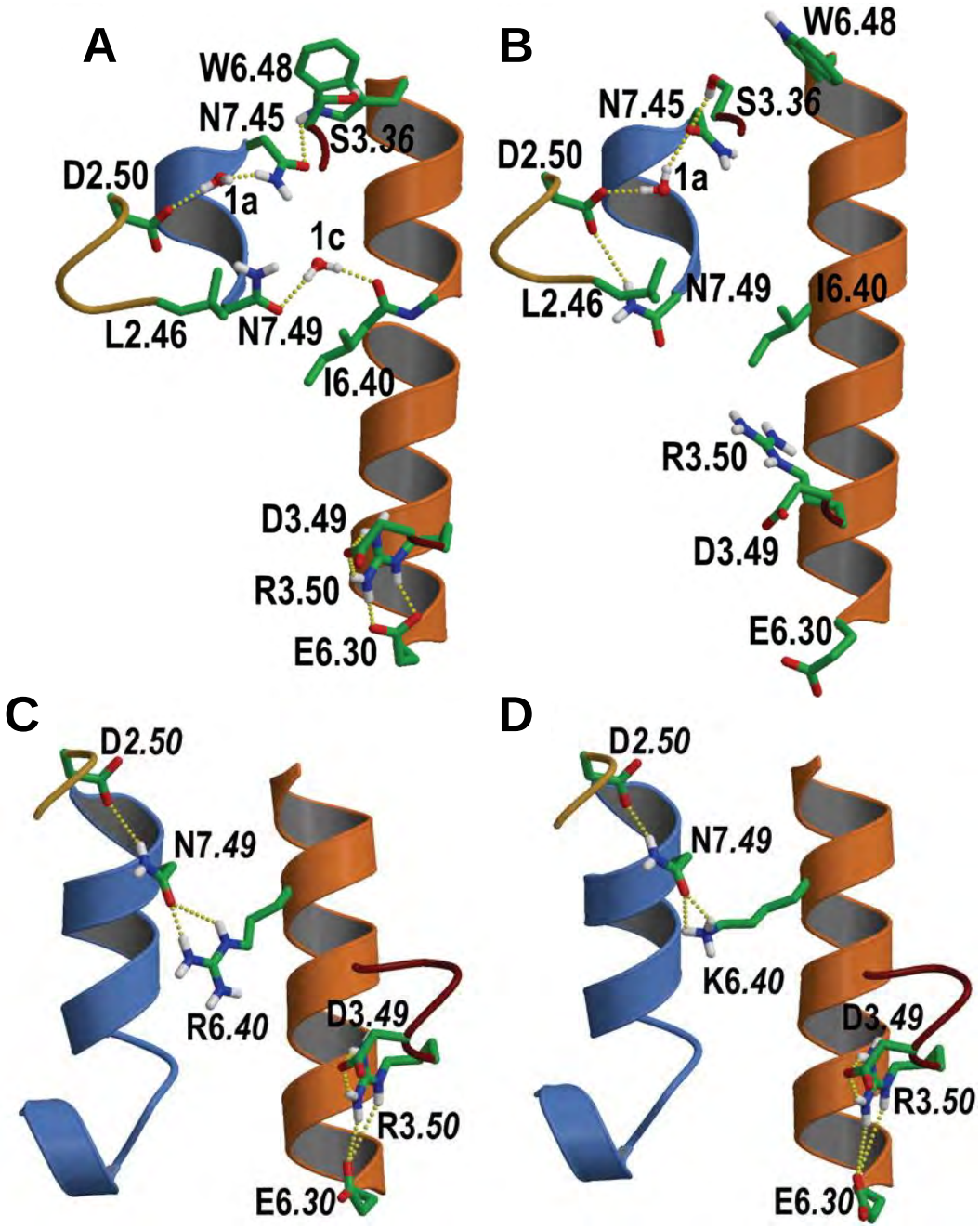

Figure 4.23 Mechanism of activation of Wt H_1R and I6.40R and I6.40K CAMs

A) Computational model of Wt H_1R in the inactive state; B) Model of Wt H_1R adopting an active conformation illustrating the interaction of $Asn^{7.49}$ and $Asp^{2.50}$; C-D) The active conformation of H_1R induced by the mutations of $Ile^{6.40}$ to C) arginine and D) lysine. These substitutions induce to reorientation of $Asn^{7.49}$ and $Asp^{2.50}$ as proposed in the activation of the Wt H_1R. The conformation of $Arg^{3.50}$ could not be modelled in C and D so has been modelled as engaging in the 'ionic lock' interaction. Colour code: golden rod, TM II; dark red, TM III; orange, TM VI, and blue, TM VII. (Bakker *et al*., 2008).

[I6.40W]V_{1a}R construct conferred a decreased AVP potency, but an apparent increase in AVP affinity. Although there was a decrease in cell-surface expression, this was not sufficient to account for the decreased maximal signalling levels demonstrating an inherent reduced ability to adopt an active receptor conformation. The apparent increase in AVP affinity may indicate long range perturbation of the ligand binding site.

Substitution of $Ile^{6.40}$ to leucine or tyrosine resulted in severe inactivation of the V_{1a}R. Both receptor constructs displayed small decreases (> 2.5-fold) in AVP binding affinity, suggesting the mutations introduced interactions that were stabilising an inactive state. This is supported by the apparent decreases in basal activity of [I6.40L]V_{1a}R and [I6.40Y]V_{1a}R to -9 and -11 % of Wt E_{max} respectively. Although the V_{1a}R displays little detectible basal activity natively, the reductions measured here further highlight the inactivating nature of the substitutions introduced. AVP potency is reduced 71.5-fold in the [I6.40L]V_{1a}R construct whereas a lesser 4.2-fold decrease is observed in the [I6.40Y]V_{1a}R construct. This being said, although both receptor constructs are expressed to levels comparable to Wt at the cell surface, only the [I6.40L]V_{1a}R construct is able to reach Wt-like maximal signalling levels. [I6.40Y]V_{1a}R displays reductions in AVP potency in a manner similar to the [I6.40F]V_{1a}R suggesting that the terminal hydroxyl of tyrosine mediates the inactivating reduction in basal activation and the benzene moiety causes the reduction in agonist potency to generate InsP-$InsP_3$. The leucine substitution of 6.40 in opsin was the only characterised construct to maintain basal levels of signalling (Han *et al*., 1998). In contrast to the findings in the V_{1a}R where tyrosine substitution generated a receptor construct that was greatly reduced in its ability to stabilise an active receptor conformation, the corresponding substitution in opsin generated the greatest level of constitutive activity, 32.6 % of light induced activity (Han *et al.*, 1998). The crystal structure of opsin incorporating the M6.40Y substitution proposes a mechanism for the high

degree of agonist-independent signalling in rhodopsin (Deupi *et al.*, 2012). This involves the stabilisation the orientations of $Tyr^{5.58}$ and $Tyr^{7.53}$ into the helical bundle through aromatic-aromatic interactions (Figure 4.24).

4.3.2 Probing interactions of $Ile^{6.40}$ with the receptor construct [I6.40D]$V_{1a}R$

In the attempt to recapitulate the interaction of $Ile^{6.40}$ with $Leu^{3.43}$ with a charge-charge interaction to recover expression and functionality, the following findings were observed. The double substitution [L3.43K/I6.40D]$V_{1a}R$ expressed at a similar level as the single [I6.40D]$V_{1a}R$ substitution. This being said, dose-responsive InsP-$InsP_3$ accumulation was re-established at detectible levels and a basal activity of 10 % of Wt E_{max} levels detected. Additionally, the construct bound AVP with higher affinity than Wt as suggested by the decreased IC_{50} (0.32 ± 0.02 nM; Wt, 0.85 ± 0.02 nM), a feature characteristic of CAMs (Figure 4.14, upper panel). The single substitution [L3.43K]$V_{1a}R$ displayed decreased binding affinity for AVP suggesting that the lysyl side chain at position 3.43 stabilises an inactive conformation, which may contribute to the increased cell-surface expression observed. This substitution does not prevent the construct from adopting an active conformation, as indicated by the Wt-like signalling capabilities through the inositol phosphate cascade. This is supported by the similar signalling capabilities were observed in the [L3.43A]$V_{1a}R$ construct generated previously but Wt-like AVP binding was maintained (Wootten, PhD thesis, University of Birmingham, 1997). An analogous substitution was generated in the LHR (L3.43R) which also increased the density of receptor at the cell surface (Latronico and Segaloff, 2007). This construct demonstrated increased constitutive cAMP accumulation but was unable to generate cAMP in response to agonist hormone although Wt-like binding affinity was maintained. Together, these data suggest that in the double substituted receptor construct [L3.43K/I6.40D]$V_{1a}R$, a charge-charge interaction confers the basal activity

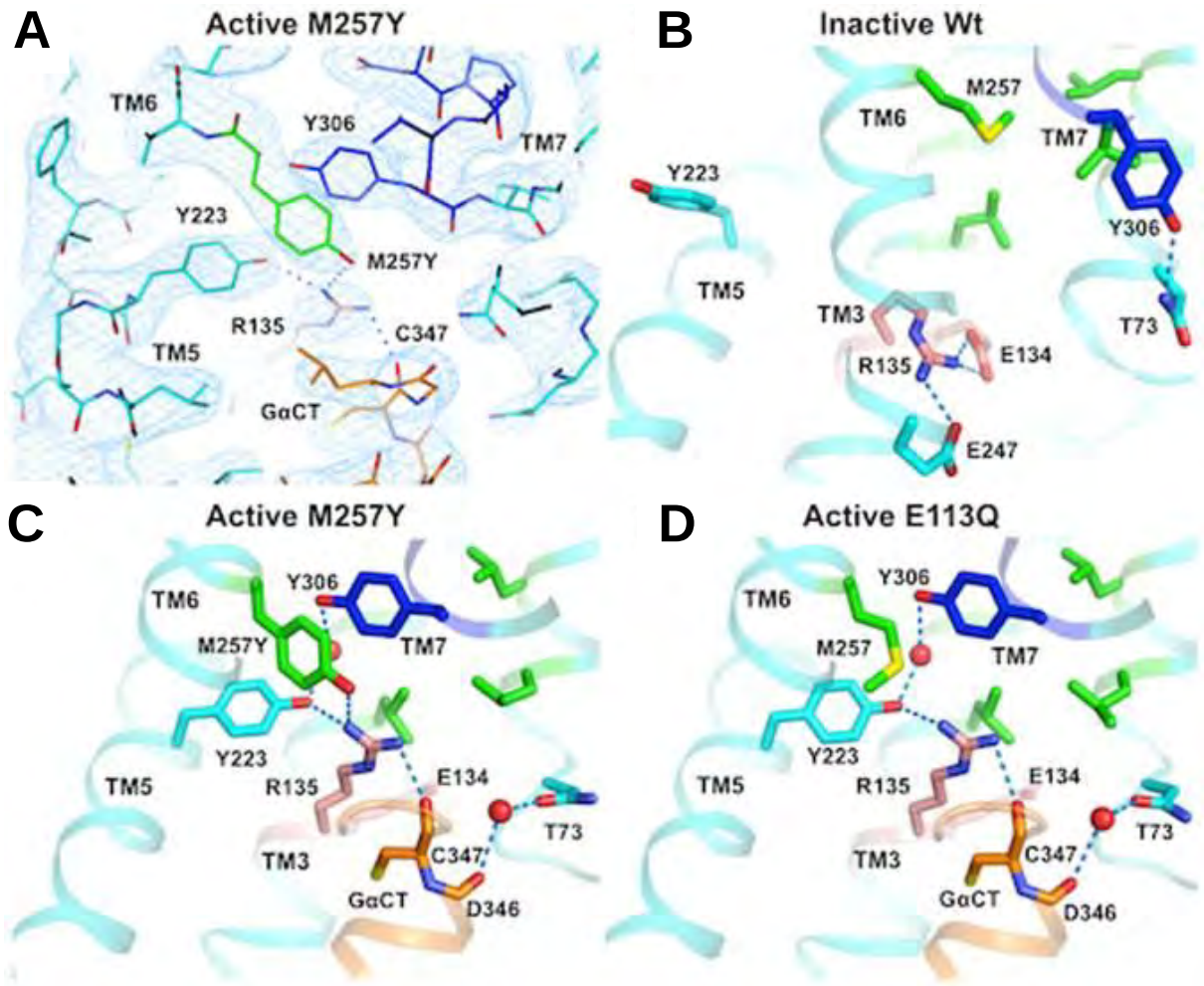

Figure 4.24 Effect of the M6.40Y mutation on the 'ionic lock' region of rhodopsin

A) blue mesh demonstrates the electron density of Y223$^{5.58}$, Y306$^{7.53}$ and CAM M257Y$^{6.40}$. B) Inactive conformation of Wt rhodopsin with hydrophobic barrier residue M257$^{6.40}$; C-D) demonstrate the similarity of the orientation of residues in the 'ionic lock' region of two constitutively active rhodopsin crystal structures (Deupi et al., 2012).

observed. One might hypothesise that this is due to the increased side chain length introduced by substitution of $Ile^{6.40}$ for lysine. Through L3.43K and I6.40D interacting, the increased side chain length introduced at 6.40 is increasing the distance between the cytoplasmic portions of TM VI and TM III, partially recapitulating the increase in distance well documented in GPCR activation required for G-protein activation.

In the attempt to stabilise the interaction of $Ile^{6.40}$ with $Asn^{7.49}$ with a charge-charge interaction to recover expression and functionality, the following findings were observed. [I6.40D/N7.49K]V_{1a}R was able to bind AVP and CA although cell-surface expression and InsP-$InsP_3$ generation were not detected. The loss of cell-surface expression was probably due to the detrimental effect of the I6.40D substitution given that the receptor construct [N7.49K]V_{1a}R was detected at the cell-surface at slightly higher levels than Wt, although generation of inositol phosphates by [N7.49K]V_{1a}R was not observed. Additionally the [N7.49K]V_{1a}R adopted a more inactive conformation as indicated by the greatly decreased (20-fold) AVP affinity. Given that the construct was able to bind AVP, albeit with reduced affinity, the lack of InsP-$InsP_3$ generation and internalisation upon agonist challenge was not due to an inability to bind AVP. The [N7.49R]V_{1a}R construct demonstrated Wt-like pharmacology indicating that the inactivating effects observed in [N7.49K]V_{1a}R are due specifically to the lysyl side chain and not the presence of a basic charge at 7.49. However, the inability of the [N7.49K]V_{1a}R construct to generate InsP-$InsP_3$ and to internalise upon agonist challenge, can be attributed to a basic charge being present at position 7.49 given that the same observations were made in the [N7.49R]V_{1a}R construct. An acidic charge at 7.49 as in the [N7.49D]V_{1a}R construct maintained the ability to internalise upon AVP challenge, further highlighting the basic charge at 7.49 being responsible for the loss of internalisation and InsP-$InsP_3$ generation.

4.3.3 Probing the interaction of Leu$^{3.43}$ and Asn$^{7.49}$

Introduction of an aspartate residue at position 3.43 was detrimental to the expression of receptor constructs [L3.43D]V_{1a}R and [L3.43D/N7.49K]V_{1a}R, which resulted in their inability to signal through the inositol phosphate pathway. In combination, the substitutions L3.43K and N7.49D caused the V_{1a}R to possess a decreased ability of AVP to generate InsP-$InsP_3$ given that the [L3.43K/N7.49D]V_{1a}R generated maximal signalling levels of only 70 % of Wt although it was very well expressed. Additionally, the construct demonstrated a severely decreased ability to internalise upon agonist challenge internalising only 20 % of receptors from the cell surface (Wt, 45 %). The [N7.49D]V_{1a}R receptor construct indicates that the decreased efficacy and inability to internalise are not attributed to the contribution of this substitution as this construct internalised upon agonist challenge and was dose-responsive in generating InsP-$InsP_3$. Together with the observed decreased AVP affinity observed in the single [L3.43K]V_{1a}R construct, these data suggest that the charge-charge interaction conferred in the [L3.43K/N7.49D]V_{1a}R maintain Wt-like conformation at the ligand binding pocket, but potentially a more inactive conformation at the intracellular side.

4.3.4 Probing the interaction of Leu$^{3.43}$ and Tyr$^{6.44}$

The substitution of Tyr$^{6.44}$ to aspartate results in a receptor that adopts a more active conformation as demonstrated by the increased affinity for AVP. However the ability to generate of InsP-$InsP_3$ was diminished given then E_{max} and AVP potency were reduced. Although the cell-surface expression was reduced to 42 % of Wt, it was not to an extent that should result in only 10 % of Wt E_{max}. For example [I6.40G]V_{1a}R expressed at a similar level but still has an E_{max} of 58 % of Wt (Table 4.2). The double substitution [L3.43K/Y6.44D]V_{1a}R was expressed at an almost identical level to [Y6.44D]V_{1a}R but the signalling capabilities were greatly enhanced. The 3.7-fold increase in AVP affinity and

increase in E_{max} from 10 % to 55 % of Wt are consistent with stabilising an R* state. Together, these data suggest that the interaction of $Leu^{3.43}$ and $Tyr^{6.44}$ contributes to the ability to signal through the inositol-phosphate pathway in the $V_{1a}R$, potentially through hydrophobic interaction of the leucine side chain and benzene ring of the native tyrosine side chain. The [Y6.44D]$V_{1a}R$ simulated the residue conserved in glycoprotein hormone receptors (Shinozaki *et al.*, 2001; Zhang *et al.*, 2005) but was disruptive to agonist-induced signalling in the $V_{1a}R$. With $Asp^{6.44}$ interacting with L3.43R of the LHR, constitutive activity was conferred and the receptor was no longer responsive to hormone agonist. In the $V_{1a}R$, [L3.43K/Y6.44D]$V_{1a}R$ recovered the reduced agonist-induced InsP-$InsP_3$ generation observed in [Y6.44D]$V_{1a}R$ but did not confer constitutive activity.

CHAPTER 5: THE ROLE OF TYR$^{5.58}$ IN $V_{1A}R$

5.1 Introduction

Understanding intramolecular interactions and structural rearrangements of transmembrane regions of GPCRs is key in elucidating activation mechanisms. The relative orientations of the TM III and TM VI are by far the most characterised, yet more subtle helical rearrangements have been identified in TM V.

TM V contains a proline residue conserved in 77 % of rhodopsin-like GPCRs (Mirzadegan *et al.*, 2003). Typically, the presence of a proline residue in an α-helix induces bend in the helix of approximately 20° (Deupi *et al.*, 2004) with the precise disruption being dictated by the local context. This distortion of the helix is induced by the steric clash introduced by the pyrrolidine ring and lack of normal main chain hydrogen bonding. Crystallographic data of GPCRs have identified that an unwinding of residues preceding this conserved proline residue removes the steric clashes associated with a typical α-helix (Sansuk *et al.*, 2011). Additionally, comparison of inactive and active rhodopsin structures reveals TM V approaches TM VI, accompanied by a rotation in TM V upon activation (Sansuk *et al.*, 2011; Standfuss *et al.*, 2011).

Although the Ballesteros-Weinstein numbering system is based around Pro$^{5.50}$, a Tyr$^{5.58}$ is equally conserved in rhodopsin-like GPCRs. The ligand-free crystal structure of opsin first identified Tyr$^{5.58}$ (Park *et al.*, 2008) as an interacting partner with Arg$^{3.50}$ which was subsequently confirmed by further rhodopsin crystal structures (Choe *et al.*, 2011; Deupi *et al.*, 2012) structures. However, in an inactive receptor conformation, Tyr$^{5.58}$ points towards the membrane (Palczewski *et al.*, 2000; Li *et al.*, 2004) suggesting its participation in protein-protein interactions in an active state only (Figure 5.1). Upon activation, disruption of the

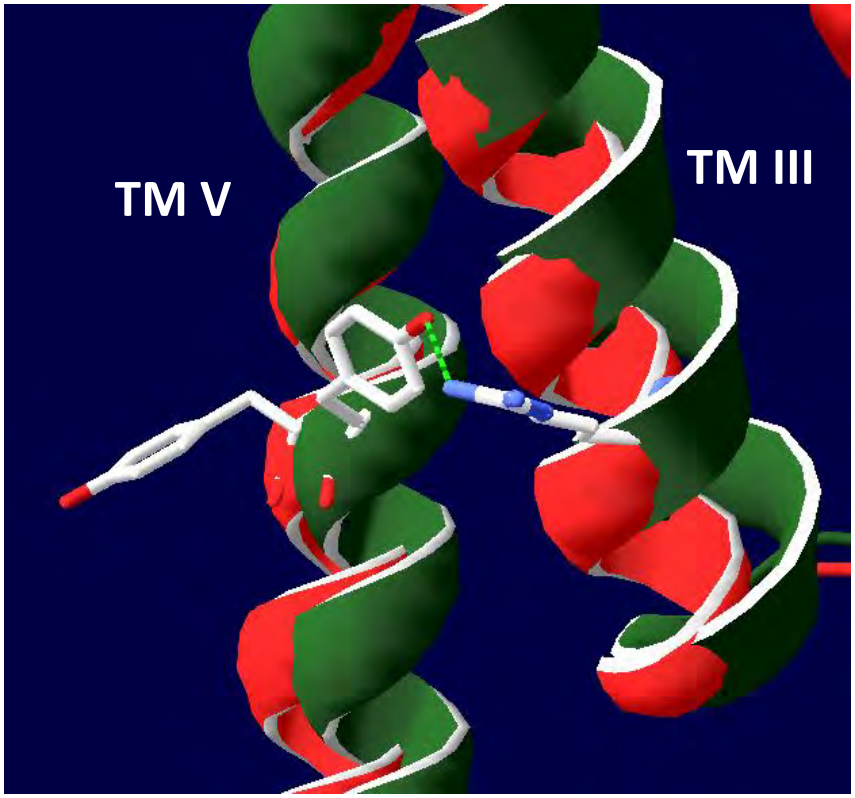

Figure 5.1 The translocation of Tyr$^{5.58}$ in receptor activation

Overlay of inactive, red (pdb: 1GZM) and active, green (pdb: 3PX0) rhodopsin crystal structures viewed from inside the helical bundle. In the inactive state, Tyr$^{5.58}$ is oriented towards the membrane. Upon activation, Tyr$^{5.58}$ is translocated with the rotation of TM V into the helical bundle and hydrogen bonds (green dashes) with the 'ionic lock' residue Arg$^{3.50}$.

hydrophobic barrier (discussed previously in Chapter 4) by the rotation of TM VI, allows the reorientation of $Tyr^{5.58}$ into the helical bundle (Standfuss *et al.*, 2011). In doing so, $Tyr^{5.58}$ connects the actions at the ligand binding pocket to rearrangements at the cytoplasmic face through an extended hydrogen bond network. $Tyr^{7.53}$ is also repositioned into the helical bundle and these tyrosine residues together disrupt the 'ionic lock' between TM III and TM VI, allowing G-protein binding. NMR studies confirm the role of $Tyr^{5.58}$ in stabilising an active intermediate of Meta II (Goncalves *et al.*, 2010). This has been exploited to obtain the crystal structure of β_1AR where the Y5.58A substitution was introduced as one of a number of point mutations to stabilise an inactive receptor conformation (Warne *et al.*, 2008). In both inactive and active structures of β_2AR, $Tyr^{5.58}$ faces into the helical bundle, adopting different conformations (Cherezov *et al.*, 2007; Rasmussen *et al.*, 2011b). $Tyr^{5.58}$ is oriented towards the membrane in the inactive structure of M3 mAChR (Kruse *et al.*, 2012), inactive H_1R (Shimamura *et al.*, 2011) and all activation intermediate structures of the A_{2A}R (Lebon and Tate, 2011; Xu *et al.*, 2011). Inactive structures of a number of GPCRs also demonstrate $Tyr^{5.58}$ positioned into the helical bundle (Chien *et al.*, 2010; Haga *et al.*, 2012; Manglik *et al.*, 2012; Wu *et al.*, 2012).

The aim of this chapter is to probe the structural requirements at this locus of $Tyr^{5.58}$ in the pharmacology, signalling and stability at the cell-surface of the V_{1a}R. By systematically substituting this conserved tyrosine residue for all 19 encoded amino acids, the role of the phenol side chain of $Tyr^{5.58}$ will attempt to be elucidated.

5.2 Results

The position of $Tyr^{5.58}$ discussed in this chapter is represented in Figure 5.2 in the $V_{1a}R$. The oligonucleotides utilised to generate the receptor constructs (as described in section 2.2.1) are presented in Table 5.1. Receptor constructs were expressed in HEK 293T cells and characterised by radioligand binding assay with respect to their ability to bind the endogenous agonist AVP and synthetic peptide antagonist CA (Figures 5.3-5.8, Table 5.2). All, $V_{1a}R$ constructs characterised by competition radioligand binding assay were expressed at 1-2 pmol/mg protein. In order to determine the effects of amino acid substitution on the receptors' signalling capabilities, receptor constructs were transiently transfected into HEK 293T cells and the accumulation of InsP-$InsP_3$ measured (Figures 5.9-5.14, Table 5.2). The effects on IC_{50}, basal and maximal signalling (E_{max}) were ascertained. All basal signalling levels were Wt-like unless stated otherwise. The signalling response of receptor constructs may be influenced by the ability of receptors to be trafficked to the cell surface. Consequently, in addition to pharmacological characterisation, whole cell ELISA utilised the HA-tag engineered at the amino terminus of all $V_{1a}R$ constructs to detect the presence of receptor constructs to quantify cell-surface expression (Figures 5.9-5.14 and summarised in Table 5.2). Receptor constructs were also challenged with AVP agonist and the ability of the receptor to internalise assessed. All levels of internalisation were comparable to Wt unless stated.

5.2.1 Substituting $Tyr^{5.58}$ for small side chain amino acids

The receptor constructs [Y5.58G]$V_{1a}R$, [Y5.58A]$V_{1a}R$ and [Y5.58P]$V_{1a}R$ substituted the large phenolic side chain of tyrosine for small side chains. [Y5.58G]$V_{1a}R$ and [Y5.58A]$V_{1a}R$ maintained Wt-like affinities for AVP agonist and CA antagonist (Figure 5.3, Table 5.2). In marked contrast, [Y5.58P]$V_{1a}R$ did not bind the [^{3}H]AVP tracer ligand at experimental concentrations used so could not be further characterised by radioligand binding studies.

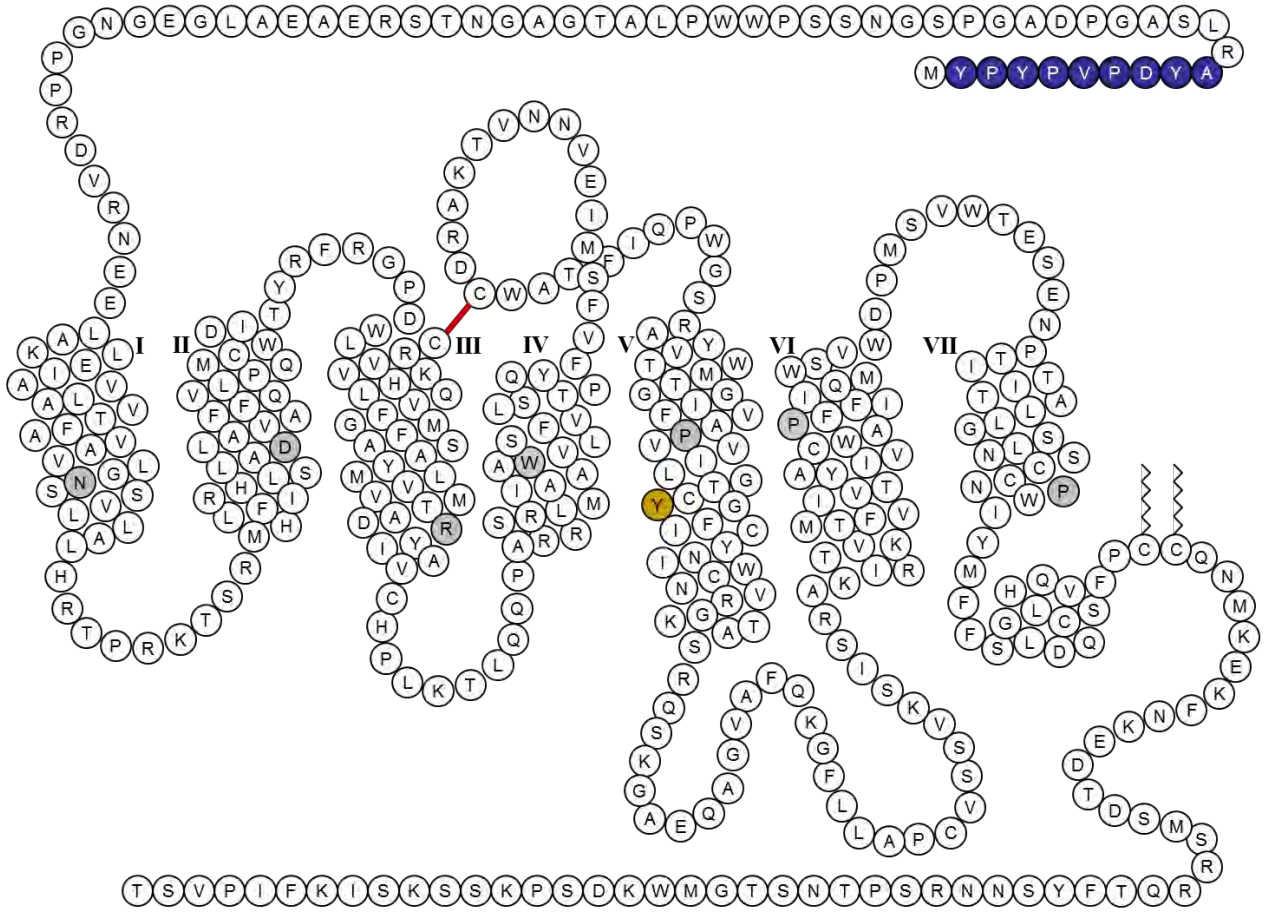

Figure 5.2 Two-dimensional representation of the $V_{1a}R$

The N-terminal, HA-epitope tag (extracellular side) is shown as blue circles. Helices are labelled by roman numerals. The most conserved residue of each helix of rhodopsin-like GPCRs is shown in grey circles and conserved disulphide bridge is shown in red. Palmitoylation sites are shown as zigzags (intracellular side). The residues discussed within this chapter are shown as yellow circles.

Receptor construct	Sense oligonucleotide	Antisense oligonucleotide
[Y5.58A]V_{1a}R	5' – GGT-ACC-TGC-**GCC**-GGC-TTC-ATC – 3'	5' – GAT-GAA-GCC-**GGC**-GCA-GGT-ACC – 3'
[Y5.58C]V_{1a}R	5' – GGT-ACC-TGC-**TGC**-GGC-TTC-ATC – 3'	5' – GAT-GAA-GCC-**GCA**-GCA-GGT-ACC – 3'
[Y5.58D]V_{1a}R	5' – GGT-ACC-TGC-**GAG**-GGC-TTC-ATC – 3'	5' – GAT-GAA-GCC-**CTC**-GCA-GGT-ACC – 3'
[Y5.58E]V_{1a}R	5' – C-TTG-GGT-ACC-TGC-**GAG**-GGC-TTC-ATC-TGC – 3'	5' – GCA-GAT-GAA-GCC-**CTC**-GCA-GGT-ACC-CAA-G – 3'
[Y5.58F]V_{1a}R	5' – GGT-ACC-TGC-**TTC**-GGC-TTC-ATC – 3'	5' – GAT-GAA-GCC-**GAA**-GCA-GGT-ACC – 3'
[Y5.58G]V_{1a}R	5' – GGT-ACC-TGC-**GGC**-GGC-TTC-ATC – 3'	5' – GAT-GAA-GCC-**GCC**-GCA-GGT-ACC – 3'
[Y5.58H]V_{1a}R	5' – GGT-ACC-TGC-**CAC**-GGC-TTC-ATC – 3'	5' – GAT-GAA-GCC-**GTG**-GCA-GGT-ACC – 3'
[Y5.58I]V_{1a}R	5' – GGT-ACC-TGC-**ATC**-GGC-TTC-ATC – 3'	5' – GAT-GAA-GCC-**GAT**-GCA-GGT-ACC – 3'
[Y5.58K]V_{1a}R	5' – GGT-ACC-TGC-**AAA**-GGC-TTC-ATC – 3'	5' – GAT-GAA-GCC-**TTT**-GCA-GGT-ACC – 3'
[Y5.58L]V_{1a}R	5' – GGT-ACC-TGC-**TTG**-GGC-TTC-ATC – 3'	5' – GAT-GAA-GCC-**CAA**-GCA-GGT-ACC – 3'
[Y5.58M]V_{1a}R	5' – GGT-ACC-TGC-**ATG**-GGC-TTC-ATC – 3'	5' – GAT-GAA-GCC-**CAT**-GCA-GGT-ACC – 3'
[Y5.58N]V_{1a}R	5' – GGT-ACC-TGC-**AAC**-GGC-TTC-ATC – 3'	5' – GAT-GAA-GCC-GT**T**-GCA-GGT-ACC – 3'
[Y5.58P]V_{1a}R	5' – GGT-ACC-TGC-**CCC**-GGC-TTC-ATC – 3'	5' – GAT-GAA-GCC-**GGG**-GCA-GGT-ACC – 3'
[Y5.58Q]V_{1a}R	5' – GGT-ACC-TGC-**CAG**-GGC-TTC-ATC – 3'	5' – GAT-GAA-GCC-**CTG**-GCA-GGT-ACC – 3'
[Y5.58R]V_{1a}R	5' – GGT-ACC-TGC-**CGC**-GGC-TTC-ATC – 3'	5' – GAT-GAA-GCC-**GCG**-GCA-GGT-ACC – 3'
[Y5.58S]V_{1a}R	5' – GGT-ACC-TGC-T**CC**-GGC-TTC-ATC – 3'	5' – GAT-GAA-GCC-**GGA**-GCA-GGT-ACC – 3'
[Y5.58T]V_{1a}R	5' – GGT-ACC-TGC-**ACC**-GGC-TTC-ATC – 3'	5' – GAT-GAA-GCC-**GGT**-GCA-GGT-ACC – 3'
[Y5.58V]V_{1a}R	5' – GGT-ACC-TGC-**GTC**-GGC-TTC-ATC – 3'	5' – GAT-GAA-GCC-**GAC**-GCA-GGT-ACC – 3'
[Y5.58W]V_{1a}R	5' – GGT-ACC-TGC-T**GG**-GGC-TTC-ATC – 3'	5' – GAT-GAA-GCC-**CCA**-GCA-GGT-ACC – 3'

Table 5.1 Oligonucleotide sequences utilised to generate receptor constructs

Receptor constructs were generated as described in section 2.2.1. The codon encoding the amino acid substituted is highlighted in red and nucleotide substitutions in bold. Non-bold bases show the complementary template sequence.

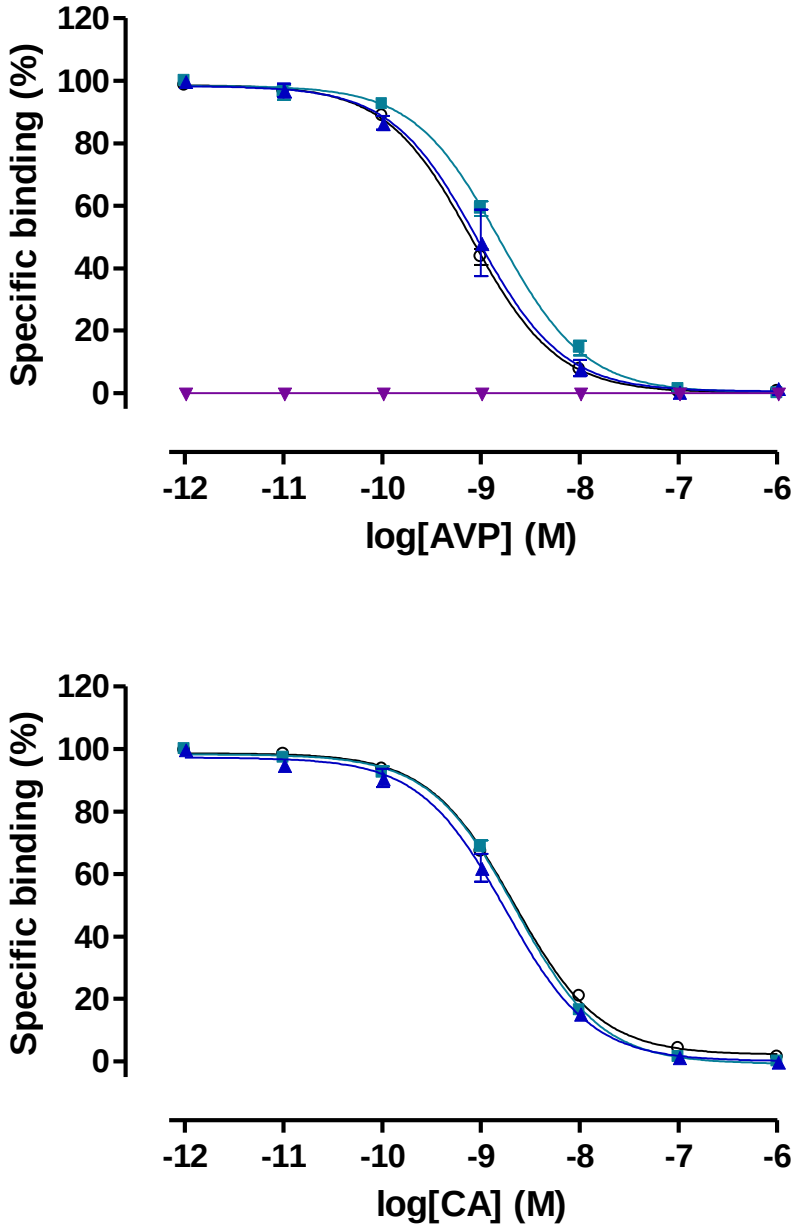

Figure 5.3 Competition radioligand binding curves of substitutions of Tyr$^{5.58}$ to small amino acids

Competition radioligand binding assays were performed on HEK 293T cells, transiently transfected with receptor constructs [Wt]$V_{1a}R$, (○); [Y5.58G]$V_{1a}R$, (■); [Y5.58A]$V_{1a}R$, (▲); and [Y5.58P]$V_{1a}R$, (▼). Upper panel: [^{3}H]AVP vs. AVP competition; lower panel: [^{3}H]AVP vs. CA competition. A theoretical Langmuir binding isotherm was fitted to data expressed as specific binding (%), defining non-specific binding by 1 μM ligand. Data are the mean ± s.e.m. of three experiments performed in triplicate.

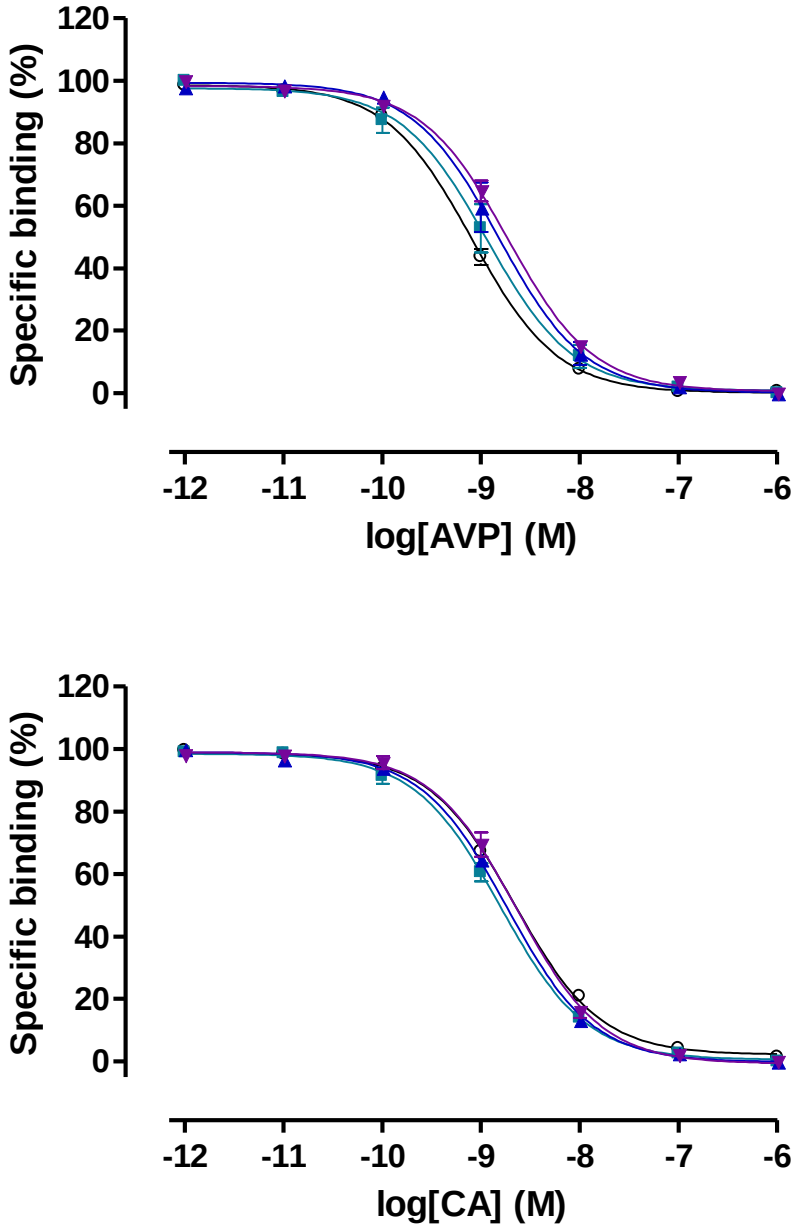

Figure 5.4 Competition radioligand binding curves of substitutions of Tyr$^{5.58}$ to small polar amino acids

Competition radioligand binding assays were performed on HEK 293T cells, transiently transfected with receptor constructs [Wt]$V_{1a}R$, (○); [Y5.58S]$V_{1a}R$, (■); [Y5.58T]$V_{1a}R$, (▲); and [Y5.58C]$V_{1a}R$, (▼). Upper panel: [^{3}H]AVP vs. AVP competition; lower panel: [^{3}H]AVP vs. CA competition. A theoretical Langmuir binding isotherm was fitted to data expressed as specific binding (%), defining non-specific binding by 1 μM ligand. Data are the mean ± s.e.m. of three experiments performed in triplicate.

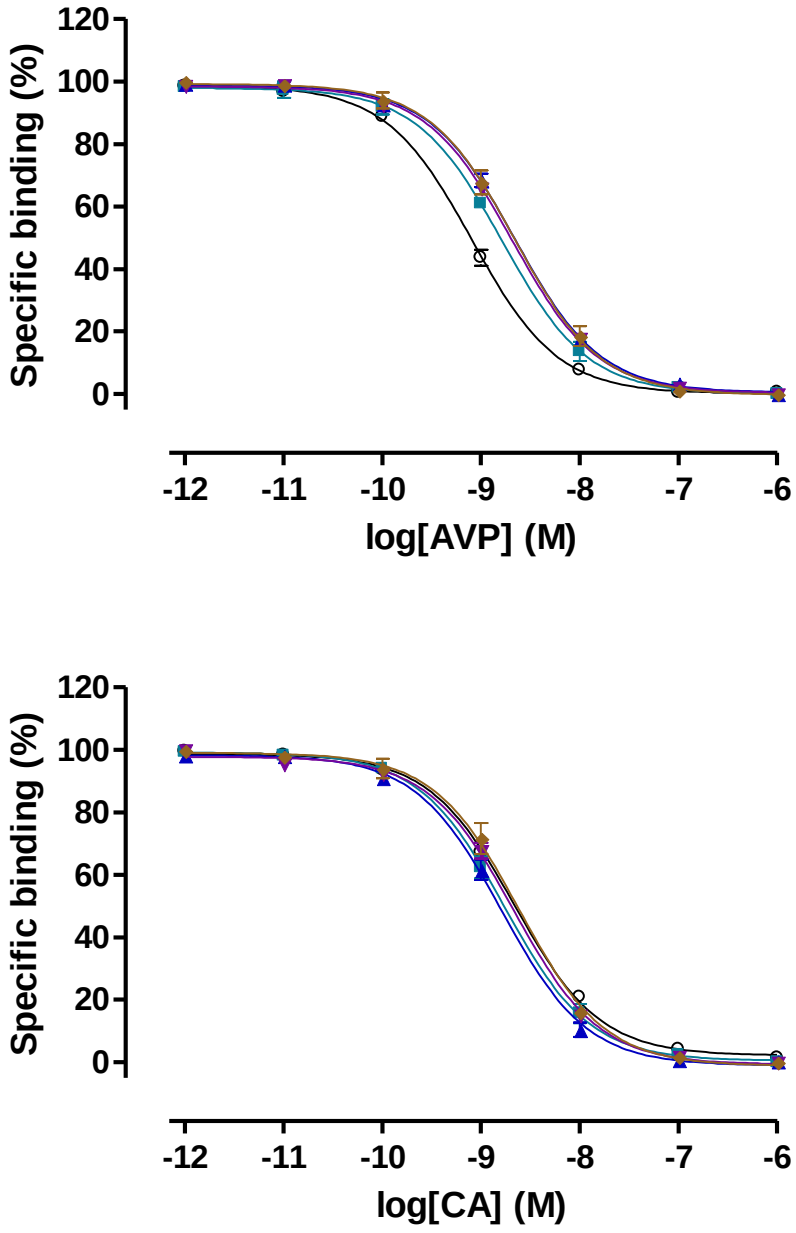

Figure 5.5 Competition radioligand binding curves of substitutions of Tyr$^{5.58}$ to hydrophobic amino acids

Competition radioligand binding assays were performed on HEK 293T cells, transiently transfected with receptor constructs [Wt]$V_{1a}R$, (○); [Y5.58V]$V_{1a}R$, (■); [Y5.58I]$V_{1a}R$, (▲); [Y5.58L]$V_{1a}R$, (▼) and [Y5.58M]$V_{1a}R$ (♦). Upper panel: [^{3}H]AVP vs. AVP competition; lower panel: [^{3}H]AVP vs. CA competition. A theoretical Langmuir binding isotherm was fitted to data expressed as specific binding (%), defining non-specific binding by 1 µM ligand. Data are the mean ± s.e.m. of three experiments performed in triplicate.

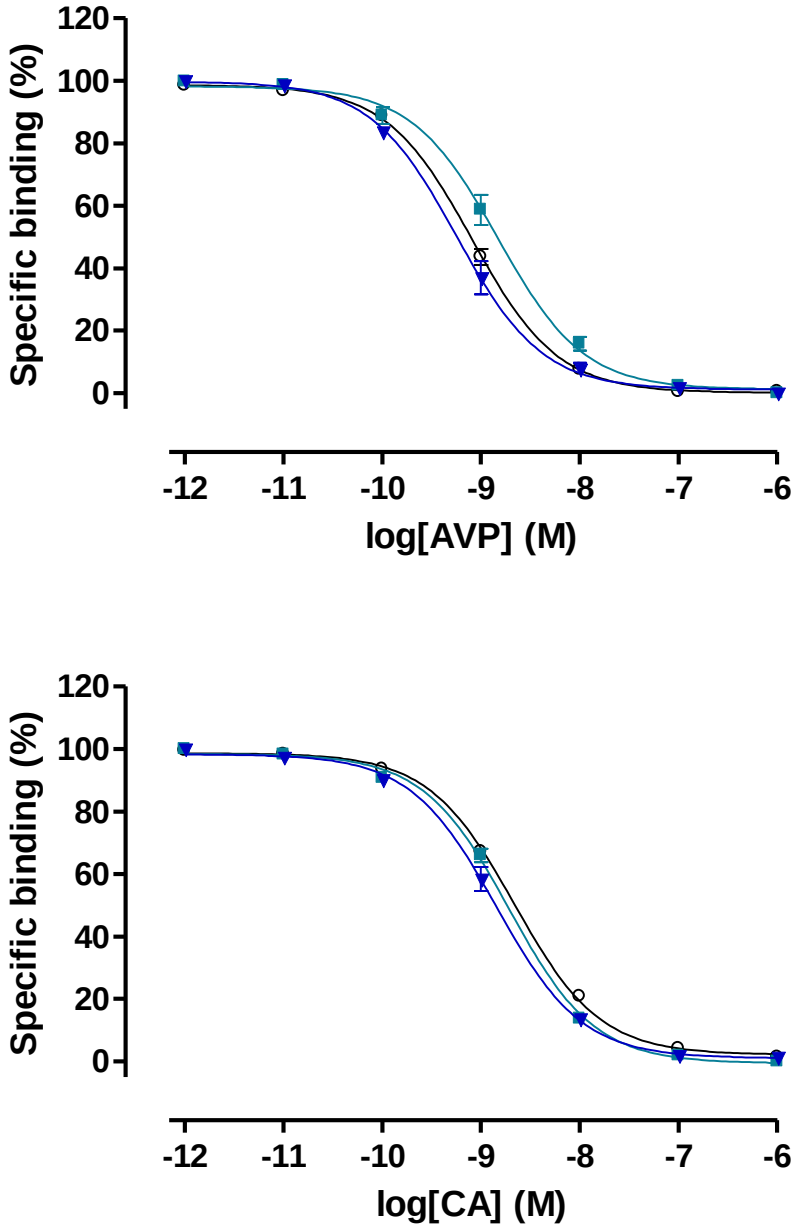

Figure 5.6 Competition radioligand binding curves of substitutions of Tyr$^{5.58}$ to aromatic amino acids

Competition radioligand binding assays were performed on HEK 293T cells, transiently transfected with receptor constructs [Wt]V_{1a}R, (○); [Y5.58F]V_{1a}R, (■) and [Y5.58W]V_{1a}R. Upper panel: [^{3}H]AVP vs. AVP competition; lower panel: [^{3}H]AVP vs. CA competition. A theoretical Langmuir binding isotherm was fitted to data expressed as specific binding (%), defining non-specific binding by 1 µM ligand. Data are the mean ± s.e.m. of three experiments performed in triplicate.

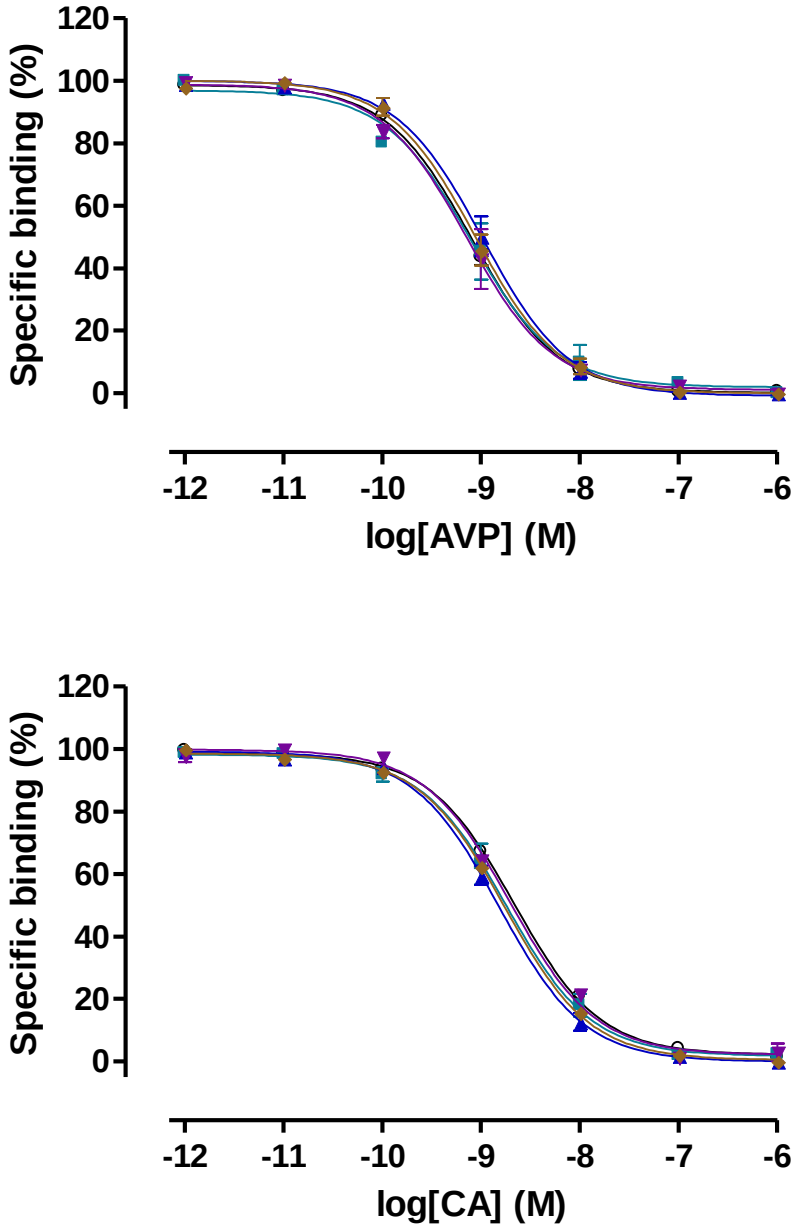

Figure 5.7 Competition radioligand binding curves of substitutions of Tyr$^{5.58}$ to acidic and amine amino acids

Competition radioligand binding assays were performed on HEK 293T cells, transiently transfected with receptor constructs [Wt]V_{1a}R, (○); [Y5.58D]V_{1a}R, (■); [Y5.58N]V_{1a}R, (▲); [Y5.58E]V_{1a}R, (▼) and [Y5.58Q]V_{1a}R (♦). Upper panel: [^{3}H]AVP vs. AVP competition; lower panel: [^{3}H]AVP vs. CA competition. A theoretical Langmuir binding isotherm was fitted to data expressed as specific binding (%), defining non-specific binding by 1 µM ligand. Data are the mean ± s.e.m. of three experiments performed in triplicate.

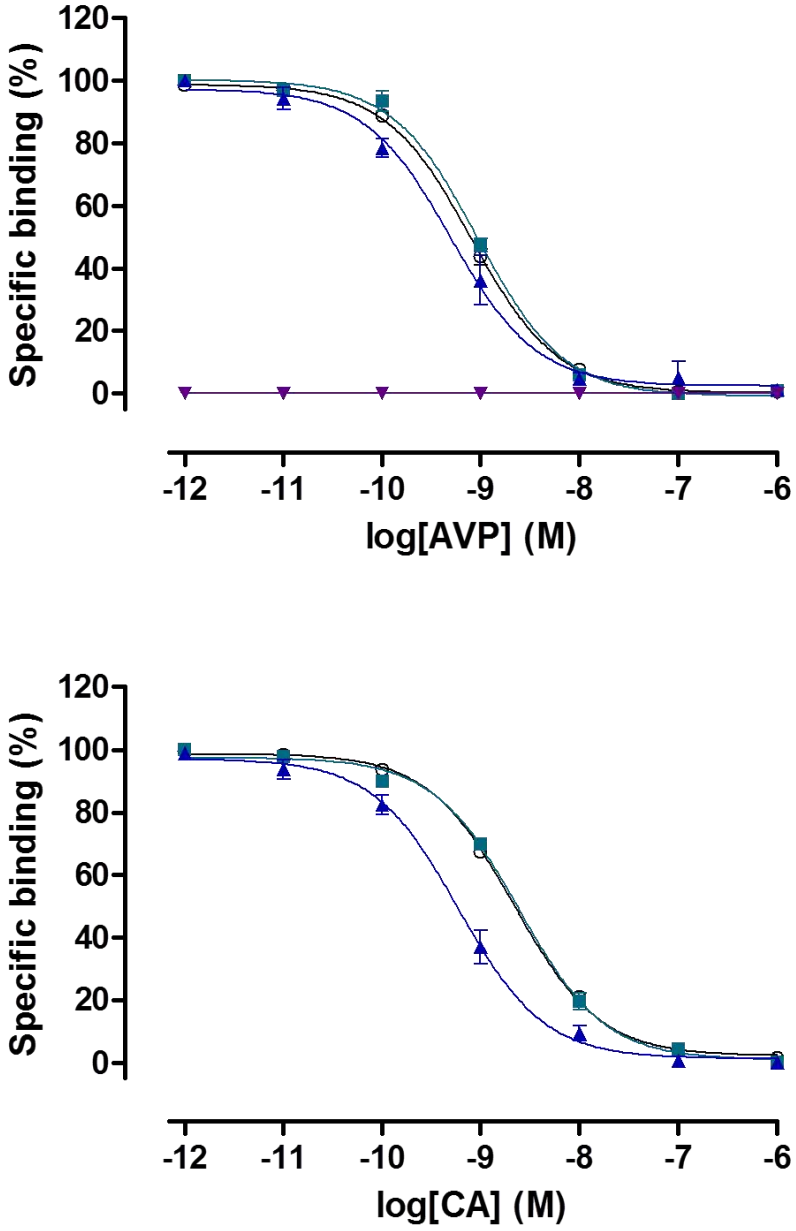

Figure 5.8 Competition radioligand binding curves of substitutions of Tyr$^{5.58}$ to basic amino acids

Competition radioligand binding assays were performed on HEK 293T cells, transiently transfected with receptor constructs [Wt]$V_{1a}R$, (○); [Y5.58H]$V_{1a}R$, (■); [Y5.58K]$V_{1a}R$, (▲) and [Y5.58R]$V_{1a}R$, (▼). Upper panel: [^{3}H]AVP vs. AVP competition; lower panel: [^{3}H]AVP vs. CA competition. A theoretical Langmuir binding isotherm was fitted to data expressed as specific binding (%), defining non-specific binding by 1 μM ligand. Data are the mean ± s.e.m. of three experiments performed in triplicate.

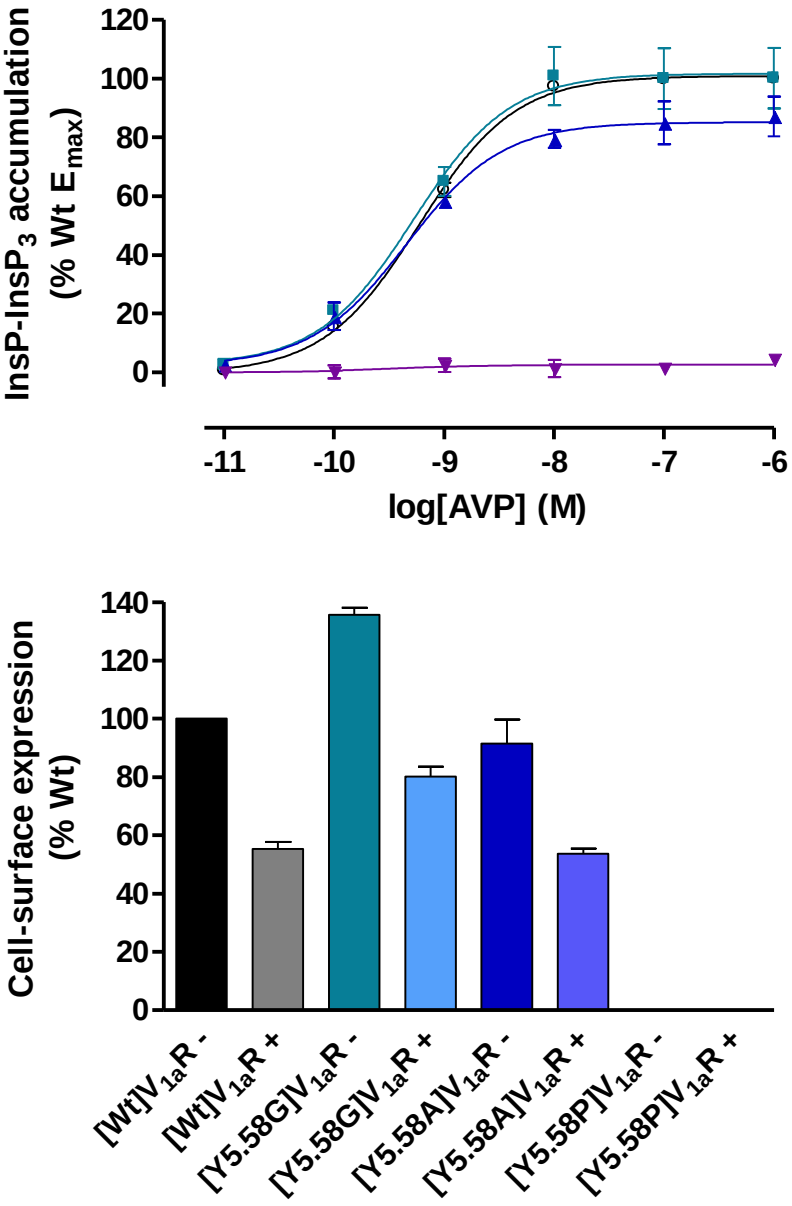

Figure 5.9 InsP-InsP$_3$ dose-response curves and cell-surface expression (+/- agonist challenge) of substitutions of Tyr$^{5.58}$ to small amino acids

Upper panel: Dose-response curves of inositol phosphates accumulation assays of HEK 293T cells, transiently transfected with receptor constructs [Wt]V_{1a}R, (○); [Y5.58G]V_{1a}R, (■); [Y5.58A]V_{1a}R, (▲); and [Y5.58P]V_{1a}R, (▼). Data are normalised to [Wt]V_{1a}R basal and maximal signalling levels, expressed as the mean ± s.e.m. of three experiments performed in triplicate. Basal signalling is plotted at 10^{-11} M. Lower panel: Cell-surface expression levels of receptor constructs were normalised to untransfected cells and unstimulated (-) [Wt]V_{1a}R expression levels. Data are stated as the mean ± s.e.m. of three experiments performed in triplicate. Stimulated (+) constructs were challenged by 10^{-7}M AVP for 30 min.

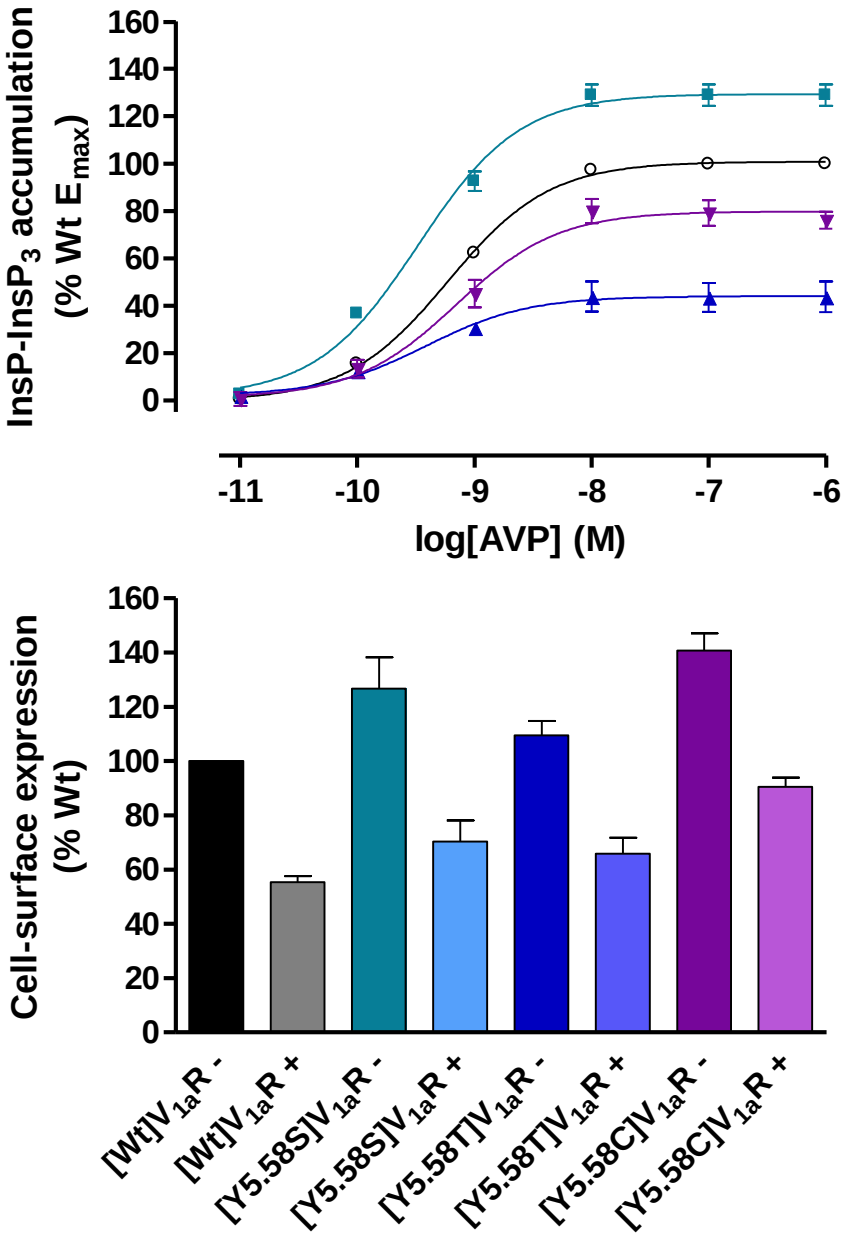

Figure 5.10 InsP-InsP$_3$ dose-response curves and cell-surface expression (+/- agonist challenge) of substitutions of Tyr$^{5.58}$ to small hydrophilic amino acids

Upper panel: Dose-response curves of inositol phosphates accumulation assays of HEK 293T cells, transiently transfected with receptor constructs [Wt]V_{1a}R, (○); [Y5.58S]V_{1a}R, (■); [Y5.58T]V_{1a}R, (▲); and [Y5.58C]V_{1a}R, (▼). Data are normalised to [Wt]V_{1a}R basal and maximal signalling levels, expressed as the mean ± s.e.m. of three experiments performed in triplicate. Basal signalling is plotted at 10^{-11} M. Lower panel: Cell-surface expression levels of receptor constructs were normalised to untransfected cells and unstimulated (-) [Wt]V_{1a}R expression levels. Data are stated as the mean ± s.e.m. of three experiments performed in triplicate. Stimulated (+) constructs were challenged by 10^{-7}M AVP for 30 min.

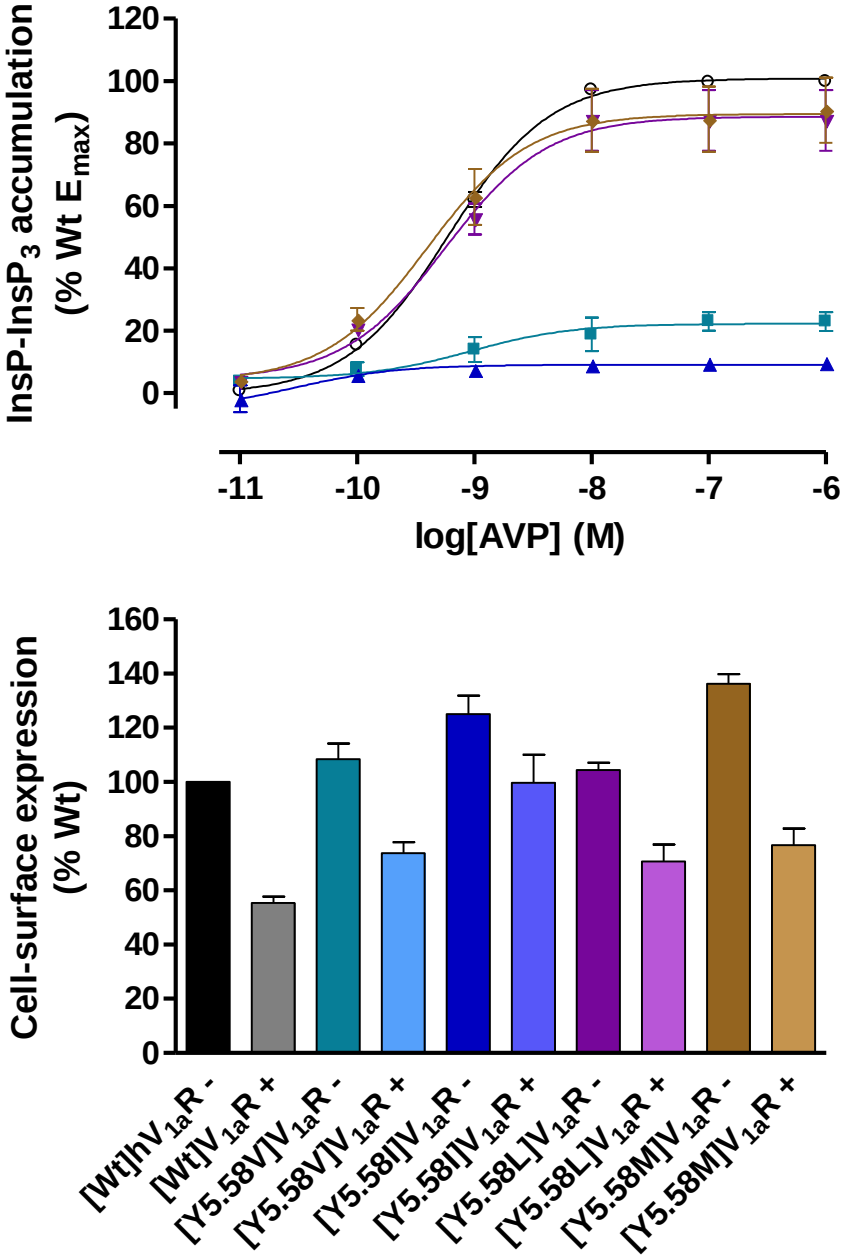

Figure 5.11 InsP-InsP$_3$ dose-response curves and cell-surface expression (+/- agonist challenge) of substitutions of Tyr$^{5.58}$ to hydrophobic amino acids

Upper panel: Dose-response curves of inositol phosphates accumulation assays of HEK 293T cells, transiently transfected with receptor constructs [Wt]V_{1a}R, (○); [Y5.58V]V_{1a}R, (■); [Y5.58I]V_{1a}R, (▲); [Y5.58L]V_{1a}R, (▼) and [Y5.58M]V_{1a}R (♦). Data are normalised to [Wt]V_{1a}R basal and maximal signalling levels, expressed as the mean ± s.e.m. of three experiments performed in triplicate. Lower panel: Cell-surface expression levels of receptor constructs were normalised to untransfected cells and unstimulated (-) [Wt]V_{1a}R expression levels. Data are stated as the mean ± s.e.m. of three experiments performed in triplicate. Stimulated (+) constructs were challenged by 10^{-7}M AVP for 30 min.

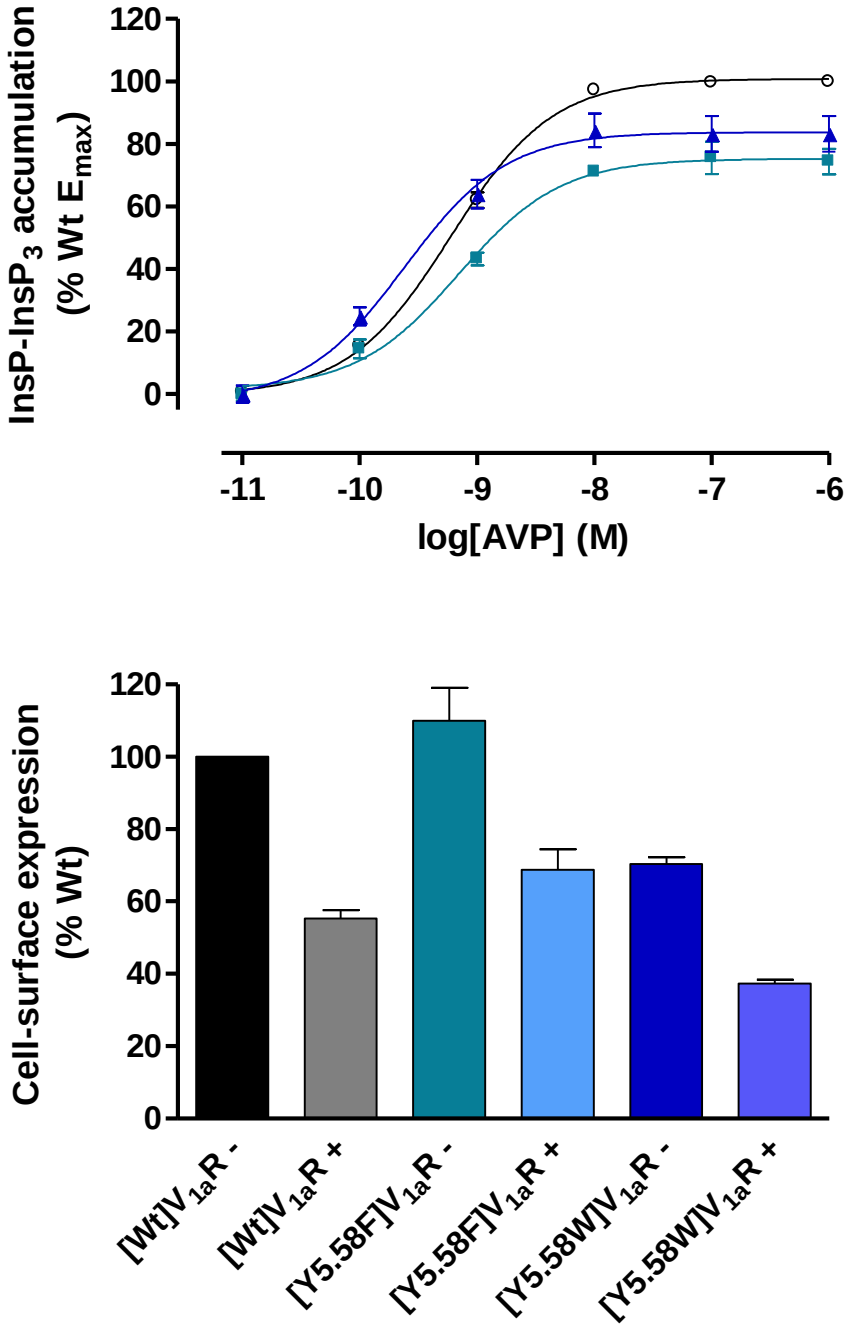

Figure 5.12 InsP-InsP$_3$ dose-response curves and cell-surface expression (+/- agonist challenge) of substitutions of Tyr$^{5.58}$ to aromatic amino acids

Upper panel: Dose-response curves of inositol phosphates accumulation assays of HEK 293T cells, transiently transfected with receptor constructs [Wt]V_{1a}R, (○); [Y5.58F]V_{1a}R, (■) and [Y5.58W]V_{1a}R, (▲). Data are normalised to [Wt]V_{1a}R basal and maximal signalling levels, expressed as the mean ± s.e.m. of three experiments performed in triplicate. Basal signalling is plotted at 10^{-11} M. Lower panel: Cell-surface expression levels of receptor constructs were normalised to untransfected cells and unstimulated (-) [Wt]V_{1a}R expression levels. Data are stated as the mean ± s.e.m. of three experiments performed in triplicate. Stimulated (+) constructs were challenged by 10^{-7}M AVP for 30 min.

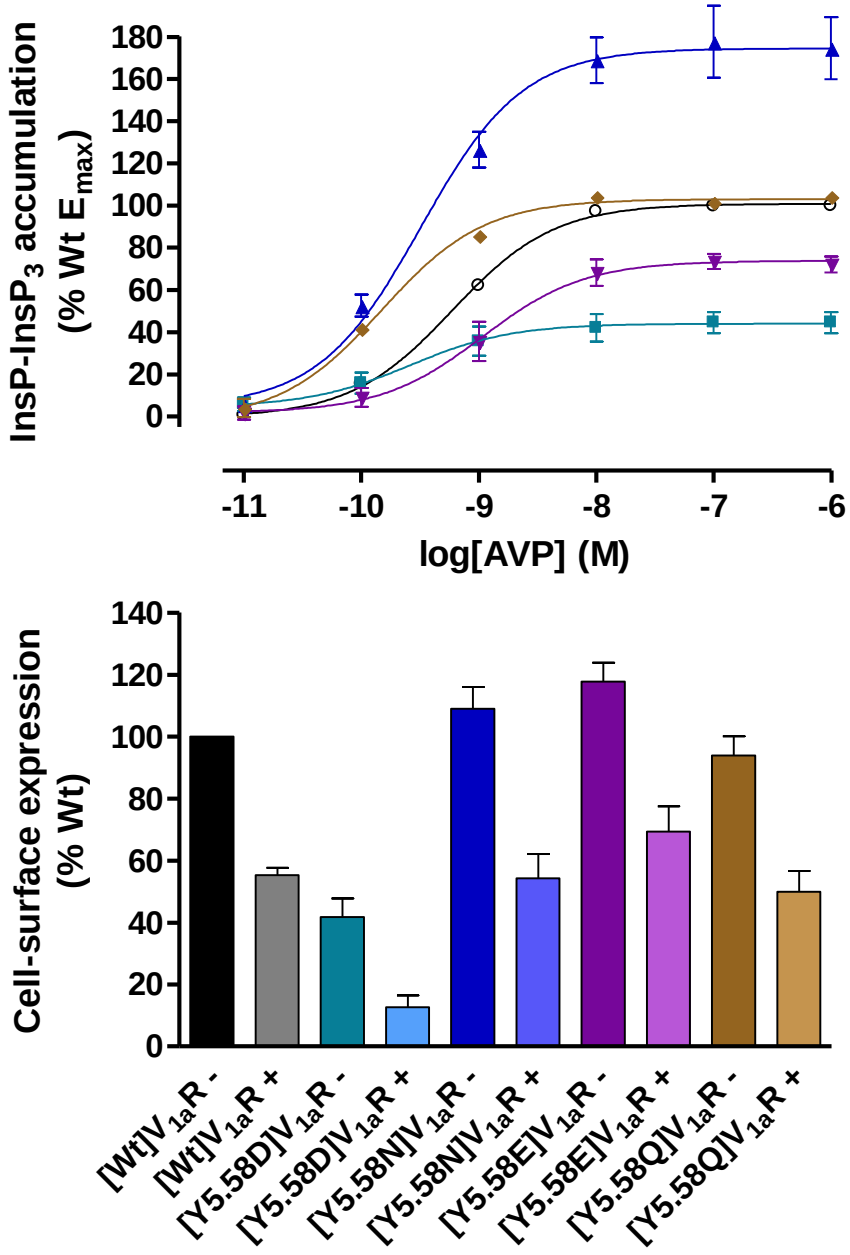

Figure 5.13 InsP-InsP$_3$ dose-response curves and cell-surface expression (+/- agonist challenge) of substitutions of Tyr$^{5.58}$ to acidic and amine amino acids

Upper panel: Dose-response curves of inositol phosphates accumulation assays of HEK 293T cells, transiently transfected with receptor constructs [Wt]V_{1a}R, (○); [Y5.58D]V_{1a}R, (■); [Y5.58N]V_{1a}R, (▲); [Y5.58E]V_{1a}R, (▼) and [Y5.58Q]V_{1a}R (♦). Data are normalised to [Wt]V_{1a}R basal and maximal signalling levels, expressed as the mean ± s.e.m. of three experiments performed in triplicate. Basal signalling is plotted at 10^{-11} M. Lower panel: Cell-surface expression levels of receptor constructs were normalised to untransfected cells and unstimulated (-) [Wt]V_{1a}R expression levels. Data are stated as the mean ± s.e.m. of three experiments performed in triplicate. Stimulated (+) constructs were challenged by 10^{-7}M AVP for 30 min.

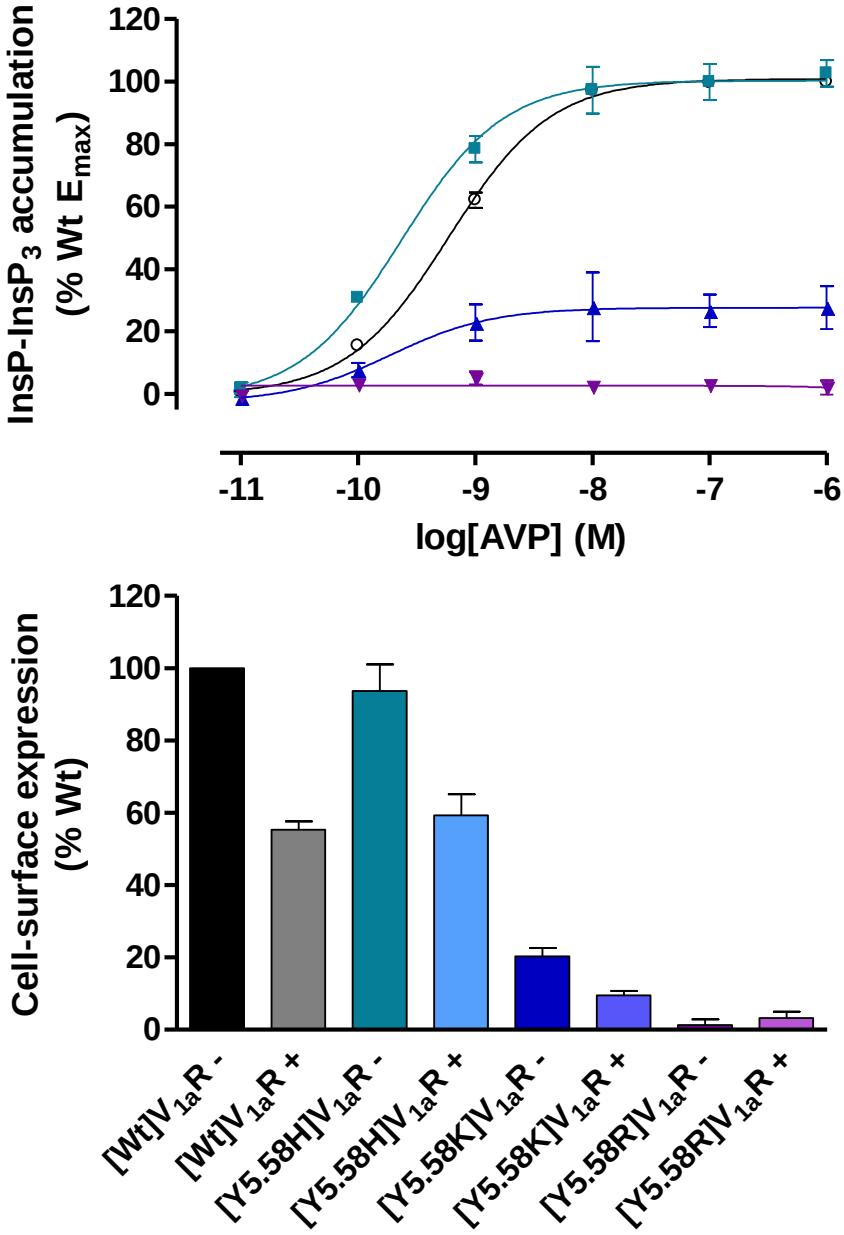

Figure 5.14 InsP-InsP$_3$ dose-response curves and cell-surface expression (+/- agonist challenge) of substitutions of Tyr$^{5.58}$ to basic amino acids

Upper panel: Dose-response curves of inositol phosphates accumulation assays of HEK 293T cells, transiently transfected with receptor constructs [Wt]V_{1a}R, (○); [Y5.58H]V_{1a}R, (■); [Y5.58K]V_{1a}R, (▲) and [Y5.58R]V_{1a}R, (▼). Data are normalised to [Wt]V_{1a}R basal and maximal signalling levels, expressed as the mean ± s.e.m. of three experiments performed in triplicate. Basal signalling is plotted at 10^{-11} M. Lower panel: Cell-surface expression levels of receptor constructs were normalised to untransfected cells and unstimulated (-) [Wt]V_{1a}R expression levels. Data are stated as the mean ± s.e.m. of three experiments performed in triplicate. Stimulated (+) constructs were challenged by 10^{-7}M AVP for 30 min.

Receptor construct	Binding affinity, K_i (nM) ± s.e.m.		InsP-$InsP_3$ accumulation (% Wt E_{max}) ± s.e.m.			Cell-surface expression (% Wt unstimulated) ± s.e.m.	
	AVP	CA	Basal	EC_{50}*	E_{max}	Unstimulated	Simulated
$V_{1a}R$	**0.45 ± 0.04**	**0.96 ± 0.10**	**0**	**0.60 ± 0.02**	**100**	**100**	**55 ± 2**
[Y5.58A]$V_{1a}R$	0.73 ± 0.41	1.14 ± 0.23	2 ± 1	0.46 ± 0.04	85 ± 0	92 ± 8	54 ± 2
[Y5.58C]$V_{1a}R$	1.52 ± 0.27	1.89 ± 0.34	1 ± 3	0.70 ± 0.15	80 ± 5	141 ± 7	91 ± 3
[Y5.58D]$V_{1a}R$	0.47 ± 0.27	0.83 ± 0.15	6 ± 3	0.27 ± 0.02	45 ± 5	42 ± 6	13 ± 4
[Y5.58E]$V_{1a}R$	0.54 ± 0.40	1.29 ± 0.07	2 ± 3	1.07 ± 0.08	74 ± 4	118 ± 6	69 ± 8
[Y5.58F]$V_{1a}R$	1.18 ± 0.34	1.43 ± 0.16	0 ± 2	0.67 ± 0.07	76 ± 5	110 ± 10	69 ± 6
[Y5.58G]$V_{1a}R$	1.12 ± 0.22	1.70 ± 0.10	3 ± 2	0.53 ± 0.06	101 ± 0	136 ± 3	80 ± 3
[Y5.58H]$V_{1a}R$	0.62 ± 0.14	1.52 ± 0.10	1 ± 2	0.25 ± 0.03	103 ± 4	94 ± 7	59 ± 6
[Y5.58I]$V_{1a}R$	1.84 ± 0.25	1.35 ± 0.15	-2 ± 4	0.05 ± 0.02	10 ± 1	125 ± 7	100 ± 10
[Y5.58K]$V_{1a}R$	0.17 ± 0.08	0.18 ± 0.06	1 ± 2	0.21 ± 0.03	28 ± 7	20 ± 2	10 ± 2
[Y5.58L]$V_{1a}R$	1.70 ± 0.15	1.72 ± 0.14	4 ± 1	0.57 ± 0.09	87 ± 10	104 ± 3	71 ± 6
[Y5.58M]$V_{1a}R$	1.88 ± 0.51	1.86 ± 0.18	4 ± 1	0.40 ± 0.01	91 ± 10	136 ± 3	77 ± 6
[Y5.58N]$V_{1a}R$	0.64 ± 0.28	1.02 ± 0.07	6 ± 2	0.32 ± 0.04	177 ± 17	109 ± 7	54 ± 8
[Y5.58P]$V_{1a}R$	Did not bind [^{3}H]AVP		0 ± 1	No detectable signalling		-3 ± 3	0 ± 1
[Y5.58Q]$V_{1a}R$	0.60 ± 0.15	0.97 ± 0.16	0 ± 1	0.15 ± 0.02	104 ± 2	94 ± 6	50 ± 7
[Y5.58R]$V_{1a}R$	Did not bind [^{3}H]AVP		0 ± 1	No detectable signalling		1 ± 2	3 ± 2
[Y5.58S]$V_{1a}R$	0.95 ± 0.40	1.09 ± 0.18	2 ± 2	0.33 ± 0.05	129 ± 5	127 ± 12	70 ± 8
[Y5.58T]$V_{1a}R$	1.38 ± 0.43	1.52 ± 0.12	2 ± 2	0.38 ± 0.07	44 ± 6	110 ± 5	66 ± 6
[Y5.58V]$V_{1a}R$	1.31 ± 0.17	1.18 ± 0.43	4 ± 2	0.85 ± 0.32	23 ± 3	108 ± 6	74 ± 4
[Y5.58W]$V_{1a}R$	0.28 ± 0.14	0.52 ± 0.16	0 ± 3	0.25 ± 0.04	84 ± 5	70 ± 2	37 ± 1

Table 5.2 Binding, signalling and cell-surface expression of Tyr$^{5.58}$ substitutions

All data are shown as the mean ± s.e.m. of three separate experiments performed in triplicate. *EC_{50} is stated as the mean ± mean of 95 % confidence intervals of three separate experiments performed in triplicate. Data in yellow indicate >2.5-fold increase in K_i or EC_{50} or >25 % reduction in E_{max}, cell-surface expression; orange >5-fold increase in K_i or EC_{50} or >50 % reduction in E_{max}, cell-surface expression or internalisation; red >10-fold increase in K_i or EC_{50} or >75 % reduction in E_{max}, cell-surface expression or internalisation. Data in green indicate >2.5-fold increase in K_i or EC_{50} or >25 % increase in E_{max}, cell-surface expression or > 50% increase in internalisation. Data in white are comparable to Wt. $^{\#}$ denotes IC_{50} ± mean of 95 % confidence intervals of three separate experiments performed in triplicate.

Both [Y5.58G]V_{1a}R and [Y5.58A]V_{1a}R generated InsP-$InsP_3$ in a Wt-like manner with respect to EC_{50} and maximal signalling (Figure 5.9, Table 5.2). However they differed with respect to cell-surface expression with [Y5.58A]V_{1a}R being essentially Wt and [Y5.58G]V_{1a}R exhibiting increased cell-surface expression (136 % of Wt expression). [Y5.58P]V_{1a}R however was not detectable at the cell-surface by ELISA and no InsP-$InsP_3$ accumulation could be detected.

5.2.2 Substituting $Tyr^{5.58}$ for small polar amino acids

[Y5.58S]V_{1a}R, [Y5.58T]V_{1a}R, [Y5.58C]V_{1a}R represent substitutions of $Tyr^{5.58}$ for amino acids possessing small hydrophilic amino acids. [Y5.58S]V_{1a}R bound AVP agonist with Wt-like affinity while [Y5.58T]V_{1a}R and [Y5.58C]V_{1a}R displayed a ~3-fold decreased affinity (Figure 5.4, Table 5.2). All three substitutions demonstrated Wt-like binding affinities for antagonist CA.

While [Y5.58S]V_{1a}R, [Y5.58T]V_{1a}R and [Y5.58C]V_{1a}R displayed Wt-like EC_{50} values of AVP-induced inositol-phosphates, maximal signalling level (E_{max}) was effected (Figure 5.10, Table 5.2). [Y5.58S]V_{1a}R, [Y5.58T]V_{1a}R and [Y5.58C]V_{1a}R achieved E_{max} of 129 %, 44 % and 80 % of Wt levels respectively (Figure 5.10, Table 5.2). ELISA demonstrated that all receptor constructs expressed as well as Wt at the cell-surface with serine and cysteine substitutions expressing at 127 % and 141 % of Wt respectively.

5.2.3 Substituting $Tyr^{5.58}$ for hydrophobic amino acids

The hydrophobic amino acids valine, isoleucine, leucine and methionine were substituted at position 5.58 generating the receptor constructs [Y5.58V]V_{1a}R, [Y5.58I]V_{1a}R, [Y5.58L]V_{1a}R and [Y5.58M]V_{1a}R. Substitution of $Tyr^{5.58}$ for valine, isoleucine, leucine and methionine decreased the binding affinity of AVP by 3-4-fold while maintaining Wt-like affinities for CA (Figure 5.5, Table 5.2).

Receptor constructs [Y5.58L]V_{1a}R and [Y5.58M]V_{1a}R signalled like Wt (Figure 5.11, Table 5.2). In contrast, [Y5.58I]V_{1a}R displayed decreased E_{max} (10% of Wt E_{max}) and an apparent 12-fold increase in IC_{50} despite being expressed well at the cell surface. It is difficult to be accurate regarding the increase in potency of AVP to generate InsP-$InsP_3$ due to the overall poor signalling capabilities of this construct. [Y5.58V]V_{1a}R also demonstrated drastic decrease in E_{max} (23 % of Wt E_{max}) but maintained Wt-like EC_{50}. [Y5.58V]V_{1a}R, [Y5.58I]V_{1a}R, [Y5.58L]V_{1a}R expressed at the cell surface at Wt-like levels and [Y5.58M]V_{1a}R displayed an increase in cell-surface expression, 136 % of Wt expression. [Y5.58I]V_{1a}R displayed the greatest decrease in the proportion of receptor internalised from the cell-surface upon AVP challenge of all amino acid substitutions within this chapter. The Y5.58I substitution resulted in a receptor construct that internalised only 20 % of total cell-surface expression (Wt, 45 % of unstimulated expression).

5.2.4 Substituting $Tyr^{5.58}$ for aromatic amino acids

[Y5.58F]V_{1a}R and [Y5.58W]V_{1a}R were generated, substituting $Tyr^{5.58}$ for phenylalanine and tryptophan respectively. Substitution of $Tyr^{5.58}$ for phenylalanine displayed a 2.6-fold decrease in AVP affinity while maintaining Wt-like CA affinity (Figure 5.6, Table 5.2). The [Y5.58W]V_{1a}R receptor construct bound both AVP and CA with Wt-like binding affinities.

[Y5.58F]V_{1a}R was Wt-like in all aspects of InsP-$InsP_3$ accumulation and cell-surface expression (Figure 5.12, Table 5.2). [Y5.58W]V_{1a}R generated a near-Wt E_{max} with a small reduction cell-surface expression (70 % of Wt expression). IC_{50} of [Y5.58W]V_{1a}R was comparable to Wt.

5.2.5 Substituting $Tyr^{5.58}$ for acidic and amine amino acids

Substitution of the $Tyr^{5.58}$ side chain for acidic amino acids generated the constructs [Y5.58D]V_{1a}R and [Y5.58E]V_{1a}R and substitutions for the polar amines [Y5.58N]V_{1a}R,

[Y5.58Q]V_{1a}R. All receptor constructs bound both agonist AVP and antagonist CA with Wt-like binding affinities (Figure 5.7, Table 5.2).

[Y5.58D]V_{1a}R displayed a basal activity of 6 % of Wt E_{max} and reduced maximal signalling at 44 % of Wt E_{max} although EC_{50} was Wt-like (Figure 5.13, Table 5.2). Cell-surface expression levels were reduced to 42 % of Wt levels. [Y5.58E]V_{1a}R demonstrated a modest reduction in maximal signalling (74 % Wt E_{max}) whilst maintaining Wt basal and EC_{50} values. Cell-surface expression of [Y5.58E]V_{1a}R was at a level comparable to Wt.

While both [Y5.58N]V_{1a}R and [Y5.58Q]V_{1a}R substitutions resulted in receptor constructs that expressed at the cell-surface at levels comparable to Wt, the signalling properties were differently enhanced (Figure 5.13, Table 5.2). A small increase in basal activity (6 % of Wt E_{max}) and an increase to 177 % of Wt E_{max} were observed for the [Y5.58N]V_{1a}R construct. [Y5.58Q]V_{1a}R produced a Wt-like maximal signalling response with a 4-fold decrease in EC_{50}. Basal signalling was unaffected.

5.2.6 Substituting $Tyr^{5.58}$ for basic amino acids

[Y5.58H]V_{1a}R, [Y5.58K]V_{1a}R and [Y5.58R]V_{1a}R were generated to assess the effect of introducing a basic side chain in the place of $Tyr^{5.58}$ in the V_{1a}R. [Y5.58H]V_{1a}R bound both AVP and CA with Wt-like binding affinities (Figure 5.8, Table 5.2). [Y5.58K]V_{1a}R displayed a 2.6-fold increase in AVP affinity and 5.3-fold increase in CA affinity. The receptor construct [Y5.58R]V_{1a}R did not bind [^{3}H]AVP at experimental concentrations used so could not be pharmacologically characterised.

The [Y5.58H]V_{1a}R generated InsP-$InsP_3$ in a Wt-like manner in all respects and expressed at the cell-surface at a level comparable to Wt (Figure 5.14, Table 5.2). Substitution of the native tyrosine for a lysine residue produced a receptor construct with markedly reduced cell-surface expression (20 % of Wt) and E_{max} (28 % of Wt E_{max}). Basal signalling was unaffected in the

[Y5.58K]V_{1a}R construct with a 2.8-fold decrease in EC_{50}. Owing to the lack of presence of [Y5.58R]V_{1a}R at the cell-surface detected by ELISA, no InsP-$InsP_3$ accumulation was detected.

5.3 Discussion

Upon substituting the conserved $Tyr^{5.58}$ to every other encoded amino acid, 17 of the 19 substitutions were functionally expressed and able to be characterised with respect to their pharmacology and signalling capabilities through the inositol phosphate pathway. The two constructs that were severely disrupted were [Y5.58P]V_{1a}R and [Y5.58R]V_{1a}R. Both proline and arginine are excluded from this locus in the rhodopsin-like GPCR family (Mirzadegan *et al.*, 2003) and their introduction had gross effects on the receptor structure. Introducing a helix-breaking, proline at position 5.58 resulted in a loss of presence at the cell surface and consequently inositol phosphate signalling. This is in agreement with observations in the human thyrotropin receptor where introducing the point mutation Y5.58P resulted in the receptor being retained in intracellular membrane compartments (Biebermann *et al.*, 1998). It is reasonable to conclude that introducing proline at position 5.58 caused major disruption to the tertiary fold of the receptor. Additionally, the large, positively charged side chain of arginine cannot be accommodated at position 5.58. This effect was not solely due to the side chain charge as the lysine substitution was better accommodated.

The 'side chain removal' substitution of [Y5.58A]V_{1a}R, effectively removes the phenol moiety of the native tyrosine residue without affecting the propensity for TM V to adopt a helical conformation. The Wt-like nature of the [Y5.58A]V_{1a}R receptor construct suggests that the loss of the phenol ring of tyrosine does not significantly perturb the receptor conformation given that the pharmacology of the construct was like Wt. Additionally, the construct is still capable of signalling though the inositol phosphate pathway as the mutation

did not affect the basal or agonist-induced signalling properties. The Y5.58A substitution in the β_1AR favoured a receptor conformation where the 'ionic lock' is intact (Balaraman *et al.*, 2010) and abolished cannabinoid-induced inhibition of cAMP accumulation in the CB2 receptor and decreased agonist binding affinity (Song and Feng, 2002). In the NK-1R, the substitution abolished SP-stimulated PI hydrolysis while maintaining high affinity binding (Huang *et al.*, 1995).

Similar to the [Y5.58A]V_{1a}R construct, the introduction of a glycine residue resulted in a receptor construct capable of signalling though the inositol phosphate pathway in a Wt-like manner with AVP and CA binding comparable to Wt. [Y5.58G]V_{1a}R was however expressed at the cell surface at a higher density than Wt. Together this suggests that the increased flexibility introduced into TM VI by glycine, is not disruptive to the integrity of the receptor nor its function.

Similarly, the introduction of a cysteine residue at position 5.58 demonstrated a substantial increase in cell-surface expression compared to Wt but maintained Wt-like signalling properties. The slight decreased affinities of AVP and CA in the [Y5.58C]V_{1a}R receptor construct does however indicate mild perturbation of the ligand binding site. The substitution to serine yielded a receptor that was Wt-like with regards to pharmacology of agonist and antagonist. The signalling capabilities of the receptor differ from Wt in only an increased E_{max}. Although there is a proportional increase in cell-surface expression, the [Y5.58G]V_{1a}R demonstrates that this may not necessarily indicate an increased efficacy of AVP in signal generation. Molecularly, [Y5.58T]V_{1a}R effectively mimics the [Y5.58S]V_{1a}R construct with the addition of a methyl group at the β-carbon. Although the construct was well expressed at the cell surface, the efficacy of AVP to generate inositol phosphates was severely disrupted to less than half of Wt. The presence of the methyl moiety also conferred a decreased AVP

affinity while maintaining Wt-like CA binding. So tyrosine, serine or threonine possess an hydroxyl group while the cysteine possesses a closely-related thiol. Despite the structural similarity, the effects of substitution by these amino acids are diverse, highlighting that the presence of an hydroxyl (as in $Tyr^{5.58}$) is insufficient to provide Wt-like functionality in the $V_{1a}R$ and the context of the hydroxyl is also important.

The perturbations in ligand binding and AVP efficacy are also evident in the β-branched, hydrophobic substitution constructs [Y5.58V]$V_{1a}R$ and [Y5.58I]$V_{1a}R$. While these constructs express at Wt-like levels at the cell surface, similarly to [Y5.58T]$V_{1a}R$, the maximal signalling levels are severely reduced. The reduction in AVP efficacy is due to the β-methyl group given that the hydrophobic substitutions [Y5.58L]$V_{1a}R$ and [Y5.58M]$V_{1a}R$ generate maximal signalling levels comparable to Wt. No expressed receptor constructs other than those that are β-branched displayed reduced AVP efficacy to this extent. This said, substitution of tyrosine to leucine or methionine also reduced the binding affinity of AVP. Together, these data suggest that the introduction of hydrophobic amino acids valine, isoleucine, leucine and methionine, in addition to threonine stabilise an inactive state. This is presumably owing to the side chain being preferentially oriented to the membrane lipids in an inactive receptor state. However, it is only the β-branched receptor constructs that demonstrate reduced signalling capabilities. These observations suggest that the large hydrophobic ring of the native tyrosine stabilise the inactive receptor state, and the γ position of the phenol moiety permits full activation in response to agonist. This is further confirmed by the [Y5.58F]$V_{1a}R$ construct that only differs from the native tyrosine by an hydroxyl group. A small decrease in AVP affinity is displayed and a near-Wt E_{max} is observed. This is in contrast to the $AT_{1a}R$ where Y5.58F resulted in no inositol phosphate response (Hunyady *et al.*, 1995). The loss in agonist binding affinity in the $AT_{1a}R$ was attributed to the impaired ability of the mutant to interact with G-protein. In the NK1R, the same substitution could

signal through the inositol phosphate pathway (Huang *et al.*, 1995). However the substitution of a bulky, hydrophobic tryptophan, the largest of all the substitutions was well tolerated in the $V_{1a}R$. In contrast, the Y5.58W substitution in the NK1R generated a receptor could only generate an inositol-phosphate signal of 6 % of Wt E_{max} (Huang *et al.*, 1995).

The contribution of the hydroxyl moiety may in part be assessed by the substitutions to acidic side chains. The constructs [Y5.58D]$V_{1a}R$ and [Y5.58E]$V_{1a}R$ did not perturb the ligand binding sites of the $V_{1a}R$ given their Wt-like pharmacology. [Y5.58D]$V_{1a}R$ did demonstrate a small increase in basal activity (6 % of Wt E_{max}) and reduced E_{max} that can be attributed to a reduction in cell-surface expression. The decreased cell-surface expression also suggests that the basal activity detected may be underestimated by more than 50 %. These data support the evidence of the hydroxyl moiety interacting with $Arg^{3.50}$ in adopting an active receptor state (Park *et al.*, 2008; Choe *et al.*, 2011). These findings were not however reproduced in the [Y5.58E]$V_{1a}R$ receptor construct suggesting that the additional methylene does not allow the interactions conferred by the activating substitution Y5.58D.

Receptor constructs [Y5.58N]$V_{1a}R$ and [Y5.58Q]$V_{1a}R$ displayed AVP and CA affinities comparable to Wt and Wt-like cell-surface expression levels. [Y5.58N]$V_{1a}R$ displayed increased basal activity of 6 % of Wt E_{max} and a 77 % increase in E_{max} with Wt-like EC_{50}. [Y5.58Q]$V_{1a}R$ maintained Wt-like basal and maximal signalling levels but displayed increased (4-fold) potency of AVP to generate InsP-$InsP_3$. The parallel increase in basal activity of [Y5.58D]$V_{1a}R$ and [Y5.58N]$V_{1a}R$ suggests that this may be attributed to the side chain length and/or the carbonyl group. Given the hydrophilic character of the side chains of aspartate and asparagine, it is reasonable that they would be more activating than tyrosine at 5.58, shifting the equilibrium towards the R* state.

This hypothesis carries to the enhanced functionality of the [Y5.58K]V_{1a}R displaying a 2.6-fold increase in AVP binding affinity suggesting the substitution stabilises a side chain oriented away from the membrane as in an active receptor state. Although in general the ligand binding site is perturbed as the binding affinity of CA was also increased more than 5-fold. Additionally a 2.9-fold increase in AVP potency in generating InsP-$InsP_3$ was observed, with the decrease in E_{max} being attributed to a parallel decreased expression. The tolerable histidine substitution may be attributed the aromatic character of histidine being less disruptive than the lysine substitution when oriented to the lipid membrane in an inactive state. In the thyroid-stimulating hormone receptor (TSHR), a Y5.58K polymorphism causes hypothyroidism by reducing basal and hormone-induced cAMP signalling and completely ablating inositol phosphate accumulation (Biebermann *et al.*, 1998).

In general, these data suggest that substitution of the conserved $Tyr^{5.58}$ is well tolerated in the V_{1a}R. It is clear that the hydrophobic phenyl portion of the tyrosine side chain contributes to the stabilisation of an inactive conformation but presumably being oriented towards the membrane in a manor analogous to rhodopsin. Additionally, it is clear that the polar character of the hydroxyl group contributes (but is not essential) to adopting an active receptor conformation. Given that in the TSHR, mutation of $Tyr^{5.58}$ to alanine, aspartate, phenylalanine, lysine, serine or tryptophan resulted in complete loss of $G_{q/11}$ coupling, it is apparent that the contribution of $Tyr^{5.58}$ to receptor structure and G-protein coupling is receptor specific. However the rate at which an active conformation is adopted and its lifetime may be more sensitive to substitution (Goncalves *et al.*, 2010).

CHAPTER 6: SUMMARY AND FUTURE WORK

Given the diverse physiological processes to which the $V_{1a}R$ contributes, the understanding of its structure and mechanisms of function are of major pharmaceutical interest. Additionally, as a member of the largest family of integral membrane proteins, the rhodopsin-like GPCRs, experimental findings in the $V_{1a}R$ are likely to have wider application. Data presented here addressed the contribution of individual amino acids in the structure and function of the $V_{1a}R$ through a mutagenic approach. Receptor function was assessed with respect to the pharmacology and signalling properties of receptor constructs generated. Additionally, the cell-surface expression and agonist-induced internalisation of $V_{1a}R$ constructs was assessed.

Chapter 3 addressed the role of individual amino acids in the ICL 2 region of the $V_{1a}R$, initially by an alanine-scanning strategy. This highlighted that residues adjacent to the conserved DRY motif play a greater contribution to the level of cell-surface expression than residues in the second half of ICL 2, adjacent to TM IV. This could be explored further by the generation of more conservative substitutions within ICL 2 to ascertain the functional requirements at particular loci to maintain cell-surface expression.

At position 3.58, a bulky hydrophobic residue is absolutely required to generate effective signalling though the inositol phosphate pathway. The receptor construct [L3.58M]$V_{1a}R$ introduced the corresponding residue observed in the related V_2R into the $V_{1a}R$ and maintained Wt-like functionality. It would be interesting to further characterise this receptor construct to ascertain whether the methionine residue could introduce G_s coupling by quantifying cAMP accumulation. Additionally, this assay could be implemented in the V_2R for receptor constructs substituting 3.60, generating the analogous receptor constructs that were generated in the $V_{1a}R$ and ghrelin-R. Substitution of $Ala^{3.60}$ in the V_2R to threonine, serine, phenylalanine and tyrosine would provide insight into the role of this residue in the

generation of cAMP, having presented here the effects on G_q coupling in receptors that possess little constitutive activity ($V_{1a}R$) and substantial constitutive activity (ghrelin-R). As an extension to this, implementing the same assay to the chimeric construct [β_2AR-$ICL2_H$]$V_{1a}R$ would provide insight as to whether G_s-coupling is introduced into the $V_{1a}R$ by substitution of the entire helical region observed in the β_2AR.

The conserved arginine cluster at the ICL 2-TM IV interface clearly contributes to the level of expression at the cell-surface given that substitution of two basic residues results in decreased expression as determined by ELISA. Substitution of all three arginine residues resulted in a greater loss in cell-surface expression. Substitution to lysine residues would prove insight into whether it is specifically the guanidinium side chain of arginine that contributes to cell-surface expression or a general basic charge in this region.

The role of $Ile^{6.40}$ in the $V_{1a}R$ was probed in Chapter 4 by the systematic substitution to all other encoded amino acids. Differences in the basal activity level of $V_{1a}R$ were observed when particular amino acids where introduced, particularly methionine, alanine and substitution to the small polar amino acids serine and threonine. Interesting, there seems to be no general effect on basal activity and the amino acid introduced at position 6.40 when compared to opsin, H_1R and MC4R. However, in the $V_{1a}R$ receptors that displayed constitutive activity, in general they were expressed at much lower levels at the cell surface although they appear to possess increased signalling though the inositol phosphate pathway at saturating agonist concentrations. This suggests that the CAMs may be adopting different R* states to Wt $V_{1a}R$ that are more efficacious in generating InsP-$InsP_3$. The use of non-hydrolysable GTP analogues would provide insight as to whether substitution of $Ile^{6.40}$ affects the coupling of $V_{1a}R$ for G-protein.

Given that the substitutions I6.40D and I6.40E were particularly detrimental to the integrity of the $V_{1a}R$, functional characterisation was problematic. Increasing the expression levels of [I6.40D]$V_{1a}R$ and [I6.40E]$V_{1a}R$ would allow more thorough and reliable characterisation to identify the effects of these substitutions that were masked by the reduced expression levels.

The substitution of $Asn^{7.49}$ to a basic amino acid ablated the inositol phosphate accumulation of the $V_{1a}R$ and internalisation when challenged by AVP. Assessing the capability of [N7.49K]$V_{1a}R$ and [N7.49R]$V_{1a}R$ to interact with β-arrestins would begin the attempt to dissect why it is that these constructs do not internalise upon agonist challenge. Additionally, the chimeric [β2AR-$ICL2_H$]$V_{1a}R$, [ghrelin-R-$ICL2_H$]$V_{1a}R$ (Chapter 3) and [I6.40F]$V_{1a}R$, [L3.43K/N7.49D]$V_{1a}R$, [Y6.44D]$V_{1a}R$ should also be characterised in this regard given that they all internalised to a lesser extent than Wt.

Chapter 5 attempted to elucidate the role of $Tyr^{5.58}$ in the structure and function of the $V_{1a}R$ with by substitution to all other 19 encoded amino acids. Of the constructs that expressed at the cell-surface at levels that were capable of being functionally analysed, all substitutions on the whole were largely well tolerated with respect to cell-surface expression. The effects on signalling through the inositol phosphate pathway were more varied but in general, all were capable of G_q coupling. This is in contrast to the TSHR whereby any substitution of $Tyr^{5.58}$ lost G_q coupling selectivity. Together this suggests that $Tyr^{5.58}$ plays a more minor role in G_q coupling in the $V_{1a}R$ than in the TSHR. However, the role of $Tyr^{5.58}$ in the $V_{1a}R$ may play a more significant role in signalling through G-protein-independent pathways. To assess this, the catalogue of receptor constructs created in Chapter 6 should be characterised by their ability to activate MAPK/ERK1/2 pathway and by extension, characterisation with respect to their ability to interact with β-arrestins as a potential scaffold for G-protein-independent signalling.

As numerous CAMs were identified in this project, it would be useful to characterise the CA antagonist used within this study as to whether it possesses inverse agonist properties. Additionally, other antagonists of the $V_{1a}R$ could be characterised in this manner. Given that the $V_{1a}R$ natively possesses little detectible basal activity though the inositol phosphate pathway, CAMs presented here would be useful tools to the pharmaceutical industry in the design of and distinction between inverse agonist and antagonist ligands.

CHAPTER 7: REFERENCES

ATTWOOD, T. K. & FINDLAY, J. B. 1994. Fingerprinting G-protein-coupled receptors. *Protein Eng,* 7**,** 195-203.

BAKKER, R. A., JONGEJAN, A., SANSUK, K., HACKSELL, U., TIMMERMAN, H., BRANN, M. R., WEINER, D. M., PARDO, L. & LEURS, R. 2008. Constitutively active mutants of the histamine H1 receptor suggest a conserved hydrophobic asparagine-cage that constrains the activation of class A G protein-coupled receptors. *Mol Pharmacol,* 73**,** 94-103.

BALARAMAN, G. S., BHATTACHARYA, S. & VAIDEHI, N. 2010. Structural insights into conformational stability of wild-type and mutant beta1-adrenergic receptor. *Biophys J,* 99**,** 568-77.

BALLESTEROS, J. & WEINSTEIN, H. 1995. Integrated methods for the construction of three dimensional models and computational probing of structure function relations in G protein-coupled receptors. *Sealfon SC, Conn PM, eds. Methods in Neurosciences, San Diego, CA: Academic Press,* 25**,** 366-428.

BALLESTEROS, J. A., JENSEN, A. D., LIAPAKIS, G., RASMUSSEN, S. G., SHI, L., GETHER, U. & JAVITCH, J. A. 2001. Activation of the beta 2-adrenergic receptor involves disruption of an ionic lock between the cytoplasmic ends of transmembrane segments 3 and 6. *J Biol Chem,* 276**,** 29171-7.

BAYBURT, T. H., LEITZ, A. J., XIE, G., OPRIAN, D. D. & SLIGAR, S. G. 2007. Transducin activation by nanoscale lipid bilayers containing one and two rhodopsins. *J Biol Chem,* 282**,** 14875-81.

BENNETT, M. P. & MITCHELL, D. C. 2008. Regulation of membrane proteins by dietary lipids: effects of cholesterol and docosahexaenoic acid acyl chain-containing phospholipids on rhodopsin stability and function. *Biophys J,* 95**,** 1206-16.

BIEBERMANN, H., SCHONEBERG, T., SCHULZ, A., KRAUSE, G., GRUTERS, A., SCHULTZ, G. & GUDERMANN, T. 1998. A conserved tyrosine residue (Y601) in transmembrane domain 5 of the human thyrotropin receptor serves as a molecular switch to determine G-protein coupling. *Faseb J,* 12**,** 1461-71.

BIRNBAUMER, M. 2000. Vasopressin receptors. *Trends Endocrinol Metab,* 11**,** 406-10.

BOSCH, O. J. & NEUMANN, I. D. 2012. Both oxytocin and vasopressin are mediators of maternal care and aggression in rodents: from central release to sites of action. *Horm Behav,* 61**,** 293-303.

BRUNS, R. F. & FERGUS, J. H. 1990. Allosteric enhancement of adenosine A1 receptor binding and function by 2-amino-3-benzoylthiophenes. *Mol Pharmacol,* 38**,** 939-49.

CARRILLO, J. J., LOPEZ-GIMENEZ, J. F. & MILLIGAN, G. 2004. Multiple interactions between transmembrane helices generate the oligomeric alpha1b-adrenoceptor. *Mol Pharmacol,* 66**,** 1123-37.

CHEN, C., SHAHABI, V., XU, W. & LIU-CHEN, L. Y. 1998. Palmitoylation of the rat mu opioid receptor. *FEBS Lett,* 441**,** 148-52.

CHEN, C. A. & MANNING, D. R. 2001. Regulation of G proteins by covalent modification. *Oncogene,* 20**,** 1643-52.

CHEN, X. P., YANG, W., FAN, Y., LUO, J. S., HONG, K., WANG, Z., YAN, J. F., CHEN, X., LU, J. X., BENOVIC, J. L. & ZHOU, N. M. 2010. Structural determinants in the second intracellular loop of the human cannabinoid CB1 receptor mediate selective coupling to G(s) and G(i). *Br J Pharmacol,* 161**,** 1817-34.

CHEREZOV, V., ROSENBAUM, D. M., HANSON, M. A., RASMUSSEN, S. G., THIAN, F. S., KOBILKA, T. S., CHOI, H. J., KUHN, P., WEIS, W. I., KOBILKA, B. K. &

STEVENS, R. C. 2007. High-resolution crystal structure of an engineered human beta2-adrenergic G protein-coupled receptor. *Science,* 318**,** 1258-65.

CHIEN, E. Y., LIU, W., ZHAO, Q., KATRITCH, V., HAN, G. W., HANSON, M. A., SHI, L., NEWMAN, A. H., JAVITCH, J. A., CHEREZOV, V. & STEVENS, R. C. 2010. Structure of the human dopamine D3 receptor in complex with a D2/D3 selective antagonist. *Science,* 330**,** 1091-5.

CHOE, H. W., KIM, Y. J., PARK, J. H., MORIZUMI, T., PAI, E. F., KRAUSS, N., HOFMANN, K. P., SCHEERER, P. & ERNST, O. P. 2011. Crystal structure of metarhodopsin II. *Nature,* 471**,** 651-5.

CHUNG, K. Y., RASMUSSEN, S. G., LIU, T., LI, S., DEVREE, B. T., CHAE, P. S., CALINSKI, D., KOBILKA, B. K., WOODS, V. L., JR. & SUNAHARA, R. K. 2011. Conformational changes in the G protein Gs induced by the beta2 adrenergic receptor. *Nature,* 477**,** 611-5.

CIECHANOVER, A. 2010. The ubiquitin system: historical perspective. *Proc Am Thorac Soc,* 7**,** 11-2.

COHEN, G. B., OPRIAN, D. D. & ROBINSON, P. R. 1992. Mechanism of activation and inactivation of opsin: role of Glu113 and Lys296. *Biochemistry,* 31**,** 12592-601.

CONN, P. J., CHRISTOPOULOS, A. & LINDSLEY, C. W. 2009. Allosteric modulators of GPCRs: a novel approach for the treatment of CNS disorders. *Nat Rev Drug Discov,* 8**,** 41-54.

CONNER, M. T., CONNER, A. C., BLAND, C. E., TAYLOR, L. H., BROWN, J. E., PARRI, H. R. & BILL, R. M. 2012. Rapid aquaporin translocation regulates cellular water flow: mechanism of hypotonicity-induced subcellular localization of aquaporin 1 water channel. *J Biol Chem,* 287**,** 11516-25.

DAAKA, Y., LUTTRELL, L. M., AHN, S., DELLA ROCCA, G. J., FERGUSON, S. S., CARON, M. G. & LEFKOWITZ, R. J. 1998. Essential role for G protein-coupled receptor endocytosis in the activation of mitogen-activated protein kinase. *J Biol Chem,* 273**,** 685-8.

DAMIAN, M., MARIE, J., LEYRIS, J. P., FEHRENTZ, J. A., VERDIE, P., MARTINEZ, J., BANERES, J. L. & MARY, S. 2012. High constitutive activity is an intrinsic feature of ghrelin receptor protein: a study with a functional monomeric GHS-R1a receptor reconstituted in lipid discs. *J Biol Chem,* 287**,** 3630-41.

DE LEAN, A., STADEL, J. M. & LEFKOWITZ, R. J. 1980. A ternary complex model explains the agonist-specific binding properties of the adenylate cyclase-coupled beta-adrenergic receptor. *J Biol Chem,* 255**,** 7108-17.

DEEN, P. M., CROES, H., VAN AUBEL, R. A., GINSEL, L. A. & VAN OS, C. H. 1995. Water channels encoded by mutant aquaporin-2 genes in nephrogenic diabetes insipidus are impaired in their cellular routing. *J Clin Invest,* 95**,** 2291-6.

DELPARIGI, A., TSCHOP, M., HEIMAN, M. L., SALBE, A. D., VOZAROVA, B., SELL, S. M., BUNT, J. C. & TATARANNI, P. A. 2002. High circulating ghrelin: a potential cause for hyperphagia and obesity in prader-willi syndrome. *J Clin Endocrinol Metab,* 87**,** 5461-4.

DEN OUDEN, D. T. & MEINDERS, A. E. 2005. Vasopressin: physiology and clinical use in patients with vasodilatory shock: a review. *Neth J Med,* 63**,** 4-13.

DEUPI, X., EDWARDS, P., SINGHAL, A., NICKLE, B., OPRIAN, D., SCHERTLER, G. & STANDFUSS, J. 2012. Stabilized G protein binding site in the structure of constitutively active metarhodopsin-II. *Proc Natl Acad Sci U S A,* 109**,** 119-24.

DEUPI, X., OLIVELLA, M., GOVAERTS, C., BALLESTEROS, J. A., CAMPILLO, M. & PARDO, L. 2004. Ser and Thr residues modulate the conformation of pro-kinked transmembrane alpha-helices. *Biophys J,* 86**,** 105-15.

DHAMI, G. K., BABWAH, A. V., STERNE-MARR, R. & FERGUSON, S. S. 2005. Phosphorylation-independent regulation of metabotropic glutamate receptor 1 signaling requires g protein-coupled receptor kinase 2 binding to the second intracellular loop. *J Biol Chem,* 280**,** 24420-7.

DORE, A. S., ROBERTSON, N., ERREY, J. C., NG, I., HOLLENSTEIN, K., TEHAN, B., HURRELL, E., BENNETT, K., CONGREVE, M., MAGNANI, F., TATE, C. G., WEIR, M. & MARSHALL, F. H. 2011. Structure of the adenosine A(2A) receptor in complex with ZM241385 and the xanthines XAC and caffeine. *Structure,* 19**,** 1283-93.

DOWNES, G. B. & GAUTAM, N. 1999. The G protein subunit gene families. *Genomics,* 62**,** 544-52.

DUVIGNEAUD, V. 1955. Hormones of the Posterior Pituitary Gland - Oxytocin and Vasopressin. *Harvey Lectures***,** 1-26.

FAHRENHOLZ, F., KLEIN, U. & GIMPL, G. 1995. Conversion of the myometrial oxytocin receptor from low to high affinity state by cholesterol. *Adv Exp Med Biol,* 395**,** 311-9.

FARRENS, D. L., ALTENBACH, C., YANG, K., HUBBELL, W. L. & KHORANA, H. G. 1996. Requirement of rigid-body motion of transmembrane helices for light activation of rhodopsin. *Science,* 274**,** 768-70.

FERGUSON, S. S. 2001. Evolving concepts in G protein-coupled receptor endocytosis: the role in receptor desensitization and signaling. *Pharmacol Rev,* 53**,** 1-24.

FERGUSON, S. S. 2007. Phosphorylation-independent attenuation of GPCR signalling. *Trends Pharmacol Sci,* 28**,** 173-9.

FERGUSON, S. S., BARAK, L. S., ZHANG, J. & CARON, M. G. 1996. G-protein-coupled receptor regulation: role of G-protein-coupled receptor kinases and arrestins. *Can J Physiol Pharmacol,* 74**,** 1095-110.

FILEP, J. & ROSENKRANZ, B. 1987. Mechanism of vasopressin-induced platelet aggregation. *Thromb Res,* 45**,** 7-15.

FREDRIKSSON, R., LAGERSTROM, M. C., LUNDIN, L. G. & SCHIOTH, H. B. 2003. The G-protein-coupled receptors in the human genome form five main families. Phylogenetic analysis, paralogon groups, and fingerprints. *Mol Pharmacol,* 63**,** 1256-72.

FUKUSHIMA, Y., SAITOH, T., ANAI, M., OGIHARA, T., INUKAI, K., FUNAKI, M., SAKODA, H., ONISHI, Y., ONO, H., FUJISHIRO, M., ISHIKAWA, T., TAKATA, K., NAGAI, R., OMATA, M. & ASANO, T. 2001. Palmitoylation of the canine histamine H2 receptor occurs at Cys(305) and is important for cell surface targeting. *Biochim Biophys Acta,* 1539**,** 181-91.

GABORIK, Z., JAGADEESH, G., ZHANG, M., SPAT, A., CATT, K. J. & HUNYADY, L. 2003. The role of a conserved region of the second intracellular loop in AT1 angiotensin receptor activation and signaling. *Endocrinology,* 144**,** 2220-8.

GANTZ, I., DELVALLE, J., WANG, L. D., TASHIRO, T., MUNZERT, G., GUO, Y. J., KONDA, Y. & YAMADA, T. 1992. Molecular basis for the interaction of histamine with the histamine H2 receptor. *J Biol Chem,* 267**,** 20840-3.

GETHER, U., LIN, S., GHANOUNI, P., BALLESTEROS, J. A., WEINSTEIN, H. & KOBILKA, B. K. 1997. Agonists induce conformational changes in transmembrane domains III and VI of the beta2 adrenoceptor. *Embo J,* 16**,** 6737-47.

GONCALVES, J. A., SOUTH, K., AHUJA, S., ZAITSEVA, E., OPEFI, C. A., EILERS, M., VOGEL, R., REEVES, P. J. & SMITH, S. O. 2010. Highly conserved tyrosine stabilizes the active state of rhodopsin. *Proc Natl Acad Sci U S A,* 107**,** 19861-6.

GONZALEZ-MAESO, J., ANG, R. L., YUEN, T., CHAN, P., WEISSTAUB, N. V., LOPEZ-GIMENEZ, J. F., ZHOU, M., OKAWA, Y., CALLADO, L. F., MILLIGAN, G.,

GINGRICH, J. A., FILIZOLA, M., MEANA, J. J. & SEALFON, S. C. 2008. Identification of a serotonin/glutamate receptor complex implicated in psychosis. *Nature,* 452**,** 93-7.

GOODMAN, O. B., JR., KRUPNICK, J. G., SANTINI, F., GUREVICH, V. V., PENN, R. B., GAGNON, A. W., KEEN, J. H. & BENOVIC, J. L. 1996. Beta-arrestin acts as a clathrin adaptor in endocytosis of the beta2-adrenergic receptor. *Nature,* 383**,** 447-50.

GOVAERTS, C., LEFORT, A., COSTAGLIOLA, S., WODAK, S. J., BALLESTEROS, J. A., VAN SANDE, J., PARDO, L. & VASSART, G. 2001. A conserved Asn in transmembrane helix 7 is an on/off switch in the activation of the thyrotropin receptor. *J Biol Chem,* 276**,** 22991-9.

GRANIER, S., MANGLIK, A., KRUSE, A. C., KOBILKA, T. S., THIAN, F. S., WEIS, W. I. & KOBILKA, B. K. 2012. Structure of the delta-opioid receptor bound to naltrindole. *Nature,* 485**,** 400-4.

GRIEBEL, G., SIMIAND, J., STEMMELIN, J., GAL, C. S. & STEINBERG, R. 2003. The vasopressin V1b receptor as a therapeutic target in stress-related disorders. *Curr Drug Targets CNS Neurol Disord,* 2**,** 191-200.

GUO, W., SHI, L., FILIZOLA, M., WEINSTEIN, H. & JAVITCH, J. A. 2005. Crosstalk in G protein-coupled receptors: changes at the transmembrane homodimer interface determine activation. *Proc Natl Acad Sci U S A,* 102**,** 17495-500.

GUREVICH, V. V., PALS-RYLAARSDAM, R., BENOVIC, J. L., HOSEY, M. M. & ONORATO, J. J. 1997. Agonist-receptor-arrestin, an alternative ternary complex with high agonist affinity. *J Biol Chem,* 272**,** 28849-52.

HADLEY, M. E. 1996. Endocrinology.

HAGA, K., KRUSE, A. C., ASADA, H., YURUGI-KOBAYASHI, T., SHIROISHI, M., ZHANG, C., WEIS, W. I., OKADA, T., KOBILKA, B. K., HAGA, T. & KOBAYASHI, T. 2012. Structure of the human M2 muscarinic acetylcholine receptor bound to an antagonist. *Nature,* 482**,** 547-51.

HAN, M., SMITH, S. O. & SAKMAR, T. P. 1998. Constitutive activation of opsin by mutation of methionine 257 on transmembrane helix 6. *Biochemistry,* 37**,** 8253-61.

HANSON, M. A., CHEREZOV, V., GRIFFITH, M. T., ROTH, C. B., JAAKOLA, V. P., CHIEN, E. Y., VELASQUEZ, J., KUHN, P. & STEVENS, R. C. 2008. A specific cholesterol binding site is established by the 2.8 A structure of the human beta2-adrenergic receptor. *Structure,* 16**,** 897-905.

HANSON, M. A., ROTH, C. B., JO, E., GRIFFITH, M. T., SCOTT, F. L., REINHART, G., DESALE, H., CLEMONS, B., CAHALAN, S. M., SCHUERER, S. C., SANNA, M. G., HAN, G. W., KUHN, P., ROSEN, H. & STEVENS, R. C. 2012. Crystal structure of a lipid G protein-coupled receptor. *Science,* 335**,** 851-5.

HARDING, P. J., ATTRILL, H., BOEHRINGER, J., ROSS, S., WADHAMS, G. H., SMITH, E., ARMITAGE, J. P. & WATTS, A. 2009. Constitutive dimerization of the G-protein coupled receptor, neurotensin receptor 1, reconstituted into phospholipid bilayers. *Biophys J,* 96**,** 964-73.

HAVLICKOVA, M., BLAHOS, J., BRABET, I., LIU, J., HRUSKOVA, B., PREZEAU, L. & PIN, J. P. 2003. The second intracellular loop of metabotropic glutamate receptors recognizes C termini of G-protein alpha-subunits. *J Biol Chem,* 278**,** 35063-70.

HAWTIN, S. R. 2005. Charged residues of the conserved DRY triplet of the vasopressin V1a receptor provide molecular determinants for cell surface delivery and internalization. *Mol Pharmacol,* 68**,** 1172-82.

HAWTIN, S. R., TOBIN, A. B., PATEL, S. & WHEATLEY, M. 2001. Palmitoylation of the vasopressin V1a receptor reveals different conformational requirements for signaling,

agonist-induced receptor phosphorylation, and sequestration. *J Biol Chem,* 276**,** 38139-46.

HEBERT, T. E., MOFFETT, S., MORELLO, J. P., LOISEL, T. P., BICHET, D. G., BARRET, C. & BOUVIER, M. 1996. A peptide derived from a beta2-adrenergic receptor transmembrane domain inhibits both receptor dimerization and activation. *J Biol Chem,* 271**,** 16384-92.

HO, B. Y., KARSCHIN, A., BRANCHEK, T., DAVIDSON, N. & LESTER, H. A. 1992. The role of conserved aspartate and serine residues in ligand binding and in function of the 5-HT1A receptor: a site-directed mutation study. *FEBS Lett,* 312**,** 259-62.

HOLST, B., CYGANKIEWICZ, A., JENSEN, T. H., ANKERSEN, M. & SCHWARTZ, T. W. 2003. High constitutive signaling of the ghrelin receptor--identification of a potent inverse agonist. *Mol Endocrinol,* 17**,** 2201-10.

HOLST, B. & SCHWARTZ, T. W. 2006. Ghrelin receptor mutations--too little height and too much hunger. *J Clin Invest,* 116**,** 637-41.

HOPKINS, A. L. & GROOM, C. R. 2002. The druggable genome. *Nat Rev Drug Discov,* 1**,** 727-30.

HORSTMAN, D. A., BRANDON, S., WILSON, A. L., GUYER, C. A., CRAGOE, E. J., JR. & LIMBIRD, L. E. 1990. An aspartate conserved among G-protein receptors confers allosteric regulation of alpha 2-adrenergic receptors by sodium. *J Biol Chem,* 265**,** 21590-5.

HOWL, J., ISMAIL, T., STRAIN, A. J., KIRK, C. J., ANDERSON, D. & WHEATLEY, M. 1991. Characterization of the human liver vasopressin receptor. Profound differences between human and rat vasopressin-receptor-mediated responses suggest only a minor role for vasopressin in regulating human hepatic function. *Biochem J,* 276 (Pt 1)**,** 189-95.

HUANG, P., CHEN, C., MAGUE, S. D., BLENDY, J. A. & LIU-CHEN, L. Y. 2012. A common single nucleotide polymorphism A118G of the mu opioid receptor alters its N-glycosylation and protein stability. *Biochem J,* 441**,** 379-86.

HUANG, R. R., HUANG, D., STRADER, C. D. & FONG, T. M. 1995. Conformational compatibility as a basis of differential affinities of tachykinins for the neurokinin-1 receptor. *Biochemistry,* 34**,** 16467-72.

HUNYADY, L., BOR, M., BALLA, T. & CATT, K. J. 1995. Critical role of a conserved intramembrane tyrosine residue in angiotensin II receptor activation. *J Biol Chem,* 270**,** 9702-5.

JAAKOLA, V. P., GRIFFITH, M. T., HANSON, M. A., CHEREZOV, V., CHIEN, E. Y., LANE, J. R., IJZERMAN, A. P. & STEVENS, R. C. 2008. The 2.6 angstrom crystal structure of a human A2A adenosine receptor bound to an antagonist. *Science,* 322**,** 1211-7.

JENKINS, J. S. & NUSSEY, S. S. 1991. The role of oxytocin: present concepts. *Clin Endocrinol (Oxf),* 34**,** 515-25.

JI, T. H., GROSSMANN, M. & JI, I. 1998. G protein-coupled receptors. I. Diversity of receptor-ligand interactions. *J Biol Chem,* 273**,** 17299-302.

JONGEJAN, A., BRUYSTERS, M., BALLESTEROS, J. A., HAAKSMA, E., BAKKER, R. A., PARDO, L. & LEURS, R. 2005. Linking agonist binding to histamine H1 receptor activation. *Nat Chem Biol,* 1**,** 98-103.

KJELSBERG, M. A., COTECCHIA, S., OSTROWSKI, J., CARON, M. G. & LEFKOWITZ, R. J. 1992. Constitutive activation of the alpha 1B-adrenergic receptor by all amino acid substitutions at a single site. Evidence for a region which constrains receptor activation. *J Biol Chem,* 267**,** 1430-3.

KLABUNDE, T. & HESSLER, G. 2002. Drug design strategies for targeting G-protein-coupled receptors. *Chembiochem,* 3**,** 928-44.

KLEIN, U., GIMPL, G. & FAHRENHOLZ, F. 1995. Alteration of the myometrial plasma membrane cholesterol content with beta-cyclodextrin modulates the binding affinity of the oxytocin receptor. *Biochemistry,* 34**,** 13784-93.

KOLAKOWSKI, L. F., JR. 1994. GCRDb: a G-protein-coupled receptor database. *Receptors Channels,* 2**,** 1-7.

KREBS, A., EDWARDS, P. C., VILLA, C., LI, J. & SCHERTLER, G. F. 2003. The three-dimensional structure of bovine rhodopsin determined by electron cryomicroscopy. *J Biol Chem,* 278**,** 50217-25.

KRUSE, A. C., HU, J., PAN, A. C., ARLOW, D. H., ROSENBAUM, D. M., ROSEMOND, E., GREEN, H. F., LIU, T., CHAE, P. S., DROR, R. O., SHAW, D. E., WEIS, W. I., WESS, J. & KOBILKA, B. K. 2012. Structure and dynamics of the M3 muscarinic acetylcholine receptor. *Nature,* 482**,** 552-6.

LATRONICO, A. C., ABELL, A. N., ARNHOLD, I. J., LIU, X., LINS, T. S., BRITO, V. N., BILLERBECK, A. E., SEGALOFF, D. L. & MENDONCA, B. B. 1998. A unique constitutively activating mutation in third transmembrane helix of luteinizing hormone receptor causes sporadic male gonadotropin-independent precocious puberty. *J Clin Endocrinol Metab,* 83**,** 2435-40.

LATRONICO, A. C. & SEGALOFF, D. L. 2007. Insights learned from L457(3.43)R, an activating mutant of the human lutropin receptor. *Mol Cell Endocrinol,* 260-262**,** 287-93.

LEBON, G. & TATE, C. G. 2011. [Structure of the adenosine-bound conformation of the human adenosine A(2A) receptor]. *Med Sci (Paris),* 27**,** 926-8.

LEBON, G., WARNE, T., EDWARDS, P. C., BENNETT, K., LANGMEAD, C. J., LESLIE, A. G. & TATE, C. G. 2011. Agonist-bound adenosine A2A receptor structures reveal common features of GPCR activation. *Nature,* 474**,** 521-5.

LECHLEITER, J., HELLMISS, R., DUERSON, K., ENNULAT, D., DAVID, N., CLAPHAM, D. & PERALTA, E. 1990. Distinct sequence elements control the specificity of G protein activation by muscarinic acetylcholine receptor subtypes. *EMBO J,* 9**,** 4381-90.

LI, J., EDWARDS, P. C., BURGHAMMER, M., VILLA, C. & SCHERTLER, G. F. 2004. Structure of bovine rhodopsin in a trigonal crystal form. *J Mol Biol,* 343**,** 1409-38.

LI, J. H., CHOU, C. L., LI, B., GAVRILOVA, O., EISNER, C., SCHNERMANN, J., ANDERSON, S. A., DENG, C. X., KNEPPER, M. A. & WESS, J. 2009. A selective EP4 PGE2 receptor agonist alleviates disease in a new mouse model of X-linked nephrogenic diabetes insipidus. *J Clin Invest,* 119**,** 3115-26.

LIANG, Y., FOTIADIS, D., FILIPEK, S., SAPERSTEIN, D. A., PALCZEWSKI, K. & ENGEL, A. 2003. Organization of the G protein-coupled receptors rhodopsin and opsin in native membranes. *J Biol Chem,* 278**,** 21655-62.

LIMBIRD, L. E. 1984. GTP and Na+ modulate receptor-adenyl cyclase coupling and receptor-mediated function. *Am J Physiol,* 247**,** E59-68.

LIU, W., CHUN, E., THOMPSON, A. A., CHUBUKOV, P., XU, F., KATRITCH, V., HAN, G. W., ROTH, C. B., HEITMAN, L. H., AP, I. J., CHEREZOV, V. & STEVENS, R. C. 2012. Structural basis for allosteric regulation of GPCRs by sodium ions. *Science,* 337**,** 232-6.

LUTTRELL, L. M., DAAKA, Y. & LEFKOWITZ, R. J. 1999. Regulation of tyrosine kinase cascades by G-protein-coupled receptors. *Curr Opin Cell Biol,* 11**,** 177-83.

MAGALHAES, A. C., DUNN, H. & FERGUSON, S. S. 2012. Regulation of GPCR activity, trafficking and localization by GPCR-interacting proteins. *Br J Pharmacol,* 165**,** 1717-36.

MANGLIK, A., KRUSE, A. C., KOBILKA, T. S., THIAN, F. S., MATHIESEN, J. M., SUNAHARA, R. K., PARDO, L., WEIS, W. I., KOBILKA, B. K. & GRANIER, S. 2012. Crystal structure of the micro-opioid receptor bound to a morphinan antagonist. *Nature,* 485**,** 321-6.

MANSOUR, A., MENG, F., MEADOR-WOODRUFF, J. H., TAYLOR, L. P., CIVELLI, O. & AKIL, H. 1992. Site-directed mutagenesis of the human dopamine D2 receptor. *Eur J Pharmacol,* 227**,** 205-14.

MARCHESE, A. & BENOVIC, J. L. 2001. Agonist-promoted ubiquitination of the G protein-coupled receptor CXCR4 mediates lysosomal sorting. *J Biol Chem,* 276**,** 45509-12.

MARINISSEN, M. J. & GUTKIND, J. S. 2001. G-protein-coupled receptors and signaling networks: emerging paradigms. *Trends Pharmacol Sci,* 22**,** 368-76.

MARION, S., OAKLEY, R. H., KIM, K. M., CARON, M. G. & BARAK, L. S. 2006. A beta-arrestin binding determinant common to the second intracellular loops of rhodopsin family G protein-coupled receptors. *J Biol Chem,* 281**,** 2932-8.

MARTIN, N. P., LEFKOWITZ, R. J. & SHENOY, S. K. 2003. Regulation of V2 vasopressin receptor degradation by agonist-promoted ubiquitination. *J Biol Chem,* 278**,** 45954-9.

MATSUSHITA, H., TOMIZAWA, K., OKIMOTO, N., NISHIKI, T., OHMORI, I. & MATSUI, H. 2010. Oxytocin mediates the antidepressant effects of mating behavior in male mice. *Neurosci Res,* 68**,** 151-3.

MAY, L. T., AVLANI, V. A., LANGMEAD, C. J., HERDON, H. J., WOOD, M. D., SEXTON, P. M. & CHRISTOPOULOS, A. 2007. Structure-function studies of allosteric agonism at M2 muscarinic acetylcholine receptors. *Mol Pharmacol,* 72**,** 463-76.

MCLOUGHLIN, D. J. & STRANGE, P. G. 2000. Mechanisms of agonism and inverse agonism at serotonin 5-HT1A receptors. *J Neurochem,* 74**,** 347-57.

MICHELL, R. H., KIRK, C. J. & BILLAH, M. M. 1979. Hormonal stimulation of phosphatidylinositol breakdown with particular reference to the hepatic effects of vasopressin. *Biochem Soc Trans,* 7**,** 861-5.

MILLAR, R. P. & NEWTON, C. L. 2010. The year in G protein-coupled receptor research. *Mol Endocrinol,* 24**,** 261-74.

MILLIGAN, G., STODDART, L. A. & SMITH, N. J. 2009. Agonism and allosterism: the pharmacology of the free fatty acid receptors FFA2 and FFA3. *Br J Pharmacol,* 158**,** 146-53.

MIRZADEGAN, T., BENKO, G., FILIPEK, S. & PALCZEWSKI, K. 2003. Sequence analyses of G-protein-coupled receptors: similarities to rhodopsin. *Biochemistry,* 42**,** 2759-67.

MITCHELL, D. C., STRAUME, M., MILLER, J. L. & LITMAN, B. J. 1990. Modulation of metarhodopsin formation by cholesterol-induced ordering of bilayer lipids. *Biochemistry,* 29**,** 9143-9.

MONOD, J., CHANGEUX, J. P. & JACOB, F. 1963. Allosteric proteins and cellular control systems. *J Mol Biol,* 6**,** 306-29.

MORO, O., LAMEH, J., HOGGER, P. & SADEE, W. 1993. Hydrophobic amino acid in the i2 loop plays a key role in receptor-G protein coupling. *J Biol Chem,* 268**,** 22273-6.

MORRIS, A. J. & SCARLATA, S. 1997. Regulation of effectors by G-protein alpha- and beta gamma-subunits. Recent insights from studies of the phospholipase c-beta isoenzymes. *Biochem Pharmacol,* 54**,** 429-35.

MURRAY, A. R., FLIESLER, S. J. & AL-UBAIDI, M. R. 2009. Rhodopsin: the functional significance of asn-linked glycosylation and other post-translational modifications. *Ophthalmic Genet,* 30**,** 109-20.

NAGASE, H., IMAIDE, S., HIRAYAMA, S., NEMOTO, T. & FUJII, H. 2012. Essential structure of opioid kappa receptor agonist nalfurafine for binding to the kappa receptor 2: Synthesis of decahydro(iminoethano)phenanthrene derivatives and their pharmacologies. *Bioorg Med Chem Lett,* 22**,** 5071-4.

NAKAJIMA, K. I. & WESS, J. 2012. Design and Functional Characterization of a Novel, Arrestin-Biased Designer G Protein-Coupled Receptor. *Mol Pharmacol*.

NAKAMURA, K., KRUPNICK, J. G., BENOVIC, J. L. & ASCOLI, M. 1998. Signaling and phosphorylation-impaired mutants of the rat follitropin receptor reveal an activation- and phosphorylation-independent but arrestin-dependent pathway for internalization. *J Biol Chem,* 273**,** 24346-54.

NEUMANN, I. D. & LANDGRAF, R. 2012. Balance of brain oxytocin and vasopressin: implications for anxiety, depression, and social behaviors. *Trends Neurosci*.

NEVE, K. A., COX, B. A., HENNINGSEN, R. A., SPANOYANNIS, A. & NEVE, R. L. 1991. Pivotal role for aspartate-80 in the regulation of dopamine D2 receptor affinity for drugs and inhibition of adenylyl cyclase. *Mol Pharmacol,* 39**,** 733-9.

NG, G. Y., MOUILLAC, B., GEORGE, S. R., CARON, M., DENNIS, M., BOUVIER, M. & O'DOWD, B. F. 1994. Desensitization, phosphorylation and palmitoylation of the human dopamine D1 receptor. *Eur J Pharmacol,* 267**,** 7-19.

NUNN, C., MAO, H., CHIDIAC, P. & ALBERT, P. R. 2006. RGS17/RGSZ2 and the RZ/A family of regulators of G-protein signaling. *Semin Cell Dev Biol,* 17**,** 390-9.

O'DOWD, B. F., HNATOWICH, M., CARON, M. G., LEFKOWITZ, R. J. & BOUVIER, M. 1989. Palmitoylation of the human beta 2-adrenergic receptor. Mutation of Cys341 in the carboxyl tail leads to an uncoupled nonpalmitoylated form of the receptor. *J Biol Chem,* 264**,** 7564-9.

OAKLEY, R. H., LAPORTE, S. A., HOLT, J. A., CARON, M. G. & BARAK, L. S. 2000. Differential affinities of visual arrestin, beta arrestin1, and beta arrestin2 for G protein-coupled receptors delineate two major classes of receptors. *J Biol Chem,* 275**,** 17201-10.

OIKAWA, R., HOSODA, C., NASA, Y., DAICHO, T., TANOUE, A., TSUJIMOTO, G., TAKAGI, N., TANONAKA, K. & TAKEO, S. 2010. Decreased susceptibility to salt-induced hypertension in subtotally nephrectomized mice lacking the vasopressin V1a receptor. *Cardiovasc Res,* 87**,** 187-94.

OKADA, T. & PALCZEWSKI, K. 2001. Crystal structure of rhodopsin: implications for vision and beyond. *Curr Opin Struct Biol,* 11**,** 420-6.

OLDHAM, W. M. & HAMM, H. E. 2006. Structural basis of function in heterotrimeric G proteins. *Q Rev Biophys,* 39**,** 117-66.

OVCHINNIKOV YU, A., ABDULAEV, N. G. & BOGACHUK, A. S. 1988. Two adjacent cysteine residues in the C-terminal cytoplasmic fragment of bovine rhodopsin are palmitylated. *FEBS Lett,* 230**,** 1-5.

PALCZEWSKI, K., KUMASAKA, T., HORI, T., BEHNKE, C. A., MOTOSHIMA, H., FOX, B. A., LE TRONG, I., TELLER, D. C., OKADA, T., STENKAMP, R. E., YAMAMOTO, M. & MIYANO, M. 2000. Crystal structure of rhodopsin: A G protein-coupled receptor. *Science,* 289**,** 739-45.

PARK, J. H., SCHEERER, P., HOFMANN, K. P., CHOE, H. W. & ERNST, O. P. 2008. Crystal structure of the ligand-free G-protein-coupled receptor opsin. *Nature,* 454**,** 183-7.

PARTHIER, C., REEDTZ-RUNGE, S., RUDOLPH, R. & STUBBS, M. T. 2009. Passing the baton in class B GPCRs: peptide hormone activation via helix induction? *Trends Biochem Sci,* 34**,** 303-10.

PENG, Z., TANG, Y., LUO, H., JIANG, F., YANG, J., SUN, L. & LI, J. D. 2011. Disease-causing mutation in PKR2 receptor reveals a critical role of positive charges in the second intracellular loop for G-protein coupling and receptor trafficking. *J Biol Chem,* 286**,** 16615-22.

PFEIFFER, M., KOCH, T., SCHRODER, H., KLUTZNY, M., KIRSCHT, S., KREIENKAMP, H. J., HOLLT, V. & SCHULZ, S. 2001. Homo- and heterodimerization of somatostatin receptor subtypes. Inactivation of sst(3) receptor function by heterodimerization with sst(2A). *J Biol Chem,* 276**,** 14027-36.

PIN, J. P., GALVEZ, T. & PREZEAU, L. 2003. Evolution, structure, and activation mechanism of family 3/C G-protein-coupled receptors. *Pharmacol Ther,* 98**,** 325-54.

PITCHER, J. A., FREEDMAN, N. J. & LEFKOWITZ, R. J. 1998. G protein-coupled receptor kinases. *Annu Rev Biochem,* 67**,** 653-92.

PONIMASKIN, E. G., HEINE, M., JOUBERT, L., SEBBEN, M., BICKMEYER, U., RICHTER, D. W. & DUMUIS, A. 2002. The 5-hydroxytryptamine(4a) receptor is palmitoylated at two different sites, and acylation is critically involved in regulation of receptor constitutive activity. *J Biol Chem,* 277**,** 2534-46.

PRONETH, B., XIANG, Z., POGOZHEVA, I. D., LITHERLAND, S. A., GORBATYUK, O. S., SHAW, A. M., MILLARD, W. J., MOSBERG, H. I. & HASKELL-LUEVANO, C. 2006. Molecular mechanism of the constitutive activation of the L250Q human melanocortin-4 receptor polymorphism. *Chem Biol Drug Des,* 67**,** 215-29.

RAMAN, D., OSAWA, S., GUREVICH, V. V. & WEISS, E. R. 2003. The interaction with the cytoplasmic loops of rhodopsin plays a crucial role in arrestin activation and binding. *J Neurochem,* 84**,** 1040-50.

RASMUSSEN, S. G., CHOI, H. J., FUNG, J. J., PARDON, E., CASAROSA, P., CHAE, P. S., DEVREE, B. T., ROSENBAUM, D. M., THIAN, F. S., KOBILKA, T. S., SCHNAPP, A., KONETZKI, I., SUNAHARA, R. K., GELLMAN, S. H., PAUTSCH, A., STEYAERT, J., WEIS, W. I. & KOBILKA, B. K. 2011a. Structure of a nanobody-stabilized active state of the beta(2) adrenoceptor. *Nature,* 469**,** 175-80.

RASMUSSEN, S. G., CHOI, H. J., ROSENBAUM, D. M., KOBILKA, T. S., THIAN, F. S., EDWARDS, P. C., BURGHAMMER, M., RATNALA, V. R., SANISHVILI, R., FISCHETTI, R. F., SCHERTLER, G. F., WEIS, W. I. & KOBILKA, B. K. 2007. Crystal structure of the human beta2 adrenergic G-protein-coupled receptor. *Nature,* 450**,** 383-7.

RASMUSSEN, S. G., DEVREE, B. T., ZOU, Y., KRUSE, A. C., CHUNG, K. Y., KOBILKA, T. S., THIAN, F. S., CHAE, P. S., PARDON, E., CALINSKI, D., MATHIESEN, J. M., SHAH, S. T., LYONS, J. A., CAFFREY, M., GELLMAN, S. H., STEYAERT, J., SKINIOTIS, G., WEIS, W. I., SUNAHARA, R. K. & KOBILKA, B. K. 2011b. Crystal structure of the beta(2) adrenergic receptor-Gs protein complex. *Nature*.

RASMUSSEN, S. G., JENSEN, A. D., LIAPAKIS, G., GHANOUNI, P., JAVITCH, J. A. & GETHER, U. 1999. Mutation of a highly conserved aspartic acid in the beta2 adrenergic receptor: constitutive activation, structural instability, and conformational rearrangement of transmembrane segment 6. *Mol Pharmacol,* 56**,** 175-84.

RIEK, R. P., RIGOUTSOS, I., NOVOTNY, J. & GRAHAM, R. M. 2001. Non-alpha-helical elements modulate polytopic membrane protein architecture. *J Mol Biol,* 306**,** 349-62.

ROBINSON, P. R., COHEN, G. B., ZHUKOVSKY, E. A. & OPRIAN, D. D. 1992. Constitutively active mutants of rhodopsin. *Neuron,* 9**,** 719-25.

ROSENBAUM, D. M., CHEREZOV, V., HANSON, M. A., RASMUSSEN, S. G., THIAN, F. S., KOBILKA, T. S., CHOI, H. J., YAO, X. J., WEIS, W. I., STEVENS, R. C. & KOBILKA, B. K. 2007. GPCR engineering yields high-resolution structural insights into beta2-adrenergic receptor function. *Science,* 318**,** 1266-73.

ROSENBAUM, D. M., ZHANG, C., LYONS, J. A., HOLL, R., ARAGAO, D., ARLOW, D. H., RASMUSSEN, S. G., CHOI, H. J., DEVREE, B. T., SUNAHARA, R. K., CHAE, P. S., GELLMAN, S. H., DROR, R. O., SHAW, D. E., WEIS, W. I., CAFFREY, M., GMEINER, P. & KOBILKA, B. K. 2011. Structure and function of an irreversible agonist-beta(2) adrenoceptor complex. *Nature,* 469**,** 236-40.

RUPRECHT, J. J., MIELKE, T., VOGEL, R., VILLA, C. & SCHERTLER, G. F. 2004. Electron crystallography reveals the structure of metarhodopsin I. *Embo J,* 23**,** 3609-20.

SADEGHI, H. & BIRNBAUMER, M. 1999. O-Glycosylation of the V2 vasopressin receptor. *Glycobiology,* 9**,** 731-7.

SAMAMA, P., COTECCHIA, S., COSTA, T. & LEFKOWITZ, R. J. 1993. A mutation-induced activated state of the beta 2-adrenergic receptor. Extending the ternary complex model. *J Biol Chem,* 268**,** 4625-36.

SAMBROOK, J., FRITSCH, E. F. & MANIATISM, T. 1989. *Molecular Cloning, 2nd ed.*

SANCHEZ-LAORDEN, B. L., HERRAIZ, C., VALENCIA, J. C., HEARING, V. J., JIMENEZ-CERVANTES, C. & GARCIA-BORRON, J. C. 2009. Aberrant trafficking of human melanocortin 1 receptor variants associated with red hair and skin cancer: Steady-state retention of mutant forms in the proximal golgi. *J Cell Physiol,* 220**,** 640-54.

SANSUK, K., DEUPI, X., TORRECILLAS, I. R., JONGEJAN, A., NIJMEIJER, S., BAKKER, R. A., PARDO, L. & LEURS, R. 2011. A structural insight into the reorientation of transmembrane domains 3 and 5 during family A G protein-coupled receptor activation. *Mol Pharmacol,* 79**,** 262-9.

SCHEER, A. & COTECCHIA, S. 1997. Constitutively active G protein-coupled receptors: potential mechanisms of receptor activation. *J Recept Signal Transduct Res,* 17**,** 57-73.

SCHEER, A., FANELLI, F., COSTA, T., DE BENEDETTI, P. G. & COTECCHIA, S. 1996. Constitutively active mutants of the alpha 1B-adrenergic receptor: role of highly conserved polar amino acids in receptor activation. *Embo J,* 15**,** 3566-78.

SCHEERER, P., PARK, J. H., HILDEBRAND, P. W., KIM, Y. J., KRAUSS, N., CHOE, H. W., HOFMANN, K. P. & ERNST, O. P. 2008. Crystal structure of opsin in its G-protein-interacting conformation. *Nature,* 455**,** 497-502.

SCHMIDT, C. J., THOMAS, T. C., LEVINE, M. A. & NEER, E. J. 1992. Specificity of G protein beta and gamma subunit interactions. *J Biol Chem,* 267**,** 13807-10.

SCHORSCHER-PETCU, A., SOTOCINAL, S., CIURA, S., DUPRE, A., RITCHIE, J., SORGE, R. E., CRAWLEY, J. N., HU, S. B., NISHIMORI, K., YOUNG, L. J., TRIBOLLET, E., QUIRION, R. & MOGIL, J. S. 2010. Oxytocin-induced analgesia and scratching are mediated by the vasopressin-1A receptor in the mouse. *J Neurosci,* 30**,** 8274-84.

SCHWARTZ, T. W., FRIMURER, T. M., HOLST, B., ROSENKILDE, M. M. & ELLING, C. E. 2006. Molecular mechanism of 7TM receptor activation--a global toggle switch model. *Annu Rev Pharmacol Toxicol,* 46**,** 481-519.

SHAN, J., WEINSTEIN, H. & MEHLER, E. L. 2010. Probing the structural determinants for the function of intracellular loop 2 in structurally cognate G-protein-coupled receptors. *Biochemistry,* 49**,** 10691-701.

SHENOY, S. K., BARAK, L. S., XIAO, K., AHN, S., BERTHOUZE, M., SHUKLA, A. K., LUTTRELL, L. M. & LEFKOWITZ, R. J. 2007. Ubiquitination of beta-arrestin links seven-transmembrane receptor endocytosis and ERK activation. *J Biol Chem,* 282**,** 29549-62.

SHI, L., LIAPAKIS, G., XU, R., GUARNIERI, F., BALLESTEROS, J. A. & JAVITCH, J. A. 2002. Beta2 adrenergic receptor activation. Modulation of the proline kink in transmembrane 6 by a rotamer toggle switch. *J Biol Chem,* 277**,** 40989-96.

SHIMAMURA, T., HIRAKI, K., TAKAHASHI, N., HORI, T., AGO, H., MASUDA, K., TAKIO, K., ISHIGURO, M. & MIYANO, M. 2008. Crystal structure of squid rhodopsin with intracellularly extended cytoplasmic region. *J Biol Chem,* 283**,** 17753-6.

SHIMAMURA, T., SHIROISHI, M., WEYAND, S., TSUJIMOTO, H., WINTER, G., KATRITCH, V., ABAGYAN, R., CHEREZOV, V., LIU, W., HAN, G. W., KOBAYASHI, T., STEVENS, R. C. & IWATA, S. 2011. Structure of the human histamine H1 receptor complex with doxepin. *Nature,* 475**,** 65-70.

SHINOZAKI, H., FANELLI, F., LIU, X., JAQUETTE, J., NAKAMURA, K. & SEGALOFF, D. L. 2001. Pleiotropic effects of substitutions of a highly conserved leucine in transmembrane helix III of the human lutropin/choriogonadotropin receptor with respect to constitutive activation and hormone responsiveness. *Mol Endocrinol,* 15**,** 972-84.

SIMON, M. I., STRATHMANN, M. P. & GAUTAM, N. 1991. Diversity of G proteins in signal transduction. *Science,* 252**,** 802-8.

SINGH, G., RAMACHANDRAN, S. & CERIONE, R. A. 2012. A constitutively active Galpha subunit provides insights into the mechanism of G protein activation. *Biochemistry,* 51**,** 3232-40.

SJOGREN, B. & NEUBIG, R. R. 2010. Thinking outside of the "RGS box": new approaches to therapeutic targeting of regulators of G protein signaling. *Mol Pharmacol,* 78**,** 550-7.

SONDEK, J., BOHM, A., LAMBRIGHT, D. G., HAMM, H. E. & SIGLER, P. B. 1996. Crystal structure of a G-protein beta gamma dimer at 2.1A resolution. *Nature,* 379**,** 369-74.

SONG, Z. H. & FENG, W. 2002. Absence of a conserved proline and presence of a conserved tyrosine in the CB2 cannabinoid receptor are crucial for its function. *FEBS Lett,* 531**,** 290-4.

SPALDING, T. A., BIRDSALL, N. J., CURTIS, C. A. & HULME, E. C. 1994. Acetylcholine mustard labels the binding site aspartate in muscarinic acetylcholine receptors. *J Biol Chem,* 269**,** 4092-7.

SPRANG, S. R. 1997. G protein mechanisms: insights from structural analysis. *Annu Rev Biochem,* 66**,** 639-78.

STACEY, M., LIN, H. H., GORDON, S. & MCKNIGHT, A. J. 2000. LNB-TM7, a group of seven-transmembrane proteins related to family-B G-protein-coupled receptors. *Trends Biochem Sci,* 25**,** 284-9.

STANDFUSS, J., EDWARDS, P. C., D'ANTONA, A., FRANSEN, M., XIE, G., OPRIAN, D. D. & SCHERTLER, G. F. 2011. The structural basis of agonist-induced activation in constitutively active rhodopsin. *Nature,* 471**,** 656-60.

STOJANOVIC, A., HWANG, I., KHORANA, H. G. & HWA, J. 2003. Retinitis pigmentosa rhodopsin mutations L125R and A164V perturb critical interhelical interactions: new insights through compensatory mutations and crystal structure analysis. *J Biol Chem,* 278**,** 39020-8.

STRAUME, M. & LITMAN, B. J. 1988. Equilibrium and dynamic bilayer structural properties of unsaturated acyl chain phosphatidylcholine-cholesterol-rhodopsin recombinant vesicles and rod outer segment disk membranes as determined from higher order analysis of fluorescence anisotropy decay. *Biochemistry,* 27**,** 7723-33.

SUGIMOTO, Y., NAKATO, T., KITA, A., TAKAHASHI, Y., HATAE, N., TABATA, H., TANAKA, S. & ICHIKAWA, A. 2004. A cluster of aromatic amino acids in the i2 loop plays a key role for Gs coupling in prostaglandin EP2 and EP3 receptors. *J Biol Chem,* 279**,** 11016-26.

SUN, Y., CHENG, Z., MA, L. & PEI, G. 2002. Beta-arrestin2 is critically involved in CXCR4-mediated chemotaxis, and this is mediated by its enhancement of p38 MAPK activation. *J Biol Chem,* 277**,** 49212-9.

SUN, Y., HUANG, J., XIANG, Y., BASTEPE, M., JUPPNER, H., KOBILKA, B. K., ZHANG, J. J. & HUANG, X. Y. 2007. Dosage-dependent switch from G protein-coupled to G protein-independent signaling by a GPCR. *Embo J,* 26**,** 53-64.

TANAKA, K., NAGAYAMA, Y., NISHIHARA, E., NAMBA, H., YAMASHITA, S. & NIWA, M. 1998. Palmitoylation of human thyrotropin receptor: slower intracellular trafficking of the palmitoylation-defective mutant. *Endocrinology,* 139**,** 803-6.

TANOUE, A., ITO, S., HONDA, K., OSHIKAWA, S., KITAGAWA, Y., KOSHIMIZU, T. A., MORI, T. & TSUJIMOTO, G. 2004. The vasopressin V1b receptor critically regulates hypothalamic-pituitary-adrenal axis activity under both stress and resting conditions. *J Clin Invest,* 113**,** 302-9.

TELLER, D. C., OKADA, T., BEHNKE, C. A., PALCZEWSKI, K. & STENKAMP, R. E. 2001. Advances in determination of a high-resolution three-dimensional structure of rhodopsin, a model of G-protein-coupled receptors (GPCRs). *Biochemistry,* 40**,** 7761-72.

THOMPSON, A. A., LIU, W., CHUN, E., KATRITCH, V., WU, H., VARDY, E., HUANG, X. P., TRAPELLA, C., GUERRINI, R., CALO, G., ROTH, B. L., CHEREZOV, V. & STEVENS, R. C. 2012. Structure of the nociceptin/orphanin FQ receptor in complex with a peptide mimetic. *Nature,* 485**,** 395-9.

TIMOSSI, C., MALDONADO, D., VIZCAINO, A., LINDAU-SHEPARD, B., CONN, P. M. & ULLOA-AGUIRRE, A. 2002. Structural determinants in the second intracellular loop of the human follicle-stimulating hormone receptor are involved in G(s) protein activation. *Mol Cell Endocrinol,* 189**,** 157-68.

TOHGO, A., PIERCE, K. L., CHOY, E. W., LEFKOWITZ, R. J. & LUTTRELL, L. M. 2002. beta-Arrestin scaffolding of the ERK cascade enhances cytosolic ERK activity but inhibits ERK-mediated transcription following angiotensin AT1a receptor stimulation. *J Biol Chem,* 277**,** 9429-36.

TRZASKOWSKI, B., LATEK, D., YUAN, S., GHOSHDASTIDER, U., DEBINSKI, A. & FILIPEK, S. 2012. Action of molecular switches in GPCRs--theoretical and experimental studies. *Curr Med Chem,* 19**,** 1090-109.

TSUNEMATSU, T., FU, L. Y., YAMANAKA, A., ICHIKI, K., TANOUE, A., SAKURAI, T. & VAN DEN POL, A. N. 2008. Vasopressin increases locomotion through a V1a receptor in orexin/hypocretin neurons: implications for water homeostasis. *J Neurosci,* 28**,** 228-38.

ULLOA-AGUIRRE, A., URIBE, A., ZARINAN, T., BUSTOS-JAIMES, I., PEREZ-SOLIS, M. A. & DIAS, J. A. 2007. Role of the intracellular domains of the human FSH receptor in G(alphaS) protein coupling and receptor expression. *Mol Cell Endocrinol,* 260-262**,** 153-62.

UNAL, H. & KARNIK, S. S. 2012. Domain coupling in GPCRs: the engine for induced conformational changes. *Trends Pharmacol Sci,* 33**,** 79-88.

URIZAR, E., CLAEYSEN, S., DEUPI, X., GOVAERTS, C., COSTAGLIOLA, S., VASSART, G. & PARDO, L. 2005. An activation switch in the rhodopsin family of G protein-coupled receptors: the thyrotropin receptor. *J Biol Chem,* 280**,** 17135-41.

VARGAS-POUSSOU, R., FORESTIER, L., DAUTZENBERG, M. D., NIAUDET, P., DECHAUX, M. & ANTIGNAC, C. 1997. Mutations in the vasopressin V2 receptor and aquaporin-2 genes in 12 families with congenital nephrogenic diabetes insipidus. *J Am Soc Nephrol,* 8**,** 1855-62.

WACKER, J. L., FELLER, D. B., TANG, X. B., DEFINO, M. C., NAMKUNG, Y., LYSSAND, J. S., MHYRE, A. J., TAN, X., JENSEN, J. B. & HAGUE, C. 2008. Disease-causing mutation in GPR54 reveals the importance of the second intracellular loop for class A G-protein-coupled receptor function. *J Biol Chem,* 283**,** 31068-78.

WALL, M. A., COLEMAN, D. E., LEE, E., INIGUEZ-LLUHI, J. A., POSNER, B. A., GILMAN, A. G. & SPRANG, S. R. 1995. The structure of the G protein heterotrimer Gi alpha 1 beta 1 gamma 2. *Cell,* 83**,** 1047-58.

WARNE, T., MOUKHAMETZIANOV, R., BAKER, J. G., NEHME, R., EDWARDS, P. C., LESLIE, A. G., SCHERTLER, G. F. & TATE, C. G. 2011. The structural basis for agonist and partial agonist action on a beta(1)-adrenergic receptor. *Nature,* 469**,** 241-4.

WARNE, T., SERRANO-VEGA, M. J., BAKER, J. G., MOUKHAMETZIANOV, R., EDWARDS, P. C., HENDERSON, R., LESLIE, A. G., TATE, C. G. & SCHERTLER, G. F. 2008. Structure of a beta1-adrenergic G-protein-coupled receptor. *Nature,* 454**,** 486-91.

WEISS, J. M., MORGAN, P. H., LUTZ, M. W. & KENAKIN, T. P. 1996. The cubic ternary complex receptor-occupancy model. III. resurrecting efficacy. *J Theor Biol,* 181**,** 381-97.

WESS, J. 2005. Allosteric binding sites on muscarinic acetylcholine receptors. *Mol Pharmacol,* 68**,** 1506-9.

WHEATLEY, M., SIMMS, J., HAWTIN, S. R., WESLEY, V. J., WOOTTEN, D., CONNER, M., LAWSON, Z., CONNER, A. C., BAKER, A., CASHMORE, Y., KENDRICK, R. & PARSLOW, R. A. 2007. Extracellular loops and ligand binding to a subfamily of Family A G-protein-coupled receptors. *Biochem Soc Trans,* 35**,** 717-20.

WHEATLEY, M., WOOTTEN, D., CONNER, M., SIMMS, J., KENDRICK, R., LOGAN, R., POYNER, D. & BARWELL, J. 2012. Lifting the lid on GPCRs: the role of extracellular loops. *Br J Pharmacol,* 165**,** 1688-703.

WHORTON, M. R., BOKOCH, M. P., RASMUSSEN, S. G., HUANG, B., ZARE, R. N., KOBILKA, B. & SUNAHARA, R. K. 2007. A monomeric G protein-coupled receptor isolated in a high-density lipoprotein particle efficiently activates its G protein. *Proc Natl Acad Sci U S A,* 104**,** 7682-7.

WOOTTEN, D. L., SIMMS, J., MASSOURA, A. J., TRIM, J. E. & WHEATLEY, M. 2011. Agonist-specific requirement for a glutamate in transmembrane helix 1 of the oxytocin receptor. *Mol Cell Endocrinol,* 333**,** 20-7.

WU, B., CHIEN, E. Y., MOL, C. D., FENALTI, G., LIU, W., KATRITCH, V., ABAGYAN, R., BROOUN, A., WELLS, P., BI, F. C., HAMEL, D. J., KUHN, P., HANDEL, T. M., CHEREZOV, V. & STEVENS, R. C. 2010. Structures of the CXCR4 chemokine GPCR with small-molecule and cyclic peptide antagonists. *Science,* 330**,** 1066-71.

WU, H., WACKER, D., MILENI, M., KATRITCH, V., HAN, G. W., VARDY, E., LIU, W., THOMPSON, A. A., HUANG, X. P., CARROLL, F. I., MASCARELLA, S. W., WESTKAEMPER, R. B., MOSIER, P. D., ROTH, B. L., CHEREZOV, V. & STEVENS, R. C. 2012. Structure of the human kappa-opioid receptor in complex with JDTic. *Nature,* 485**,** 327-32.

XU, F., WU, H., KATRITCH, V., HAN, G. W., JACOBSON, K. A., GAO, Z. G., CHEREZOV, V. & STEVENS, R. C. 2011. Structure of an agonist-bound human A2A adenosine receptor. *Science,* 332**,** 322-7.

YAO, X., PARNOT, C., DEUPI, X., RATNALA, V. R., SWAMINATH, G., FARRENS, D. & KOBILKA, B. 2006. Coupling ligand structure to specific conformational switches in the beta2-adrenoceptor. *Nat Chem Biol,* 2**,** 417-22.

ZHANG, M., MIZRACHI, D., FANELLI, F. & SEGALOFF, D. L. 2005. The formation of a salt bridge between helices 3 and 6 is responsible for the constitutive activity and lack of hormone responsiveness of the naturally occurring L457R mutation of the human lutropin receptor. *J Biol Chem,* 280**,** 26169-76.

ZHENG, H., PEARSALL, E. A., HURST, D. P., ZHANG, Y., CHU, J., ZHOU, Y., REGGIO, P. H., LOH, H. H. & LAW, P. Y. 2012. Palmitoylation and Membrane Cholesterol Stabilize mu-Opioid Receptor Homodimerization and G Protein Coupling. *BMC Cell Biol,* 13**,** 6.